공학박사 학위논문

Study of Two-Dimensional Shear Effects on Flow and Pollutant Transport in Meandering Channels

사행수로에서 흐름 및 오염물질 혼합에 미치는
2차원 전단 효과에 대한 연구

2018년 2월

서울대학교 대학원

건설환경공학부

신 재 현

ABSTRACT OF DISSERTATION

Study of Two-Dimensional Shear Effects on Flow and Pollutant Transport in Meandering Channels

by

Jaehyun Shin

Doctor of Philosophy in Civil and Environmental Engineering

Seoul National University

Professor Il Won Seo, Advisor

In this study, the depth-averaged two-dimensional model was used to simulate the shear effects on meandering river flows and pollutant transport with reasonable accuracy and efficiency. To validate the numerical model, large-scale experiments were conducted in the River Experiment Channel (REC) large-scale meandering channels, in which the data of flow by acoustic Doppler current profiler (ADCP) measurement and pollutant transport by tracer tests in meandering channels were collected. Using velocity measurements, the effect of the secondary current on the primary flow distribution was analyzed. First, the relations of the secondary flow strength to the depth to radius-of-curvature of the channel and channel roughness were found. Then, the vertical profile equation for the secondary flow was

developed reflecting the nonlinear term effects on the secondary flow which were omitted in the previous studies. The proposed equation generated a vertical profile that showed a decrease in the maximum secondary flow strength at the top and bottom of the profile, which is different from the existing equations.

The proposed velocity profile equation was inserted into the momentum equations with the dispersion stress method for the two-dimensional flow solver HDM-2D, in order to induce the shear effect of secondary flow, which is normally neglected in the depth averaging process. The simulation results using the proposed equation to the dispersion stress method showed that the simulation of the Rozovskii channel showed improvement over the dispersion stress model using deVriend and Kikkawa's velocity equation, which was based on the linear behavior between the secondary flow and primary flow, as well as over the model with no-dispersion stress in the distributions of primary flow velocity. The validation results with REC meandering channels revealed that the 2D hydrodynamic model with dispersion stress term gave a better fit of primary flow distribution to the experimental data than the simulation without the dispersion stress term.

To find the characteristics of pollutant transport in meandering channels, the two-dimensional dispersion coefficients were calculated using the vertical velocity profiles which represents shear dispersion from the ADCP measurements, and the results were compared with the values calculated by applying 2D stream-tube routing procedure to the concentration curves obtained from 2D transient tracer experiments. The velocity driven two-dimensional dispersion coefficient in rivers

which was calculated using the shear flow dispersion coefficient equation developed by Fischer et al. (1979) is easy to obtain since it did not require the tracer test experiments. The results showed that non-dimensional longitudinal dispersion coefficient, D_L / hu^*, by velocity profile ranges from 4 to 6 which is close to Elder's result, while non-dimensional transverse dispersion coefficient, D_T / hu^*, ranges from 0.05 to 0.4. However, the dispersion coefficients calculated using the 2D stream-tube routing procedure were quite large: 4-5 times larger than velocity driven values for longitudinal dispersion coefficients, 1-3 times larger for the transverse dispersion coefficients. These differences could be explained by the fact that the concentration-driven dispersion coefficient included the mixing effects due to the irregularities of the channel, storage zones and numerical dispersion while velocity-driven coefficients only accounted for shear flow effects. Then, CTM-2D advection-dispersion model was applied to simulate mixing in meandering channels and the dispersion stress term improved accuracy by 1%. The calibrated dispersion coefficients by the CTM-2D model were between the velocity-driven results and concentration driven results. The simulation results proved the applicability of the CTM-2D model in reproducing concentration curves in meandering channels.

Keywords: 2D shallow water model, 2D advection-dispersion model, meandering channel, dispersion stress, dispersion coefficients, primary flow distribution, secondary current, vertical velocity profile, nonlinear effects

Student Number: 2012-30246

TABLE OF CONTENTS

LIST OF TABLES

LIST OF FIGURES

LIST OF SYMBOLS

Latin Uppercase

A	Cross-sectional area
C	Chezy coefficient
D_s	Rate of dissipation
F	Function
H	Depth of fluid
R_c	Radius of curvature
S_n	Sinuosity
U	Depth averaged longitudinal velocity
U_*	Average shear velocity of section
$\overline{U}$	Cross-sectional averaged longitudinal velocity
V	Depth averaged transverse velocity
W	Width of channel
Z	Depth of fluid

Latin Lowercase

f_n	Normalized value of v_n

f_s	Normalized value of v_s
g	Gravitational acceleration
h	Fluid depth
p	Pressure
r	Radius
s'	Longitudinal distance from entrance of bend
s''	Longitudinal distance from exit of bend
$\bar{u}$	Depth averaged longitudinal velocity
u_s	Velocity at fluid surface
u	Longitudinal velocity
v	Transverse velocity
v_z	Transverse velocity at the fluid surface
z	Vertical location

Greek Lowercase

γ	Unit mass
ε	Turbulent dissipation rate
κ	Von Karman constant
η	Normalized vertical distance z / h
μ	Viscosity
ρ	Density
τ	Shear stress

Chapter 1 Introduction

1.1 Research Background and Necessity

In majority of natural rivers and channels, the stream is usually formed in a meandering shape by the influence of uneven river morphology and bed topography. Modeling the flow characteristics of meandering channel bends proves to be a challenge due to the complication in the flow structure compared to those in straight channels. The flow resembles a helical flow structure formed in the meander bend, which is how the secondary flow affects the movement in the apex. The secondary flow in meandering channels is caused by the local imbalance between the transverse water pressure forces generated by super elevation of the water surface and the vertically varying centrifugal force (Henderson, 1966). The local force imbalance causes a secondary cell to form, so that the lower part of the water column flows inside the bend, while the surface part of the water column flows to the outside of the bend, which affects the local scouring and sedimentation occurring at the bend areas. Furthermore, the secondary flow affects the transverse dispersion rate through the mass and momentum redistributions by the helical flow structure. The advective momentum transport by the secondary flow also causes longitudinal velocity redistribution (Blanckaert, 2004), in which the primary flow is shifted outward at the bend, as shown in Fig. 1.1. Thus, understanding of the secondary flow in bends is necessary, in order to analyze the transverse distribution of the longitudinal velocity, as well as to study the mixing of sediments and pollutants in meandering channels.

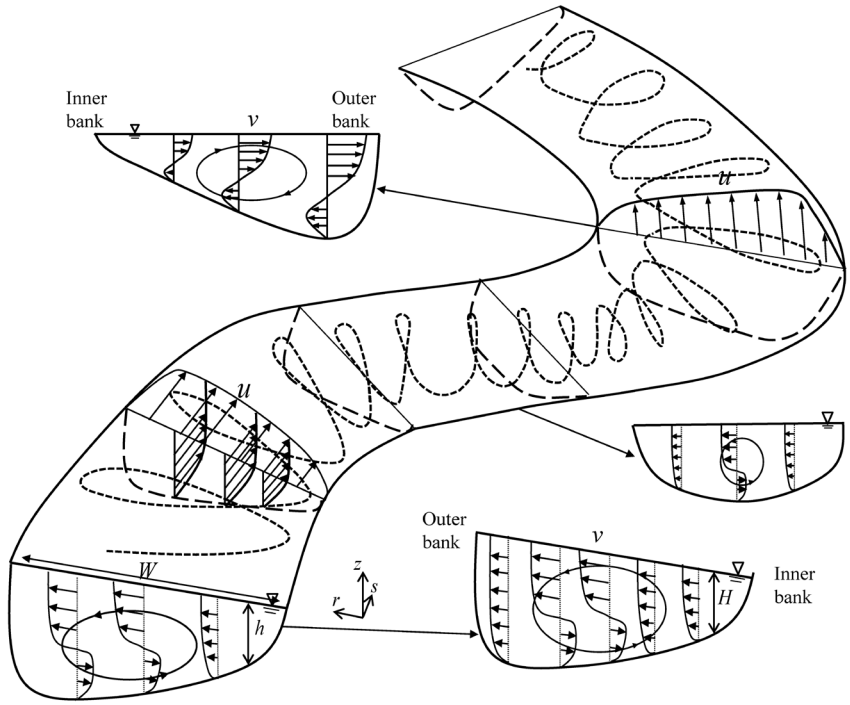

Fig. 1.1 Schematic diagram of flow and force balance in the meandering channel

The understanding of the secondary flow in bends is necessary since it affects the channel morphology, sediment transport and pollutant mixing in the area. Pollution mixing problems in water bodies are caused by industrial development or contaminant spill accidents. They are considered especially important since it affects the intake water facilities and the ecosystem. Therefore careful measures must be taken for water pollution control and management. To regulate water pollution problems, insight of the pollutant mixing and spread is necessary. The pollutant can be assumed as particles that spread out on the river due to the flow and difference of velocity, and this concept is defined as dispersion of particles. To find out the accurate movement and transport of these particles, the characteristics of secondary flow must be carefully analyzed and studied.

When a pollutant is first inserted into an open channel, it spreads and goes through several stages of shear dispersion as in Figure 1.2. In the first stage which is considered the near field, the vertical mixing mainly occurs in most open channels in which the depth is smaller than the width of the channel. In the second stage known as the intermediate field, the transverse mixing mainly takes place (Fischer et al., 1979). The mixing stage of the intermediate field is very long compared to the near field mixing (Seo et al, 2016). Therefore, for accurate analysis of the mixing in rivers, study of the two-dimensional mixing is required. Also, the analysis of two-dimensional (2D) dispersion in rivers and open channels is necessary due to possible pollutant accidents that could occur which would affect water intake facilities in the intermediate field.

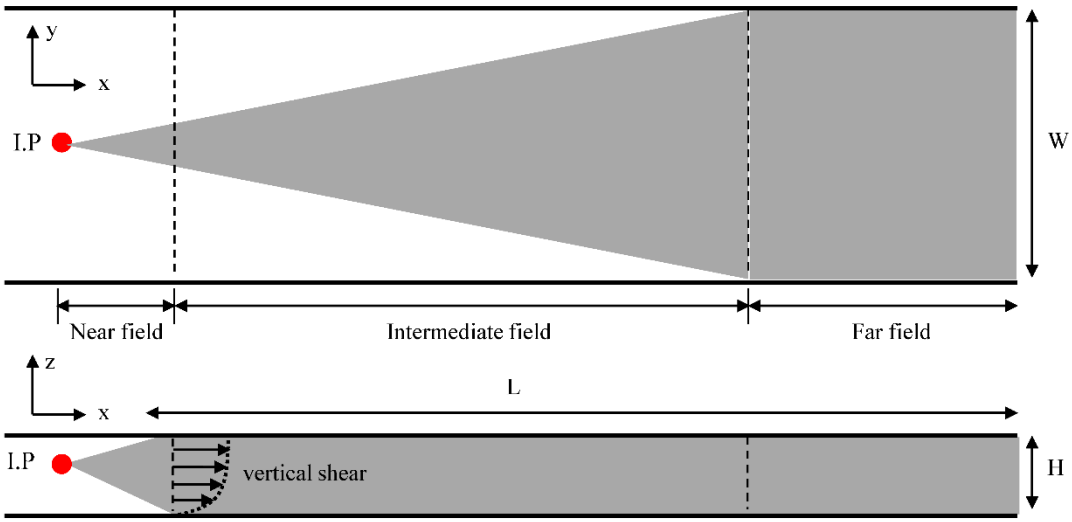

Fig. 1.2 Conceptual diagram of stages of pollutant mixing in rivers

(adapted from Kim, 2012)

Physical models have been used to reproduce the flow in natural meandering channels. Real flow situations are usually too extensive for precise examination and study so instead of creating a prototype of the same size, the model would be a small scaled physical re-creation of the target area. However, the time and effort needed to create the actual physical models were high and scaling problems including similitude such as Froude and Reynolds number were always an issue regarding true representation of the full size flume. Therefore assuming that the equations that govern the motion of fluid are known, constructing a conceptual or numerical model of the real world and carrying out a numerical experiment became more feasible as development of computers expanded and numerical modeling techniques expanded in the latter twentieth century. The numerical studies could be applied to the Navier-Stokes equation or the advection dispersion equation for solving flow and pollutant mixing problems.

In the modeling of flow in meandering channels, although three-dimensional (3D) models showed the highest accuracy in reproducing the complex flow in curved reaches, the applicability of using 3D hydrodynamic models is relatively limited, compared to the two-dimensional (2D) depth-averaged models, due to their high computational requirements. For the modeling of flow and mass transport in a relatively shallow water system, such as open channels and rivers, the usage of 2D depth-averaged models is more common. However, in the existing 2D numerical models frequently used in rivers, the depth-averaging sequence of 3D Navier Stokes equations causes the loss of three-dimensional information in the momentum terms.

This information can be partially retrieved by introducing the dispersion stress terms, which involves the integration of the discrepancy of the averaged and fluctuated transverse velocity in the momentum equations. In the dispersion stress method, the terms using vertical profiles of both longitudinal and transverse velocity were inserted, so the secondary current effect was included in the momentum equation (Seo and Song, 2012). Thus, in order to apply the dispersion stress method to the 2D depth-averaged momentum equation, vertical profile equations for both longitudinal and transverse velocities are needed.

Even though many researchers have studied the vertical profile of the transverse velocity in curved channels, most equations were derived by neglecting the nonlinear terms in the momentum equation. Rozovskii (1957) and Kikkawa (1976) derived the vertical profile equations of the secondary flow from the momentum equations using a logarithmic form assumption, without considering nonlinear relations between primary and secondary flows. The perturbation method was used by de Vriend (1977), who assumed the depth of the meandering channel is smaller than the radius-of-curvature, to derive another secondary flow equation. Since the former equations were still complicated, Odgaard (1986) connected the vertical profile of the secondary flow to the surface velocity, to formulate into a linear profile. Although the author considered the easiest method for implementation, it was too simple to account for the complex mechanisms of velocity deviations from the mean at the top and bottom parts of the profile. Therefore, for accurate representation of the secondary flow, equations for the vertical profile should have

the nonlinearity reflected. This knowledge of flow characteristics is essential for analysis of tracer mixing in meandering channels.

For the analysis of two-dimensional pollutant mixing, advection-dispersion model can be used for modeling the contaminant transport. These type of models require dispersion coefficients, which could be calculated using the shear velocity driven method and the concentration data driven method. The mixing characteristics of pollutants by shear flow can be defined by using dispersion coefficients from the derivation shown by Taylor (1954). The equation showed that the vertical deviations of velocity are related to shear flow which affect the dispersion coefficients. Due to the recent advancement in accurate velocity measuring systems such as the use of ADCP commenced to the acquisition of velocity data that could be used for velocity profile development. The measured vertical velocity profile could serve as data to calculate dispersion coefficients for the prediction of mixing coefficients without the need for actual tracer tests. This can be used in situations where the concentration is unknown so the dispersion coefficients are predicted using only the hydraulic data such as pollutant accidents. Former research lacked the 2D dispersion coefficient estimation by vertical velocity in natural channels. This method could be compared to the traditional method of using tracer test concentration data for routing for its applicability. The two methods could be used as parameters for the advection dispersion model for pollutant transport modeling. Overall, these research can provide how the shear effects flow and pollutant transport in curved channels, which will be the main scope of this research.

1.2 Objectives and Scope

This study aims to investigate the interaction between the flow structures and contaminant transports in meandering channels. Thus, the key objectives are to find the vertical velocity structure in the meandering bends and determine its shear effects on the flow and pollutant mixing. These methods were validated using the measured velocity data and tracer test results from a large-scale meandering channels at the River Experiment Center (REC) of Korea Institute of Civil Engineering and Building Technology (KICT).

The detailed scope of the study is given below:

First, a profile of the vertical structure of the secondary flow profile was created for the dispersion stress method of the flow model HDM-2D using experimental data from the REC. An analysis of the previous equations for the secondary flow was conducted to find the key variables that affect the formation of the secondary flow structure. A new vertical profile equation of the transverse velocity based on the experimental results was developed by considering the nonlinear relationship between the longitudinal and transverse flows, which was neglected in the previous equations. The dependence of the secondary flow on certain variables, such as the depth to radius-of-curvature ratio, was analyzed using experimental results obtained from the meandering experimental channels. The proposed equation for the vertical profile of the transverse velocity was incorporated into the momentum equations of the 2D finite element model in the dispersion stress form, in order to induce the secondary flow effect in the primary flow in modeling curved channels.

Second, a large-scale meandering channel experiment was conducted in the REC for the measurement of primary flow and vertical flow profiles to find the effects of curvature to the secondary flow strength and its characteristics, and tracer tests were conducted to acquire the concentration distribution data for dispersion coefficients. Also, the vertical profile equation from the first objective was developed by using the measured vertical profile. The vertical velocity profiles was integrated with the equation by Taylor (1954) to find the spatial variation of the dispersion coefficient in measured sections of the open channel assuming the shear dispersion is mainly influenced by the flow deviation in the vertical profile. Then, tracer test results were analyzed for the contaminant spread in meandering channels. Further comparisons with observation results such as two-dimensional stream-tube routing procedures using tracer test results was also undertaken to find the accuracy and reliability of the predicted dispersion coefficients.

Third, the predicted dispersion coefficients were used in the unsteady depth-averaged two-dimensional advection-dispersion pollutant model, CTM-2D, to find the applicability of the velocity driven dispersion coefficients and concentration driven dispersion coefficients. This modeling showed the effect of two-dimensional shear on dispersion coefficients. The meander sinuosity and geographical characteristics that affect transport mixing was analyzed. Completion of the these objectives leads to increase of knowledge of flow structure in meandering bends and its effects to pollutant mixing, which is critical for modeling and field studies overall.

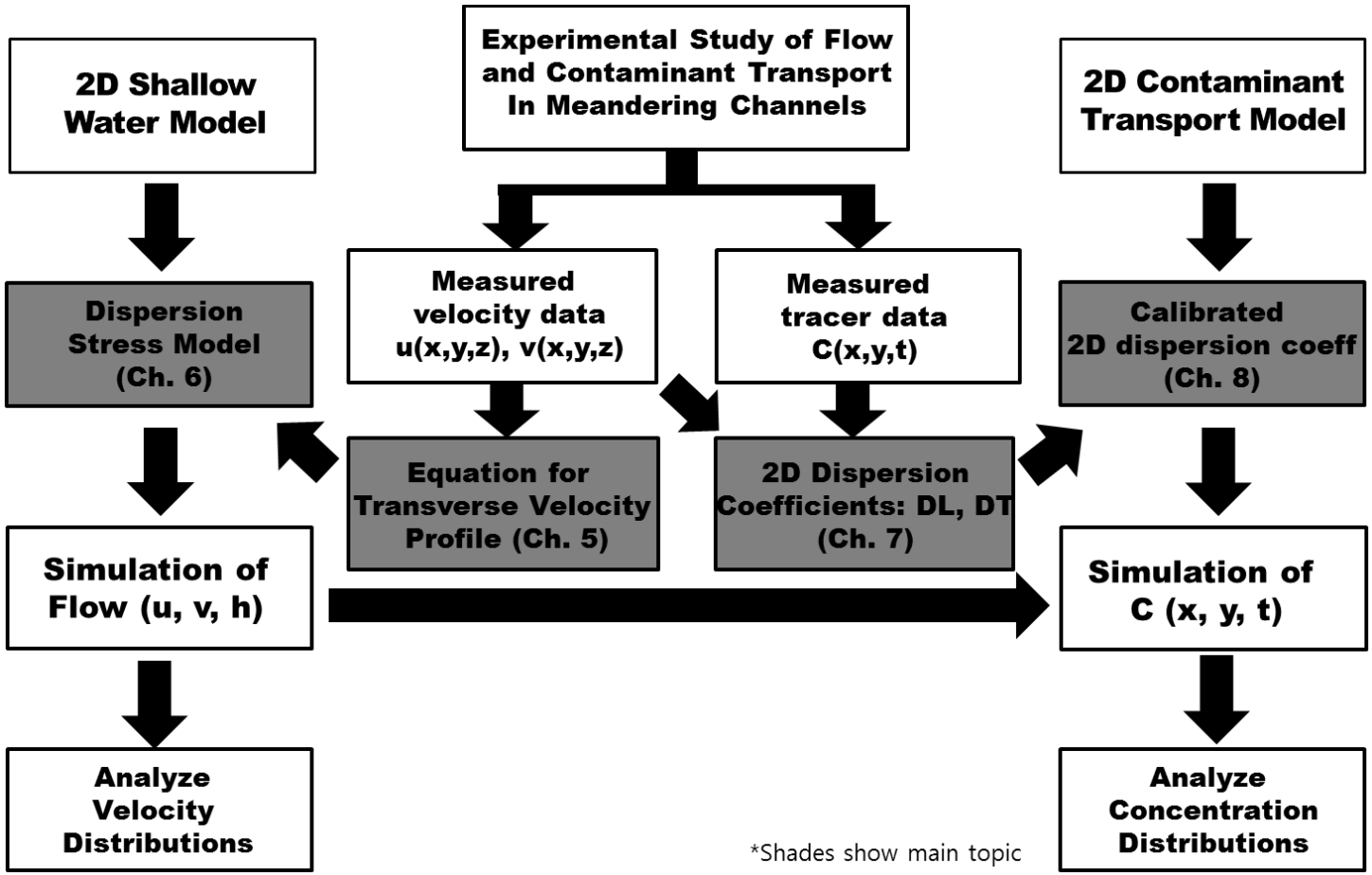

Figure 1.3 Research Diagram

2. Theoretical Research

2.1 Meandering Channel Classification

For the study of meandering channels, first the basic concept and understanding of the open flow occurrence of meandering will be introduced. The classification of straight and meandering channels can be described by certain features, which can be somewhat arbitrary. Meandering is usually recognized by the tortuosity of the course and is formed by the erosion and deposition of gravel, sand and other types of sediment. Some classification methods first involve the single channel and multi-channel patterns with several distinct variables.

A variable that can be used to explain a meandering channel in sinuosity. The channel sinuosity can be computed with

$$Sn = \frac{\text{channel length}}{\text{straight-line valley length}} \tag{2.1}$$

The difference between the actual lengths to straight-line length can show the sinuosity of the channel. Describing the meandering characteristics another term used is the degree of regularity, where three categories of meander regularity can be

shown (Knighton, 2014); regular meanders with a clearly repeated pattern with the maximum deviation angle below 90, regular meanders with a maximum deviation angle above 90, and vague repeated patterns in irregular meanders,

Another variable which could be used to distinguish the meander characteristics are meander wavelength and radius of curvature which could be acquired by single measurement or by averaging over several bends. The wavelength is connected to the sine/cosine generated curve, where it becomes a typical explanation of a simple model form of a meandering channel. The sine generated curve can be shown with the following equation

$$\theta = \omega \sin kx \tag{2.2}$$

where θ = channel direction, x = flow direction along the reach, ω = the maximum angle between a channel segment and the mean down valley axis, k = the meander wavenumber. Other individual bend statistics involve radius of curvature and width of the channel. Although the actual relation between the flow characteristic and meander geometry was somewhat ambiguous, various researches were done by deriving the transverse velocity using the momentum equations with variables such as radius of curvature, sinuosity, and width over height of the channel which will be introduced in Chapter 2.3.

2.2 Theoretical Concept of Secondary Flow

The secondary flow is created as the water body in the upper part of the channel is driven outward and the water near the bottom is driven inward. This is due to several reasons, one being the result of the centrifugal force applied to the water. Also, the bottom friction and pressure gradient due to the decline of the water surface creates this phenomenon. The flow characteristics around a bend are induced by the following process. (Henderson, 1966). The analysis assumes that the loss of energy involving the meander apex flow is negligible and will be ignored in the derivation. First the Euler equation is

$$\frac{\partial}{\partial x}(p+\gamma z)+\rho a_k = 0 \qquad (2.3)$$

p is the pressure, γ is the unit mass, z is the vertical location, ρ is the density, and a_k is the velocity in the *s* direction in Fig 1.1

If we take the *r*-direction inwards across the width of the section, then $a_k = v^2 / r$ is formed by dynamic theory. If the pressure is hydrostatic, $\frac{\partial}{\partial k}(p+\gamma z)/\partial s = -\gamma \partial h / \partial n$, since at all points the following is equitable, $p+\gamma z = \gamma h$. Then the Euler equation becomes

$$\frac{dh}{dn} = \frac{v^2}{gr} \tag{2.4}$$

where h is the water depth, v is the fluid velocity, g is the gravitational acceleration, and r is the distance from the center of curvature to the thalweg. This equation illustrates that h would increase from the inner to the outer bank with n increase since v^2 / gr is always positive which is one of the reasons a superelevation of the water surface is composed.

In the curved channel apex areas, the secondary currents always occur since the velocity v is not constant vertically throughout the channel and changes from top to bottom and inner to outer bank, lower near the bed. Whereas the water surface gradient dh / dn is nearly the same vertically which accompanies a constant transverse pressure gradient in a vertical profile standpoint, and the pressure distribution is nearly hydrostatic in these open channels. So adding up the forces shows that near the bed the inward pressure is dominant inducing inner flow at the lower levels of the water body and compensated by outward flow at the upper levels and which results in a rotating pattern. So in the meandering areas of the channel the transverse velocity is highly non uniform over the depth.

However, in deriving equations of the transverse velocity, nonlinear terms that account for interactions between the primary flow and secondary flow were usually neglected. Fig. 2.1 shows a representation of the curvature induced secondary flow caused by the addition of outward centrifugal force and inward pressure gradient. In

mild curved channels, interactions between the longitudinal and transverse flow would be small, and the secondary flow increase would depend on the term H / R_c to grow linearly. But nonlinear behavior by the sharper curves would cause the decrease and irregularity of the outward centrifugal force, which would then lead to the overall decrease of secondary flow strength in the top and bottom parts of the water flow. In this regard, Blanckaert and de Vriend (2003, 2010), Ottavenger et al. (2013) and Wei et al. (2016) used the equation developed by de Vriend (1977), and showed that the commonly used linear models, in which secondary current effects linearly depend on H / R_c, may overestimate the strength of the curvature inducement. Thus, they introduced a nonlinear method concerning the term $C_f^{-1} H / R_c$ as the major control parameter, using depth to radius-of-curvature and the dimensionless Chezy friction coefficient, C_f, which is given as $C_f = C^2 / g$. The parameter size would gradually decrease, to include the feedback between the longitudinal velocity and secondary circulation. The nonlinear behavior by the secondary currents would cause the decrease and irregularity of the outward centrifugal force, which would then lead to the overall decrease of secondary flow strength in the top and bottom parts of the water flow, as shown in Fig. 2. Thus, this study proposes a revised equation for the vertical profile of secondary currents, in which the nonlinear term is sustained to include the effect of secondary flows in sharp curved channels.

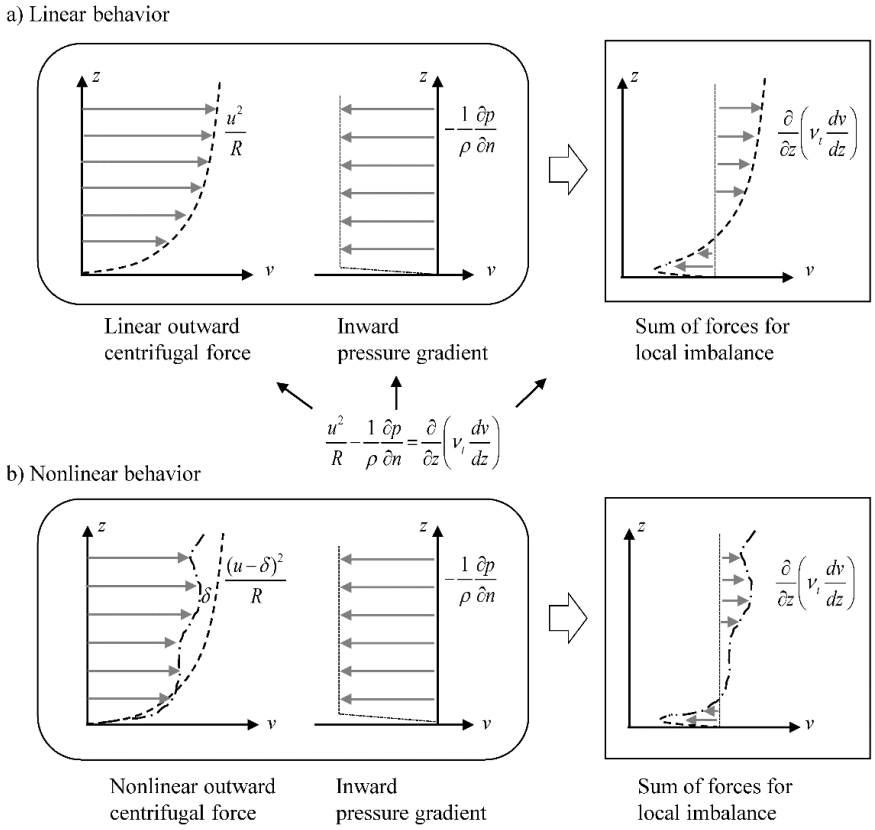

Fig. 2.1 Schematic representation of curvature induced secondary flow with linear and nonlinear behavior (Adapted from Wei et al., 2016)

2.3 Vertical Profile Equation of Secondary Flow

Previous studies regarding the subject of secondary flow are the following. Several researches by laboratory experiments and theoretical equations have been continued to find the structure of the velocity of the secondary flow. Since the mid-19th century the occurrence of secondary flow has been observed by many researchers. Thompson (1876) had found this by introducing seeds and dyes in a channel bend and recorded the flow characteristics of the spiral motion that was observed in the open channel. Prandtl (1952) used the term secondary flow and defined its concept. Later researchers gave attention to the derivation of the vertical profile equation from the equations of motion and continuity for meandering channels for knowledge of secondary flow. Rozovskii (1957), Kikkawa (1976), de Vriend (1977), etc. assumed that the depth was considered to be much less than the width and radius of curvature in natural open channels and derived the vertical profile which ends up in a form where the upper part of the velocity profile to move outward while the lower part of the profile moved inward as in Figure 1.1

Rozovskii (1957) studied the flow in meandering open channels with several experiments and summarized in the derived equations. One of the derived equations was the vertical profile of fully developed transverse velocity, which was compared with data from a single bend experiment using growth and decay functions, to show the changes and variation of secondary flow strength in meandering channels. The research assumed the logarithmic profile of the longitudinal velocity, then obtained the transverse velocity profile in the case of a smooth bed, as follows:

$$\frac{v(\eta)}{\overline{u}} = \frac{1}{\kappa^2}\frac{H}{R_c}\left[F_1(\eta) - \frac{g^{1/2}}{\kappa C}F_2(\eta)\right] \tag{2.5}$$

$$F_1(\eta) = \int \frac{2\ln\eta}{\eta - 1}d\eta \tag{2.6a}$$

$$F_2(\eta) = \int \frac{\ln^2\eta}{\eta - 1}d\eta \tag{2.6b}$$

where, v is the transverse velocity, η is the dimensionless distance from the bed, H is the depth, $\overline{u}$ is the depth-averaged longitudinal velocity, κ is the von Kármán coefficient, C is the Chezy coefficient, R_c is the radius of curvature, and g is the acceleration of gravity. This assumed that when the radius of curvature was many times larger than the channel depth, there was an equilibrium of the pressure force, centrifugal force, and turbulent shear stress. The author also suggested a growth and decay pattern equation using exponential functions to illustrate the changes to the secondary flow along the streamwise direction in the curvature in channels as the following.

$$U_2(s,\eta) = U_2(\eta)\left[1 - \exp\left(\frac{2\kappa g^{1/2}}{C}\frac{s'}{h}\right)\right] \tag{2.7}$$

as the growth term,

$$U_2(s,\eta) = U_2(\eta)\left[\exp\left(\frac{2\kappa g^{1/2}}{C}\frac{s''}{h}\right)\right] \tag{2.8}$$

as the decay term, where s' = longitudinal distance from the entrance of the bend, and s'' = longitudinal distance from the exit of the bend.

Kikkawa (1976) also developed the equation for transverse velocity from the equation of motion assuming the flow is in equilibrium, the eddy viscosity is constant within the cross section of the channel, and the channel has a sufficiently large radius. The derived equation is

$$\frac{v(\eta)}{U} = F^2\frac{1}{\kappa}\frac{H}{R_c}\left[F_A(\eta) - \frac{1}{\kappa}\frac{U_*}{U}F_B(\eta)\right] \tag{2.9}$$

$$F_A(\eta) = -15\left(\eta^2\ln\eta - \frac{1}{2}\eta^2 + \frac{15}{54}\right) \tag{2.10}$$

$$F_B(\eta) = \frac{15}{2}\left(\eta^2\ln^2\eta - \eta^2\ln\eta + \frac{1}{2}\eta^2 - \frac{19}{54}\right) \tag{2.11}$$

where U is the cross-sectional averaged longitudinal velocity, $F = \left(\frac{\bar{u}}{U}\right)^2$ is the radial distribution of the depth averaged velocity normalized by U, and U_* is the cross-sectional averaged shear velocity. This equation shows that the channel water depth compared to the radius of curvature has a linear effect on the secondary flow strength, which is similar to the Rozovskii equation. The research also showed that

the velocity profiles observed at cross sections in curved open channels showing the distribution of the secondary flow by deriving the vertical profile from the equation of motion. The derivation procedure will be shown later as this research shows a revised version of the equation.

A transverse velocity profile equation was created by de Vriend (1977) using the perturbation method. The ratio of the depth to the radius of curvature was selected as the perturbation parameter, and the dependent variables of the equation were expanded in a power series, so higher order terms of the second order could be neglected to obtain the solution. Using the depth-averaged model to simplify the three-dimensional meandering channel into a two-dimensional problem, it has the following secondary flow and main flow functions, F_s and F_m, respectively.

$$\frac{v(\eta)}{U} = -\frac{1}{\kappa^2}\left(\frac{H}{R_c}\right)^2 \frac{R_c}{r_\psi} F_s(\eta) \tag{2.12}$$

$$F_s(\eta) = 2F_1(\eta) + \frac{\sqrt{g}}{\kappa C} F_2(\eta) - 2\left(1 - \frac{\sqrt{g}}{\kappa C}\right) \times F_m(\eta) \tag{2.13}$$

$$F_m(\eta) = 1 + \frac{\sqrt{g}}{\kappa C}(1 + \ln\eta) \tag{2.14}$$

$$F_1(\eta) = \int_0^1 \frac{\ln\eta}{\eta - 1} d\eta \tag{2.15a}$$

$$F_2(\eta) = \int_0^1 \frac{\ln^2\eta}{\eta - 1} d\eta \tag{2.15b}$$

where, U_n is the Euclidian norm of longitudinal velocity, and r_ψ is the local radius of curvature in the streamline system. This equation shows that the logarithmic profile of the longitudinal flow could affect the characteristic and shape of the secondary currents. The research observed that the steady flow in shallow rivers of moderate curvature with gradual depth can be described by shallow water equations. It also showed that the secondary circulation in curved channel flow could give rise to considerable deformations of the main velocity distribution.

Odgaard (1986) considered the velocity profile of the secondary flow cell as of circular motion type, and using this presumption, introduced a linear transverse velocity profile with the following:

$$v(\eta) = v + 2u_s\left(\eta - \frac{1}{2}\right) \tag{2.16}$$

$$u_s = v\frac{2m+1}{2\kappa^2 m}\frac{H}{R_c} \tag{2.17}$$

where, $u_s =$ longitudinal velocity at the water surface, and $m = \kappa C / g^{1/2}$. This equation utilizes the longitudinal velocity at the water surface. With this equation, the author developed a 2D model for simulating the flow and bed topography in a meandering alluvial channel.

With v_s becoming the transverse velocity at the fluid surface, Baek (2006) derived the following equation using the transverse water slope equation for the

surface velocity by Chang (1988). After deriving the surface velocity the vertical profile by Odgaard was used for the following equation.

$$v_s(s) = \frac{A_1}{A_2}\{1 - \exp(-A_2 s)\} + v_s^i \exp(-A_2 s) \tag{2.18}$$

$$A_1 = \frac{2m+1}{m(m+1)}\frac{\bar{u}}{r_c} \qquad A_2 = \frac{2\kappa^2}{m+1}\frac{1}{h} \tag{2.19}$$

with v_s being the secondary flow occurring at the early stages of the flow. It is similar to the equation that was proposed by Rozovskii (1957) with exponential distribution. The first term represents the increase of the flow velocity and the second term represents the decrease of the flow velocity. The controlling parameters for the model were width-depth, radius-width, resistant characteristics, and Froude number. Using the two terms H / R_c and the H / W term, an empirical equation was created to show the transverse velocity profile. The developed model was able to predict the secondary flow component and transverse bed slope reacting to the curvature changes in a channel with an oscillating form since those changes were important to the transverse mass shift.

These equations such as the case of Rozovkii equation and Kikkawa equation are based on the assumption that the radius of the river is large compared to the depth of the channel. For the Kikkawa equation the derivation sequence neglects the

nonlinear convective terms of the momentum equations as they become the two orders of magnitude which later causes overestimation in the top and bottom part of the channel. The de Vriend equation assumes that the channel depth over curvature is small enough so that the terms of the order $O(H/R_c)^2$ are neglected to yield the equation when using the perturbation method for derivation. The Odgaard and Baek equation uses a linear profile which is acceptable in many natural channels but for sharp curvatures, the secondary current size of the top and bottom of the vertical profile is decreased due to the nonlinear interaction between the secondary and the main flow. These results show the necessity of a revised equation for the vertical profile of secondary currents. The first two equations Eq. 2.5 and 2.9 have the similarity that the transverse velocity size is directly related to H/R_c and the longitudinal velocity. By using the term H/R_c, a new equation using the momentum equation derivation such as the above equations and field experimental data results will be created for the vertical profile of transverse velocity in Chapter 5.

2.4 Methods of Secondary Flow Application

2.4.1 Secondary Flow Modeling

After the development of vertical secondary velocity equations, other attempts with modeling the meandering flow was conducted by the following researchers. Flokstra (1977) viewed that the depth averaged calculations for flow should have effective stresses if the secondary currents were put into effect. Leschziner and Rodi (1979) presented the development and decay of spiral movements as the flow progresses in the downstream direction. And then they compared their computed vertical distributions of transverse velocity and longitudinal velocity profiles with those of Rozovskii (1957) and got a very satisfactory agreement. de Vriend (1980) observed that the steady flow in shallow rivers of moderate curvature with gradual depth can be described by shallow water equations. Then derived vertical velocity profiles were verified with experiments. He also showed that the secondary circulation in curved channel flow could give rise to considerable deformations of the main velocity distribution. He suggested that the development of the additional cell should be a matter of hydrodynamic instability.

Falcon (1984) showed that for steady uniform curved flow in open channel bends, secondary flow velocity can be obtained by a simple Boussinesq turbulence model. But Falcon also pointed out that for bank recession and accurate calculation for transverse bed shear stress other turbulence models needed to be introduced. Odgaard (1989) developed a model for simulating the flow and bed topography in a

meandering alluvial channel. The model was tested with both laboratory and field data. The controlling parameters for the model were width-depth, radius-width, resistance characteristics, and Froude number. Johannesson and Parker (1989) developed equations which would suppose the distributions of the depth averaged longitudinal velocity in curved rivers. The paper showed that the convective transport of the flow momentum by the secondary flow induced the longitudinal flow to move outward in the curves. Shiono (1991) dealt with the study of flow of water in open channels with complex cross sections changing the depth ratio of the overbank/inner bank flow. The development of measurement equipment and laser technology led to more careful observations in laboratory experiments. Tominaga and Nezu (1991) used a FLDA (Fiber-optic Laser Doppler Anemometer) for measurements in fully developed compound open channel flows, which led the researcher to be able to measure secondary flow velocities in 3d. Molls and Chaudary (1995) developed a 2D depth averaged equation model with incorporating a constant eddy-viscosity model to approximate the turbulent Reynolds stress. The model was then applied to experimental researches of the above such as the 180 degree channel bend that was observed by Rozovskii. Later researches used the measurement techniques and compared them by using the moment of momentum method and dispersion stress method for two-dimensional modeling to reproduce the secondary flow effects. First, the moment of momentum method was reviewed.

Table 2.1 Main Literature Review Classification (Secondary Flow)

Topic	Researcher	Details
Concept	Thompson(1876)	Spiral motion shown in channel bend by seeds and dye
	Prandtl (1952)	Concept of secondary currents
Experiment and transverse equation	Rozovskii (1957)	Flow of water in bends of open channels
	Kikkawa (1976)	Velocity profiles observed at cross sections in curved open channels by functions
	de Vriend(1980)	Steady flow of shallow rivers of moderate curvature with gradual depth
Model verification with developed model	Falcon (1984)	For steady uniform curved flow in open-channels bends, secondary flow velocity have been obtained by simple Boussinesq turbulence model
	Odgaard (1989)	Model for simulating the flow and bed topography in a meandering alluvial channel is developed. Model is tested with both laboratory and field data. Controlling parameters are Width-depth, radius-width, resistant characteristics, Froude number
	Tominaga, Nezu (1991)	Measurements in fully developed compound open channel flows conducted with FLDA, able to measure secondary velocities in 3D

	Molls (1995)	2D depth averaged equation model developed with incorporating constant eddy-viscosity model to approximate the turbulent Reynolds stress.
	Lien (1999)	2D depth averaged model for simulating and examining flow patterns in channel bends, data from de Vriend and Rozovskii were compared for model application showing the secondary flow effect
Experiment	Shiono (1991)	Study of flow of water in open channels with complex cross sections changing the depth ratio of the overbank/inner bank flow
	Blanckaert (2001)	3D measurements of flow were made in an outer half-section of an open channel bend for a rough turbulent flow
	Patra (2004)	Flow and velocity distribution in meandering compound channels with overbank flow is described
	Baek (2006)	Equation proposed to describe the transverse velocity along sinuous channels with alternating bends
Moment of Momentum method	Ghamry (1999)	Vertically averaged and moment model, which the depth averaged continuity and momentum equations are coupled with additional moment of momentum equations
	Vasquez (2006)	Two-dimensional finite element river morphology based on the vertically averaged and moment of momentum equations.
	Finnie (1999)	Used secondary flow correction method developed by Bernard and Schneider to apply it into a depth averaged flow model RMA2

Other 2D models considering secondary flow	Jia (1999)	Developed CCHE2D, a flow and sediment transport model used a semi-empirical function of Engelund to apply the effects of the secondary flow in curved channels
	Blanckaert (2003)	Model where the terms represent the advective transport of downstream momentum by transverse currents retained in the downstream momentum equations
	Duan (2004)	Developed two-dimensional numerical model using the Odgaard equation for transverse flow for the dispersion term calculations
	Begnudelli (2010)	Two dimensional model with the dispersion stress term for secondary flow consideration as the transfer of energy out of the circulating flows
	Kimura (2010)	Model considering the lag of development of secondary current behind the streamline curvature with deformations of mean vertical velocity profiles
	Sukhodolov (2011)	Vertical profile of tangential velocity was described by a logarithmic law and modified for the pool in curvature
	Song (2012)	Model applying the dispersion stress for secondary flow and changeable slip boundary conditions for simulating curvature channels
	Yang (2014)	Secondary flow effects in open channel confluence flow using dissipation and dispersion terms in the momentum equation
	Akhtar (2015)	Simulated curvilinear stretch in a natural river using a depth averaged model with the dispersion stress term

Maria and Silva (1999) expressed the friction factor of rough turbulent meandering flows as the function of sinuosity and position (which is determined by, among other factors, the local channel curvature). Blanckaert and Graf (2001) conducted laboratory experiments on 3D measurements of flow that were made in an outer half section of an open channel bend for a rough turbulent flow. The core of the maximum velocity was found at the separation between the center region and the outer bank region and patterns of cross sectional velocities contained two circulation cells. Olsen (2003) developed a 3D CFD model used to compute the formulation of the meandering pattern in an originally straight alluvial channel. Bed changes were calculated with comparison with results from physical models, and showed the secondary current velocity profiles. Patra (2004) described the flow and velocity distribution in meandering compound channels with overbank flow. Due to the secondary flow, a modified form of the power law equation was proposed.

Equations proposed by Baek et al. (2006) described the transverse velocity along sinuous channels with alternating bends. Equations were verified with experimental data sets obtained from laboratory results. Seo and Jung (2010) compared several theoretical velocity distribution profiles of secondary currents. Then the existing equations were compared with experimental data from measured data from a sinuous channel experiment introduced by Baek et al., and the sensitivity analysis displayed that the deviation of the transverse velocity tends to enlarge with the increase of sinuosity. Sukhodolov (2011) showed the effect of channel curvature in turbulent flow and the flow structure changes between the transition in riffles and

pools in the meandering bend. Also the vertical profile of tangential velocity was described by a logarithmic law and modified for the pool area. Riley and Rhoads (2012) took field measurements in confluent meandering rivers and compared it to numerical modeling. The patterns of flow and channel morphology were different from the normal meandering channels and the complex helical motion due to the high junction angle at the confluence was observed. Jing et al (2012) used a renormalized k-ε turbulence flow model to simulate the flow in the upper Yellow River with five meandering points. The two-dimensional flow model showed that there were deviations between the positions of the thalweg and the main streamline, and it was able to reproduce it due to adding the circulation flow term which was a source term added to the momentum equations of the model.

Zarrati, Tamai and Jin (2005) developed a depth averaged model for predicting water surface profiles for meandering channels. They applied the model to three meandering channels (two simple and one compound) data. The model was found to predict well the water surface profile and velocity distribution for simple channels and also for the main channel of compound meandering channel. Uijttewall (2014) summarized many researches on shallow water curved flows and commented that reproducing the details of flow patterns and understanding the morphodynamical consequences of flow curvature is an important research topic, and the large width to depth ratio and radius of curvature is a key factor in transverse velocity. As the radius of the curvature decreases, the secondary flow of the first kind gains influence in affecting the streamwise momentum distribution.

2.4.2 Moment of Momentum Method

The moment of momentum method uses the 2D vertically averaged moment model (VAM) which was developed for the momentum redistributions. Originally Johannesson and Parker (1989) presented an analytical model for calculating the lateral distribution of the depth-averaged flow velocity in curved rivers. This made it possible to take into account the convective acceleration of the secondary flow that would suppress the growth of the magnitude of the primary flow. This became the basis of the later models of the moment of momentum method. The equations include the incorporation of assumed distribution of vertical velocity components with quadratic vertical velocity and pressure distributions which resemble transport equations, and are shown as below

$$\frac{\partial q_x}{\partial t}+\frac{\partial}{\partial x}\left(\frac{q_x^2}{h}\right)+\frac{\partial}{\partial y}\left(\frac{q_x q_y}{h}\right)+\frac{1}{3}\left(\frac{\partial h u_1^2}{\partial x}+\frac{\partial h u_1 v_1}{\partial y}\right)+gh\frac{\partial}{\partial x}(h+z_0)+\frac{g}{2}\frac{\partial h h_1}{\partial x}+\frac{2g}{3}\frac{\partial h h_2}{\partial x}$$
$$+gh_1\frac{\partial z_b}{\partial x}-\frac{1}{\rho}\frac{\partial h\overline{\sigma}_x}{\partial x}-\frac{1}{\rho}\frac{\partial h\overline{\tau}_{xy}}{\partial y}+\frac{1}{\rho}\tau_{xzb}=0 \qquad (2.20a)$$

$$\frac{\partial q_y}{\partial t}+\frac{\partial}{\partial y}\left(\frac{q_y^2}{h}\right)+\frac{\partial}{\partial x}\left(\frac{q_y q_x}{h}\right)+\frac{1}{3}\left(\frac{\partial h v_1^2}{\partial y}+\frac{\partial h u_1 v_1}{\partial x}\right)+gh\frac{\partial}{\partial y}(h+z_b)+\frac{g}{2}\frac{\partial h h_1}{\partial y}+\frac{2g}{3}\frac{\partial h h_2}{\partial y}$$
$$+gh_1\frac{\partial z_b}{\partial y}-\frac{1}{\rho}\frac{\partial h\overline{\sigma}_y}{\partial y}-\frac{1}{\rho}\frac{\partial h\overline{\tau}_{yx}}{\partial x}+\frac{1}{\rho}\tau_{yzb}=0 \qquad (2.20b)$$

$$\frac{\partial u}{\partial t}+\frac{\partial}{\partial x}\left(\frac{q_x u}{h}\right)+\nu\frac{\partial}{\partial y}\left(\frac{q_x}{h}\right)+\frac{q_y}{h}\frac{\partial u}{\partial y}+\frac{3}{2}\left(\frac{gh_1}{3h}\frac{\partial h}{\partial x}-\frac{g}{3}\frac{\partial h_1}{\partial x}+\frac{8gh_2}{3h}\frac{\partial\overline{z}}{\partial x}-\frac{4\overline{\sigma}_x}{\rho h}\frac{\partial\overline{z}}{\partial x}\right)$$
$$+\frac{3}{2}\left(-\frac{4\overline{\tau}_{xy}}{\rho h}\frac{\partial\overline{z}}{\partial y}+\frac{4\overline{\tau}_{xz}}{\rho h}-\frac{2}{\rho h}\tau_{xzb}\right)=0 \qquad (2.21a)$$

$$\frac{\partial v}{\partial t}+\frac{\partial}{\partial y}\left(\frac{q_y v}{h}\right)+u\frac{\partial}{\partial x}\left(\frac{q_y}{h}\right)+\frac{q_y}{h}\frac{\partial v}{\partial x}+\frac{3}{2}\left(\frac{gh_1}{3h}\frac{\partial h}{\partial y}-\frac{g}{3}\frac{\partial h_1}{\partial y}+\frac{8gh_2}{3h}\frac{\partial \bar{z}}{\partial y}-\frac{4\bar{\sigma}_y}{\rho h}\frac{\partial \bar{z}}{\partial y}\right)$$
$$+\frac{3}{2}\left(-\frac{4\bar{\tau}_{yx}}{\rho h}\frac{\partial \bar{z}}{\partial x}+\frac{4\bar{\tau}_{yz}}{\rho h}-\frac{2}{\rho h}\tau_{yzb}\right)=0 \qquad (2.21b)$$

where $q_{x,}\ q_y$ is the flow discharge in the longitudinal and transverse direction respectively, $\bar{z}$ is the mean flow depth, h_1 as the hydraulic head in excess of the hydrostatic at the bed, h_2 as the mid-depth head in excess of the average of heads in the bed and surface, $\bar{\tau}_{xy},\ \bar{\tau}_{yx},\ \bar{\tau}_{xz},\ \bar{\tau}_{yz}$ is the vertically averaged total turbulent shear stress in the *y* direction on *x* surface, *x* direction on *y* surface, *z* direction on *x* surface, *z* direction on *y* surface respectively, $\bar{\sigma}_x,\ \bar{\sigma}_y$ is the total turbulent normal stress in the longitudinal and transverse direction respectively, $\tau_{xzb},\ \tau_{yzb}$ is the bed shear stress in the longitudinal and transverse direction respectively.

Then Yeh and Kennedy (1993) developed a moment model in which derivation was involving an integral differential formulation in open channels to apply the secondary flow and the curvature effects on the transverse velocity profile. The research implied that the momentum calculation is important to explain the relations between the primary and secondary flow. Quadratic transverse velocity distributions would be assumed as Fig 2.2.

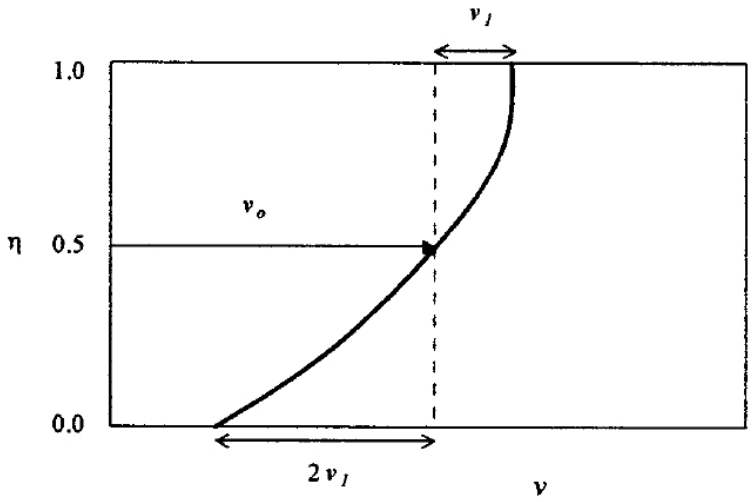

Figure 2.2 Assumed quadratic transverse velocity distribution of VAM

(Ghamry and Steffler, 2002)

Ghamry and Steffler (2002) introduced the 2D VAM model, in which the depth-averaged continuity and momentum equations are coupled with additional moment of momentum equations which were derived from the balance of the momentum flux of the convective terms, stress term, and pressure gradient term for secondary flow closure purposes. Vasquez et al. (2005) applied the 2D finite element river morphology based on the VAM equations, and they maintained their model was capable of reproducing the main effects of the flow in bends in a quasi-three dimensional way. Using the original model developed by Ghamry and Steffler, the research showed that the model could be coupled with a bed load sediment model for morphodynamic applications. Compared to the former research with linear velocity profiles, 2D research dealing with the nonlinearity of the development in secondary flow such as the moment of momentum method (Jin and Steffler, 1993, Yeh and Kennedy, 1993, Ghamry and Steffler, 2002) was conducted for better accuracy. However, since it was composed of solving several additional differential equations the computational cost was high as shown in Eq. (2.20) and Eq. (2.21).

2.4.3 Dispersion Stress Method

The dispersion stress method is the one method that can be used in order to represent free surface open flow in meandering channels in which the vertical variations of the velocity would be re-applied as they are usually neglected in the depth-averaging process. It is associated with the terms where the integration of the products of the fluctuating velocity components are directly calculated by incorporating vertical velocity profiles of both longitudinal and transverse velocities, as in Fig 2.3. The following dispersion stress term is used in many models

$$S_{ij} = \int_0^h \left(u_1'(\eta) - U_1\right)\left(u_2'(\eta) - U_2\right) d\eta \qquad (2.22)$$

where S_{ij} as the dispersion stress term using Einstein summation for *i, j* = 1, 2; u_1', u_2' is the deviation of vertical velocity from the mean in *x, y* directions respectively; U_1, U_2 is the depth averaged velocity in the *x, y* directions respectively; η as the dimensionless relative depth to the bed. By using the discrepancy between the depth-averaged and the actual velocity distribution, the neglected vertical variations are reassigned into the momentum equations. This approach is useful as it can be calculated using a vertical velocity profile without solving additional transport equations. There were several attempts in developing methods for applying the dispersion stress to the momentum flow, which appears as the Navier-Stokes momentum equations are depth averaged.

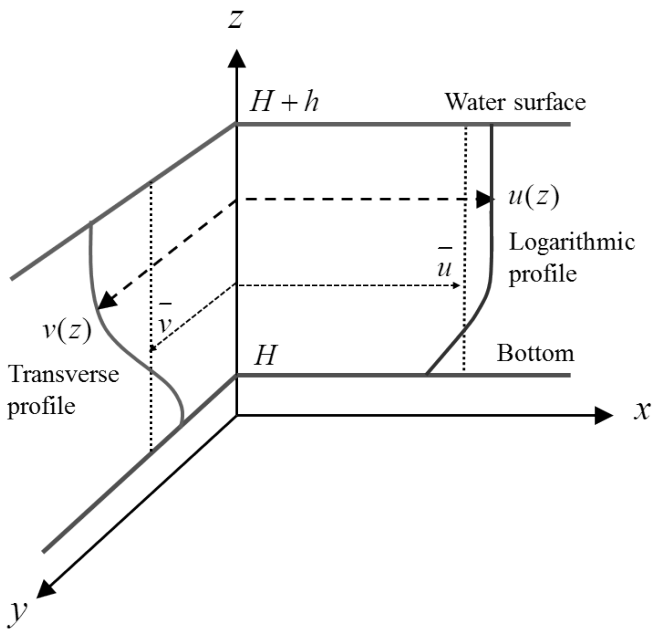

Figure 2.3 Vertical profiles of non-uniform velocity for dispersion stress

One was introduced by Bernard and Schneider (1992) where the dispersion stress terms were used as a secondary flow correction method to reproduce the secondary flow that was shown in a bendway flume experiment in the Waterways Experiment Station into a finite volume program STREMR. This consisted of a method that corrects the crosswise vorticity as the main flow direction is diverted using a dispersion term that arises from depth averaging the Navier-Stokes momentum equations.

$$\frac{\partial \Omega}{\partial t} + u\frac{\partial \Omega}{\partial x} + v\frac{\partial \Omega}{\partial y} = \frac{A_s\sqrt{C_f}\,|u|^2}{Rh\left(1+\frac{9h^2}{R^2}\right)} - D_s\sqrt{C_f}\,\Omega\frac{|u|}{h} + \frac{1}{h}\nabla\left(\nu h\nabla\Omega\right) \tag{2.23}$$

with Ω as the streamline vorticity, C_f as the friction coefficient, R as the radius of curvature, A_s as the empirical coefficient for the rate of vorticity production, D_s as the empirical coefficient for the rate of dissipation. The second and third term on the left is the vortex advection, and the first term on the right is the vorticity production, second term being the vorticity dissipation, and the third term being the vortex diffusion. The solution will then be used to calculate the streamwise stress from the deviation of velocity from the depth averaged velocity.

$$\tau_s = \rho h|\mathbf{u}|\Omega\sqrt{C_f} \tag{2.24}$$

Using the streamwise stress the equation below for the accelerations induced by secondary currents is calculated.

$$S = \left(S_x, S_y\right) \approx \rho^{-1} \frac{u}{|u|}\left[\mathbf{n} \cdot \nabla(h\tau_s) + \frac{2h\tau_s}{R}\right] \tag{2.25}$$

with $\mathbf{n}$ as the unit vector normal to the depth averaged velocity vector $\mathbf{u}$ with components (u,v). The accelerations that resulted from the non-uniformity of the velocity field $S = \left(S_x, S_y\right)$ were inserted into the shallow water equations and it was solved again with the corrections applied. This allowed to express the developing and decaying process of secondary flows as the flow passes through curved channels. Another attempt was first used by Flokstra (1977) where the dispersion stress terms where applied, later with Molls and Chaudhry (1995) with a secondary flow equation from by deVriend.

Lien (1999) also developed a 2D depth averaged model for simulating and examining flow patterns in channels bends. The experimental data from de Vriend and Rozovskii were compared for model application showing the secondary flow effect. This research showed that the dispersion stress play a major role in transverse convection of the momentum shifting from the inner bank to the outer bank. Shiono and Muto (1998) presented that when h/H (H is the main channel water depth, and h is the flood plain water depth) increased, the flow running along

the main channel were little dominant in meandering channels with straight flood plain. Jia and Wang (1999) presented the CCHE2D model, in which the introduced two dimensional and sediment transport model used a semi-empirical function of Engelund (1974) to apply the effects of the secondary flow in curved channels when calculating bed load transport.

Finnie et al. (1999) used the secondary flow correction method developed by Bernard and Schneider to apply it into a depth averaged flow model RMA2, which is a hydrodynamic finite element model developed by the US Army Corps of Engineers. A transport equation for streamwise vorticity was solved and the results were converted into additional accelerations in the momentum equation due to secondary currents. Tominaga et al (2000) showed the effects of vegetation and spur dikes in curved channels where the secondary flow was generated on the region outside the vegetation zones. The flow model applied a dispersion term to take the vertical distribution of mean velocities into account. Wilson (2001) attempted to use the TELEMAC-2D flow model to calculate for straight and meandering channels for overbank flow, but due to the model limitations it could not properly show the effects of the secondary flow in the meandering channel. Later changes to the model involved method of secondary flow corrections developed by Bernard and Schneider (1992) was applied to later versions of the flow model.

Begnudelli et al (2010) dealt with the two dimensional hydrodynamic numerical model calculating the Reynolds stress equation. It had the dispersion stress term for secondary flow consideration as the transfer of energy out of the circulating flows. The results showed that the mass dispersion using transverse velocity profiles had

more affect than momentum dispersion in velocity distributions. Kimura et al (2010) used 4 different types of models for shallow water equations. The model which considered the lag of development of secondary current behind the streamline curvature with deformations of mean vertical velocity profiles proved to be acceptable in showing the effect of flow circulation in curved channels. Song et al. (2012) found the importance of the effects of the secondary current in a confluent channel and natural stream using the de Vriend equation for the dispersion stress term. Also the research stated that the pressure gradient term of the momentum equations were the main factor that triggered the velocity redistribution. Yang et al (2014) studied the secondary flow effects in open channel confluence flow using dissipation and dispersion terms in the momentum equation. The dispersion terms would reflect the vertical non-uniformity of transverse velocity and would affect the prediction of the size of the separation zone as it was over predicted without the terms. It was observed that the influence of dispersion terms is both flow condition and location dependent in the confluent channel. Akhtar et al (2015) simulated the curvilinear stretch in a natural river using a depth averaged model with the dispersion stress term and found the effect of the tensor in flow field increases as the sinuosity in the river increased especially in channels with multiple meanders.

The aforementioned models adopted vertical profile equations for the secondary flow into the dispersion stress term in 2D flow models in order to incorporate the secondary flow effects. However, the vertical profile equations in early research based their assumptions on mild curvature, so the non-linear terms of the

momentum equation were discarded (Rozovskii, 1957, Kikkawa, 1976), or the perturbation method was applied so the equation was limited to less sharp curves (de Vriend, 1977). Therefore previous dispersion stress models incorporated with the existing secondary velocity profiles had limitations where the some models overestimated the effect of the secondary flow strength especially in the case for sharp meanders (Lien, 1999). The other dispersion stress models calculating additional vorticity term or Reynolds stress term would be expensive compared to other two dimensional models (Bernard and Schneider, 1992, Begnudelli, 2010). Others used the linear Odgaard equation for transverse flow for the dispersion stress integration into the momentum equations which could not reflect the nonlinear characteristics of the flow (Duan, 2004, Aktar, 2015).

Therefore later research on modeling flows introduced nonlinear terms using vertical profile equations. Blanckaert and de Vriend (2003, 2010), Ottavenger et al. (2013), and Wei et al. (2016) used the equation developed by de Vriend (1977) and showed that the commonly used linear closure submodels which uses the developed vertical profile equations regarding secondary currents may overestimate the strength of the curvature inducement and introduced a nonlinear submodel concerning the term $C_f^{-1}H / R_c$ as the major control parameter to include the feedback between the downstream velocity and secondary circulation. Ottavenger et al (2013) used the model to apply the nonlinearity to bed morphology in curved bends and showed the influence of the downslope gravitational force through the nonlinear effects. Wei et al. (2016) also used the developed nonlinear submodel to

find the dependence of secondary flow strength on the curvature ratio parameter in bends with continuous experiments. These models showed better application to sharp curvature flows, but the compared flow experiments were limited on single bend flows and laboratory experiments.

The previous equations for vertical profile of transverse velocity are usually based on the assumption that the radius of the curvature is large compared to the depth of the channel such as the case of Rozovkii equation. For the Kikkawa equation the derivation sequence neglects the nonlinear convective terms of the momentum equations as they become the second order of magnitude compared to the other terms which later causes overestimation in the top and bottom part of the channel. The de Vriend equation assumes that the channel depth over curvature is small enough so that the terms of the order $O(H / R_c)^2$ are neglected to yield the solution when using the perturbation method. The Odgaard equation used a linear profile which is acceptable in many natural channels. But for sharp curvatures, the secondary current size of the top and bottom of the vertical profile decreases due to the nonlinear interaction between the secondary and the main flow.

Although the moment of momentum equations had the nonlinearity of the secondary flows in meandering channels, the computational cost was high due to additional equation calculations. In this regard, a revised equation for the vertical profile of secondary currents needs to be proposed in which the non-linear term would be sustained to include the effect of sharp channels

2.5 Dispersion Coefficients

2.5.1 Theoretical and experimental approaches

For the study of contaminant dispersion and its coefficient researches, Taylor (1954) originally explained that the mixing properties of pollutant dispersion by shear flow that can be described with the dispersion coefficients, which is the combination of molecular diffusion and variation of velocity. Assuming that the dispersion coefficients are more dependent on the vertical deviations of velocity rather than molecular diffusion of particles, the 2D coefficients could be derived from the relation as the following

$$D_L = -\frac{1}{h}\int_0^h u' \int_0^z \frac{1}{\varepsilon_v}\int_0^z u'\, dzdzdz \tag{2.26a}$$

$$D_T = -\frac{1}{h}\int_0^h v' \int_0^z \frac{1}{\varepsilon_v}\int_0^z v'\, dzdzdz \tag{2.26b}$$

where u', v' is the discrepancy of velocity in the *x, y* directions respectively; ε_v is the vertical mixing coefficient; D_L, D_T are the longitudinal and transverse dispersion coefficients. Therefore, the vertical deviations of velocity can be measured in open channels to find out the spatial dispersion coefficients in the experiment channel. The dispersion coefficients derived shear velocity can serve as a efficient prediction for the actual contaminant spread since measurement of contaminant mixing by concentration curves requires a tracer experiment.

Table 2.2 Main Literature Review Classification (Dispersion)

Topic	Researcher	Details
Concept	Taylor (1954)	Introduced the mixing properties of pollutant in shear flow with dispersion coefficients
	Elder (1959)	Used the analysis and equation by Taylor to describe the diffusion of fluid and longitudinal dispersion of particles
	Fischer (1979)	Dispersion spread in theoretical equation development
Experiment and dispersion estimation	Yotsukura and Sayre (1976)	A mathematical model is presented to predict the steady two-dimensional distribution tracer test results and suggests criterion for meandering streams
	Beltaos (1980)	Shows analytical solution to 1D dispersion and introduces the dimensionless shape factor for stream-tube methods.
	Almquist and Holley (1985)	Laboratory experiment showing the secondary affects in transverse mixing
	Rutherford (1994)	Explains the predictive rates of the mixing of tracers considering river curvature, vertical and transverse mixing studies and their models are described
	Boxall et al. (2003)	Showed the vertical velocity shear induced by the channel curvature

	Seo et al (2006)	The routing procedure combined with the stream-tube concept was first introduced to reflect the irregularities in curved streams and were comparable with the stream-tube moment method, also the sinuosity to transverse dispersion relations were shown
	Jeon et al. (2007)	Created a transverse dispersion coefficient using the sinuosity of the channel
	Albers and Steffler (2007)	Affects of secondary currents have more effect in tracer cloud mixing than turbulent diffusion alone, comparison with moment method
	Marion and Zaramella (2010)	Showed that the transverse mixing was activated due to the increase of lateral velocity fluctuations on bend apexes
	Baek and Seo (2011)	Streamwise and vertical variation of the transverse velocity along a curved channel could be interpolated to find the affect of secondary flow on dispersion
	Baek and Seo (2013)	Developed a variation of the transverse dispersion coefficient equation using a dimensionless hydraulic parameter including radius of curvature
	Sharma and Ahmad (2014)	Secondary currents on channel bends accelerate the lateral mixing and adds to the transverse coefficients
	Baek and Seo (2016)	The 2D STRP using tracer tests were compared with the former equations using channel characteristics, and showed the routing procedure as an acceptable method for calculating dispersion reflecting the irregularities of the river geometry and curvature
	Seo et al. (2016)	Tracer experiments were conducted for tracer tests to find the relations of the transverse

		dispersion coefficient to the velocity over shear velocity, width over depth. The longitudinal dispersion coefficient was shown be much higher that then value suggested by Elder
Dispersion estimation using ADCP	Bogle (1997)	Originally used the cross sectional velocity distribution data to calculate the longitudinal dispersion and showed the values may lead to over-prediction in delta channels
	Carr and Rehmann (1997)	The one dimensional longitudinal dispersion coefficient K was derived from the ADCP velocities using the Fischer equation showing half of the value from the tracer studies.
	Shen et al (2010)	Used acoustic doppler current profilers to measure longitudinal velocity in order to estimate the dispersion coefficient as an alternative to the tracer test approach
	Kim (2012)	Derived longitudinal dispersion coefficient using measured vertical velocity data from ADCP in natural channels both one and two dimensional methods
	Launay et al. (2015)	Longitudinal dispersion coefficients were derived using the velocity field by ADCP and proved that the cross-sectional distribution affects more than the vertical distribution in 1D.
	Schwab and Rehmann (2015)	1D dispersion has main effect by transverse variations as known, but vertical variations of velocity to dispersion was effected by the ratio of mixing times and should be considered in certain shown conditions such as small transverse variation.
	Zhu et al. (2017)	The ADCP measurements used for longitudinal dispersion were calibrated for a 1D solution which produced quick results but was unable to predict the tail of the curves and dead zones

Later, for the two-dimensional dispersion coefficient research, several approaches both analytical, empirical were undertaken to find the transverse and longitudinal dispersion coefficients. For the analytical approach, Elder (1959) used Taylor's equation for calculating a longitudinal dispersion coefficient considering a turbulent flow down an infinitely wide inclined plane assuming the von Kármán logarithmic velocity profile for the longitudinal flow.

$$u'(y) = \frac{u^*}{\kappa}(1 + \ln y') \tag{2.27}$$

where u^* is shear velocity and κ as the von Kármán coefficient. Then for the open channel flow shear stress is given as the following.

$$\tau = \rho\varepsilon\frac{du}{dy} = \tau_0(1 - y') \tag{2.28a}$$

$$\varepsilon(y) = \frac{\tau_0}{\rho}\frac{(1-y')}{\frac{du}{dy}} = \frac{\tau_0}{\rho}\frac{(1-y')}{\frac{u^*}{\kappa}\frac{1}{y'}\frac{1}{d}} = \kappa y'(1-y')du^* \tag{2.28b}$$

Then equation 2.27 and 2.28 is inserted into equation 2.26 and double integrated for

the equation below

$$C' = \frac{\partial \overline{C}}{\partial x}\frac{d}{\kappa^2}\left(\sum_{n=1}^{\infty}\frac{1}{n^2}\left(\frac{d-y}{d}\right)^n - 0.648\right) \tag{2.29}$$

The above equation is integrated again for

$$K = \frac{0.404}{\kappa^3} du^* \tag{2.30}$$

$$K = 5.93 du^* \quad (\kappa = 0.41) \tag{2.31}$$

And the longitudinal coefficient becomes 5.93 assuming the von Kármán constant is 0.41. This equation shows a guideline for the longitudinal dispersion coefficient that is the combination of turbulent lateral diffusion and convection of the mean flow usable in large rivers, as the analysis by Taylor in circular pipes were extended to open channel flows. This value is different from the one-dimensional dispersion coefficient which is used in the one-dimensional advection-dispersion equation (1D ADE) as the following

$$\frac{\partial S}{\partial t} + V\frac{\partial S}{\partial x} = \frac{\partial}{\partial x}\left(K\frac{\partial S}{\partial x}\right) \tag{2.32}$$

where V is the cross-sectional mean velocity; S is the cross sectional mean concentration, K is the bulk longitudinal dispersion coefficient also known as the 1D dispersion coefficient. This value has both the lateral shear and vertical shear of the velocity combined into one value, so it is different from the vertical shear velocity driven two-dimensional dispersion coefficients that is the topic of this study.

For the empirical approaches, equations that could reflect the channel characteristics to find the dispersion coefficient for the channel, were developed using measured data using tracer tests. Other approaches involved using the routing method to determine the case specific dispersion coefficients by tracer tests also. The first approach conducted 2D tracer studies in natural open channels to calculate the dispersion coefficients (Yotsukura et al., 1970; Yotsukura and Sayre, 1976; Beltaos, 1980; Holley and Nerat, 1983; Seo et al., 2006; Seo et al., 2016). The tracer studies were mainly focused on to obtain the transverse dispersion coefficient, and the previous researches suggested the dimensionless value of transverse dispersion coefficients D_T / hu^* in the range of 0.15-3.00 (Rutherford, 1994). This was due to the reason that most of the field studies of tracer tests in the 1970s and 1980s were conducted with steady-state assumption and only the transverse dispersion coefficient was able to be calculated. Later experiments with transient conditions

then enabled the retrieval of both longitudinal and transverse dispersion from the data of two-dimensional concentration-time curves.

The details of each research are the following. Fischer et al. (1979) claimed that higher values for the transverse mixing coefficient are expected if the channel has the sharp curves even though values or ranges of the transverse dispersion coefficient were not exactly suggested. Based on the analysis of data collected in Missouri River by Yotsukura et al. (1970) and Sayre and Yeh (1973), the authors suggested that a gently meandering river is one which follows the condition given below:

$$\frac{\overline{U}}{U^*}\frac{W}{R_c} \le 2 \tag{2.33}$$

where $\overline{U}$ is the reach-average of the depth-averaged velocity.

Later, using the equation by Yotsukura and Sayre (1976), Almquist and Holley (1985) stated that the secondary flow affects the transverse mixing in open channels by using experimental results conducted in a laboratory meandering channel suggested the gently meandering river guideline where the secondary currents are strong enough to increase the transverse mixing as:

$$\frac{\overline{U}}{U^*}\frac{W}{R_c} \geq 1 \tag{2.34}$$

For research concerning the channel characteristics, Fischer (1969) studied the effect of channel curvature on the transverse mixing by utilizing velocity profiles of the secondary currents given by Rozovskii (1951). Using the results of circular channel laboratory tests, the researcher suggested the equation given below:

$$\frac{D_T}{HU^*} = 25\left(\frac{U}{U^*}\right)^2\left(\frac{H}{R_c}\right)^2 \tag{2.35}$$

Yotsukura and Sayre (1976) asserted that a better correlation between the transverse dispersion coefficient and channel characteristics could be obtained substituting channel width for water depth in Eq. (2.35) based on the field data sets acquired at the bend area in Missouri River. Their result was

$$\frac{D_T}{HU^*} = 0.4\left(\frac{U}{U^*}\right)^2\left(\frac{W}{R_c}\right)^2 \tag{2.36}$$

Rutherford (1994) proposed criteria ranges of the transverse dispersion coefficient as follows in straight and meandering natural channels for classification,

$$\frac{D_T}{HU^*} = (0.15 \sim 0.30) \quad \text{for straight, } (0.30 \sim 0.90) \text{for gently meandering}$$

$$= (1.00 \sim 3.00) \quad \text{for sharp curved channel} \qquad (2.37)$$

Following Fischer (1969)'s approach, Boxall and Guymer (2003) showed that the change of vertical velocity shear induced by the channel curvature is directly proportional to the variation of transverse mixing coefficient. Tracer tests were performed in a natural meandering channel for the prediction of primary and secondary flow fields and the generalized method of moments were conducted to find the tracer data mixing movement. Growth and decay terms of transverse velocity with longitudinal distance, instead of the fully developed velocity were introduced to reflect the stream-wise variations of the transverse velocity.

Later Jeon et al (2007) came up with an empirical equation using the sinuosity of the channel

$$\frac{D_T}{hu_*} = 0.029\left(\frac{\overline{u}}{u_*}\right)^{0.463}\left(\frac{W}{h}\right)^{0.299}(S_n)^{0.733} \qquad (2.38)$$

where S_n is the sinuosity which is the ratio between the thalweg length and the downward straight-line distance.

Baek and Seo (2008) and Baek and Seo (2011) also derived the theoretical equations in which they utilized velocity profiles of the secondary currents given by Kikkawa et al. (1976) and Odgaard (1986) respectively. By incorporating the stream-wise variations of the transverse velocity, their equations could represent the variation of the transverse dispersion coefficient along the curved channel. Baek and Seo (2008)'s equation read as:

$$\frac{D_T}{HU^*} = \alpha \left(\frac{U}{U^*} \right)^2 \left(\frac{H}{R_c} \right)^2 f(x) \tag{2.39}$$

where α is a dimensionless constant which depends on von Kármán constant and the shear velocity; $f(x)$ is a sine function of the stream-wise distance.

Later Baek and Seo (2013) developed a variation of the equation in which the transverse dispersion coefficient used a dimensionless hydraulic parameter regarding radius of curvature of the channel which is

$$\frac{D_T}{hu_*} = (\alpha P)^2 \left(1 - \exp\left(-\frac{\beta}{P}\right)\right)^2 \tag{2.40}$$

with α, β are the regression coefficients; P as the dimensionless hydraulic parameter that is $P = \frac{U}{U^*}\frac{H}{R_c}$

The secondary flow regarding vertical velocity deviations affecting dispersion and transverse mixing were examined by the following studies. Albers and Steffler (2007) stated that the effects of secondary currents had more effect in tracer cloud mixing than turbulent diffusion acting alone by using vertically averaged and moment equation method; Marion and Zaramella (2010) concluded that the transverse mixing was activated due to the increase of lateral velocity fluctuations on bend apex; Sharma and Ahmad (2014) published that the secondary currents on channel bends accelerates the lateral mixing and positively affects to the transverse dispersion coefficients. These former studies show that the channel curvature have effect on the secondary flow which then influences the transverse mixing.

Baek and Seo (2011) developed a theoretical equation to explain the streamwise variation for the transverse velocity. The variation equation and the former equation by Odgaard were combined to an equation of transverse velocity, then was inserted into the equation by Fischer for integration into transverse dispersion coefficient in

curved channels. The Odgaard equation can be changed as a function of longitudinal s and vertical coordinates z as

$$v(s,z)=\left(2\frac{z}{h}-1\right)\left[\frac{A_1}{A_2}\{1-\exp(-A_2 s)\}+v_s^i\exp(-A_{2s})\right] \tag{2.41}$$

Then using Eq. (2.41) and inserting it into the Fischer equation for the triple integration results in the normalized transverse dispersion coefficient as

$$\frac{D_T}{hu_*}=\frac{1}{6\kappa}\left(\frac{v_s}{u_*}\right)^2 \tag{2.42}$$

The surface velocity derived before then can be used to include the longitudinal variation of the transverse dispersion coefficient as Eq. (2.41) is imbedded in Eq. (2.43) resulting in the equation below. This can describe the secondary flow affecting the periodic characteristics of the escalation and diminishment of the transverse dispersion in bend alternation in open channels.

$$\frac{D_T}{hu_*} = \frac{\left[\frac{A_1}{A_2}\{1-\exp(-A_2 s)\} + v_s^i \exp(-A_{2s})\right]^2}{6\kappa u_*^2} \tag{2.43}$$

2.5.2 Velocity driven dispersion coefficient researches

Following the theoretical equation by Fischer and the shear flow dispersion approach, The previous studies considering the use of ADCP velocity were mainly focused on the one-dimensional longitudinal dispersion assuming the contaminants have gone through full lateral mixing in the far field. (Bogle, 1997; Carr and Rehmann, 2007), so it used the depth-averaged longitudinal velocities.

Shen et al (2010) used the acoustic doppler current profilers to measure longitudinal velocity in order to estimate the dispersion coefficient as an alternative to the tracer test approach. The dead zones in the river could be reproduced better than the advection dispersion equation approach due to the lack of terms to describe the storage. A similar research was done by Kim (2012) as the paper also calculated the longitudinal dispersion coefficient from the ADCP measurements. Other researches by Launay et al., (2015), Zhu et al., (2017) were also based on the depth-averaged velocity of longitudinal flow and its shear dispersion due to the longitudinal flow distribution and was applied in the far-field mixing section shown in Figure 1.2

Later, Lee and Seo (2013) used the data from laboratory flume experiments on a meandering channel to use the vertical velocity components to predict the

longitudinal and transverse dispersion coefficients. It presented the results in a spatial two dimensional form and the results were transformed into a Cartesian form. The results showed that the relation between the maximum velocities at the thalweg was different with the maximum point of dispersion coefficients. This is due to the reason the constructed meander channel was in a rectangular shape, so the maximum velocity point was located at the inner side of the bank, while the maximum point of the dispersion coefficients were placed near the outer side of the bank.

These former researches on secondary flow effect on dispersion coefficients do not have measured velocity vertical data in natural channels used for two dimensional dispersion coefficient estimation. Elder (1959)'s equation showed the preliminary approach similar to this research but was limited to analytical advancement assuming a wide plane. The research by Shen et al (2010) and Kim (2012) was used ADCP measured data for vertical profile acquisition for dispersion coefficient calculations, but it was limited to longitudinal coefficients and two dimensions and one dimensional dispersion derivation of K. This paper will use the developed equation and the results of the measured vertical velocity profiles for the two dimension dispersion coefficient estimation to be compared to observed results and input for numerical advection dispersion models. Usually in large rivers, the depth-averaged longitudinal flow distribution played an important role in producing the longitudinal dispersion, since when contaminants had undergone full lateral mixing, the dispersion was driven by the transverse shear mostly (Schwab and

Rehmann, 2015). Exceptions were the cases of certain conditions in which the depth-averaged transverse distribution shear was minimal and only the vertical components were large enough.

But in this research, we focused on the intermediate field mixing where vertical shear can dominate, so the calculation of 2D dispersion coefficients was needed, therefore the measured vertical profile of the flow was utilized for calculation of both longitudinal and transverse dispersion coefficients.

2.5.3 STRP method

In this study, the two-dimensional stream-tube routing procedure (2D STRP) was used to calculate the transverse dispersion coefficient based on the dosage profiles, which were converted from the two-dimensional concentration-time curves obtained in the tracer tests. The stream-tube method was also used as a fixed value of discharge is attached to a fixed streamline, by moving the coordinate system back and forth across the cross-section along with the flow; thus, it can efficiently deal with the lateral migration of the water flow in irregular curved rivers and the tracer cloud in meandering rivers. (Seo et al., 2016)

First, the steady-state equation can be obtained by integrating the 2D advection-dispersion Eq. (2.43) with respect to time as (Beltaos, 1975, Seo et al., 2016):

$$\frac{\partial C}{\partial t}+u\frac{\partial C}{\partial x}+v\frac{\partial C}{\partial y}=\frac{1}{h}\frac{\partial}{\partial x}\left(hD_L\frac{\partial C}{\partial x}\right)+\frac{1}{h}\frac{\partial}{\partial y}\left(hD_T\frac{\partial C}{\partial y}\right) \tag{2.44}$$

$$u\frac{\partial \theta}{\partial x}+v\frac{\partial \theta}{\partial y}=\frac{1}{h}\frac{\partial}{\partial x}\left(hD_L\frac{\partial \theta}{\partial x}\right)+\frac{1}{h}\frac{\partial}{\partial y}\left(hD_T\frac{\partial \theta}{\partial y}\right) \tag{2.45}$$

where θ is dosage of tracer which is defined as:

$$\theta(x,y)=\int_0^\infty C(x,y,t)dt \tag{2.46}$$

For the steady-state concentration condition the longitudinal dispersion can be negligible, and if the transverse velocity is also negligibly small, then Eq. (2.45) can be simplified as:

$$u\frac{\partial \theta}{\partial x}=D_T\frac{\partial^2 \theta}{\partial y^2} \tag{2.47}$$

Applying the stream-tube concept originally suggested by Yotsukura and Cobb (1972) into Eq. (2.46), and normalizing yields

$$\frac{\partial S}{\partial x}=B_C\frac{\partial^2 S}{\partial \eta^2} \tag{2.48}$$

and B_c is the bulk dispersion coefficient, given by:

$$B_C = \frac{\psi H^2 U}{Q^2} D_T \tag{2.49}$$

where Ψ is the normalized shape factor found to have a range of 1.0~3.6 (Sayre, 1979; Beltaos, 1980).

The analytical solution to Eq. (2.48) for a vertical line source being instantaneously injected at x = 0, η = ω can be obtained as:

$$S(x,\eta) = \frac{\Theta}{\sqrt{4\pi B_C x}} \exp\left(-\frac{(\eta-\omega)^2}{4B_C x} \right) \tag{2.50}$$

Then, following the similar approach of the 1D routing procedure by Fischer (1968), the routing equation can be derived by substituting the measured concentration profile for Θ in Eq. (2.51) as follows (Seo et al., 2006):

$$S(x_2,\eta) = \int_0^1 \frac{S(x_1,\omega)}{\sqrt{4\pi B_C (x_2 - x_1)}} \exp\left(-\frac{(\eta-\omega)^2}{4B_C (x_2 - x_1)} \right) d\omega \tag{2.51}$$

where $S(x_2,\eta)$ is the predicted dosage profile as a function of the normalized cumulative discharge, η at downstream section, x_2 ; $S(x_1,\eta)$ the measured

dosage profile as a function of η at upstream section, x_1; ω the normalized dummy variable of integration. This results in the 1D-STRP, and to calculate D_T from Eq. (2.51), the dosage profile at a downstream section is calculated using the measured profile at an upstream section as the input data, after an initial guess value of D_T is chosen. Then, the calculated profile is matched with the measured profile and repeated until optimal value of D_T is found.

For the 2D-STRP to calculate the both the longitudinal and transverse dispersion coefficients, the observed concentration-time curves (Baek and Seo, 2010) are used similar to the 1D-STRP. The stream-tube model equation for transient condition can be derived applying the stream-tube concept to Eq. (2.43) without any conversion of the concentration into the dosage, and the result is

$$\frac{\partial C}{\partial t} = D_L \frac{\partial^2 C}{\partial x^2} + S_T \frac{\partial^2 C}{\partial \eta^2} \tag{2.52}$$

where $S_T = UB_C$. The input is assumed to be a distributed series of separate slugs, and the initial condition is given as $C(x,\eta,0) = f(x,\eta)$. Then, the analytical solution of Eq. (2.52) can be derived by superposition integral (Seo et al, 2016) as:

$$C(x,\eta,t) = \int_0^1 \int_{-\infty}^{\infty} \frac{f(\zeta,\omega)}{4\pi t\sqrt{D_L S_T}} \exp\left(-\frac{(x-\zeta)^2}{4D_L t}\right) \exp\left(-\frac{(\eta-\omega)^2}{4S_T t}\right) d\zeta\, d\omega \tag{2.53}$$

where ζ the dummy variable of integration. The routing equation for the spatial concentration profile at time t_2 can be derived by substituting the measured concentration profile at time t_1 for $f(\zeta,\omega)$ in Eq. (2.53).

$$C(x,\eta,t_2)=\int_0^1\int_{-\infty}^{\infty}\frac{C(\zeta,\omega,t_1)}{4\pi(t_2-t_1)\sqrt{D_L S_T}}\exp\left(-\frac{(x-\zeta)^2}{4D_L(t_2-t_1)}\right)\exp\left(-\frac{(\eta-\omega)^2}{4S_T(t_2-t_1)}\right)d\zeta\,d\omega \tag{2.54}$$

where $C(x,\eta,t_2)=$ spatial profile of predicted concentration at t_2 ; and $C(x,\omega,t_1)=$ spatial profile of measured concentration at t_1 (Seo et al, 2016). Employing the frozen-cloud approximation (Fischer, 1968), Eq. (2.54) can be converted into the routing equation for the temporal concentration profile as:

$$C\left(x_2,\eta,t\right)=\int_0^1\frac{\left[\int_{-\infty}^{\infty}\frac{C\left(x_1,\omega,\tau\right)U}{\sqrt{4\pi D_L\left(\overline{t_2}-\overline{t_1}\right)}}\exp\left(-\frac{U^2\left(\overline{t_2}-\overline{t_1}-t+\tau\right)^2}{4D_L\left(\overline{t_2}-\overline{t_1}\right)}\right)d\tau\right]}{\sqrt{4\pi B_C\left(x_2-x_1\right)}}\exp\left(-\frac{\left(\eta-\omega\right)^2}{4B_C\left(x_2-x_1\right)}\right)d\omega \tag{2.55}$$

where $C(x_2,\eta,t)$ is the temporal profile of the predicted concentration at the downstream section, x_2 ; $C\left(x_1,\omega,\tau\right)$ is the temporal profile of measured concentration at the upstream section, x_1 ; τ is the dummy time variable of

integration; and $\overline{t_1}$ and $\overline{t_2}$ are the mean times of passage in sections x_1 and x_2, respectively (Seo et al, 2016).

The actual calculation of the longitudinal and transverse dispersion coefficients by Eq. (2.55) is similar to the 1D-STRP, Eq. (2.51), except there are two unknown variables in the 2D STRP. Therefore the former method of initial guess for optimal values of D_T are not possible; therefore multiple regression techniques should be used to fit the predicted concentration to the measured concentration because two parameters are determined simultaneously through only one equation. The routing occurs with the concentration time curves at successive transverse points of the cumulative discharge, having η from the upstream section to the downstream section (Seo, 2016).

Therefore, the 2D STRP is the 1D routing equation for the longitudinal dispersion coefficient connected with the 1D-STRP equation for the transverse dispersion. Since it uses the stream-tube concept, irregularities of the channel can be reflected, and the pattern of the stream-wise variation of the dispersion coefficients can be revealed because they are calculated at each section the along river. This method and the velocity driven dispersion coefficient method will be compared in Chapter 7.

Chapter 3. Model Development

3.1 2D Shallow Water Model

3.1.1 Governing Equations

In this research using the equation for the secondary flow, the equation will be inserted into a dispersion stress form to the 2D finite element solver HDM-2D, a depth-averaged numerical model. As the model was developed for use in scaled down river laboratory channels and natural rivers, most cases have the depth of the channel assumed to be smaller than the width which lets the user to use a depth-averaged solver. The HDM-2D used in this research uses the depth averaged momentum equations as below (Song et al., 2012).

$$\frac{\partial u_i}{\partial t} + u_j \frac{\partial u_i}{\partial x_j} = -g\frac{\partial Z}{\partial x_i} - g\frac{\partial H}{\partial x_i} + \nu_T \frac{\partial^2 u_i}{\partial x_j \partial x_j} - gn^2 \frac{u_i \sqrt{u_j u_j}}{h^{4/3}} - \frac{\partial S_{ij}}{\partial x_j} \tag{3.1}$$

The equation is in a tenser form where t is time, u_1, u_2 is velocity in x, y directions respectively, Z as the bottom elevation, ν_T as the eddy viscosity coefficient, n as the Manning coefficient, S_{ij} as the dispersion stress term.

The HDM-2D model is a unsteady two-dimensional depth averaged flow model by Petrov-Galerkin stabilization approach. Originally, the shallow water equations can be written in either conservative or non-conservative form.

The conservative form is useful for situations where the conservative finite element scheme is needed so the conservation of mass and momentum can be guaranteed in the numerical solution. The non-conservative form can be used for the simpler form of the viscous terms and a numerical approximation in which the upwinding procedure is straight forward concerning the velocity direction (Song et al., 2012). In differential non-conservative form, the set of variables $u_i(x,y,t)$ and $h(x,y,t)$ is a solution of the following equations:

$$\frac{\partial h}{\partial t} + h\frac{\partial u_j}{\partial x_j} + u_j\frac{\partial h}{\partial x_j} = 0 \tag{3.2}$$

$$\frac{\partial u_i}{\partial t} + u_j\frac{\partial u_i}{\partial x_j} = -g\frac{\partial (H+h)}{\partial x_i} + \frac{\partial}{\partial x_j}\left(\nu_T\frac{\partial u_i}{\partial x_j}\right) - gn^2\frac{u_i\sqrt{u_j u_j}}{h^{4/3}} \tag{3.3}$$

where t is time; u_1, u_2 are the vertically averaged velocity components corresponding to x, y directions, respectively; g is acceleration of gravity; H bottom elevation and h flow depth, and n is Manning's roughness coefficient.

3.1.2 Dispersion stress method

For the dispersion stress method that was originally applied to the HDM-2D flow model, the vertical distribution of transverse velocity proposed by de Vriend (1977) was employed to include the effect of secondary flow in the mathematical and numerical models. de Vriend (1977) proposed a mathematical model for the shallow meandering channel by using the perturbation method to derive the lateral velocity distributions over the depth. The velocity distributions over the depth in the Cartesian coordinates proposed by de Vriend (1977) are expressed by

$$u_1(\zeta) = u_1 f_m(\zeta) - hU_1 f_s(\zeta) \tag{3.6a}$$

$$u_2(\zeta) = u_2 f_m(\zeta) - hU_2 f_s(\zeta) \tag{3.6b}$$

where u_1 is the depth-averaged velocity in x-direction; u_2 is the depth-averaged velocity in y-direction; $u_1(\zeta)$ is the vertical distribution of x-component velocity; $u_2(\zeta)$ is the vertical distribution of y-component velocity; $\zeta = (z-H)/h$ is dimensionless distance from the bed; and U_1 and U_2 are represented by

$$U_1 = \frac{\delta}{2\kappa \|\mathbf{u}\|^3}\left[\left(\|\mathbf{u}\|^2 + u_2^2\right)\left(u_1\frac{\partial u_1}{\partial x} + u_2\frac{\partial u_1}{\partial y}\right) - u_1u_2\left(u_1\frac{\partial u_2}{\partial x} + u_2\frac{\partial u_2}{\partial y}\right)\right] \tag{3.7a}$$

$$U_2 = \frac{\delta}{2\kappa\|\mathbf{u}\|^3}\left[\left(\|\mathbf{u}\|^2 + u_1^2\right)\left(u_1\frac{\partial u_2}{\partial x} + u_2\frac{\partial u_2}{\partial y}\right) - u_1u_2\left(u_1\frac{\partial u_1}{\partial x} + u_2\frac{\partial u_1}{\partial y}\right)\right] \quad (3.7b)$$

where $\|\mathbf{u}\|$ is the Euclidian norm of velocity, δ is the ratio of the characteristic depth to radius of curvature. The main flow function, $f_m(\zeta)$ and the secondary flow function, $f_s(\zeta)$ are defined by the equations (2.12-2.15). The vertical velocity profiles are assumed to have a synthesis of the distribution of the secondary flow with the Chézy coefficient and the von Kármán constant and the logarithmic distribution of main flow. Two components of the secondary flow in curved channels where one is perpendicular to the main flow direction and the other one in the direction of the main flow are considered in the velocity profiles (Song et al., 2012) This becomes the main factor to shift the streamwise momentum from the inner region of a bend toward the outer region and to increase the main velocity near the outer bank with the consideration of transverse secondary flow.

For the dispersion stress term in the original HDM-2D, the first term S_{11} indicates the integration of the products of the discrepancy between the mean and the vertically varying velocity distribution in the *x* direction (Song et al, 2012). In the original model for the application of the dispersion stress with the differentiation of the transverse velocity, the term used by de Vriend was first applied

$$F_s(\eta) = 2F_1(\eta) + \frac{\sqrt{g}}{\kappa C} F_2(\eta) - 2\left(1 - \frac{\sqrt{g}}{\kappa C}\right) f_m(\eta) \tag{3.8}$$

$$S_{11} = \frac{1}{h}\int_H^{H+h} (u_1(z) - U_1)^2 = U_1^2 \left(\frac{\sqrt{g}}{\kappa C}\right)^2 - 2hU_1V_1 \frac{\sqrt{g}}{\kappa C} FF_1 + h^2 V_1^2 FF_2 \tag{3.9}$$

$$FF_1 = \int_0^1 (1 + \ln\eta) F_s(\eta) d\eta \qquad FF_2 = \int_0^1 F_s^2(\eta) d\eta \tag{3.10}$$

The second term S_{12} and the third term S_{21} show the integration of the products of the discrepancy in the x- and y- directions. The fourth term S_{22} shows the integration of the products of the discrepancy y-direction.

$$\begin{aligned} S_{12} = S_{21} &= \int_0^1 (u_1(\eta) - U_1)(u_2(\eta) - U_2) d\eta \\ &= U_1 U_2 \left(\frac{\sqrt{g}}{\kappa C}\right)^2 - h(U_1V_1 + U_2V_2)\frac{\sqrt{g}}{\kappa C} FF_1 + h^2 V_1 V_2 FF_2 \end{aligned} \tag{3.11}$$

$$S_{22} = \int_0^1 (u_2(\eta) - U_2)^2 d\eta = U_2^2 \left(\frac{\sqrt{g}}{\kappa C}\right)^2 - 2hU_2V_2)\frac{\sqrt{g}}{\kappa C} FF_1 + h^2{}_1 V_2 FF_2 \tag{3.12}$$

These terms allow the momentum equation to reproduce the secondary flow characteristics from the vertical variance omitted depth-averaged equations. This method has some similarities to the quasi-3D models, as the treat the water body with sets of horizontal layers to show the diversified vertical variance without calculating the actual momentum equation in the vertical direction.

3.2 2D Advection Dispersion Model

For the modeling of dispersion in rivers for two dimensional problems, the advection dispersion equation solved with numerical methods can be used. The numerical results may show nonphysical oscillation for smearing since the advective transport is prevalent compared to dispersive transport. Recent studies introduced methods of finite element algorithms to reduce the problems of typical Eulerian methods.

This research uses the developed CTM-2D model developed in Seoul National University which is an advection dispersion numerical finite element model. (Seo et al, 2008). This model utilizes the velocity magnitude results from the flow model HDM-2D to be used in solving pollutant transport problems. The SUPG method was used for the spatial and temporal discretization. A heterogeneous dispersion coefficient tensor for meandering streams was adopted to accurately represent the distinction of natural channels. The generalized equation for the depth averaged advection dispersion used in the model is as below.

$$\frac{\partial(h\overline{C})}{\partial t}+\frac{\partial\left(\overline{u}h\overline{C}\right)}{\partial x}+\frac{\partial\left(\overline{v}h\overline{C}\right)}{\partial y}=\frac{\partial}{\partial x}\left[h\left(D_{xx}\frac{\partial\overline{C}}{\partial x}+D_{xy}\frac{\partial\overline{C}}{\partial y}\right)\right]+\frac{\partial}{\partial y}\left[h\left(D_{yx}\frac{\partial\overline{C}}{\partial x}+D_{yy}\frac{\partial\overline{C}}{\partial y}\right)\right]$$
$$+Q+kh\overline{C} \tag{3.8}$$

where $\overline{C}$ is the depth averaged concentration; $D_{xx}, D_{xy}, D_{yx}, D_{yy}$ is the dispersion coefficient; and h is the water depth, u is the depth averaged velocity from the flow solver HDM-2D results. Q is the function for source term, k as the decay ($k < 0$) coefficient for reactive contaminant materials. The dispersion coefficient tensor derived by Alavian (1986) was used for the numerical calculation.

$$D_{xx} = D_L \frac{\overline{u}^2}{U^2} + D_T \frac{\overline{v}^2}{U^2} \tag{3.9a}$$

$$D_{xy} = D_{yx} = (D_L - D_T) \frac{\overline{u}\,\overline{v}}{U^2} \tag{3.9b}$$

$$D_{yy} = D_T \frac{\overline{u}^2}{U^2} + D_L \frac{\overline{v}^2}{U^2} \tag{3.9c}$$

where D_L, D_T is the longitudinal and transverse coefficient by coordinate transformation from Cartesian to natural coordinates. This allows the seamless conversion of Fischer equation to Alavian equation. The model was used for simulating pollutant transport simulations assuming accidents in the Han River, and the showed its applicability by analysis of effect to water intake facilities since the model was two dimensional and the pollutant spread could be represented more accurately than one dimensional models.

Chapter 4. Field Experiments

4.1 Field Site

To find the effects of the secondary current in meandering channels, a large scale channel experiment was conducted at the Andong River Experiment Center (REC) of Korea Institute of Civil Engineering and Building Technology (KICT) in which a real-scale size meandering channel was installed in order to simulate open channel flows in a controlled outdoor environment. The center is positioned near Andong city in the Nakdong basin which located at the southeastern part of the Korean Peninsula. The meandering flume is about 11 meters wide and 600 meters long with three different sinuosity shown in Figure 4.1. The channels were classified as A312, A315, A317, which is related to their sinuosities of 1.2, 1.5, and 1.7 respectively, where 1.5 and 1.7 sinuosities are considered to be sharper than most natural rivers. The full discharge capability of the REC is 10.0 m^3/s using large pumping facilities which draws its water supply from the Nakdong River. This makes it possible to conduct various river experiments almost free from scale effects. The experiments were conducted for the creation of a vertical profile equation of the secondary current and comparison of the flow with the simulated results from the developed model. The description of the 5 experiments conducted in 2016 was listed in Table 4.1. One measured experiment was conducted for the A312 channel, and two experiments for the A315 and A317 channel.

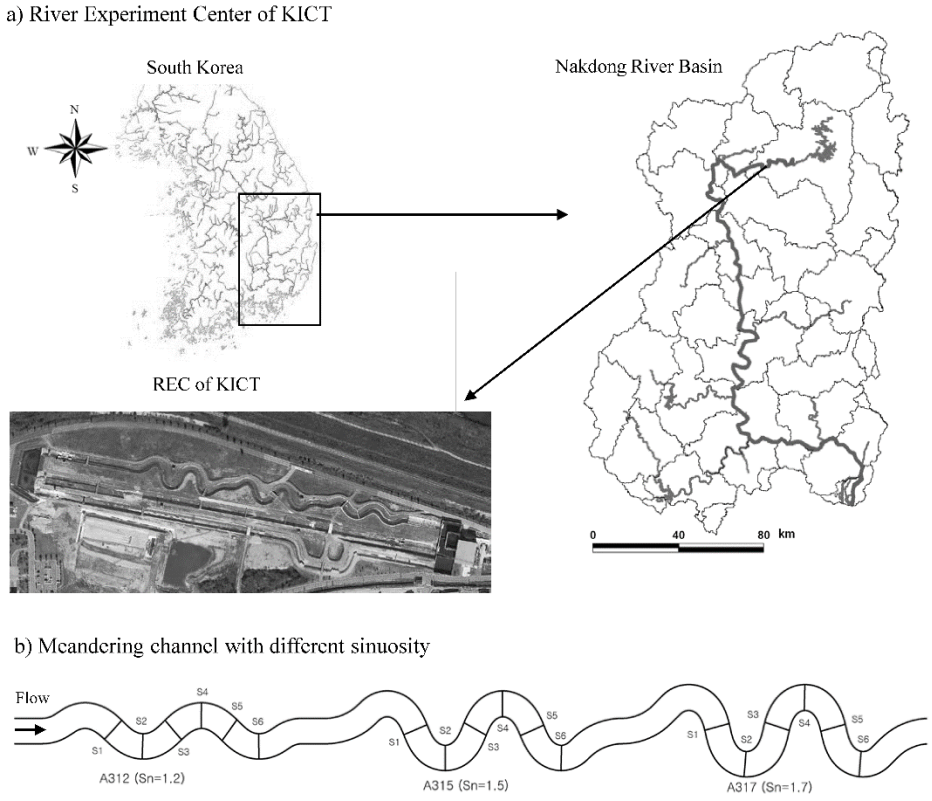

Figure 4.1 Field Site of Experiment

Table 4.1. Summary of hydraulic data measured in the meandering channels

Case	Flume (Sinuosity)	Experiment date	Discharge	Depth	R_c
R312-1	A312 (Sn = 1.2)	Mar 31, 2016	1.61	0.49	15.52
R315-1	A315 (Sn = 1.5)	April, 25, 2016	1.01	0.42	12.88
R315-2	A315 (Sn = 1.5)	Sept 8, 2016	1.45	0.48	12.88
R317-1	A317 (Sn = 1.7)	April, 26, 2016	0.82	0.46	12.04
R317-2	A317 (Sn = 1.7)	Sept 9, 2016	1.26	0.52	12.04

4.2 Experimental Set-up

The flow velocity measurements were conducted with an Acoustic Doppler Current Profiler (ADCP) and Acoustic Doppler Velocimetry (ADV). The ADCP is the Acoustic Doppler current profiler which is a hydroacoustic current meter similar to a sonar, capable of measuring water current velocities over a depth range using the Doppler effect of sound waves scattered back from particles within the water column. The experimental equipment used in this study was the SONTEK S5, a multi-band acoustic frequency capable product with profiling ranges up to 0.06 to 5 m depth and velocity up to 20 m/s shown in Fig. 4.2a). The accuracy of the equipment is known to be ± 0.2 cm/s, and with a transducer configuration of five transducers with a 4 beam 3.0 MHz and a 1.0 MHz vertical beam echosounder (Sontek, 2015). The equipment does not measure point by point, but simultaneously receives profiles along an entire water column, which enables to do river section measurements mush faster than point by point measurements.

The ADV is the Acoustic Doppler Velocimeter known as Flowtracker 2 by Sontek which was designed to record instantaneous velocity components at a single point with a relatively high frequency shown in Fig. 4.2b). The measurements were performed by measuring velocity of particles in a remote sampling volume based on the Doppler shift effect. The ADV is usually operated so the user averages a single point of a river section about to 40 seconds, while the ADCP is operated on a boat for maneuvering the river for the data across the section.

a) Sontek S5 ADCP

b) Flowtracker 2 ADV

Figure 4.2 Measurement equipment used for the experiment

4.3 Data Collection

The ADCP operation with the moving boat was done with two people to pull the boat connected to a tether line, as the channel width during the experiment was about 5-6 meters shown in Figure 4.3a). To find the appropriate number for measuring transects, the R315-1 experiment was measured up to 10 times as in Figure 4.4, and 6 times per transect was selected as the appropriate number. So the ADCP boat was operated 6 times per each section, so the measurements were taken 3 times per direction, which is larger that the recommended value of over 4 times per section by USGS standards (Mueller et al., 2009).

The ADV was measured with a width of 1 meter using the one point method for depth averaging calculation as in Figure 4.3b) to find if the ADCP values were correct. The measuring time for averaging each point was 40 seconds, which was based on the USGS standards (Turnipseed and Sauer, 2010).

The ADCP was attached to a mount on the port side of the bow of a 2.5 m long, Styrofoam - hull boat. The four transducers of the ADCP were positioned m below the water surface depending on flow conditions during each survey date. The ADCP cannot measure velocities within a blanking distance of about 0.05 m below the transducers. Also, the bottom 10% of the measured flow depth was removed to correct for acoustic side-lobe interference and near the surface. The sampling interval of the ADCP ranged between 1.3-1.7 s and vertical bin sizes were either 0.1 m or 0.25 m within each ensemble.

a) Topography survey

b) DEM from survey results

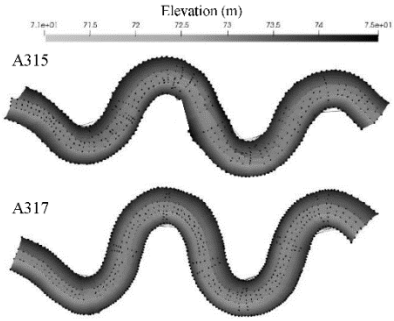

c) ADCP measurements by boat

d) A3-E21 measurement results

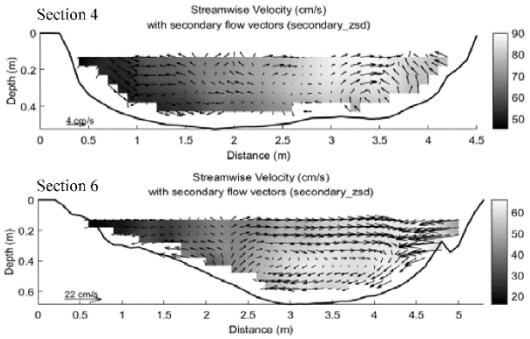

Figure 4.3 KICT REC Experiment Measurements

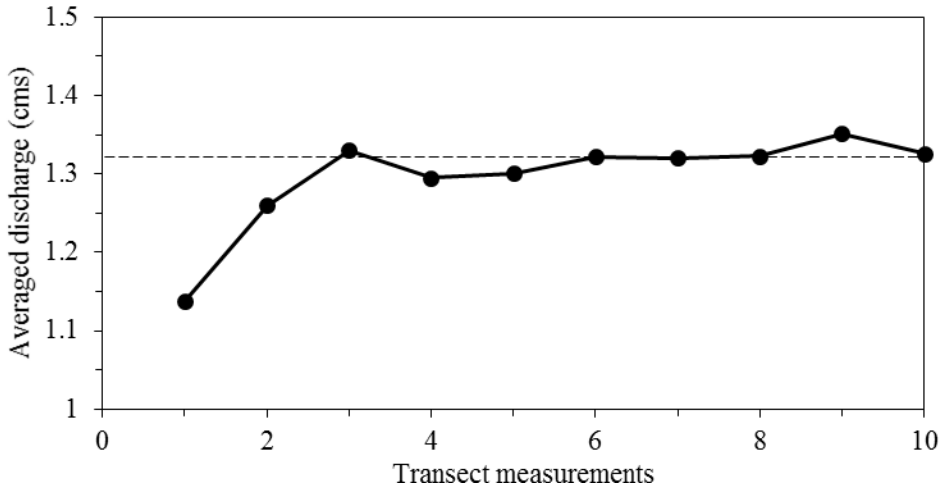

Fig 4.4 Averaged discharge for ADCP per measurements

Three-dimensional velocity and bathymetry data were obtained at several cross sections distributed throughout each meander. Cross sections were placed with tag lines in a distance of 30 – 50 m each. The flow characteristics were measured at the sections of the channels to find out the characteristics of the secondary flow structure. Cross sections were generally positioned with 6 sections per channel with half at the apex of the curvature, and half at the center of the straight part of the channel as in Fig. 4.5 and Fig. 4.6 for the A315 and A317 channel. Cross sections at both sites were oriented orthogonally to the direction of the local channel centerline. Simultaneous measurements of downstream, cross-stream, and vertical velocities and bottom depth were obtained with the ADCP by moving-boat deployment.

Boat position and velocity were determined using a differential global positioning system (DGPS) receiver for satellite differential receivers. The DGPS-receiver provides time-stamped geographic coordinates at 10 Hz with up to sub-meter accuracy and was integrated with the ADCP to georeference velocity data at each ensemble. Real-time GPS data were also used to navigate the boat as accurately as possible along the predetermined cross sections. Multiple traverses, or transects, of each cross section were surveyed to obtain spatially and temporally averaged values of velocity and to resolve details of secondary-flow patterns, while minimizing disturbances arising from turbulent velocity fluctuations and boat motion. This enables accurate averaging of several measurements when conducting continuous acquisition of data as each boat movement cannot go through an exact path as the experiment is conducted on a natural scale.

Figure 4.5 KICT REC Top view on sinuosity 1.5

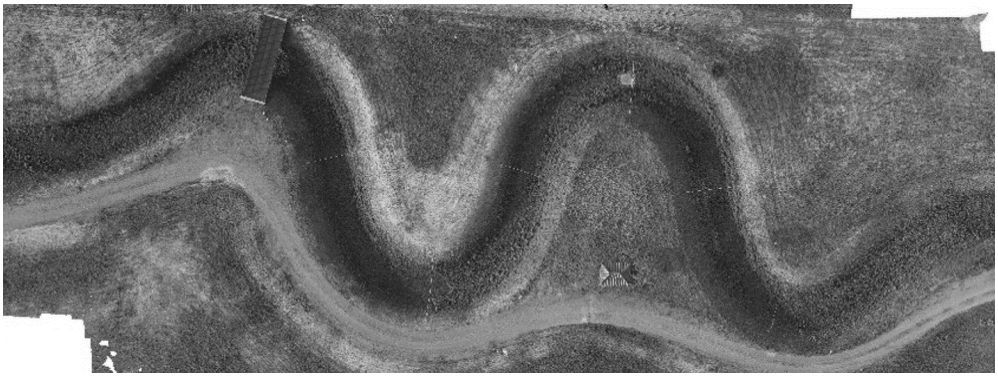

Figure 4.6 KICT REC Top view on sinuosity 1.7

4.4 Analysis for Velocity Data

The Velocity Mapping Toolbox (VMT), an ADCP post-processing software package based on a MATLAB based toolbox (Parsons et al., 2013), was used to compute spatially and temporally averaged velocity data for each cross section from repeat sectional measurements of 3D velocities. The program is capable of processing, analyzing and displaying cross sectional velocity data collected along multiple ADCP transects and was used to average the repeating moving boat measurements. The velocity contours of the temporally-averaged longitudinal velocity at bend and straight sections of the A312, A315, and A317 are shown in Fig. 4.7, 4.8, 4.9 respectively. The section locations follow the Fig. 4.1(b)

The measured data can be interpolated to grid nodes using a least-squares regression line fit through transects at each cross section with the velocity ensembles and GPS coordinates. The measured velocity components were used to derive the depth-averaged vector plots of downstream and cross-stream velocities for the individual cross sections. To identify the secondary flow structure formation within complex meandering flows at the channel, the program also rotates velocity vectors for each line in an ensemble to the direction of the depth-averaged velocity vector. Secondary flow is then defined by velocity components perpendicular to this rotation. Previous studies of river hydrodynamics have used this rotation method to detect helical motion in strongly converging flows (Rozovskii, 1957, Rhoads and Kenworthy, 1998; Lane et al., 2000).

a) Section 1

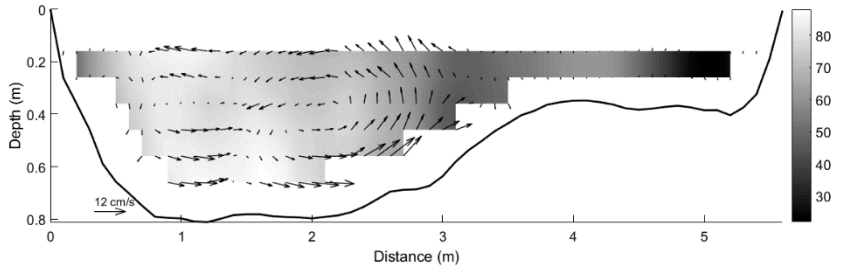

b) Section 2

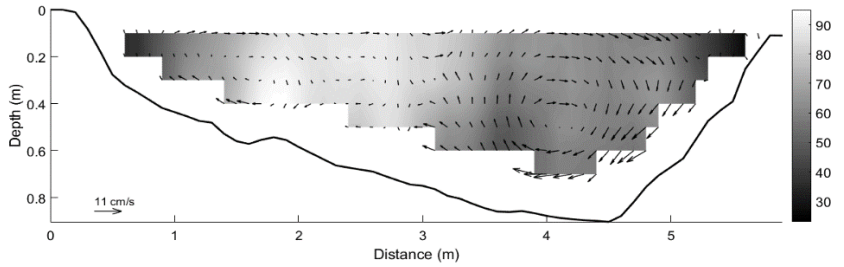

c) Section 3

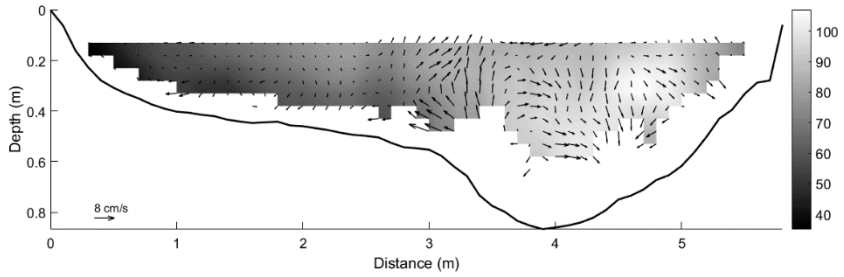

Figure 4.7 Secondary flow measurement for Case R312-1

d) Section 4

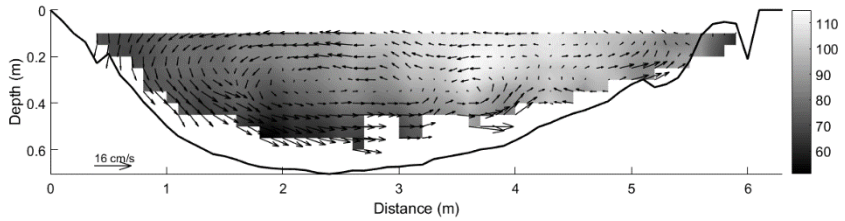

e) Section 5

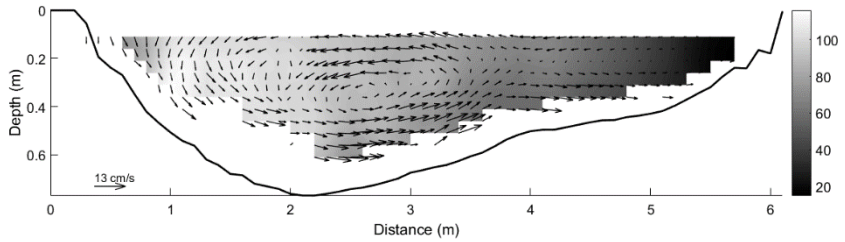

f) Section 6

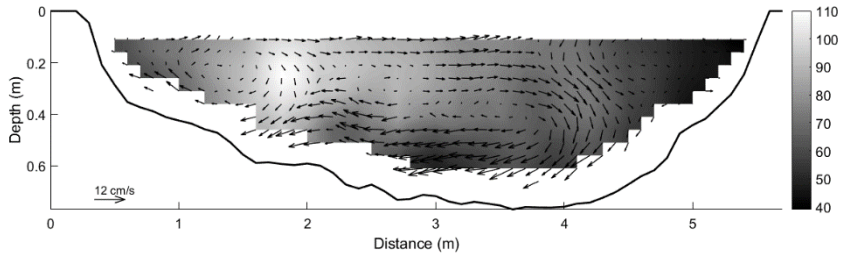

Figure 4.7 Secondary flow measurement for Case R312-1 (cont)

a) Section 1

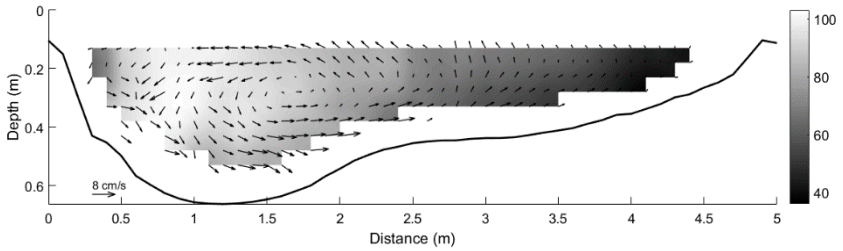

b) Section 2

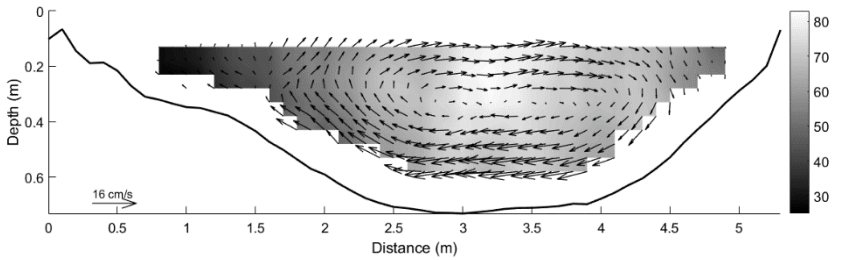

c) Section 3

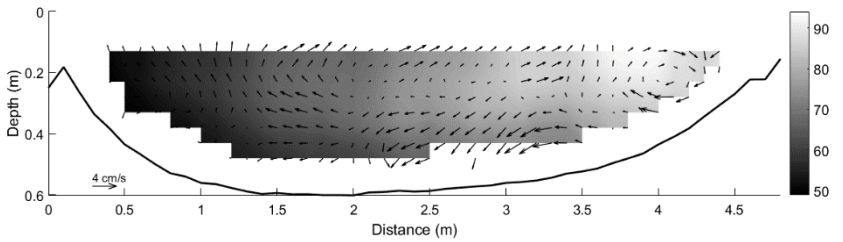

Figure 4.8 Secondary flow measurement for Case R315-2

d) Section 4

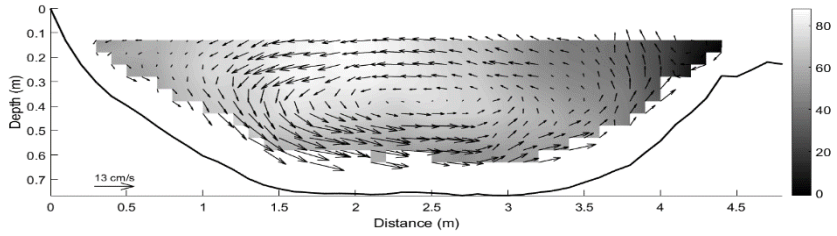

e) Section 5

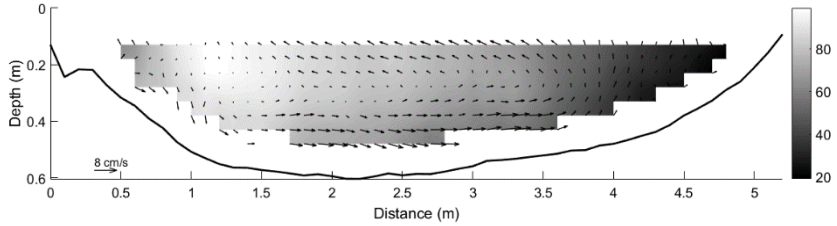

f) Section 6

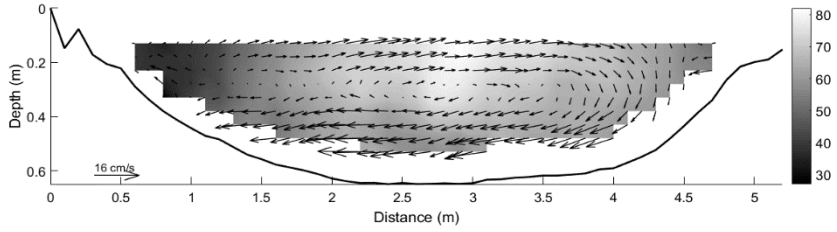

Figure 4.8 Secondary flow measurement for Case R315-2 (cont)

a) Section 1

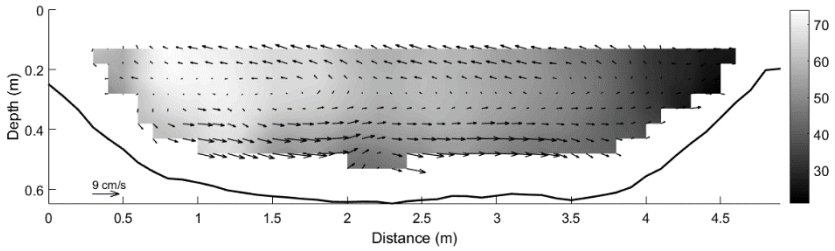

b) Section 2

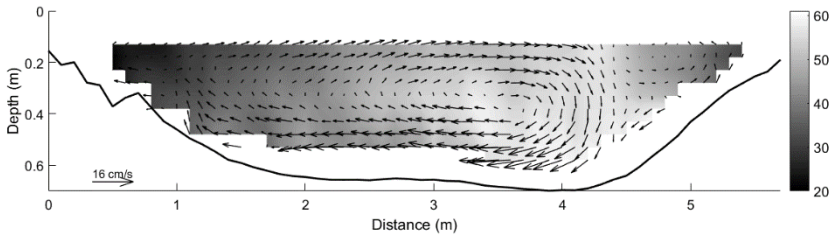

c) Section 3

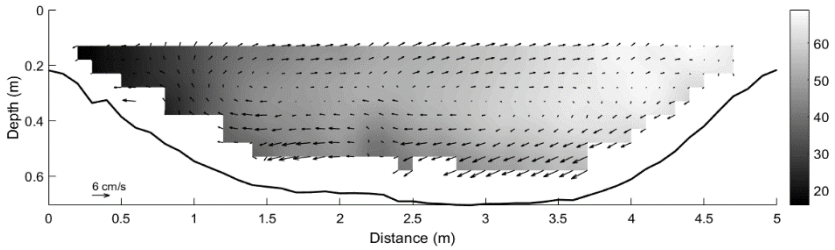

Figure 4.9 Secondary flow measurement for Case R317-2

d) Section 4

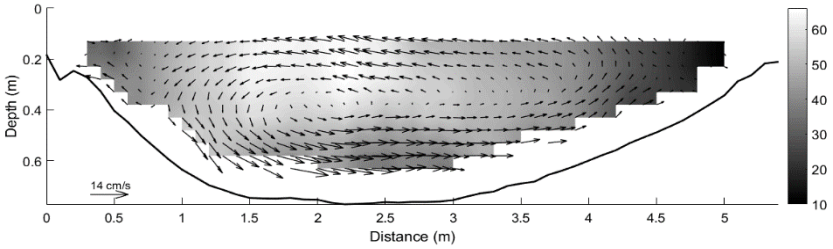

e) Section 5

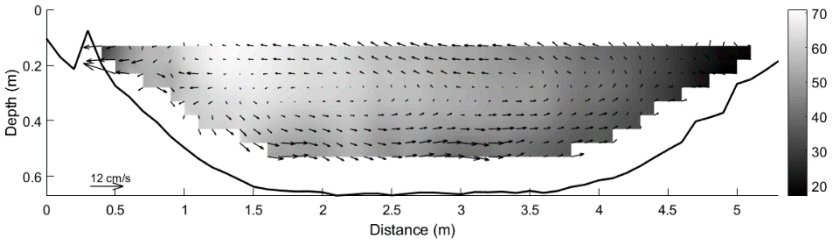

f) Section 6

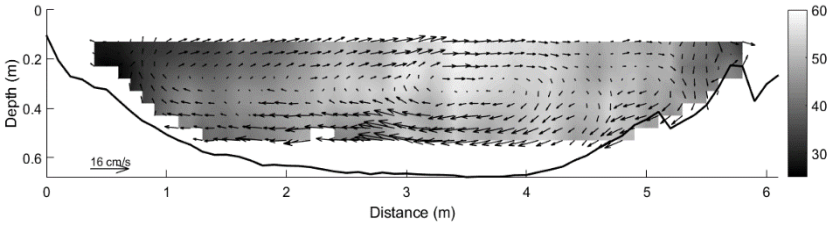

Figure 4.9 Secondary flow measurement for Case R317-2 (cont)

Time-averaged values of downstream (U), cross-stream (V), and vertical (W) velocity were computed for bins within each ensemble in relation to the cross-section orientation. Also, measurements of near-surface water temperature were recorded at each ensemble by the ADCP transducers for the modification of velocities if necessary. The acquired measured data were averaged as 6 measurements by boat were conducted for each section, with 3 measurements per direction and projected by VMT program to a straight line plane using the measured irregular ship tracks. Since the measurements were taken as a continuous boat-moving area, the sections were interpolated with a span and width interval of 0.1 m after the ensemble measurements.

The primary flow measurement results for each sections are plotted into Figure 4.10 as the projected and interpolated data for transects were created for a representation of the velocity field in the channel. The A315 channel measured vectors are depicted in Figure 4.10a), showing the distribution of primary flow as it passes through the meander. The results of the experiment show that the secondary flow affects to the transverse distribution of the primary flow velocity in REC meandering channels. As shown in Figure 4.10 the peak of the longitudinal velocity is located at the outer part of the bend, which is expected in curved channels with sinuosity of 1.5 and 1.7. It is assumed that sinuosity is one of the variables that has effect to the strength of the secondary current. This could be found from the tendency that the velocity distribution is more skewed to the outer bend in A317 as in Figure 4.10b), than the 1.5 sinuosity A315 channel in Figure 4.10a).

a) A 315

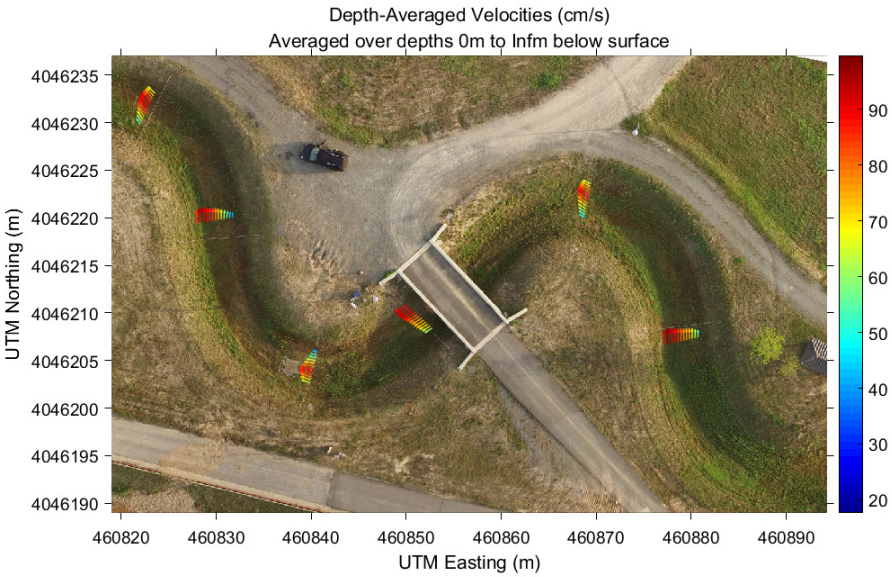

b) A 317

Figure 4.10 Measured primary velocity vectors of each sections

The measured secondary current results by sinuosity are shown in Figure 4.11(a) and this result show the secondary flow strength is increasing as the sinuosity increases. Figure 4.11(b) with 4.11(a) illustrates that the effect of secondary flow strength in the primary velocity distribution form. The increase in curvature caused the center region secondary cell to become stronger which led to the core of maximum longitudinal velocity to shift toward the outward direction as maintained in the previous researches (Blanckaert, 2004). The A312 experiment with sinuosity 1.2 has the least secondary strength, which leads to the lesser effect in longitudinal velocity skewness in Figure 4.11(b) compared to the A315 and A317 experiments with higher sinuosity. This shows that the modeling of secondary flow would be imperative for accurate representation of the flow distribution in meandering channels. By using the experimental results a relation between the depths over radius of curvature and the secondary flow strength is shown in Figure 4.12(a). In this study, non-dimensional index of the secondary flow strength is

$$SFS = \left(\overline{v'^2}\right)^{1/2} / U_m = \left[\frac{1}{h}\int_0^h (v-\overline{v})^2 dz\right]^{1/2} / U_m \qquad (4.1)$$

where v is a transverse velocity at vertical position; $\overline{v}$ is the depth averaged transverse velocity; U_m is the averaged longitudinal velocity. This figure shows that the relations are not an exact linear pattern, and the power form would be an

acceptable choice in description of the relation. The relation was transferred into a power law form with the exponent to be determined as 0.935, which will be used later in the development of a new equation for the vertical profile of the secondary current. Another term that may affect the secondary flow strength is the Chezy coefficient. The Chezy coefficient in this research was calculated by using the below equation, which is

$$C = \sqrt{RS_0} / U \tag{4.2}$$

where R is the hydraulic radius, and S_0 is the bottom slope. Figure 4.12(b) shows the relation of the Chezy coefficient to the secondary magnitude results. Higher values of the coefficient caused a slight decrease in the *SFS*, but the value of bottom slope and hydraulic radius in such meandering channels is difficult to calculate considering the variance of the parameters due to the meander. Therefore, this relation was not used in the development of the equation for vertical profile for transverse velocity. Figure 4.13 shows the secondary flow strength relations to mean velocity over shear velocity and width over radius of curvature. The mean velocity over shear velocity showed no relations, and the width over radius of curvature showed relations dependent on the radius of curvature such as 4.13(b), but the former relation of H/R_c was selected since both terms were dependent on the radius of curvature R_c, and more literature reviews used the former term.

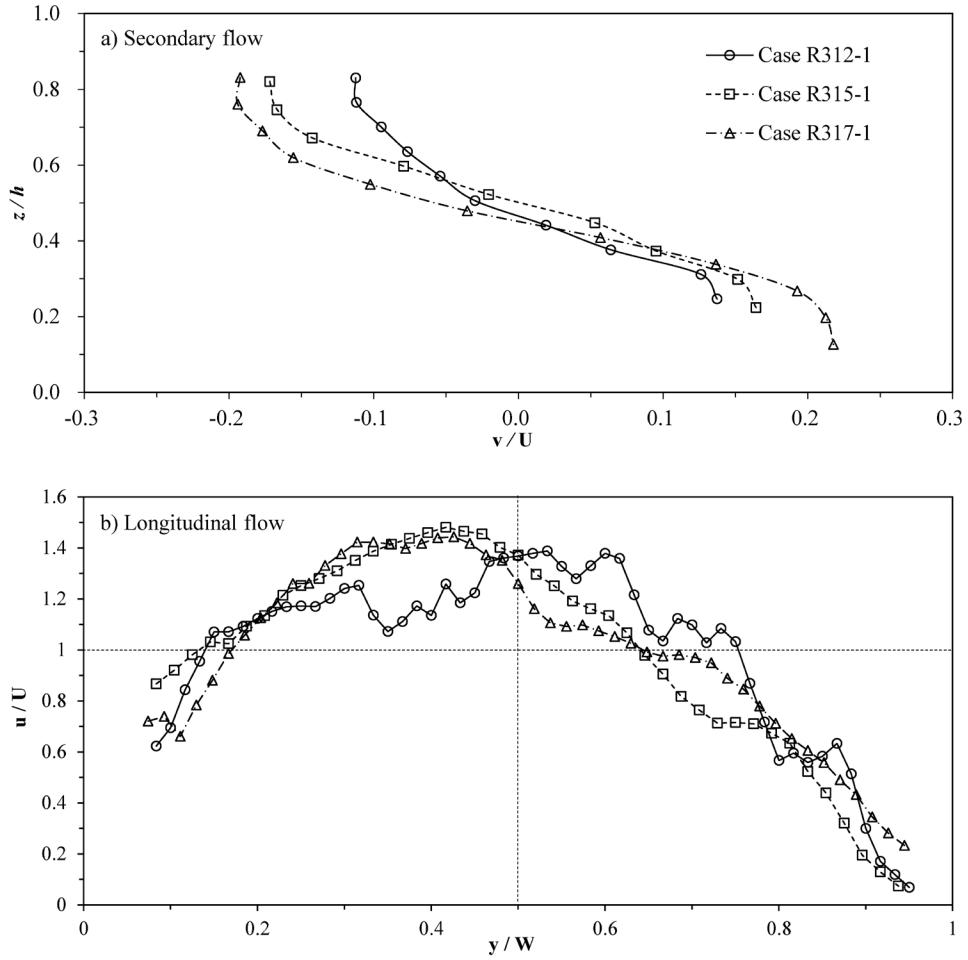

Figure 4.11 Velocity profile of secondary current and longitudinal velocity distribution (section 4) of REC meandering channel

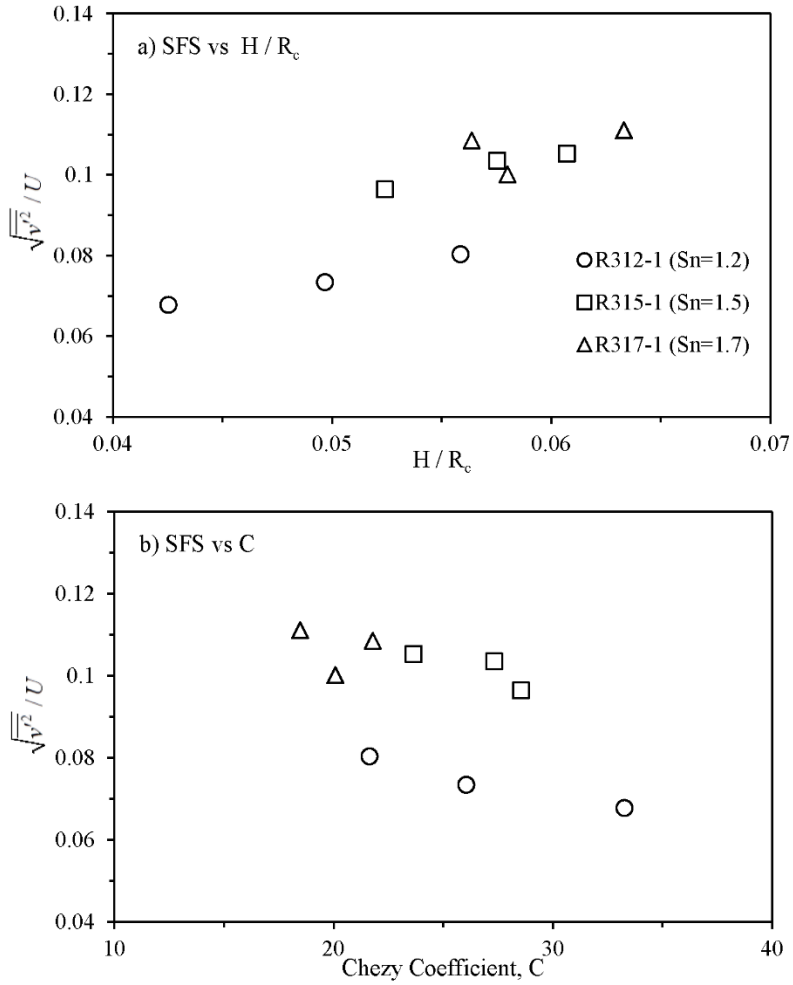

Figure 4.12 Variation of Secondary Flow Strength with H/R_c and Chezy coefficient

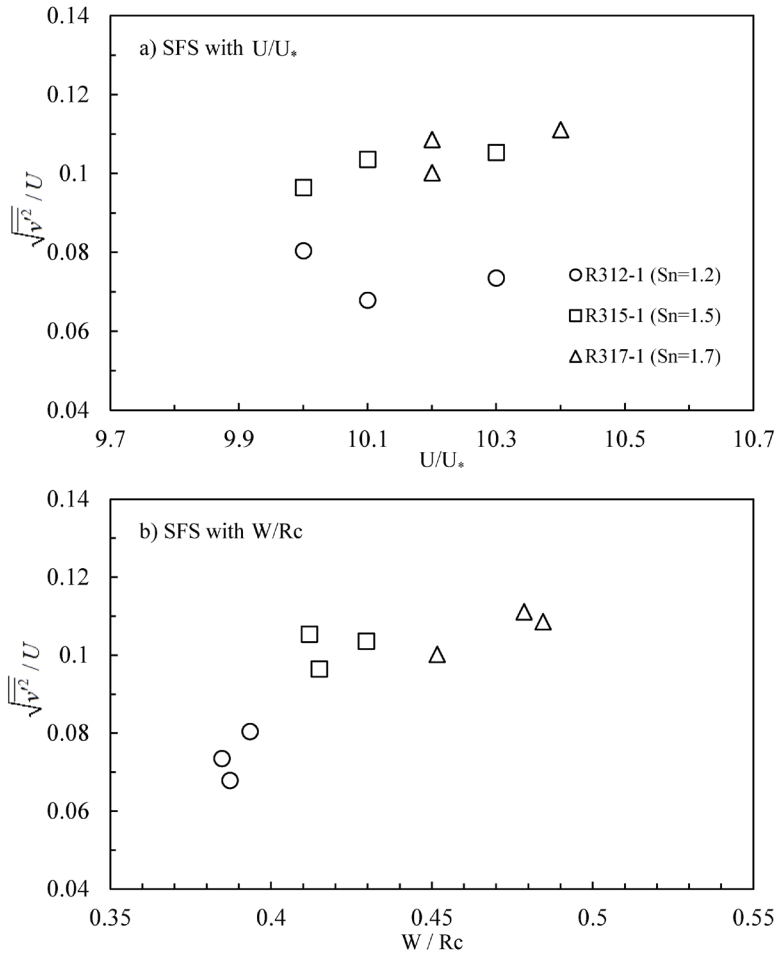

Figure 4.13 Variation of Secondary Flow Strength with U/U_* and W/R_c

4.5 Analysis for Concentration Data

For the tracer input experiments, Rhodamine WT was selected for the tracers. Rhodamine WT is a fluorescence dye with reddish color that has been selected in previous tracer tests for mixing research in open channels since it is convenient to detect in low background concentrations. (Rowinski et al. 2007; Sun et al. 2011). In this study, the Rhodamine WT was made 20% solute using the dosage formula by Kilpatrick (1970) and was released into the injection area.

$$V_s = 2.0 \times 10^{-3} \left(\frac{Q_m L}{U} \right)^{0.93} C_p \tag{4.3}$$

where V_s is the volume of stock Rhodamine WT 20% dye in liters; Q_m is the maximum discharge the downstream site (m^3/s); L is the distance to the downstream site (m); and C_p is the peak concentration at downstream site.

The tracer tests were conducted using an in situ electronic fluorometer (YSI 600-OMS sonde with 6130 Rhodamine WT sensor). The dye concentrations were measured at 5 points on evenly lateral distributed sensors per section using the installed tag lines for the section measurement. The concentrations were recorded at every 1 second to obtain the concentration-time curves per sensor. The range of the YSI 600-OMS sonde was 0-200 $\mu g / L$ (ppb), and the accuracy was 5% of the

measured data or 1 $\mu g / L$, whichever is greater. The resolution of the instrument sensor was 0.1 $\mu g / L$, and the water temperature range was -5 to 50°C. Before each field experiment, the sensors were calibrated with standard solutions before use. For the injection, 150 mL of 20,000,000 ppb Rhodamine WT solution was instantaneously injected to the A315 and A317 channels shown in Fig. 4.1. The first cross section was installed after the vertical mixing was finished, using the equation by Fischer et al. (1979) as in

$$L_V = 0.4\frac{\overline{U}h^2}{\varepsilon_v} \tag{4.4}$$

where L_V is the length needed to finish vertical mixing; $\overline{U}$ is the cross-sectional averaged velocity. So the initial Taylor period for mixing where the variance of the dispersing cloud grows linearly with time and the initial skew degenerates into the normal distribution is calculated to be 56.63 seconds, and the length is about 30.01 m. All the first sections of each experiment are located after the 30 m, however as the actual tracer test was conducted in the case R315-2 in Table 4.2 the arrival time was shown to be just shorter than the initial Taylor period. The concentration characteristics of the measurement of the 2 experiments was listed in Table 4.2. As the mixing continued on throughout the channel from section 1 to section 6 as in Fig.

4.2, the peak concentration detected from the sensors decreased while the variance of the concentration increased. The detailed concentration-time curves measured at each measured point by sensor were plotted in Figs. 4.14 and 4.15. In most point measurements, the concentration-time curves show an asymmetric distribution with left skewness and a falling limb. The long tails in the falling limbs were frequently observed in the measurements using the Eulerian method, and it occurred due to the flow structures of the test site. This makes the dispersion calculation with moment-based methods difficult, and routing methods were more appropriate in calculation. As the tracer cloud moved downstream, the variance of the concentration-time curves increased as transverse mixing occurred. The A317 in Figure 4.15 shows that more mixing has occurred than A315 in Figure 4.14 at the beginning sections as the concentration difference between sensors are low, due to the strongly developed secondary flows. At the earlier sections of the channel, the peak of the tracer cloud was not located at the center of the section but was shifted to the left/right bank. Then at the latter sections, the tracer cloud was transported to the opposite bank. This was the case for meandering streams, as the tracer moved back and forth each side of the bank throughout the channel and the skewness of concentration changed. Therefore, the stream-tube method should be used with routing procedures for the accurate calculation of dispersion coefficients. Since the stream-tube method has a fixed value of discharge attached to a streamline by moving the coordinate system along with the flow, this method allows the user to take consideration of the discharge distribution shifts in meandering channels and irregularity of the channel.

Table 4.2. Description of concentration data from experiments

Case	Section no.	C_p (ppb)	t_p (sec)	σ_t^2
R315-2	1	53.3	51.0	152.0
	2	31.8	86.0	358.8
	3	27.0	114.0	411.4
	4	20.3	137.0	632.3
	5	18.3	170.0	899.2
	6	15.1	208.0	1,193.1
R317-2	1	32.0	85.0	362.0
	2	22.9	129.0	738.8
	3	20.7	171.0	1,263.6
	4	14.5	217.0	2,381.9
	5	12.7	278.0	2,710.9
	6	9.8	319.0	3,580.9

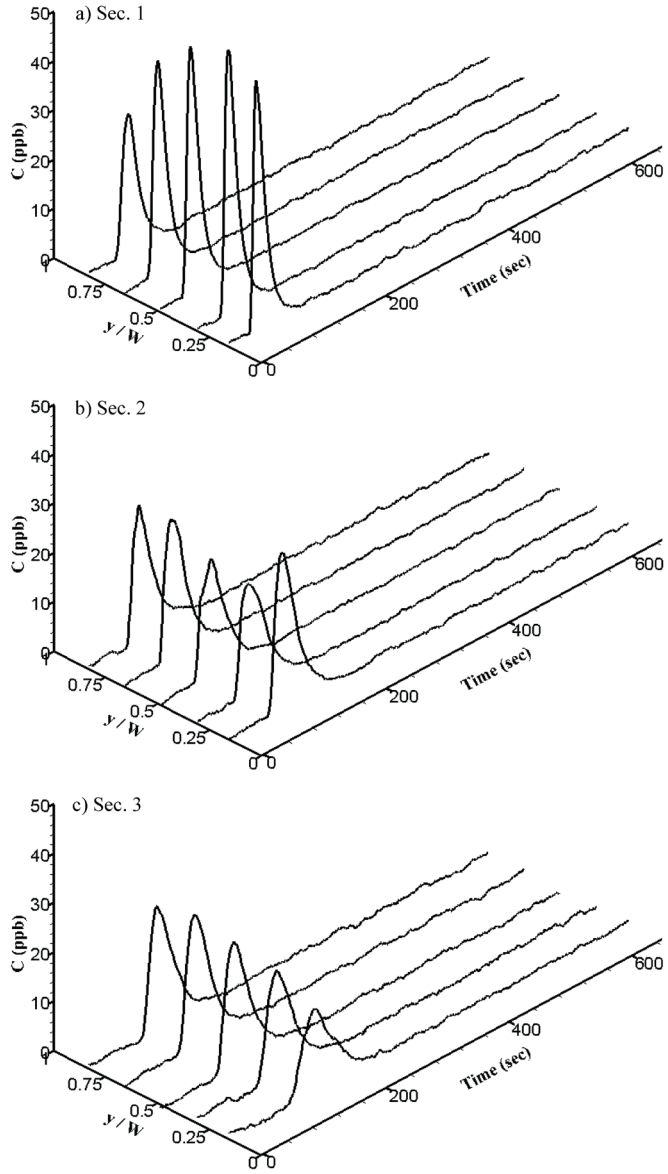

Figure 4.13 Time-concentration curves for Case R315-2

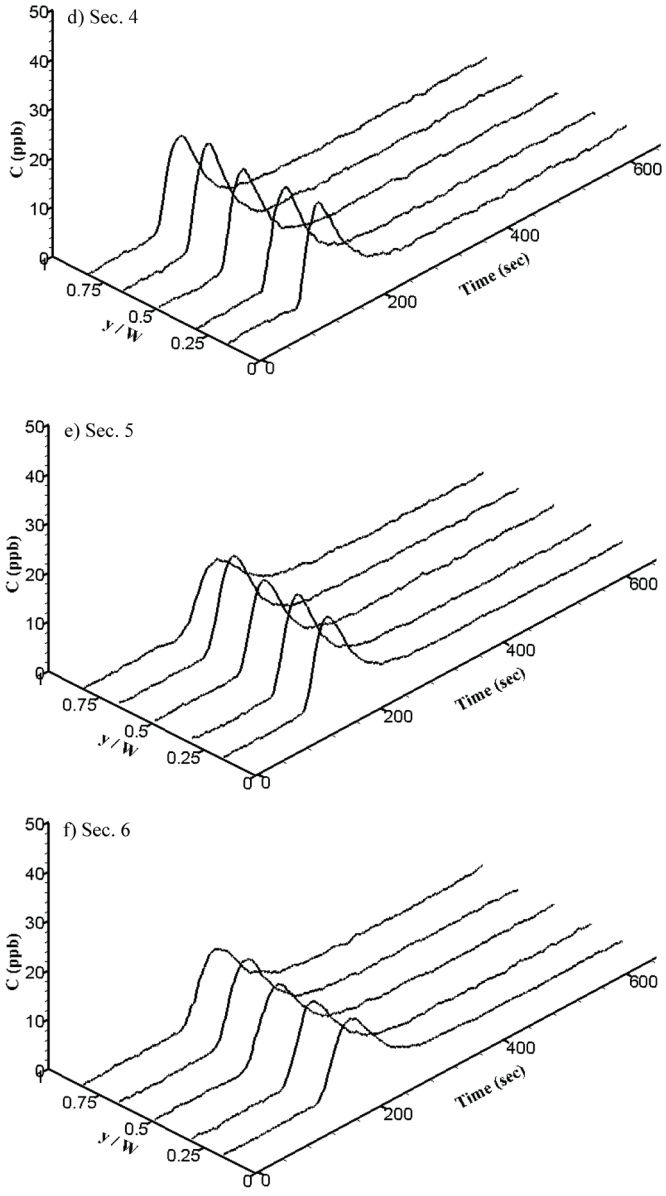

Figure 4.13 Time-concentration curves for Case R315-2 (cont)

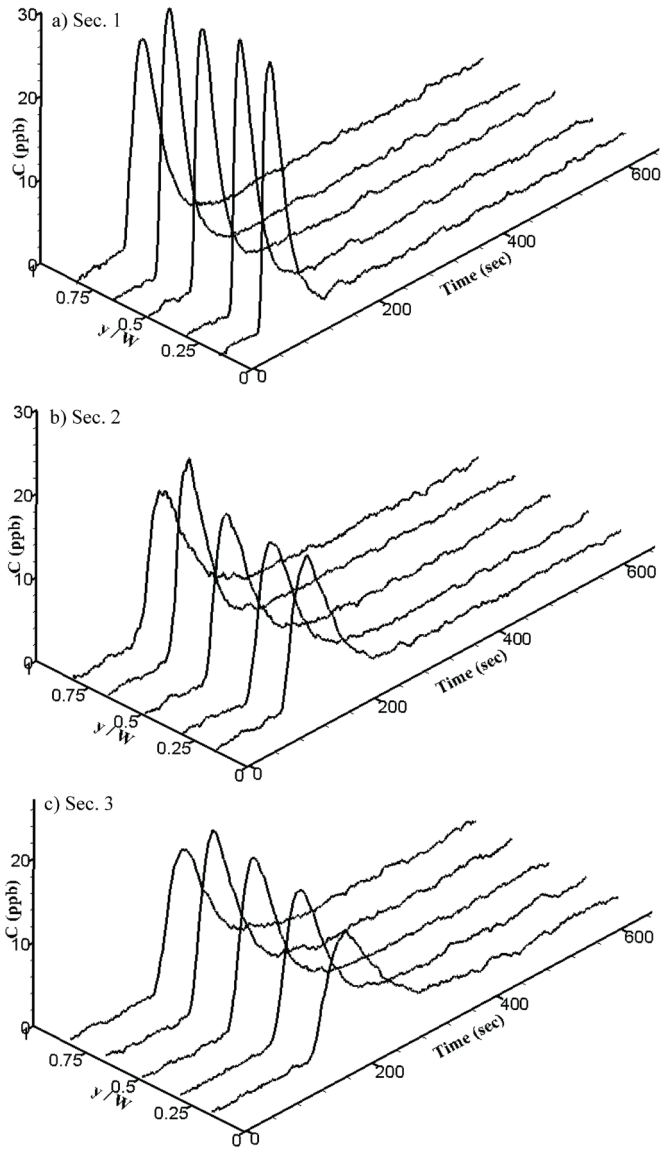

Figure 4.14 Time-concentration curves for Case R317-2

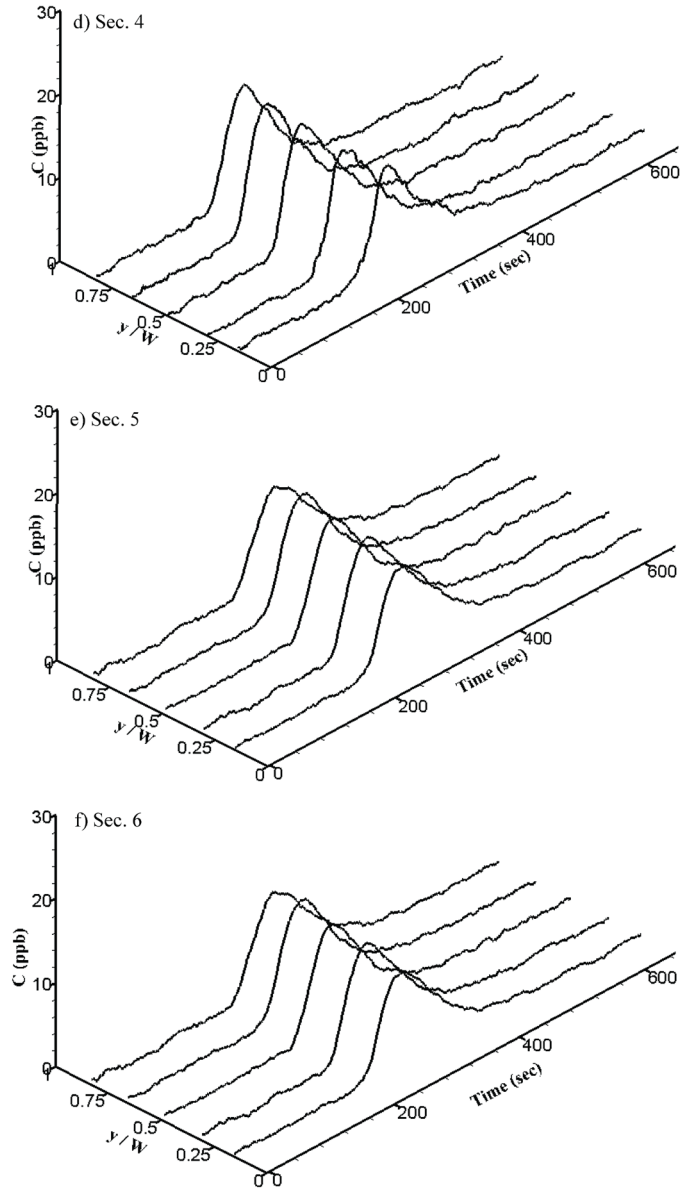

Figure 4.14 Time-concentration curves for Case R317-2 (cont)

Chapter 5. Derivation of the Transverse Velocity Profile

5.1 Development of the Velocity Profile Equation

For application of the dispersion stress method vertical profiles of the secondary current were necessary. The development of the transverse velocity equations was first based on the 3D Navier Stokes equation in the cylindrical coordinates, as shown in Figure 1b), with steady flow assumption (Kikkawa, 1973, Chang, 1988).

$$\frac{\partial u}{\partial t}+u\frac{\partial u}{\partial s}+v\frac{\partial u}{\partial r}+w\frac{\partial u}{\partial z}=-\frac{uv}{r}+gS+\frac{1}{\rho}\frac{\partial \tau_s}{\partial z} \tag{5.1}$$

$$\frac{\partial v}{\partial t}+u\frac{\partial v}{\partial s}+v\frac{\partial v}{\partial r}+w\frac{\partial v}{\partial z}=-\frac{u^2}{r}+gS_r+\frac{1}{\rho}\frac{\partial \tau_r}{\partial z} \tag{5.2}$$

where u, v, w are the velocity components of the *s, r, z* directions for the cylindrical coordinates respectively; r as the transverse coordinate point; ρ as the water density; S_r as the transverse water surface slope; S as longitudinal water surface slope; τ_s, τ_r as the shear stresses in the *s, r* directions respectively.

For the fully developed flow $\partial v/\partial s,\ \partial u/\partial s = 0$, the time derivatives drop out considering steady flow, and velocity components regarding *v* and *w* are small compared to *u* in a wide channel. The equations of motion become the following after dropping second order terms.

$$gS + \frac{1}{\rho}\frac{\partial \tau_s}{\partial z} = 0 \tag{5.3}$$

$$\frac{u^2}{r} - gS_r - \frac{1}{\rho}\frac{\partial \tau_r}{\partial z} = 0 \tag{5.4}$$

By assuming isotropic turbulence, the shear stresses τ_s and τ_r in turbulent flows can be expressed in terms of the eddy viscosity and velocity gradients such as

$$\tau_s = \varepsilon \frac{\partial u}{\partial z} \tag{5.5a}$$

$$\tau_r = \varepsilon \frac{\partial v}{\partial z} \tag{5.5b}$$

where ε is eddy viscosity. Then by using the logarithmic law for the vertical velocity profile, the longitudinal velocity in a cross section is assumed to be the following, using δ as a nonlinear term containing uncertainty to show the decrease or irregularity of longitudinal velocity which can be found in sharp bends (Wei et al., 2016) as in Figure 1.2. The figure shows that nonlinear behavior by the secondary currents would cause the decrease and irregularity of the outward

centrifugal force, which then leads to the overall decrease of secondary flow strength in the top and bottom parts of the water flow. The revised logarithmic equation is as below

$$u(\eta) = \overline{u}\left[1 + \frac{\sqrt{g}}{\kappa C}\{\ln(\eta - \delta) + 1\}\right] \tag{5.6}$$

where δ is the nonlinear term. This term would enable the neglected nonlinear characteristics of the depth-averaged model to be shown. Assuming the distribution of longitudinal velocity of Eq. (5.6) and the turbulent viscosity in Eq (5.5) to follow a curve, the solution of the problem of distribution of transverse components could be attempted. With a similar derivation method by Rozovskii (1957) for Eq. (2.5), Eq. (5.4) becomes the following by substituting with $\eta = \frac{Z}{H}$,

$$\frac{\partial}{\partial \eta}\left(\varepsilon \frac{\partial v}{\partial \eta}\right) = H^2\left(gS_r - \frac{u^2}{r}\right) \tag{5.7}$$

To get the transverse inclination of the water surface S_r, the pressure force associated with transverse surface inclination is balanced by the centripetal force for

$$\int_0^D \frac{u^2}{r}\rho ds dr dz - \rho g S_r ds dr dz = 0 \tag{5.8}$$

$$S_r = \frac{\int_0^D \frac{\overline{u}^2}{r} dz}{gr} = \frac{C_r U^2}{gr} \tag{5.9}$$

where C_r is a correction factor which is assumed to be 1. Then by substituting u with Eq. (5.8) and carrying out the integration similar to Rozovskii (1957),

$$\varepsilon \frac{\partial v}{\partial \eta} = \frac{H^2 \overline{u^2} g}{C^2 R_c} \left[\left\{ \frac{R_c S_r C^2}{\overline{u^2}} - \frac{\left(1 + \frac{\sqrt{g}}{\kappa C}\right)^2 C^2}{g} \right\} \eta - \frac{2}{\kappa} \frac{\left(1 + \frac{\sqrt{g}}{\kappa C}\right)^2 C^2}{\sqrt{g}} \{\eta \ln(\eta - \delta) - \eta\} \right.$$
$$\left. - \frac{1}{\kappa} \{\eta \ln^2(\eta - \delta) - 2\eta \ln(\eta - \delta) + 2\eta\} \right] \tag{5.10}$$

Then, using the approximation of a mean value of eddy viscosity along the vertical, the eddy viscosity is assumed to be $\varepsilon = U_* H / 15$. This value of eddy viscosity is inserted into Eq. (5.10), and the equation is integrated by using the

boundary condition that friction on the free surface equals zero, $\frac{1}{H}\left(\varepsilon\frac{\partial v}{\partial \eta}\right)=0$.

The result of the integration is the following, with the main form of the equation similar to Rozovskii and Kikkawa of equation Eq. (2.5) and Eq. (2.9):

$$\frac{v(\eta)}{U}=\frac{15}{\kappa}\frac{H}{R_c}\left[F_A(\eta)-\frac{\sqrt{g}}{\kappa C}F_B(\eta)\right] \tag{5.11}$$

$$F_A(\eta)=-\left(\frac{2\eta^2\ln(\eta-\delta)-\eta^2+C_1}{2}\right) \tag{5.12a}$$

$$F_B(\eta)=\left(\frac{2\eta^2\ln^2(\eta-\delta)-2\eta^2\ln(\eta-\delta)+\eta^2+C_2}{4}\right) \tag{5.12b}$$

The constants of integration comes from the boundary condition that the friction on the free surface equals zero, which is similar to the case by Rozovskii and Kikkawa of Eq. (2.5) and Eq. (2.9) for C_1 and C_2 for the constants of 16/27 and 7/9. Therefore, it is different from the deVriend equation, which has a bottom no-slip conditions, while the developed equation has a slip condition in the bottom. This is due to the difference in the derivation procedure, as the deVriend equation uses the perturbation method that is different from the other methods with bottom slip conditions.

In this study, for the applicability of the developed equation, the term δ that was inserted into the longitudinal velocity profile was replaced into the single coefficient β to the main equation, since this research faced limitations in acquiring the exact δ value from the experiment results since it was used in three minor terms. So this nonlinear coefficient β was introduced manually to the main equation as a compromise to apply the experimental results of this research as one single term to the main equation to apply the nonlinear effect to the equation instead of using a direct derivation result. Various data using continuous laboratory experiment results could be better suited to find the exact δ value, but since the δ in three terms were difficult to find and differentiate in this research since the actual measured data are the velocity size of transverse flow like the main equation, a compromise using an empirical approach of one single coefficient β was used.

The β coefficient could be empirical by calibration to the experiment data, or could be used in the form of $\beta = \omega\left(H / R_c\right)$, where ω can vary from 20–30, depending on the channel. This enabled the equation to keep the nonlinear term, and limit the growth of the secondary flow in the top and bottom layers of the water flow in sharper curvatures. So this β coefficient limit the growth of the top and bottom layers will reflect the gradual damping in the overall secondary flow strength as it increases with the depth over radius-of-curvature that will be shown in later figures and experimental comparisons. This would enable the neglected nonlinear characteristics of the depth-averaged model to be shown.

By considering the sensitivity of depth over radius-of-curvature, the H / R_c term was changed to a non-dimensional factor for the exponent using the measured data from the experiment; the final form of the vertical profile for the secondary flow then became the following:

$$\frac{v(\eta)}{U} = \frac{15}{\kappa}\left(\frac{H}{R_c}\right)^{\alpha}\left[F_A'(\eta) - \beta \times \frac{\sqrt{g}}{\kappa C} F_B'(\eta)\right] \tag{5.13}$$

$$F_A'(\eta) = -\left(\frac{2\eta^2 \ln \eta - \eta^2 + C_1}{2}\right) \tag{5.14a}$$

$$F_B'(\eta) = \left(\frac{2\eta^2 \ln^2 \eta - 2\eta^2 \ln \eta + \eta^2 + C_2}{4}\right) \tag{5.14b}$$

In this study, the coefficients α and β were found based on the measured experimental data; constant α was determined to be 0.935 from the relation between secondary flow strength and the depth over radius of curvature results shown in Fig. 4.11(a). The coefficient β was determined to be over 1.0–2.0 through comparisons with the measured velocity data of Fig. 5.1, and affected the term F_B' of the proposed equation for the vertical profile. This enables the vertical velocity profile to be more applicable to channels with various curvatures, especially high sharpness and multiple meanders.

5.2 Validation of Profile

To find the acceptability of the transverse velocity profiles, the proposed equation was compared with the experimental data of the REC meandering channel. Fig. 5.1 shows the comparison with the experimental data of A315 channel, and Table 5.1 lists the average root-mean-square errors (RMSE) of the proposed equation and existing equations. Table 5.1 shows that the proposed equation in this study shows the least RMSE for all cases of the meandering channels. Fig. 5.1 reveals that the proposed equation shows better fit in the top and bottom layers of the secondary flow of the vertical profile in full sized experiments with multiple curves, while the other equations show overestimation at the points. This was possible, since a nonlinear term was reflected in the proposed equation, and the sharp channels created the nonlinear behavior, where the strong secondary flow would affect the top and bottom areas of the vertical profile which is also depicted in the research by Kikkawa (1979).

As previously mentioned, the maximum longitudinal velocity was located at the outer part of the bend shown in Fig. 4.10(b), and it is postulated that the depth over radius-of-curvature is one of the variables that affects the strength of the secondary current. Also, when the sinuosity increases, there was a tendency for the distribution to be more skewed to the outer bend. For closer analysis and investigation of the effects of the H / R_c on the proposed equation for secondary flow velocity, the H / R_c term was increased in increments, to find the relation to the size of secondary flow.

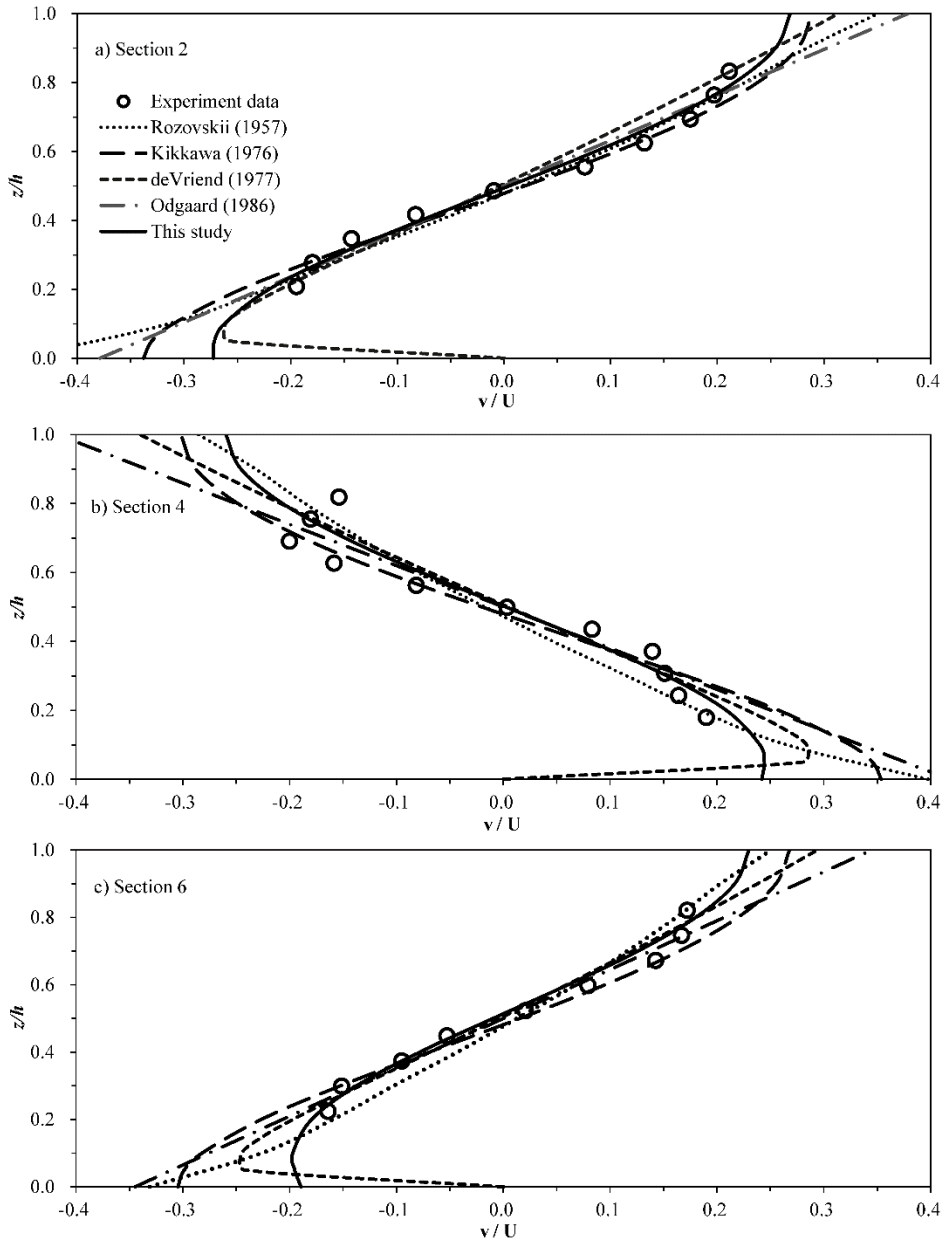

Figure 5.1 Comparison of the transverse velocity profiles (R315-2)

Table 5.1 Average RMS errors of velocity profile formulas

Equation	R315-1	R317-1	R315-2	R317-2	Average
Rozovskii	5.33	5.06	3.69	5.48	4.89
Kikkawa (1976)	5.35	3.67	3.41	4.26	4.17
de Vriend	4.52	3.35	4.09	4.15	4.03
Odgaard (1986)	4.77	5.83	3.43	5.85	4.98
This study	4.36	3.44	2.74	4.17	3.67

Fig. 5.2 shows the higher H / R_c increases the size of the secondary flow. Note that as the depth over radius-of-curvature term increases, the growth of secondary flow size is limited in the top and bottom parts of the vertical profile. This is due to the $\beta = \omega\left(H / R_c\right)$ coefficient introduced in the proposed equation with ω as 20, which serves as a coefficient to reflect the gradual damping in the secondary flow strength as it increases with the depth over radius-of-curvature. This state is also seen in Fig. 5.3, as the secondary flow strength is plotted with H / R_c, which shows attenuation of the secondary flow strength as H / R_c increases, compared to the dotted line showing secondary flow strength without nonlinear terms. This attenuation of secondary strength with high H / R_c term were also shown in the laboratory experiments (Wei et al, 2016) where the researchers maintained that with increasing values of the term, the growth becomes less than linear due to the nonlinear interactions between the primary and secondary flow (Blanckaert, 2009).

The secondary flow would cause the decrease of the longitudinal flow by nonlinear behavior caused by strong secondary flows in multiple meanders, which affects the outward centrifugal force; then the irregular decrease of the centrifugal force will cause the decrease of secondary flow strength in the top and bottom parts of the water flow, as shown in Fig. 2. Figs. 5.2 and 5.3 show that the proposed secondary flow equation can reflect the nonlinear behavior in sharp channels to represent the attenuation of secondary flow strength.

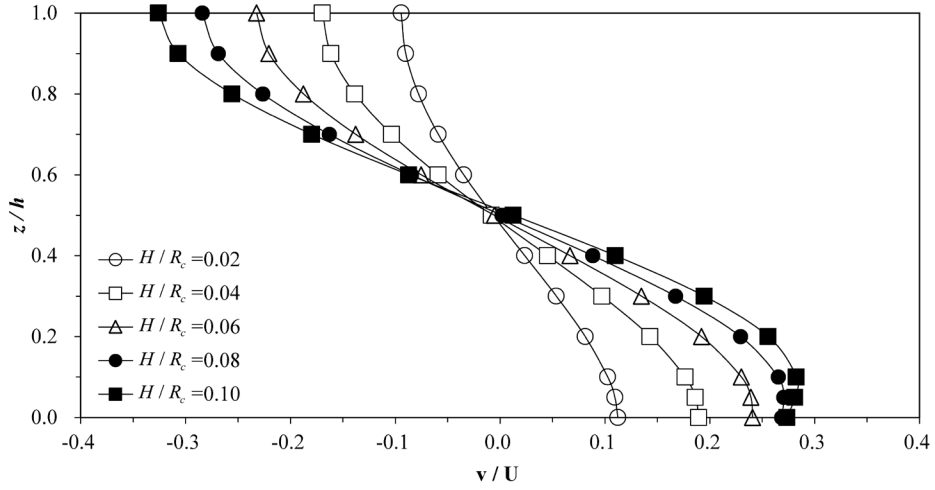

Figure 5.2 Vertical distribution of secondary flow profile computed by the proposed equation

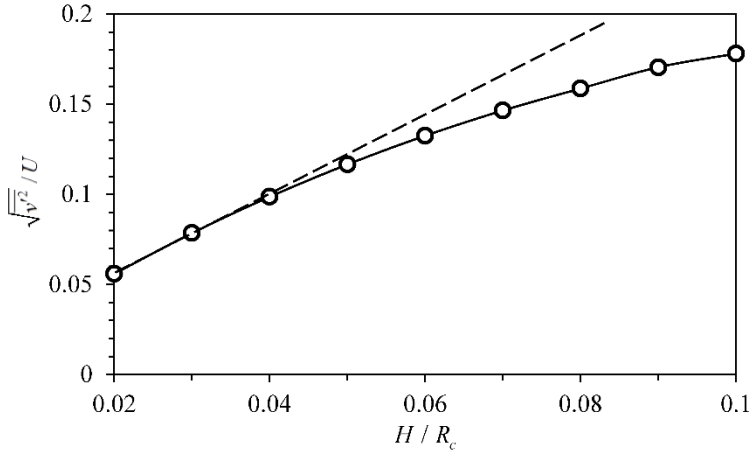

Figure 5.3 Secondary flow strength changes with H / R_c using vertical profile equation

Chapter 6. Applications of 2D Flow Model

6.1 Development of DS Model

For the dispersion stress model application the developed equation of 5.13 and 5.14 is inserted into the equation of 2.22. This study decomposed the velocity components into depth-averaged velocities and their deviations, and inserted them into the integration of the products of the velocity fluctuations. The first term S_{11} of the result of dispersion S_{xy} indicates the integration of the products of the discrepancy between the mean and the vertically varying velocity distribution in the x direction.

$$S_{11} = \int h^2 U_1^2 F_S(\xi)^2 - 2hu_1 U_1 F_M(\xi) F_S(\xi) + 2hu_1 U_1 F_S(\xi) + h^2 U_1^2 F_M(\xi)^2 \, d\xi \qquad (6.1)$$

F_M is the integrated result of the vertical profile of the longitudinal velocity by de Vriend and F_S is the integrated result of the created equation.

$$\begin{aligned} S_{12} = S_{21} = \int (u_1(\eta) - U_1)(u_2(\eta) - U_2) d\eta = \int \; & u_1 u_2 F_M(\xi)^2 - u_1 U_2 h F_M(\xi) F_S(\xi) \\ & - u_1 u_2 F_M(\xi) - hu_2 U_1 F_M(\xi) F_S(\xi) + h^2 U_1 U_2 F_S(\xi) - hu_2 F_S(\xi) \\ & - u_1 u_2 F_M(\xi) + hu_1 U_2 F_S(\xi) - u_1 u_2 \; d\xi \end{aligned} \qquad (6.2)$$

$$S_{22} = \int h^2 U_2^2 F_S(\xi)^2 - 2hu_2 U_2 F_M(\xi) F_S(\xi) + 2hu_2 U_2 F_S(\xi) + h^2 U_2^2 \, d\xi \qquad (6.3)$$

The second term S_{12} and the third term S_{21} show the integration of the products of the discrepancy in the x- and y- directions. The fourth term S_{22} shows the integration of the products of the discrepancy y-direction. These equations inserted into the HDM-2D will create the dispersion stress effect to apply the secondary flow discrepancies to be produced in the two dimensional model. Then the proposed equations of the velocity deviation that were derived in natural coordinates were changed into Cartesian coordinates by the following equations:

$$u_2'(\eta) = U_1 F_m(\eta) - hU_1' F_s(\eta) \qquad (6.4a)$$

$$u_2'(\eta) = U_2 F_m(\eta) - hU_2' F_s(\eta) \qquad (6.4b)$$

where, u_1' , u_2' are the longitudinal and transverse velocity components in Cartesian coordinates, respectively; U_1', U_2' are the unit normal vector for the longitudinal and transverse directions, respectively; and F_m and F_s are the longitudinal and secondary flow functions, respectively.

The above equations, Eqs. (6.4a) and (6.4), make the flow in the longitudinal direction change due to the influence of the secondary flow included in the second terms. This study used the logarithmic equation by de Vriend (1979) for the profile of the longitudinal flow F_m, while applying the proposed profile of the transverse

velocity of this research of Eq. 5.13 and 5.14 for F_s, which was different from the secondary flow equation by de Vriend, which was used by the original HDM-2D (Song et al., 2012). The relations for the depth to radius-of-curvature ratio were applied to the proposed transverse flow equation, which was then applied to the dispersion stress model. In this way, the nonlinear effect was included in the secondary current. So the governing equations with terms S_{xy} are included in the momentum equations for the following equation

$$\frac{\partial u_i}{\partial t} + u_j \frac{\partial u_i}{\partial x_j} + g\frac{\partial H}{\partial x_i} + g\frac{\partial h}{\partial x_i} - \frac{\partial}{\partial x_j}\left(\nu \frac{\partial u_i}{\partial x_j}\right) + gn^2 \frac{u_i \sqrt{u_j u_j}}{h^{4/3}} + \frac{\partial S_{ij}}{\partial x_j} = 0 \qquad (6.5)$$

The final term of the momentum equations includes the influence of secondary current in the channel apex. The discrepancy between the mean and the vertically varying velocity distributions which were omitted in the depth-averaging process are reproduced in this way. This will enable more accurate two-dimensional flow modeling in both laboratory and natural channels.

6.2 Laboratory Channels

6.2.1 SNU M2 Channel

The M2 experimental setup consists of two meandering channels which are S-curved which may resemble the curving characteristics of natural streams. This channel has taken into account the geometric and hydraulic properties of meandering streams. The laboratory channel used in this study, which had a rectangular cross-section, were 1 m wide, and 0.6 m deep, with a sinuosity of 1.50. A side-view micro-ADV equipment, a high-precision instrument used to measure 3-D water velocity was used to measure the three-dimensional distributions of velocity and turbulence. Sections S1 ~ S12 of M2 channel were measured shown in Fig. 6.1. This enabled the accurate measurement and analysis of the secondary flow characteristics.

Then the longitudinal velocity measured data was compared to the depth-averaged model simulated values. The simulation results with the dispersion stress terms showed that the longitudinal velocity profile throughout the channel is changed toward the outer side of the apex due to the effect of the secondary flow. The results of the comparison of the measured data and the simulated data from the meandering channel in the first apex showed that the revised data with the dispersion stress proved to have better representation of the experiment. The RMSE for the revised data from the first apex showed to be changed from 0.87 to 0.75. The results of the comparison of the measured data and the simulated data from the meandering channel in the second apex also show similar results that the revised data with the dispersion stress method proves to be better with the error decreasing as the RMSE becomes 0.67 to 0.50.

(units: cm)

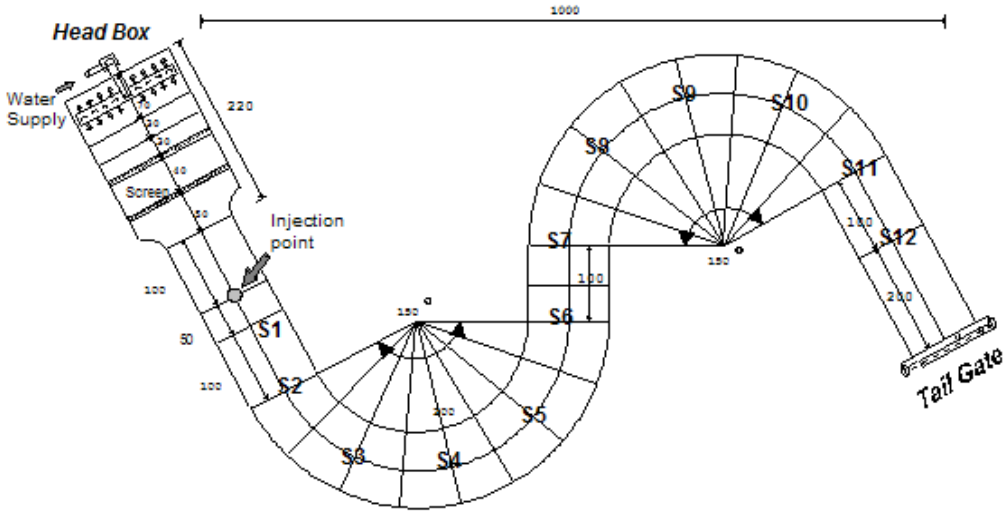

Figure 6.1 M2 Experimental Setup

Table 6.1 M2 Channel Experimental Conditions

Case	H (m)	V (m/s)	Q (cms)
1	0.30	0.2	0.06

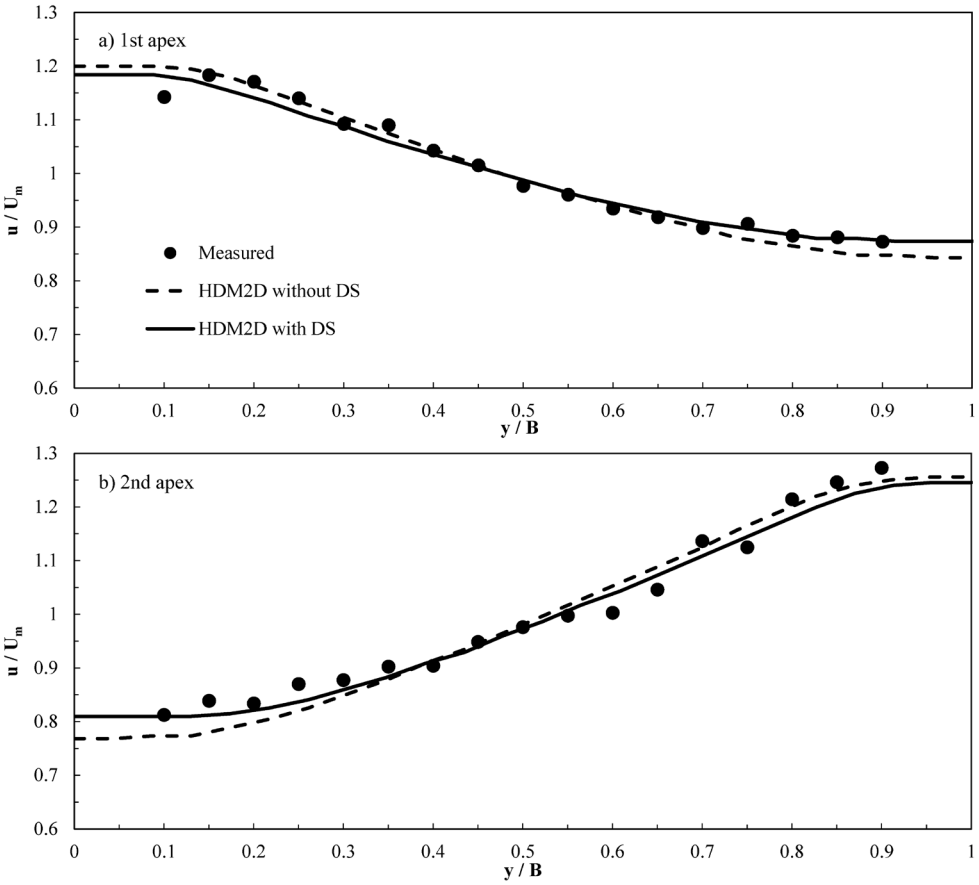

Figure 6.2 Simulation of the longitudinal velocity using constant eddy viscosity

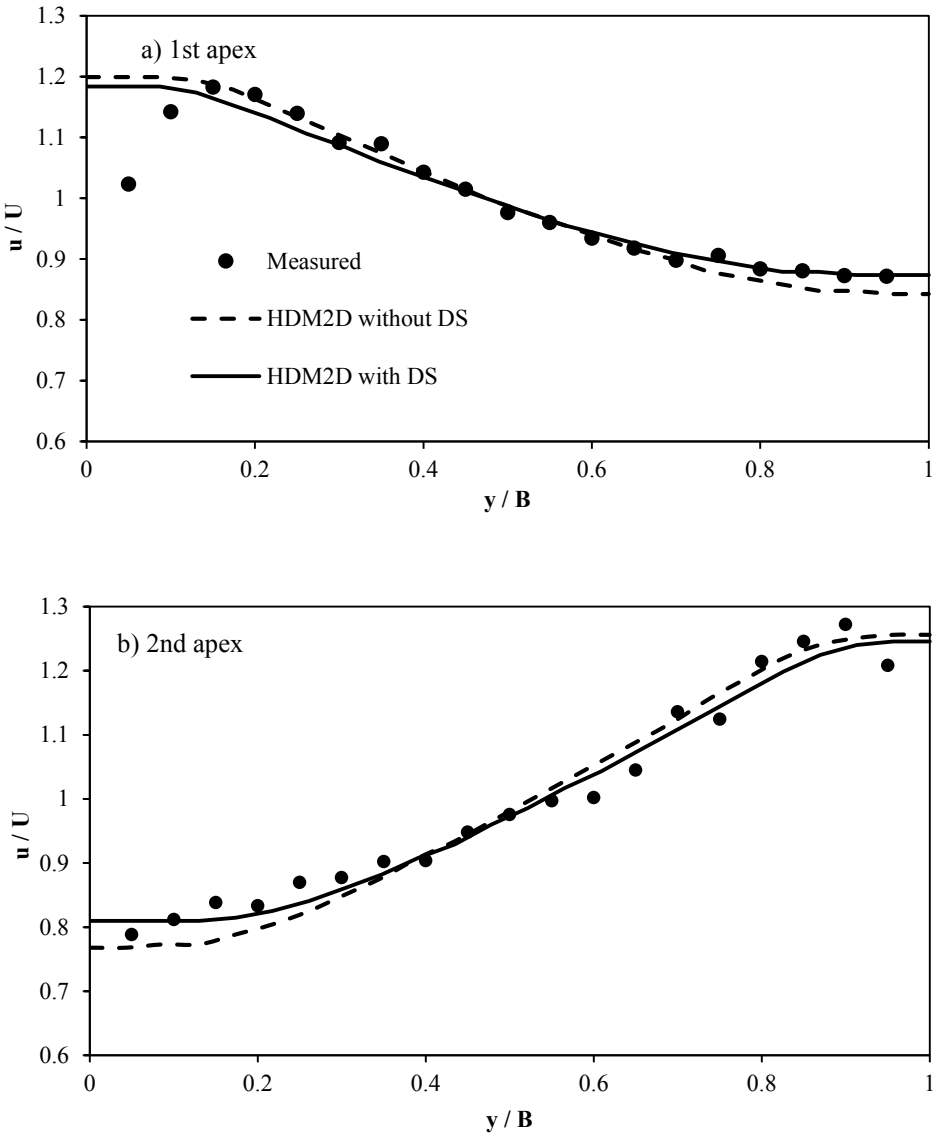

Figure 6.3 Simulation of the longitudinal velocity using parabolic eddy viscosity

6.2.2 Shumate Channel

Flow features in confluent channel are complicated, and are characterized with one separation zone or recirculation zone immediately downstream of the confluence in the inner bank side and one contracted flow region in the outer bank side. Due to the change of flow direction, the centrifugal force induces a surface radial flow opposite to the deflection, and a bottom inward current. In turn, the flow from the main channel has a secondary current rotating against the secondary current of branch channel. More detailed descriptions are given as follows. For confluence flow, the two flows from the main and branch channel are joining, thereby setting up a shearing action to the flow from the other and the surface dividing is evolved. The shear plane is not vertical, but skewed, due to the combined effects of the relative magnitudes of the merging flows and the non-uniform vertical velocity profile. The non-uniform vertical velocity profile induces three-dimensionality into these flow features and the secondary vortex appears in the main channel downstream of the side channel and rotates clockwise looking downstream. A similar secondary vortex rotating against the secondary current of branch channel forms along the other side of the main channel as well. Both vortices decay in strength as they proceed downstream, primarily due to fluid viscosity. Therefore, the consideration of secondary current effect in confluent channel is important.

The revised model in this research was applied to the open-channel confluence flow problem of Shumate (1998) who measured the velocities and the water depths using an acoustic Doppler velocimeter and a point gauge. The channel information

is shown below. Among 6 measurements, the combination of the main channel discharge, Q_m = 0.043 m^3/s and the branch channel discharge, Q_b = 0.127 m^3/s was employed to activate the influence of secondary current more strongly. The computational meshes which contain 6,420 nodes and 6,132 elements were constructed. Finer meshes were used near the confluence and lower part of main channel to capture the recirculation phenomena more precisely. The coordinate system was defined with the origin located at the upstream corner of the junction and with the non-dimensionalized coordinates of $x^* = x / B$ and $y^* = y / B$.

The velocity data confirm the development of coherent helical motion at this confluent meander bend. A clockwise-rotating helical cell is inherited from flow curvature in the upstream of the junction and is deflected by tributary flow toward the inner part of the confluence. Advection of momentum in this cell drives high velocity fluid outward toward the mixing interface near the center of the confluence and downward to a separation zone.

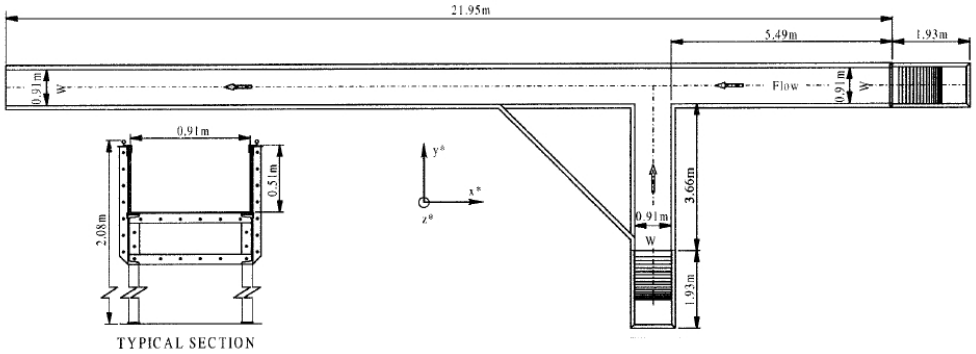

Figure 6.4 Diagram for confluent channel (Weber et al., 2001)

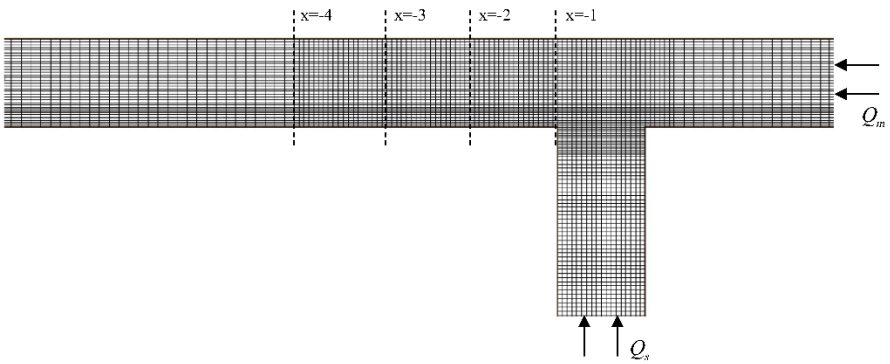

Figure 6.5 Mesh layout and measured sections for confluent channel (After Shumate, 1998)

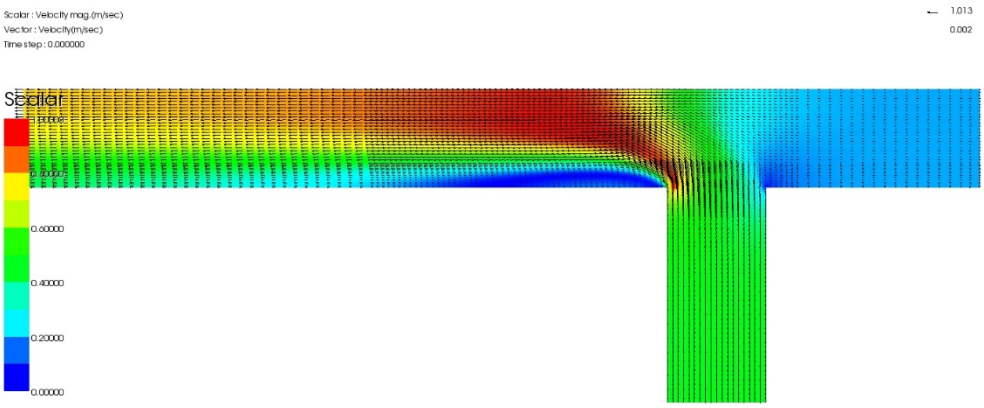

Figure 6.6 Velocity contours for confluent channel

A second helical cell with counterclockwise circulation seems to emerge along the outer section with the downstream channel. The development and evolution of twin surface-convergent helical cells at this confluent meander bend are comparable to patterns of helicity at high-angle symmetrical junctions. As flow from the tributary along the outer side of the channel downstream of the confluence, it is not deflected laterally toward the thalweg. Instead, flow accelerates to maintain continuity, and in so doing, precludes development of flow separation at the downstream junction corner. The location of a separation zone is quite similar to the confluence conceptual model

The velocity contours with and without the consideration of secondary current effect were plotted in Figs. 6.7 and 6.8 with each point location after Fig. 6.5. The contours exhibited similar flow patterns until the flows from the main and branch channel met. Both of the results had stagnation point at the upstream corner of the junction. However, beyond the junction, the separation zone and contracted flow without the consideration of dispersion terms extended more broadly compared to the result with dispersion terms.

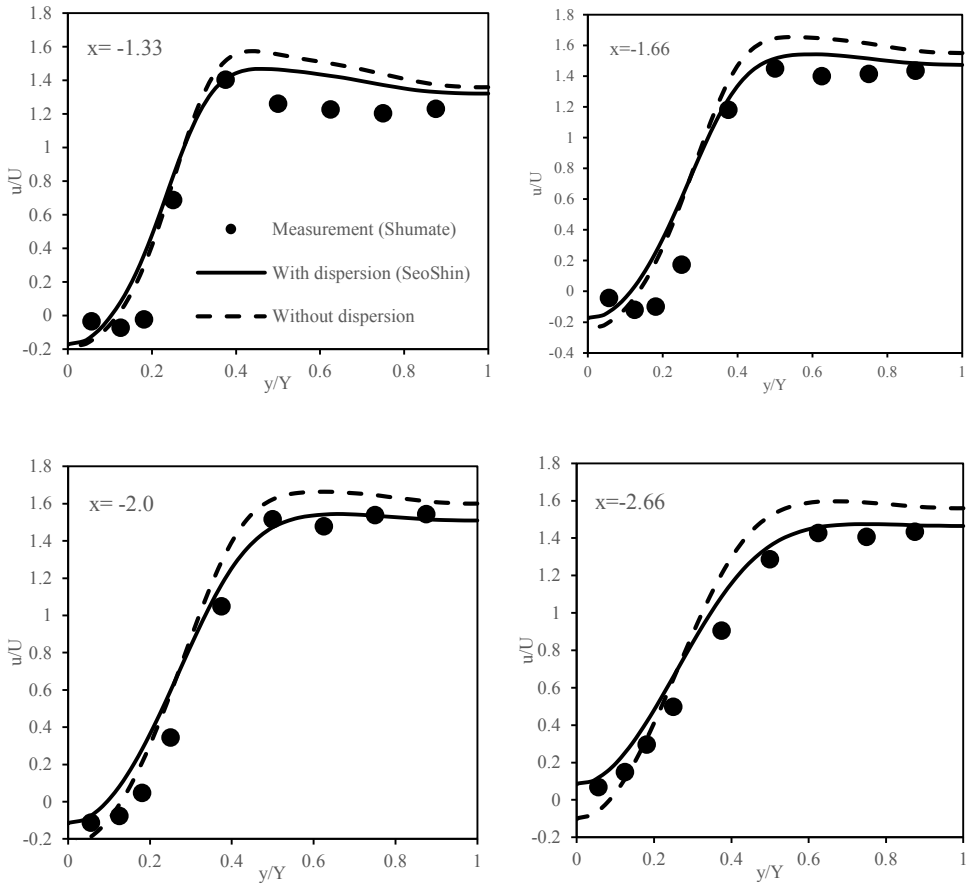

Figure 6.7 Comparison of velocity distribution for simulation and experiment

(Unit: m/s)

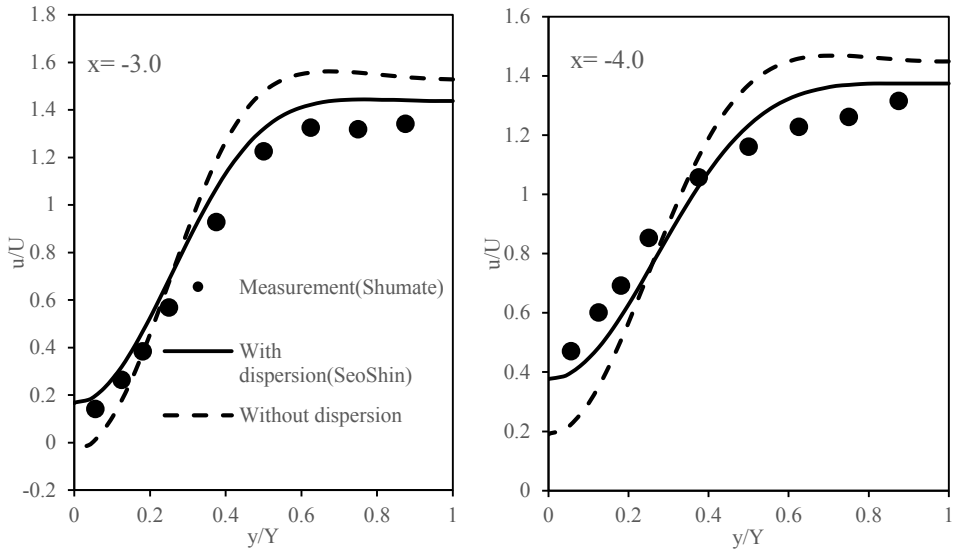

Figure 6.8 Comparison of velocity distribution for simulation and experiment at x=-3.0, -4.0 (Unit: m/s)

6.2.3 Rozovskii Channel

For another validation of the model, the experiment data obtained by Rozovskii (1957) in a U-curved channel was used. Rozovskii collected the velocity data in a sharp bend channel, in which the ratio of width to mean radius-of-curvature was 1.0. It was expected that the experimental results in this channel would exhibit highly 3D flow characteristics, because it was a curve with a width-to-mean radius ratio of 0.4 and more, which is considered to be sharp. The cross-section of the bend was rectangular, and connected to straight inlet and outlet reaches of the same cross-section. The approach channel was 6 m long, while the exit channel was 3 m long. The entire channel was horizontal with a 180 degree bend. The discharge in the channel was 0.0123 m^3/s, and the water depth was 0.6 m.

This experiment showed that there is a gradual increase of transverse circulation at the entrance portion of the bend, and a similar decrease at the second half of the bend, followed by a decay of secondary flow effects at the straight run part of the bend, as shown in the velocity distribution results in Fig. 6.9. The simulated results contained the super-elevation of the flow as it goes through the sharp bend. Fig. 6.10 shows that when the flow enters the bend, the velocity at the inner bank becomes larger, and that at the outer bank becomes smaller. The simulated velocity profile becomes uniform again after a short distance downstream of the bend exit. The figure indicates that the velocity distributions change through the meander as the flow enters the bend due to the secondary flow effect.

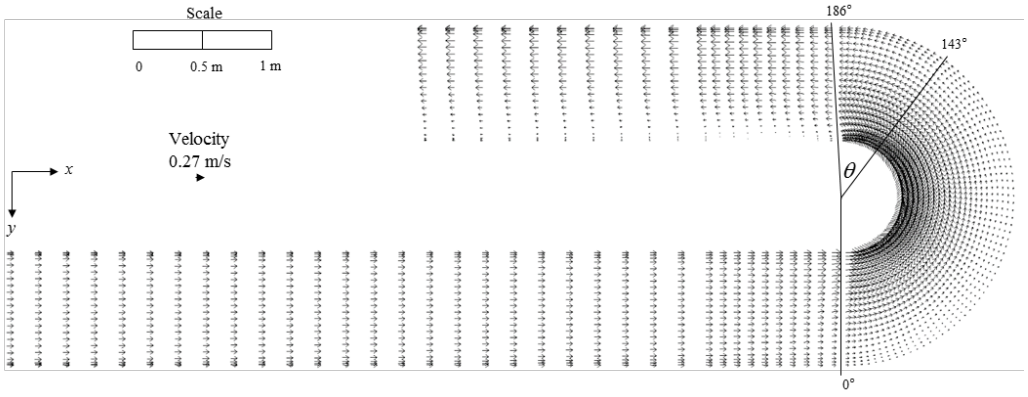

Figure 6.9 Simulated velocity distribution by HDM-2D in the Rozovskii channel

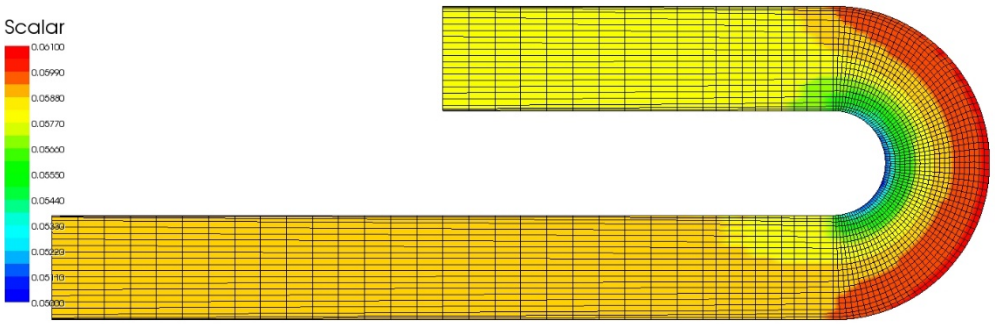

Figure 6.10 Depth contour of the Rozovskii channel by HDM-2D

Fig. 6.11 indicates that due to the secondary flow effect, as the flow enters the bend, the velocity distributions change through the bend. The figure shows the results at degrees 143 and 186, where the secondary current is fully developed, and is exiting out of the bend. This validation conducted comparisons between the experiment results, a model without dispersion stress terms, and models using dispersion stress term using 3 different equations that have linear and nonlinear effects. The linear dispersion stress model using Kikkawa's velocity equation, which excluded the nonlinear effects, seems to overestimate the secondary flow influence in the channel. Also, the dispersion stress method that was implemented using the de Vriend equation in the original HDM-2D displays less changes to the primary flow distribution, compared to the proposed model in this study, as in Table 6.2, which shows it had a smaller mean absolute percentage error (MAPE) than the proposed equation applied model. The MAPE uses the difference between the actual value and predicted value and divides with the actual value and was used instead of the RMSE since the differences were more representable compared to the M2 experiments and vertical velocity profile comparisons which had low MAPE differences. The error results show that the primary flow distribution can be better reproduced by the proposed model than the simulations without the dispersion stress term, or the simulation with the dispersion stress term using the de Vriend equation, or the linear dispersion stress term for the transverse velocity profile.

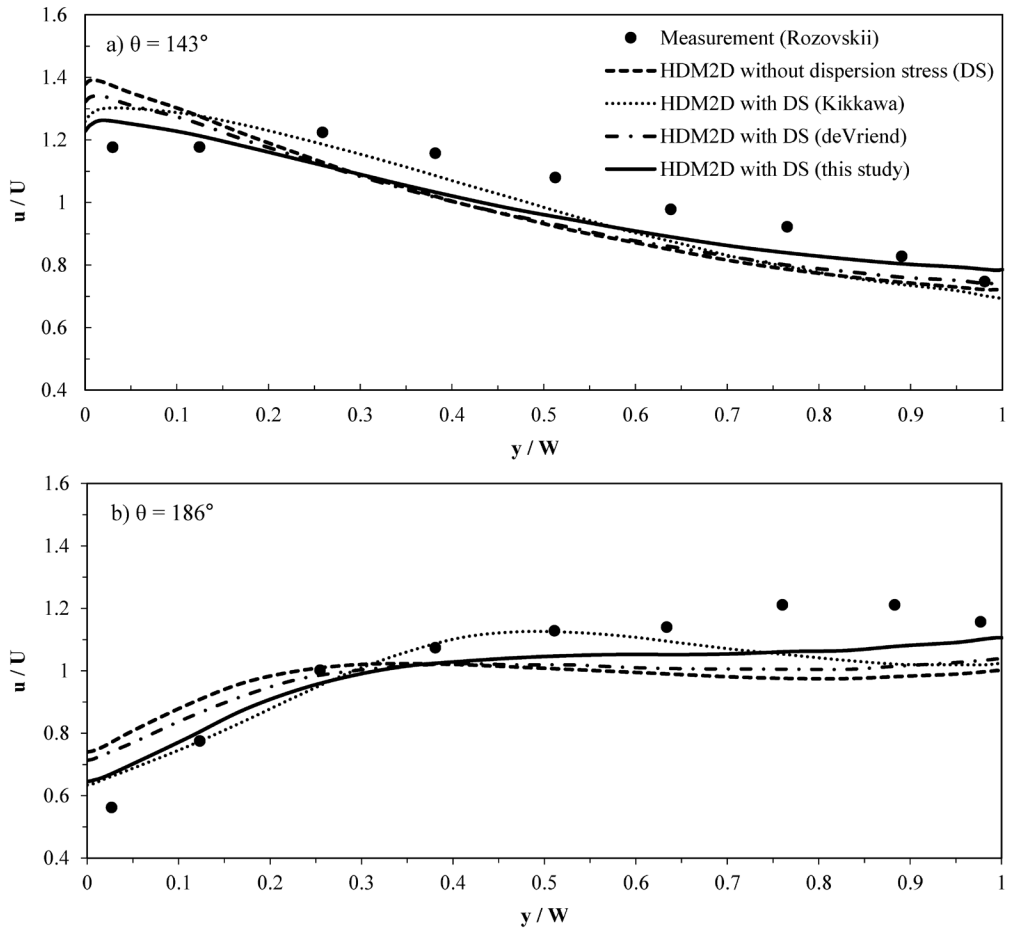

Figure 6.11 Comparison of simulated velocity distribution with experimental data

Table 6.2. Rozovskii channel data comparison with HDM-2D dispersion stress by MAPE

Model / Degree	143°	186°	Average
Without DS	8.7 %	16.2 %	12.5 %
With DS (Kikkawa,	8.3%	11.3%	9.8 %
With DS (de Vriend,	7.6 %	14.3 %	10.9 %
This study	5.6 %	10.4 %	8.0 %

6.3 REC Channels

The dispersion stress model incorporated with the proposed velocity profile was tested against the experimental data obtained from the REC meandering channel. Both river survey data and the depth data measured using ADCP were used for the mesh generation of the 2D numerical model, HDM-2D. Since the measurements were taken as a continuous boat-moving area, the averaging of the sections were done by spatial averaging, with a span and width interval of 0.1 m. First, a digital surface map of the A315 channel was created with drone-captured images to create the mesh for the model such as Fig. 6.12 and 6.13. Although the meandering channel was originally constructed to be a trapezoidal section, continuous experiments caused the channel to change to a more natural form with erosion and deposition around the banks, as shown in Fig. 6.14. Then the mesh generation of the meandering channel was completed using the surface elevation map.

The results of the experiment showed that the secondary flow affects the velocity distribution in strong meandering channels. The peak of the velocity was located at the outer part of the bend, which is expected in natural meandering channels. This could be found where 1.7 sinuosity channel seemed to have the velocity distribution more skewed to the outer bend than the 1.5 sinuosity channel. To find the effect of the dispersion stress on the flow modeling, the experimental results were compared with the modeling results that have dispersion stress term and no dispersion stress term.

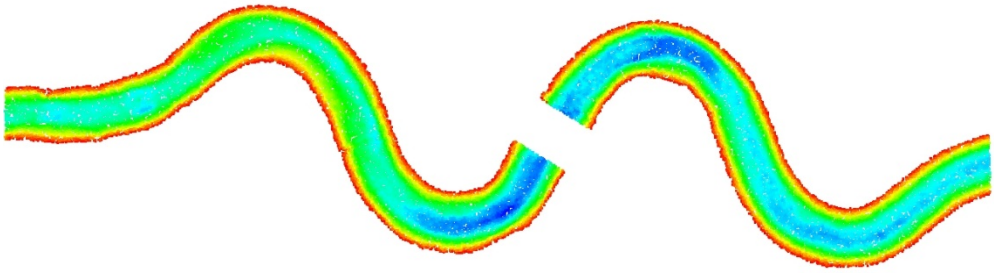

Figure 6.12 Elevation of the meander channel by drone capture and image processing

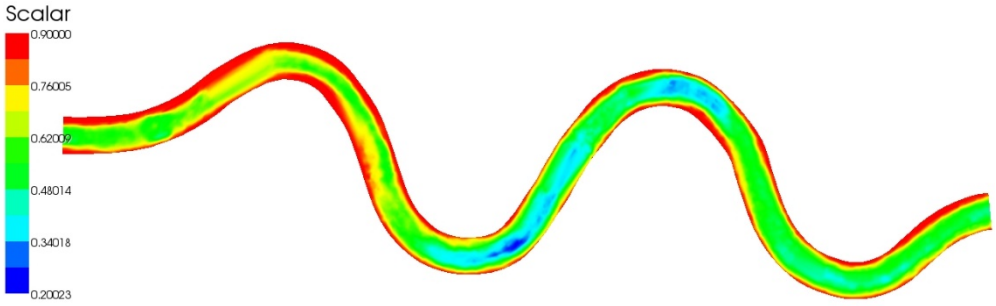

Figure 6.13 Meander mesh generation and elevation of sinuosity 1.5

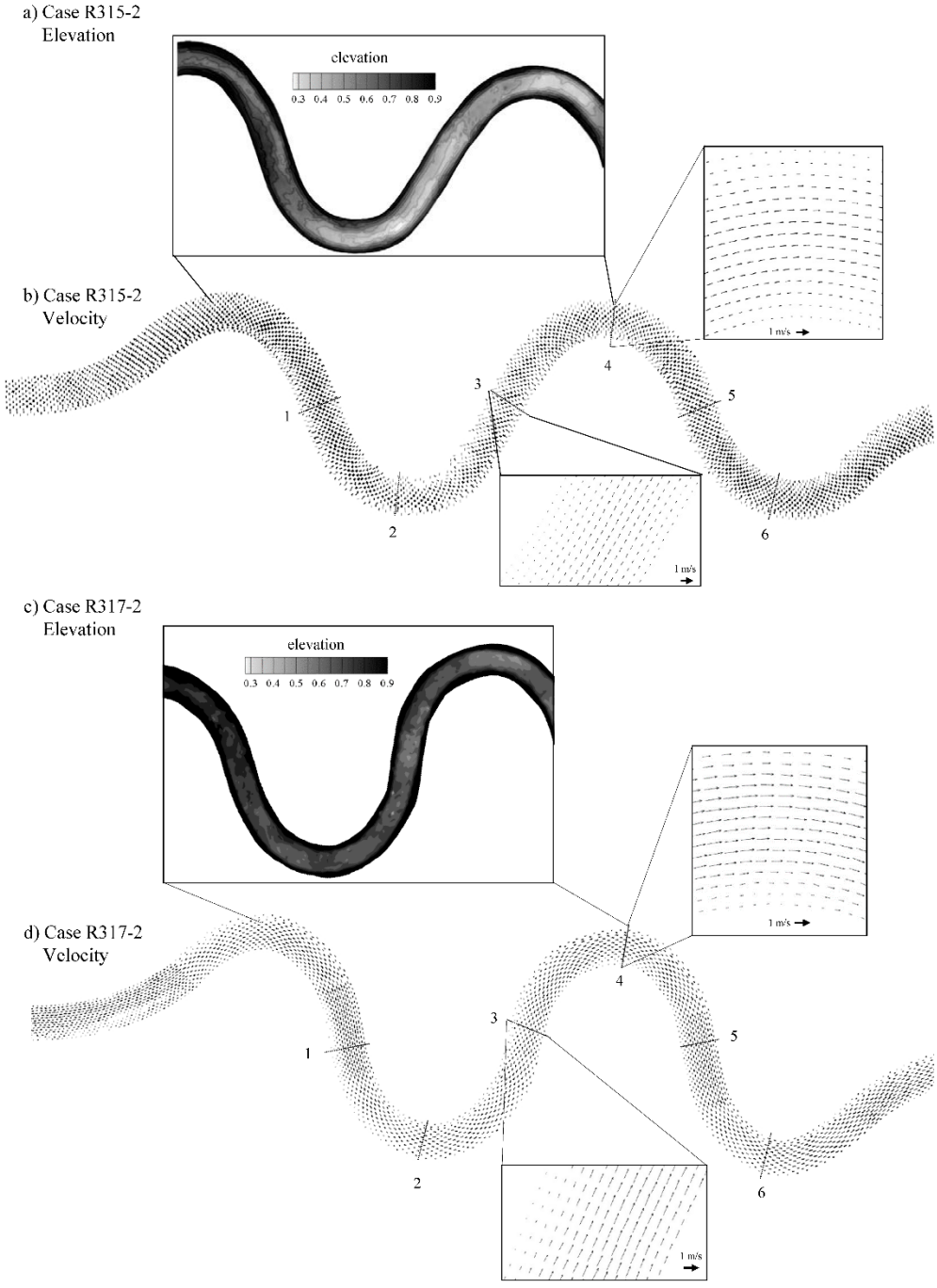

6.14 Computed velocity distributions in the REC meandering channels

The maximum primary velocity was developed along the thalweg line, and most of the even number sections located at the apex had the primary velocity distribution skewed toward the outer bank due to the secondary flow effect, as shown in Figs. 6.14(b) and (d). For the odd number sections, the position of the maximum primary velocity was affected by the upstream section, due to the history effect of the secondary flow. This history effect was considered to have arisen by the phase lag between the channel centerline and the discharge centerline or thalweg line (Chang, 1988). Figs. 6.15 and 16 show comparisons of the simulation by HDM-2D model with the measured data, in order to closely demonstrate the applicability of the dispersion stress term with the proposed equation to the transverse velocity. For both A315 and A317 channels, agreements between the measured data and the simulation are generally good. The HDM-2D models with the dispersion stress terms included produced the primary flow distribution that would be closer to the measured experimental results, which is more skewed towards the outer bank. Table 6.3 summarizes the results of the quantitative analysis between the experimental data and the numerical simulation, which was done specifically at the meander apex of the bends. This table shows that the dispersion stress decreases the MAPE, compared to the simulation without dispersion stress. The dispersion stress term skewed the primary distribution toward the outer bank in the apex sections, which is similar to the measured results. Overall the results show that the dispersion stress model with the proposed velocity profile could reproduce the secondary current effect in sinuous channels quite well.

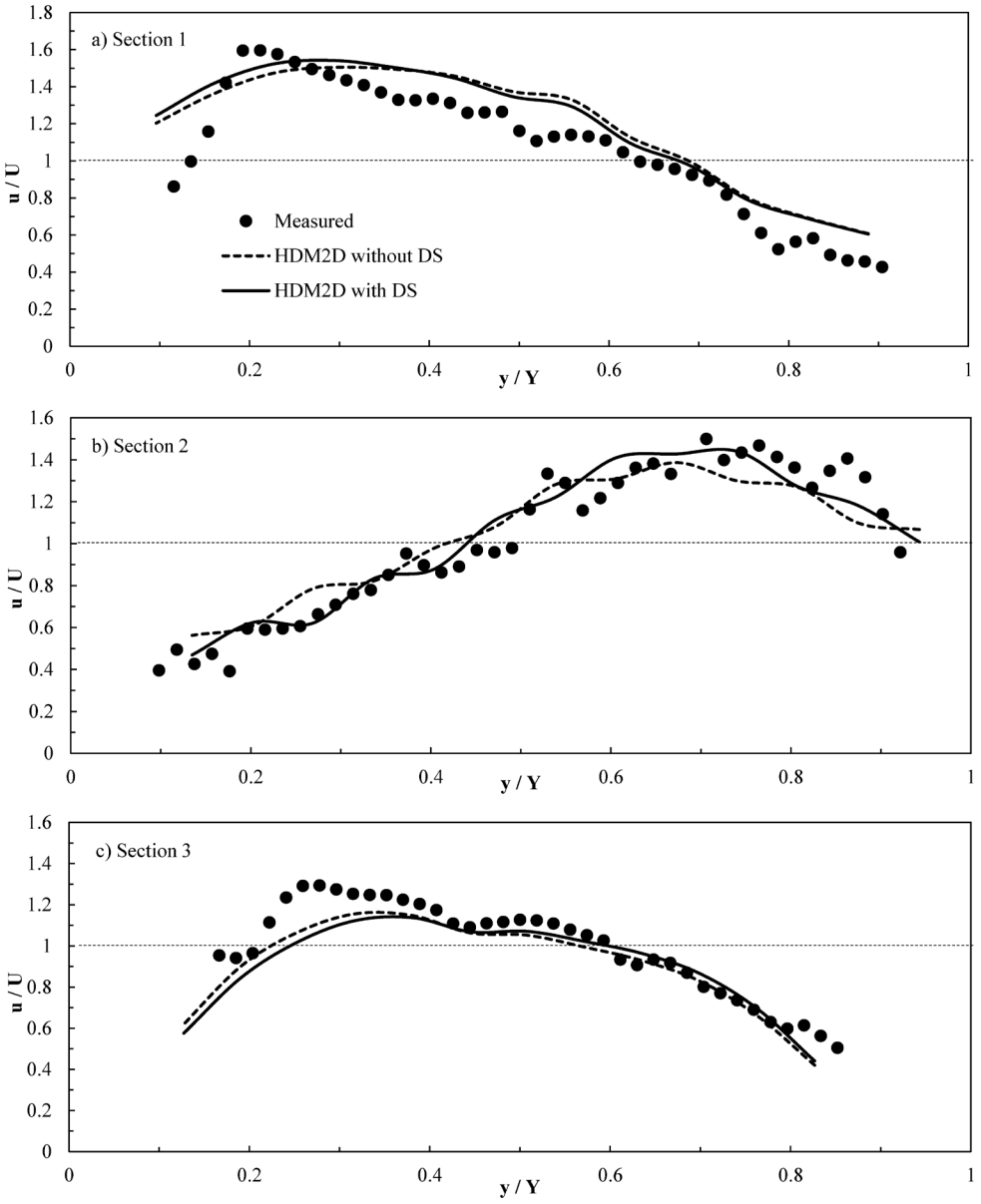

Figure 6.15 Comparison of simulated velocity distributions with measured data

Case R315-2

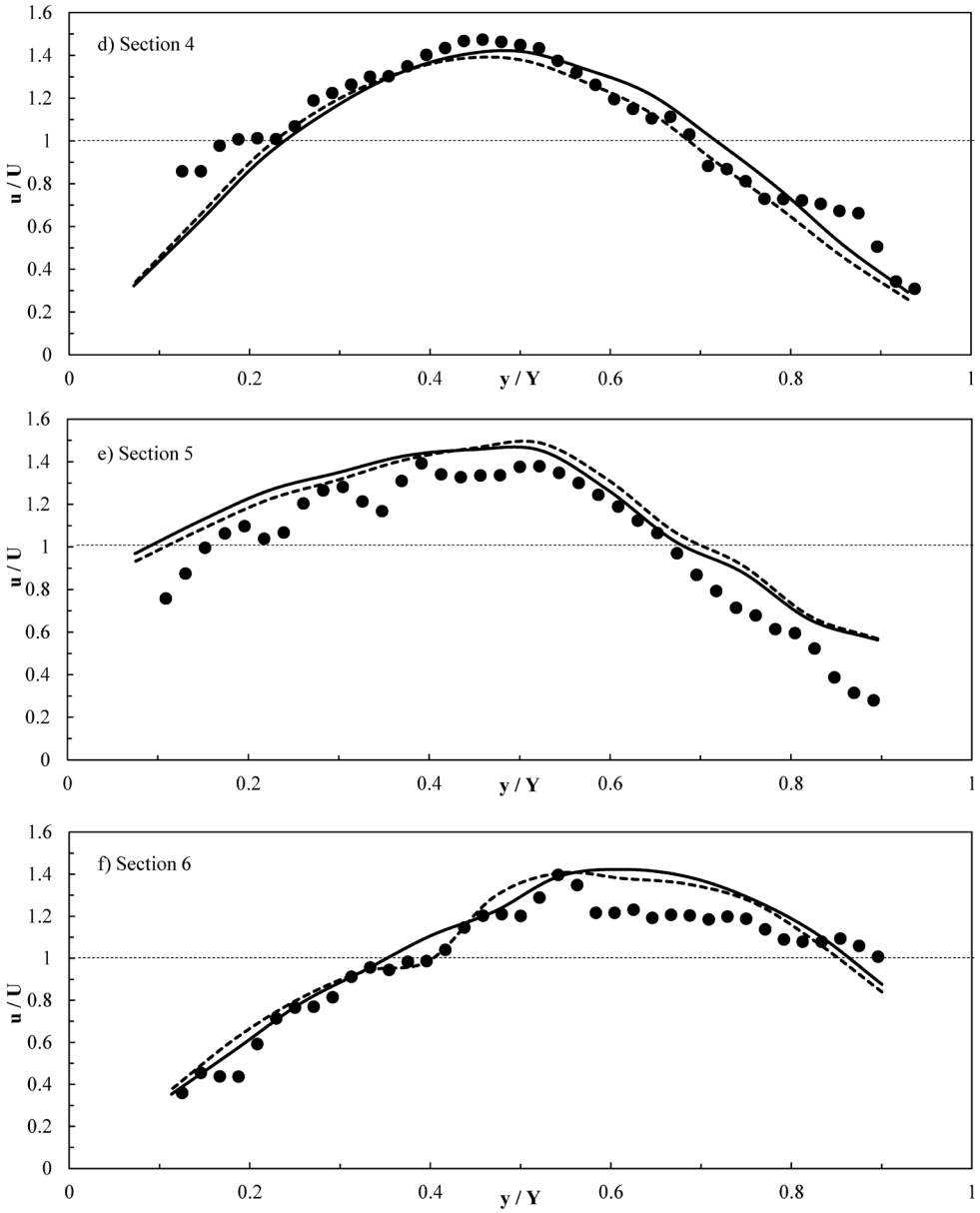

Figure 6.15 Comparison of simulated velocity distributions with measured data

Case R315-2 (cont)

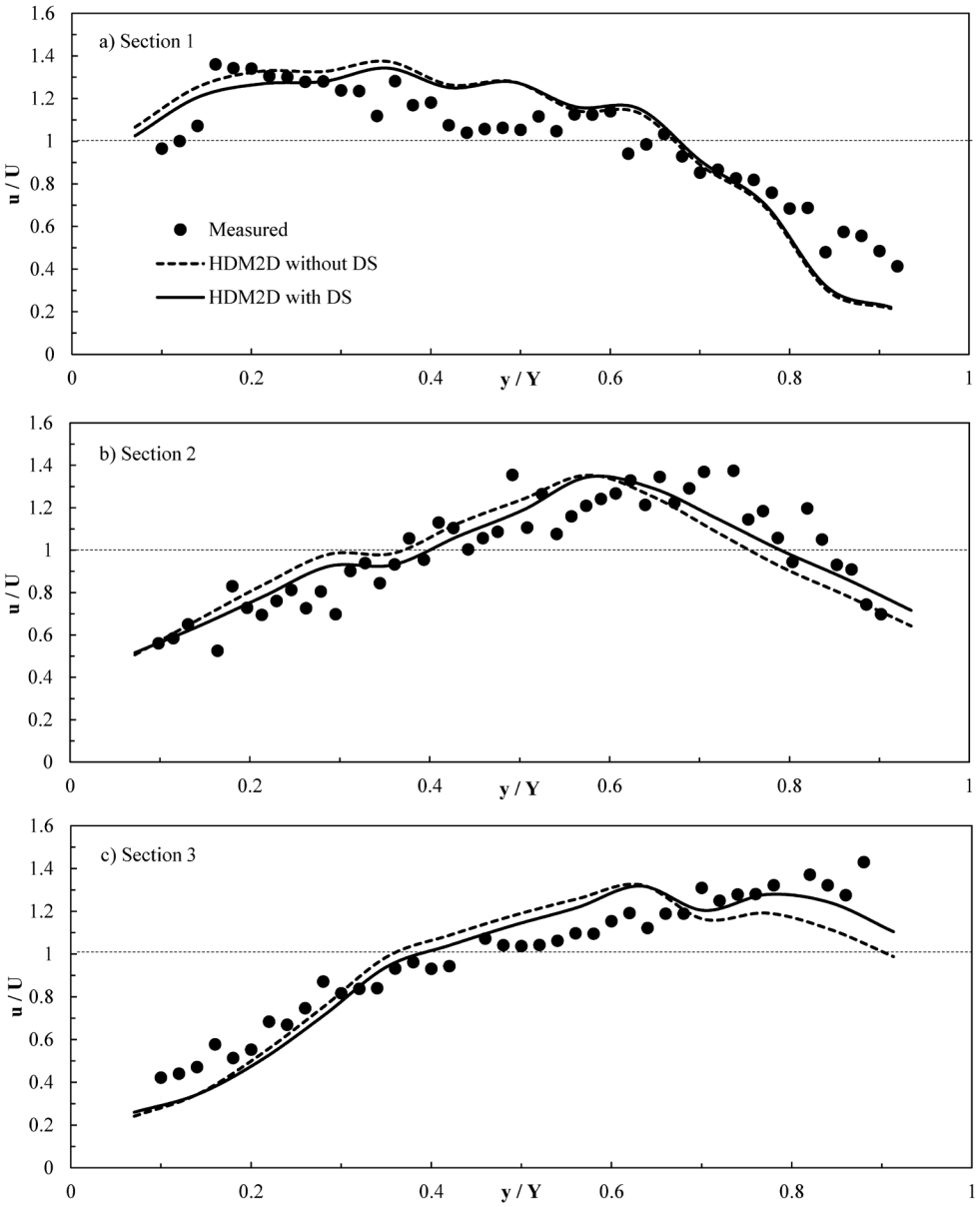

Figure 6.16 Comparison of simulated velocity distributions with measured data

Case R317-2

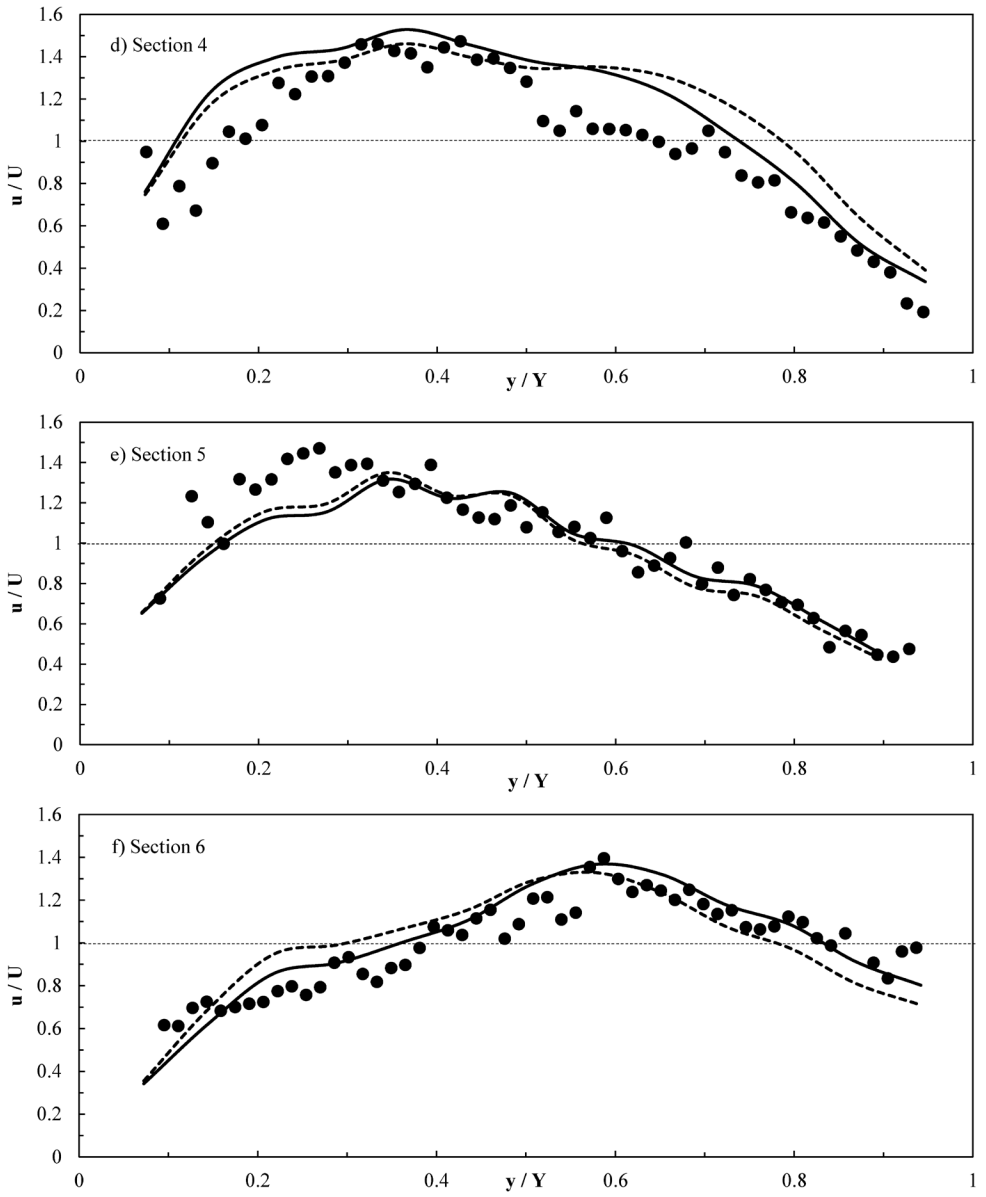

Figure 6.16 Comparison of simulated velocity distributions with measured data

Case R317-2 (cont)

Table 6.3 Average MAPE of HDM-2D simulations

Case	R315-1	R317-1	R315-2	R317-2	Average
Without DS	10.2 %	15.0 %	11.5 %	14.8 %	12.9 %
With DS	8.1 %	11.8 %	9.4 %	12.4 %	10.4 %

6.4 Application to Virtual Meandering Channels

As aforementioned the results of the experiments in the REC meandering channel showed that the secondary flow affects the transverse distribution of the primary flow velocity. As shown in the above research, the maximum longitudinal velocity was located at the outer part of the bend, Thus, it is postulated that sinuosity is one of the variables that affects the strength of the secondary current and one can find tendency that the distribution is more skewed to the outer bend when the sinuosity increased. For closer analysis and investigation of the effects of the channel sinuosity to the primary flow distribution in HDM-2D modeling, artificially designed meandering channels with higher sinuosity were created using the sine-generated curve, which is the same method as used to construct the REC meandering channel of KICT. The following equation was used for the sine-generated curve (Chang, 1988).

$$\phi = \omega \sin\left(2\pi \frac{S}{M}\right) \tag{6.6}$$

where ϕ is the angle of channel path, ω the maximum angle of deflection, M is the streamwise distance in the meander period, and S is the distance in the streamwise direction. Thus, the virtual meandering channels with the sinuosity 2.0,

2.5, 3.0 were created as shown in Figure 6.17 with the HDM-2D flow results. The meander path of the virtual meandering channels are all symmetrical, and thus might be different from the meander path of the natural meandering rivers (Chang, 1988). For the cross section of the artificial channel, a beta function proposed by Seo and Baek (2004) was used to create the bed elevation similar to natural channels.

$$\frac{h}{H} = \frac{\Gamma(\alpha' + \beta')}{\Gamma(\alpha')\Gamma(\beta')}(y')^{\alpha'-1}(1-y')^{\beta'-1} \tag{6.7}$$

where Γ as the gamma function; α, β are real number parameters controlling the shape of the channel section; y' as the dimensionless lateral location point; h/H as the dimensionless ratio of the depth at location point. When α and β are equal, the section becomes symmetrical and become more skewed as the difference increases.

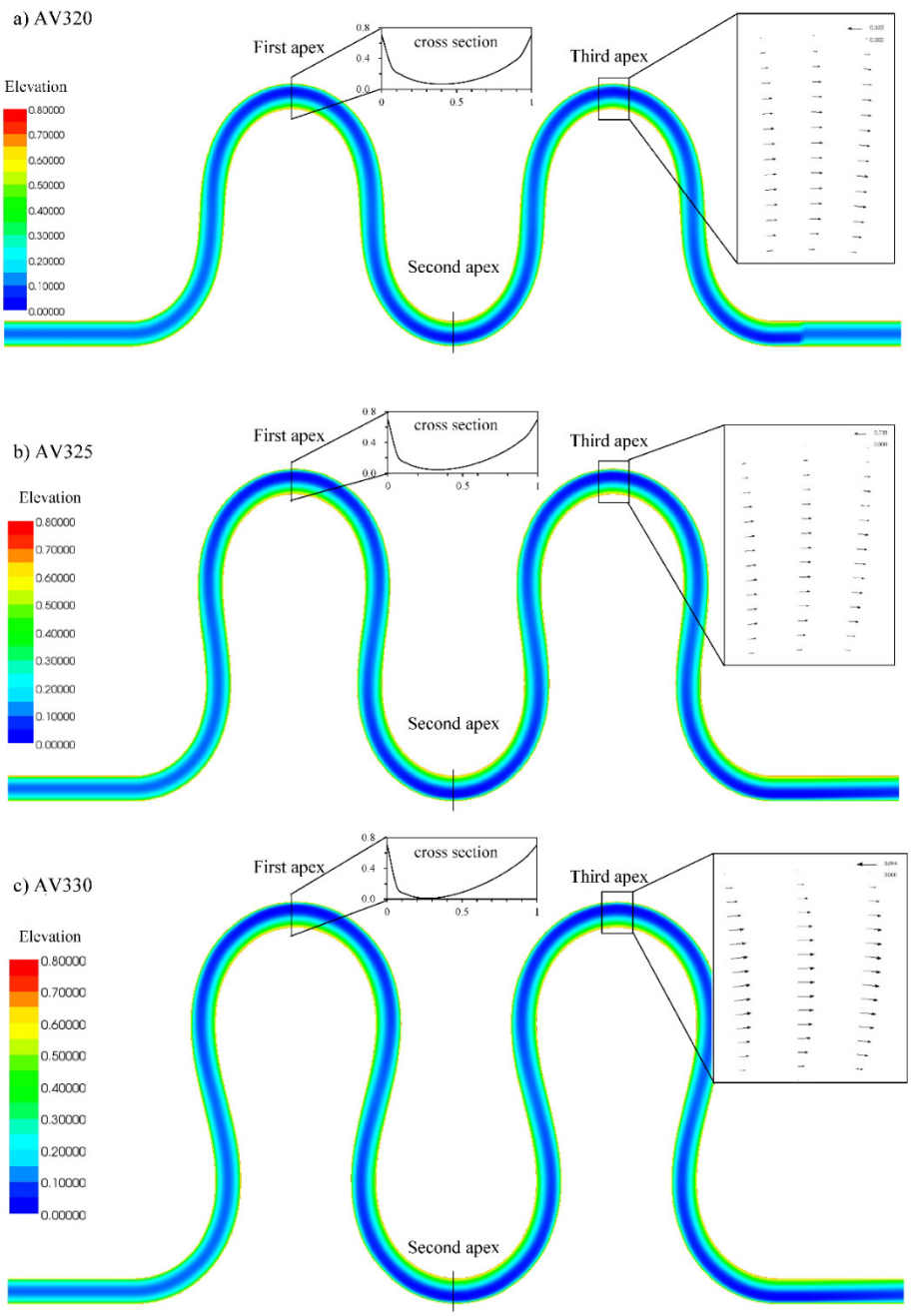

Fig. 6.17. Simulated velocity distributions and elevation for AV320, AV325, and AV330

The HDM-2D was employed for this simulation for similar boundary conditions such as A315 and A317 of the REC meandering channel for a comparison of sinuosity effects in the flow distribution and dispersion stress. Figure 6.18 shows the simulated results of HDM-2D model using dispersion stress showing primary flow distribution for the virtual meandering channels as well as real channels. The dispersion stress model results show that the higher sinuosity tended to increase the skewness of the primary flow distribution in comparison of each second apexes. This is assumed to be that the secondary flow strength increased with increase of sinuosity, which resulted in higher skewness and a result characteristic similar to Figure 4.10 which used actual measured results from the REC meandering channels. The apex 2 showed the largest difference between the dispersion stress model and the non-dispersion stress model and this is assumed to be the effect of meanders that are located at the first and third apex. Whether apex 1 and 3 are the entrance and exit apexes the second apex located at the middle have effect from both meanders, and the history effect is of account at this virtual experiment. This shows that the HDM-2D with the dispersion stress term could show the effects of sinuosity to represent actual channels. Although this was not an actual experiment, it is a result which could show a tendency in sharp channels and is a topic for further examination and study.

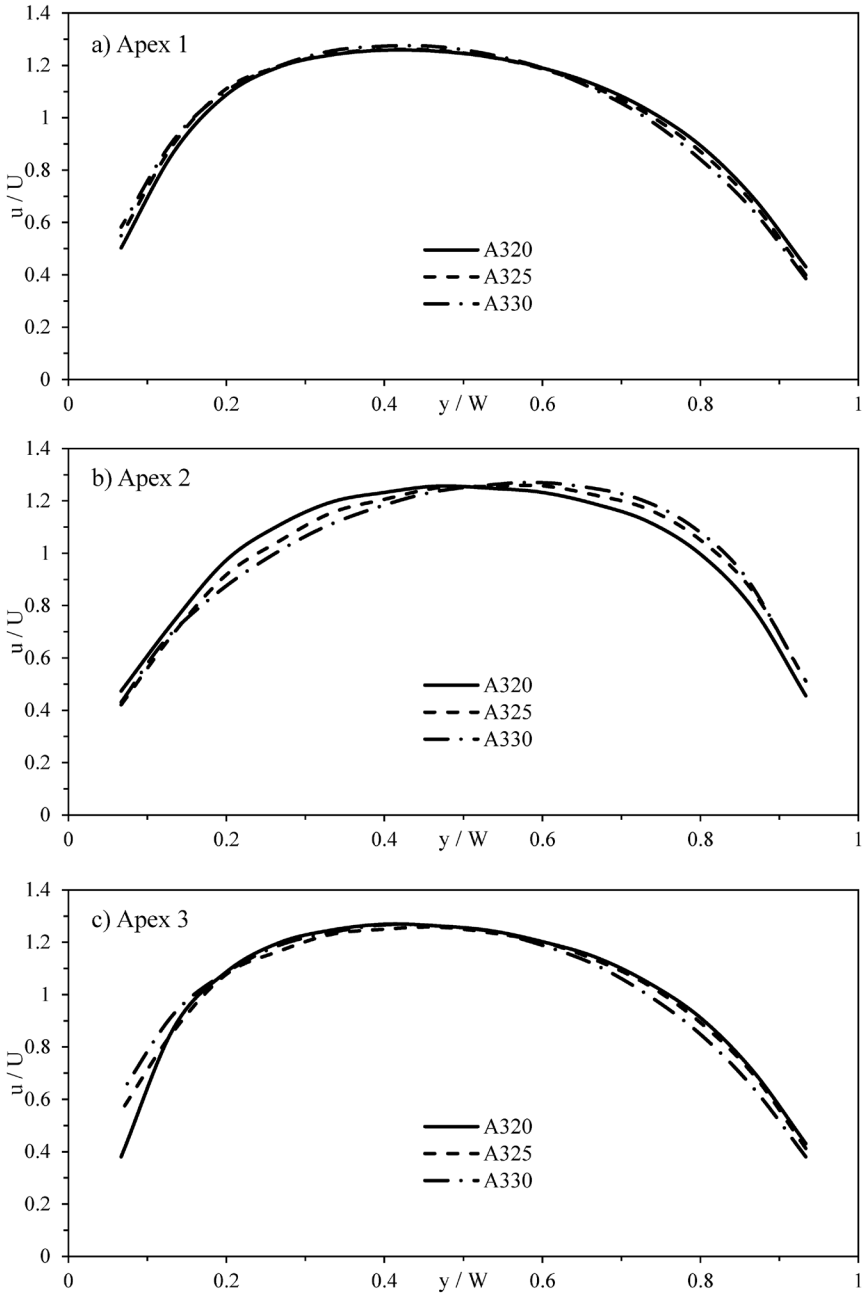

Fig. 6.18 Transverse distribution of primary flow bend apexes of each simulated channel

Chapter 7. Derivation of Dispersion Coefficients

7.1 Dispersion Coefficient Derivation using Velocity Profile

The ADCP velocity measurements of the KICT REC had vertical profiles and its deviations were to be used for dispersion coefficient calculation. Fischer et al. (1979) equation based on Taylor (1954) was used for the triple integration of the measured velocity data in each section for the depth averaged shear dispersion tensors for two-dimensional mixing. Since the ADCP has a blanking distance in the upper areas of the water body and reflecting influences in the bottom of the channel distorts the Doppler effect, the results at the bottom are also discarded. Therefore for triple integration of the velocity deviations for the dispersion coefficient calculation, an extrapolation method was needed for the accurate representation of the actual longitudinal velocity profile.

Several extrapolation methods were taken into consideration, and for this purpose the power law of 1/7 was used for the longitudinal vertical profile estimation. The 1/7 power law was used frequently in many discharge calculations in ADCP software and is one of the recommended extrapolation method of vertical profiles in ADCP manuals by USGS (2012). The variation of the methods of extrapolation could cause uncertainty on the result of dispersion calculation (Lee and Seo, 2013). In the case of longitudinal transport in 1D, the effect of vertical profile was minimal compared to the transverse profile (Schwab and Rehmann, 2015). To find the differences between the vertical profiles of the longitudinal flow, this research

compared the measured velocity data between power law and log profile in the mid-channel of the even sections. The result showed that there is little difference and both profiles are similar, so the 1/7 power law was mainly used in later calculations. Whereas, the transverse velocity profile did not use additional extrapolation, since the data from former laboratory experiments show that the highest and lowest part of the water body in open channel flows have smaller transverse flow and the possibility of overestimation was at stake. Therefore the selection of the extrapolation method should depend according to the experiment conditions, and comparison with other methods could be necessary.

To use the equation by Fischer to calculate the dispersion coefficient, it contained a value for the vertical turbulent diffusion coefficient, and the momentum based on the logarithmic law velocity profile was selected as below (Fischer, 1979) for calculation of Eq. (7.1),

$$\varepsilon_v = \kappa d u_* (z/d)\left[1-(z/d)\right] \tag{7.1}$$

where κ is the von Kármán constant. d is the local depth of the channel, u_* is the shear velocity, z is the vertical point of depth.

The calculation results for the longitudinal dispersion coefficients had similarity with the velocity magnitude in each sections shown in Figs. 7.1-7.2. This was due to

the reason that the higher velocities tend to have larger velocity deviation from the mean velocity for the triple integration used for the dispersion calculations also shown in Lee and Seo (2013). Since the bottom velocities tended to become near zero in the water body, the higher the longitudinal velocity was, the larger the vertical profile also became and the velocity deviations from the mean also increased accordingly. This was also noted in Lee and Seo (2013), where the maximum point of the longitudinal dispersion was located at the near bank of the apex where the maximum velocity was located, which was due to the rectangular shapes of the laboratory flume. In the KICT REC in this experiment, the maximum point of longitudinal dispersion was located more to the outer bank of the apex, since the sinuosity and natural channel shape led the point of maximum velocity more to the outer side of the apex. This was due to the secondary current developed in the apex of channel, although the first apex had the effects of the first meander only, while the second and third apexes had the effects of the former meander also affecting the secondary currents, so the maximum point was shifted near the middle of the channel which was also similar to the longitudinal dispersion coefficients.

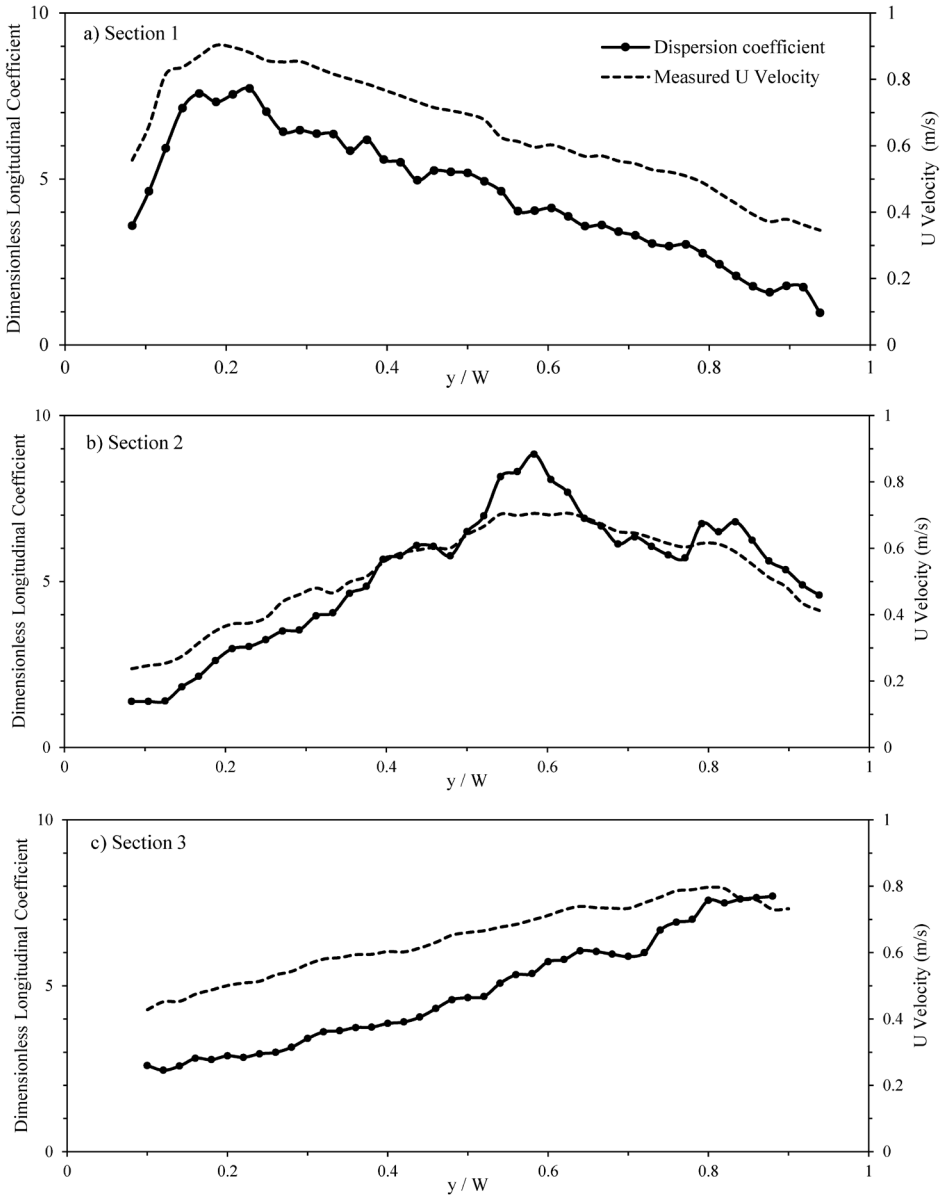

Figure 7.1 Longitudinal dispersion coefficients from Case R315-2

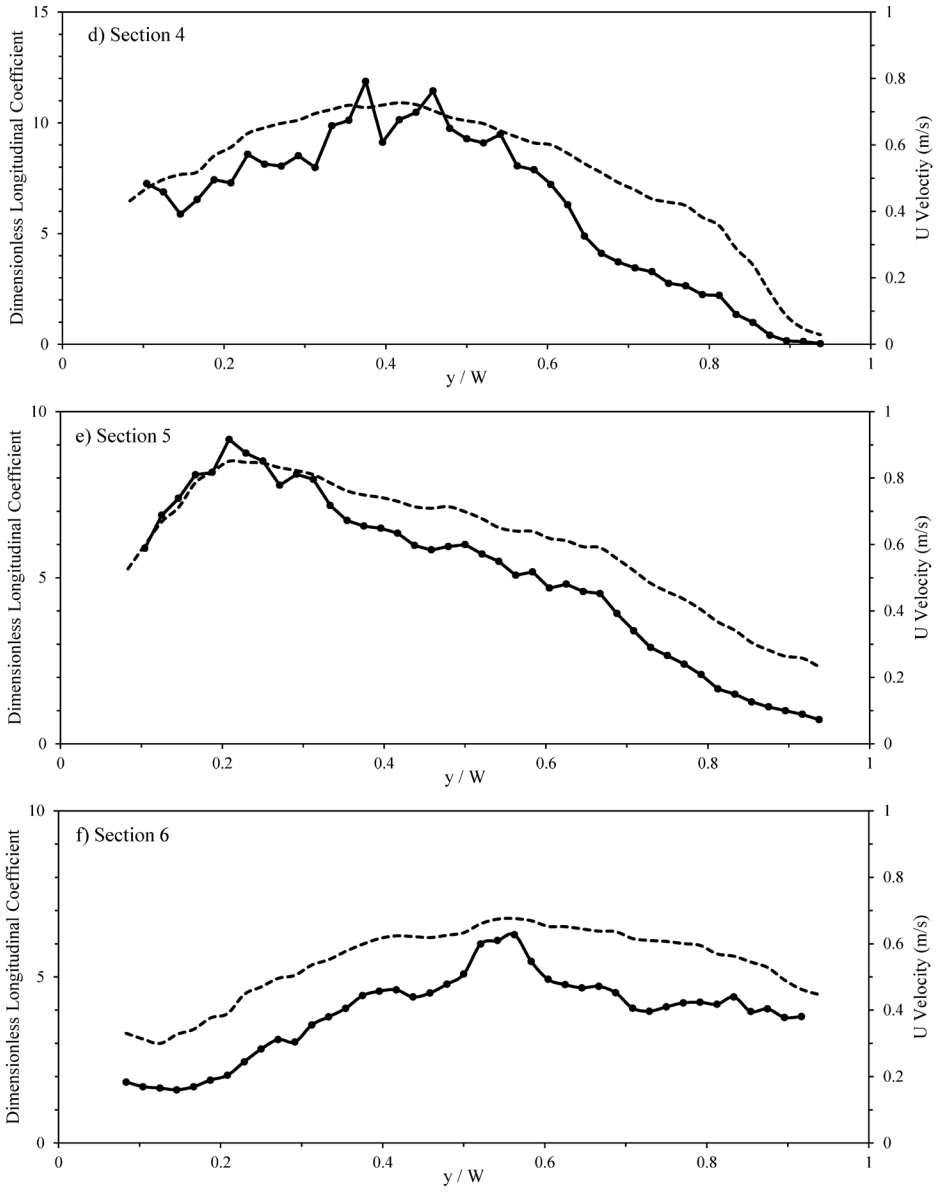

Figure 7.1 Longitudinal dispersion coefficients from Case R315-2 (cont)

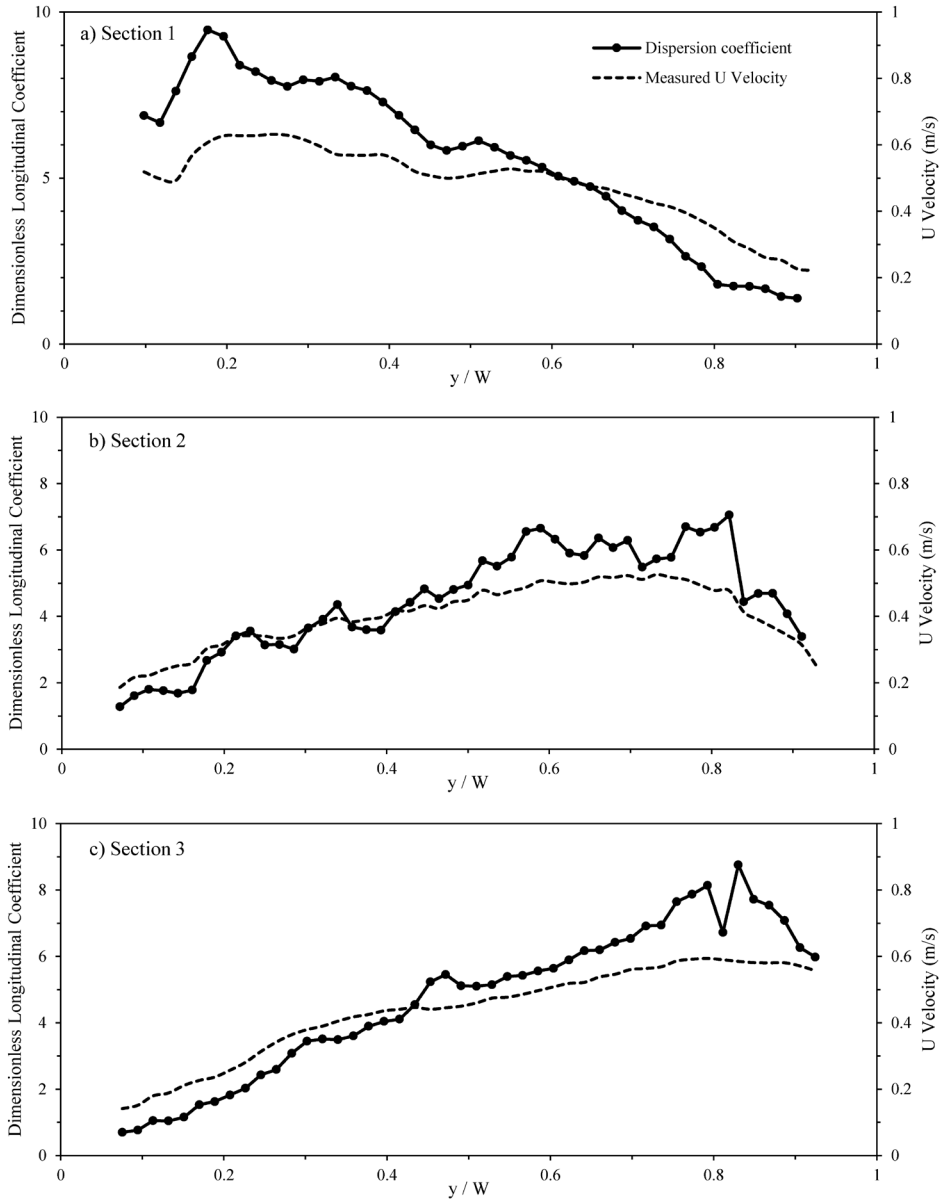

Figure 7.2 Longitudinal dispersion coefficients from Case R317-2

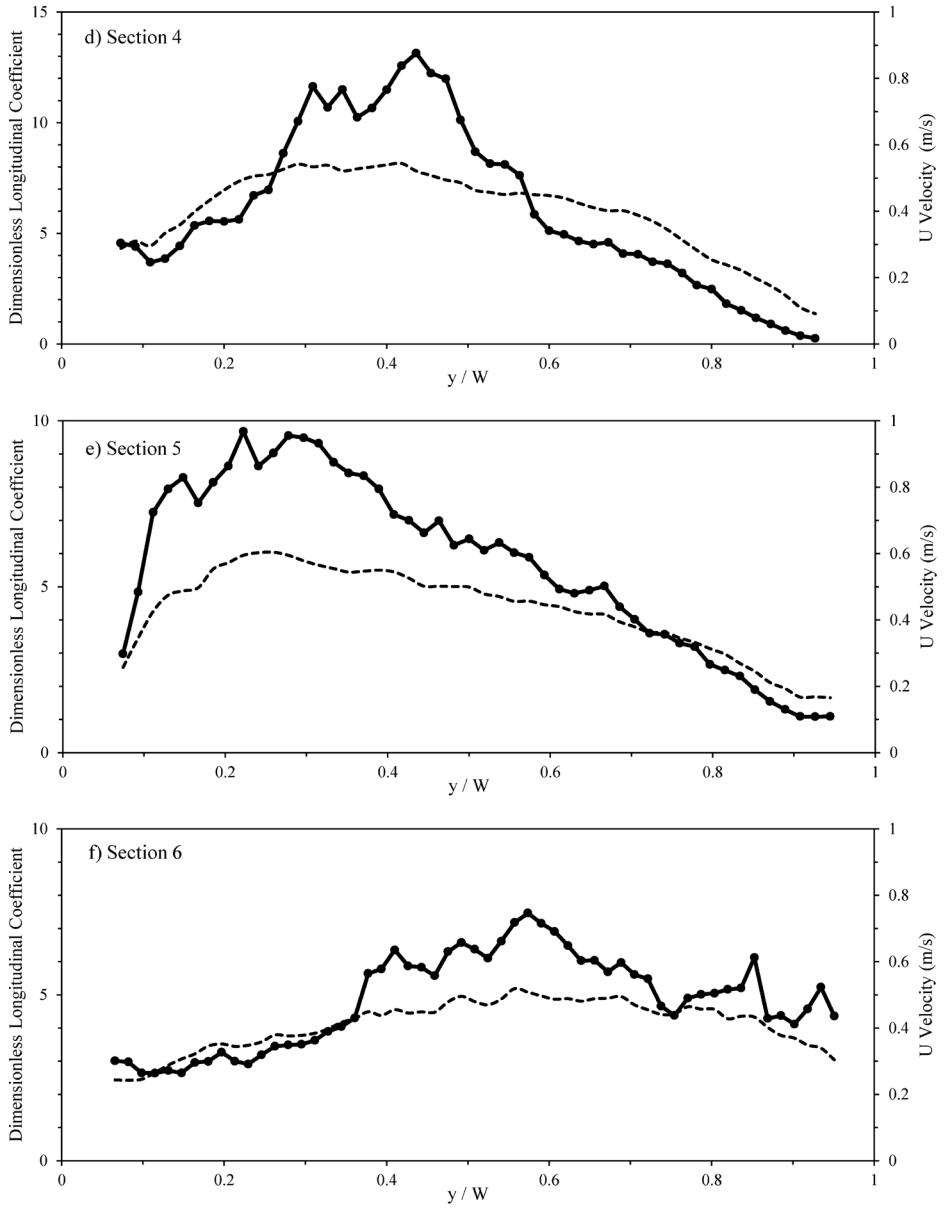

Figure 7.2 Longitudinal dispersion coefficients from Case R317-2 (cont)

The transverse dispersion coefficient calculation results in Figs. 7.3-7.4 showed the maximum point was located near the outer bank at the first apex as in section 2, while in later apexes the maximum point was near the middle of the channel. This characteristic was similar to the longitudinal dispersion coefficients but the points were nearer to the center of the channel. It showed that the sections at the middle of the apex as in the odd sections showed clearly less values than the dispersion coefficients in the apexes as in even sections; and this was different from the longitudinal dispersion coefficients which still showed high values even at the odd sections between the apexes. The research analysis shows that instead of the absolute size of the velocity, the deviation of the velocity was more important in calculating transverse coefficients than longitudinal coefficients. Since longitudinal velocity was a power form with the highest value toward the top of the water body and zero near the bottom of the channel, the mean value became larger with increased velocities. However, in the case of transverse velocities the mean value was near zero at most points of the channel, and only a slight change occurred in the apex of the channel. Therefore, the deviations were increased more at the pinnacle of the channel curvature, whereas in the mid sections the deviations decreased so the transverse dispersion coefficients also decreased greatly. This situation was somewhat similar to the former laboratory experiment in Lee and Seo (2013) where the apex areas showed definitely higher values than the mid sections, but the position of the maximum values were different, as this research was conducted in a near-natural channel with different water depths overall, while the former experiment results had the same depth throughout the channel.

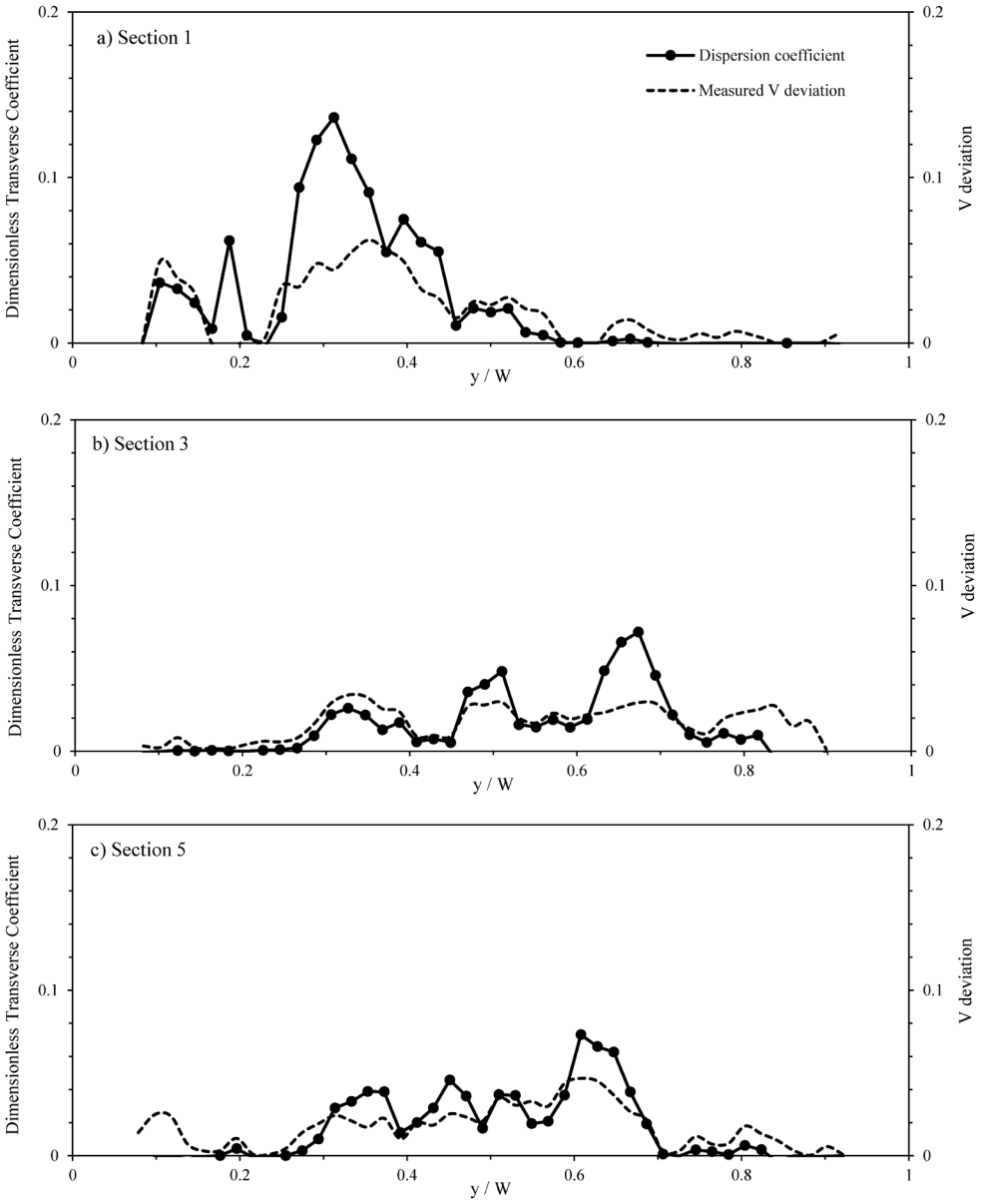

Figure 7.3 Transverse Dispersion coefficients from R315-2 mid apex

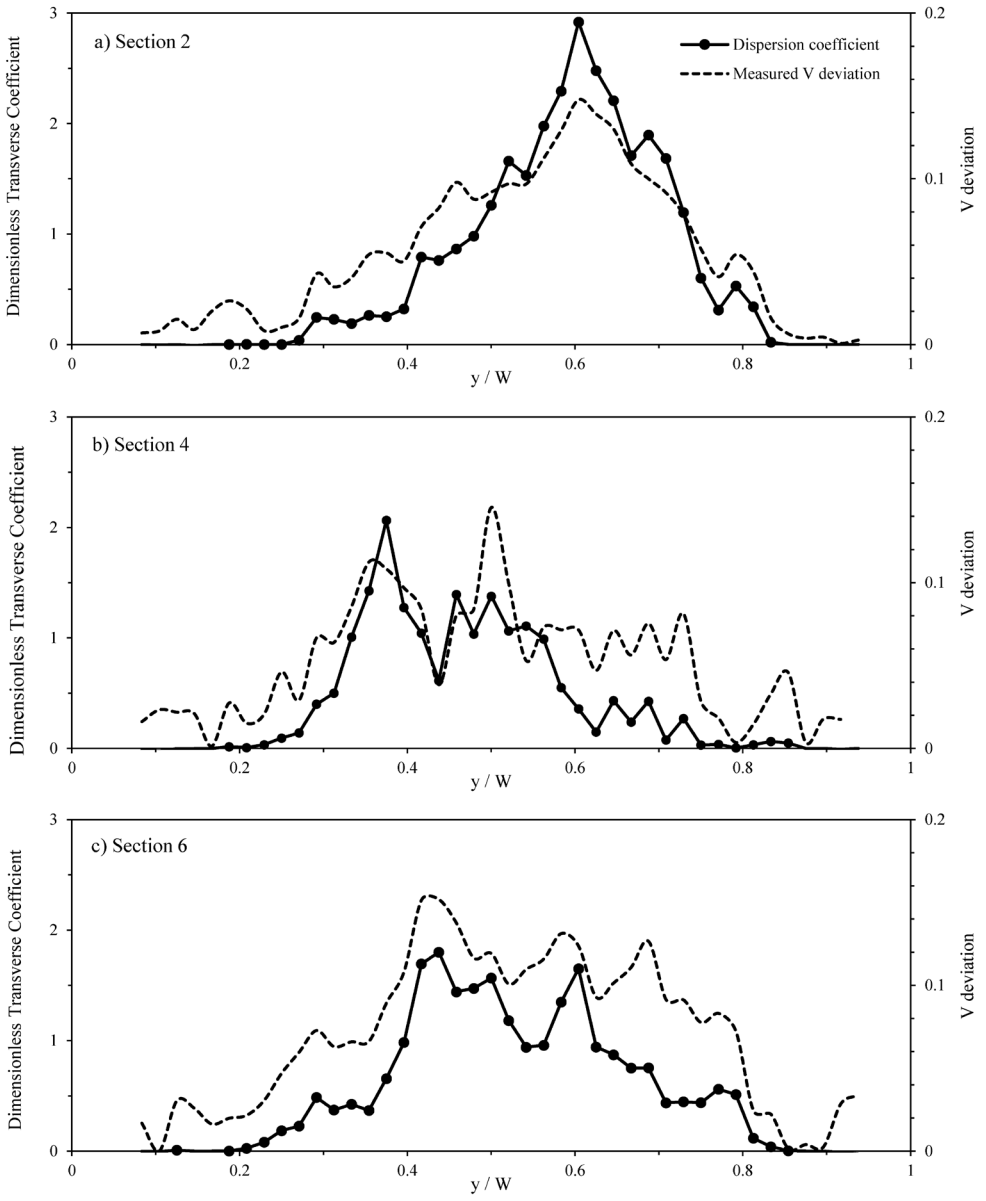

Figure 7.3 Transverse Dispersion coefficients from R315-2 apex (cont)

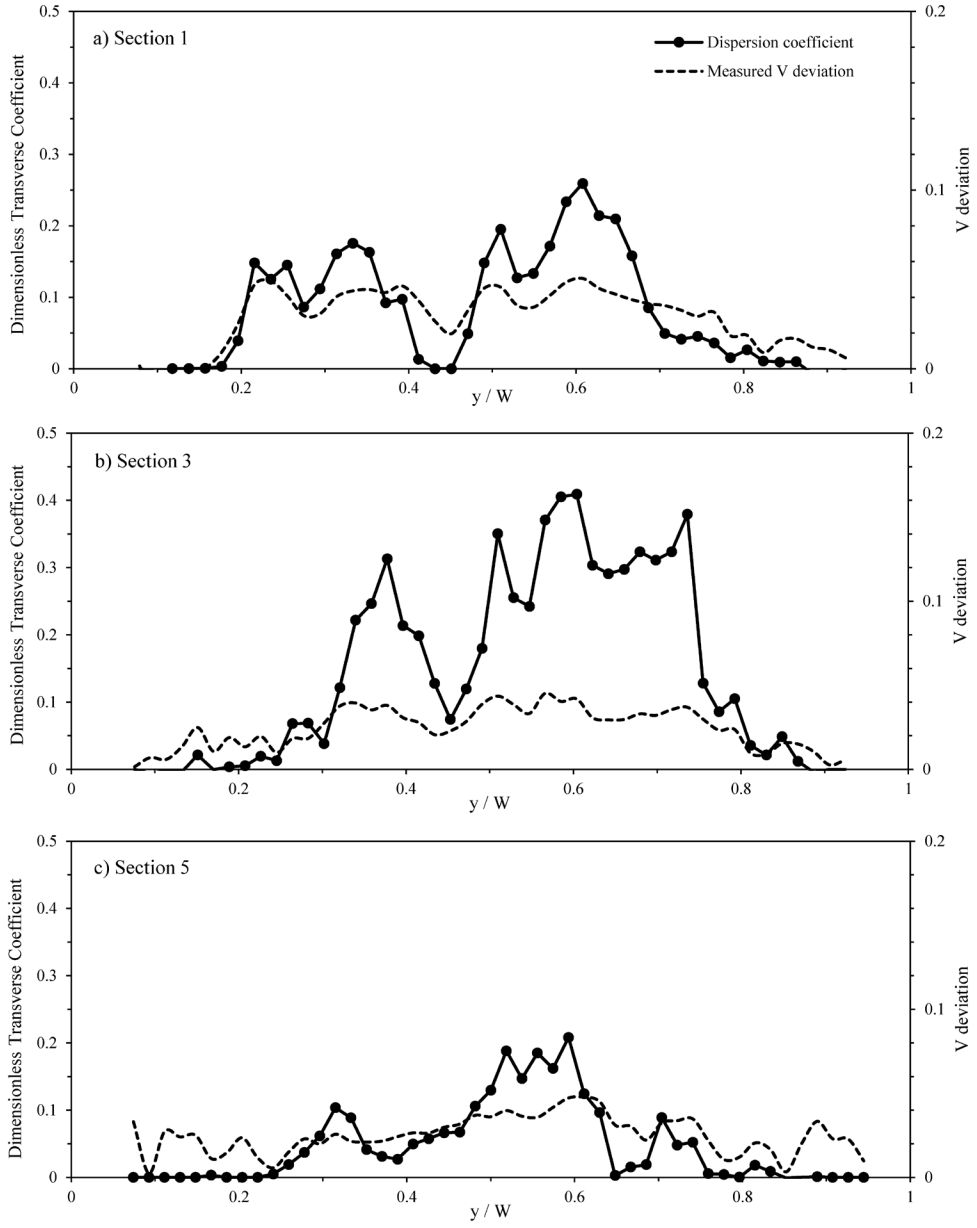

Figure 7.4 Transverse Dispersion coefficients from R317-2 mid apex

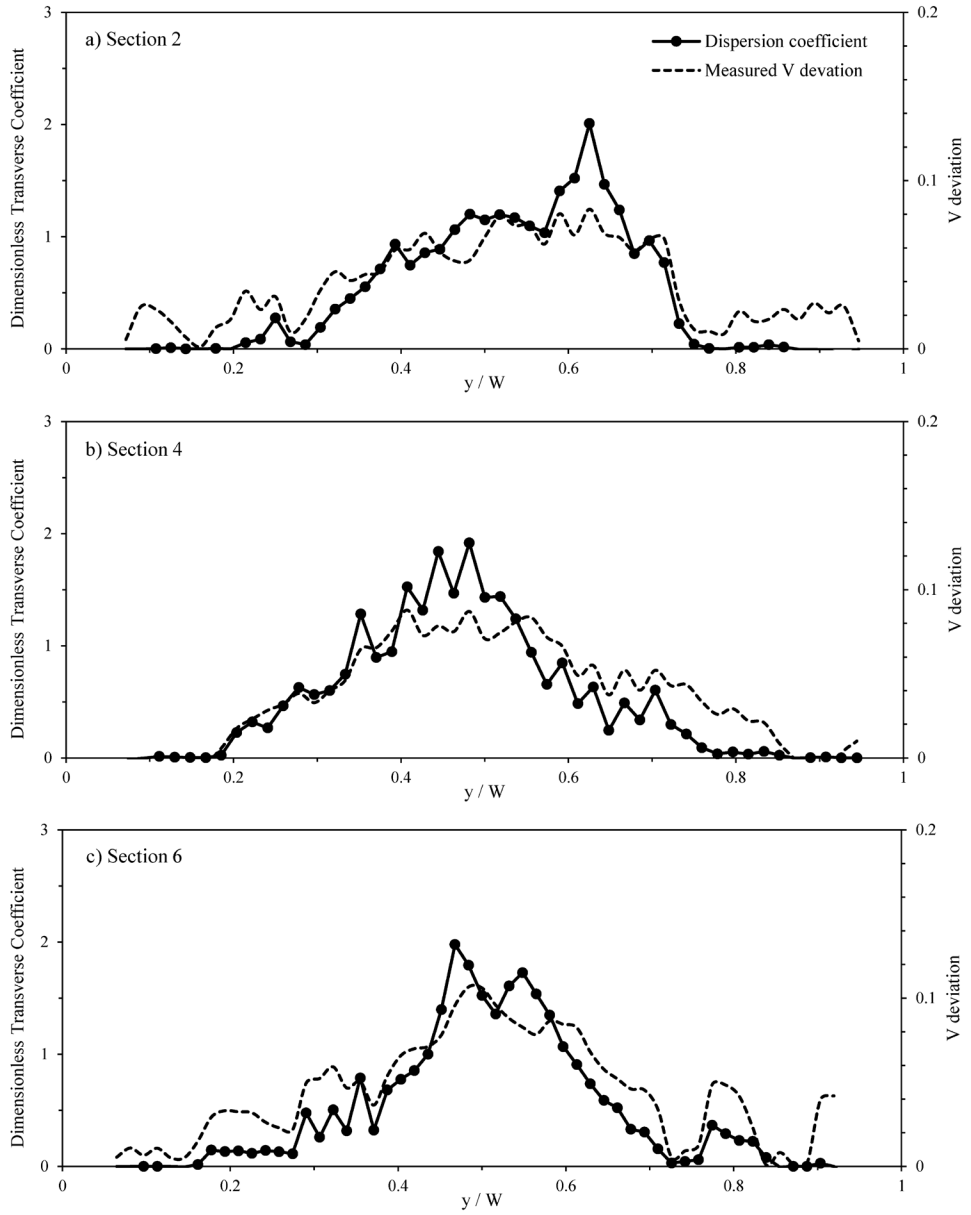

Figure 7.4 Transverse Dispersion coefficients from R317-2 apex (cont)

The calculated dispersion coefficients were interpolated in Figure 7.5 and 7.6 to find the spatial distribution of coefficients throughout the KICT REC channel. This enables the data to be inserted into a 2D ADE model for later advection dispersion calculation. It could be used to be compared to the established method of using single parameters for dispersion coefficient inputs. In the case of longitudinal dispersion coefficients, where the correlation between the velocity and the coefficients proved to be high, an approach using the velocity size for transformation into coefficients could be used in future research. These results also showed that the longitudinal dispersion coefficients were mostly larger than the 5.93 value that was calculated by Elder (1959) using Taylor (1954)'s equations, and showed the measured velocity deviations were larger than the logarithmic assumption and analytical result done by Elder due to the channel geometric configuration and transverse deviation that was also combined in the calculated value. To confirm that these values were acceptable, comparison with the routing method 2D STRP using tracer test experiments was then conducted.

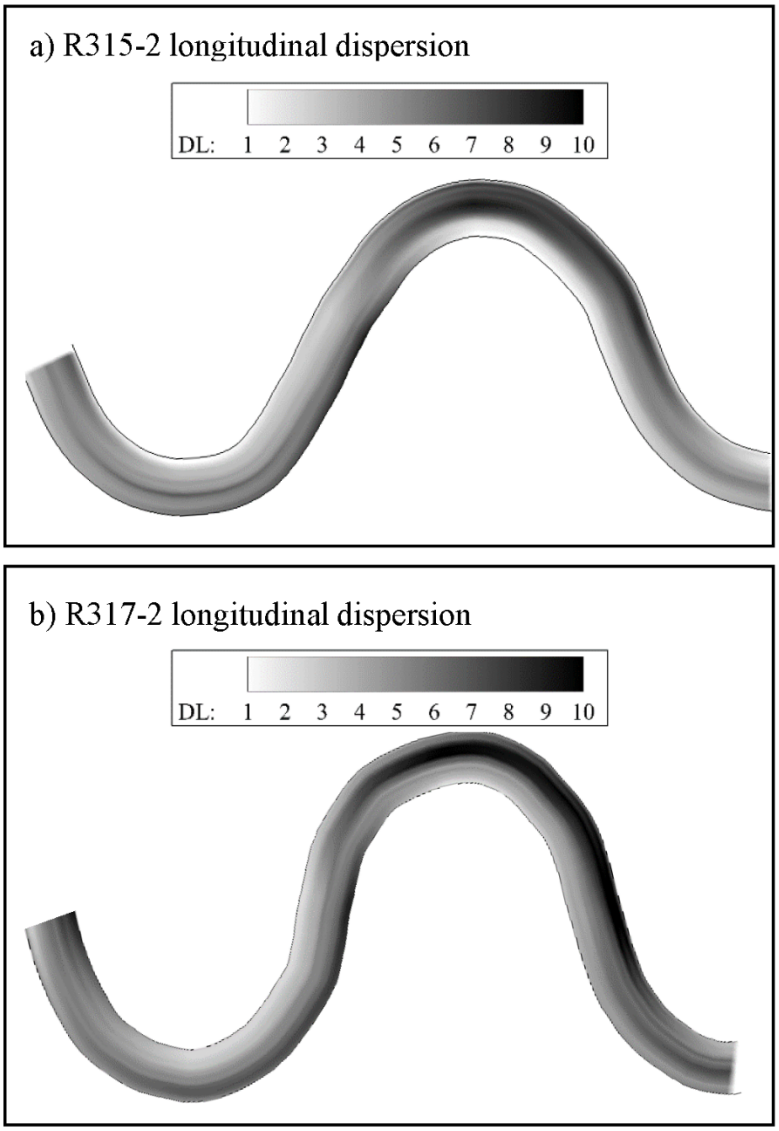

Fig. 7.5 Spatial interpolated velocity driven longitudinal dispersion coefficients

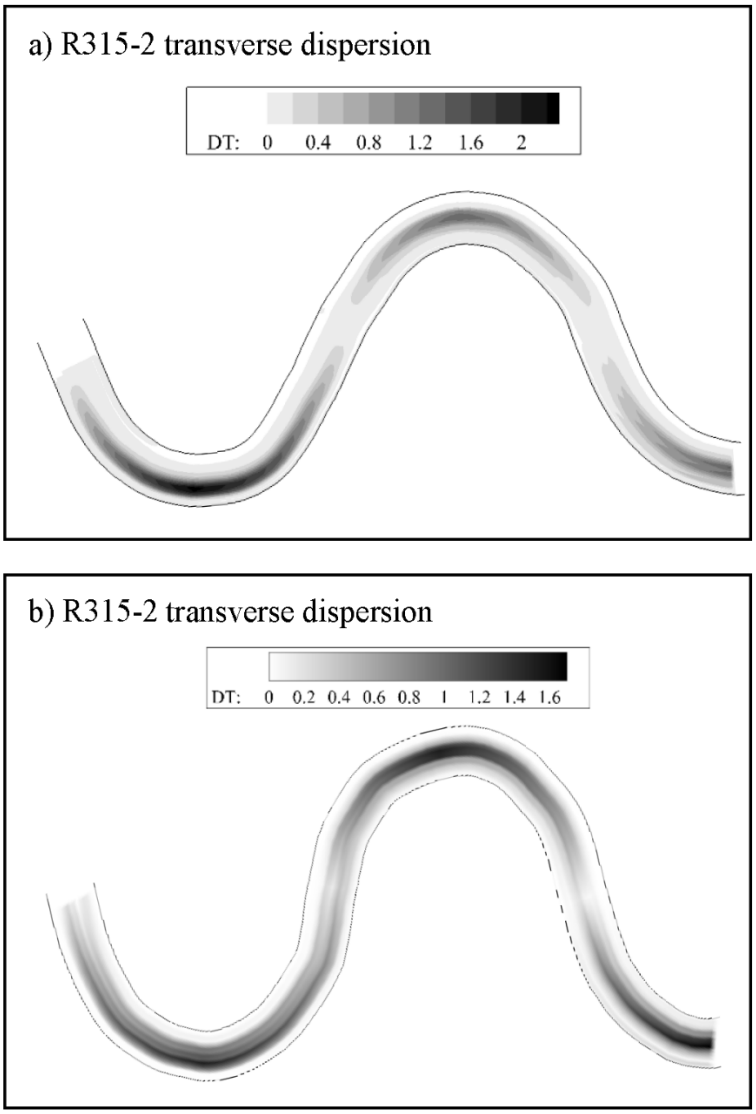

Fig. 7.6 Spatial interpolated velocity driven transverse dispersion coefficients

7.2 Dispersion Coefficient Derivation using Concentration Curves

For calculation of the dispersion coefficients by using the 2D STRP, the Fischer et al. (1979) Eq. (2.26) was used. The predicted time-concentration curves at the downstream were calculated using the measured upstream time-concentration curves shown in Figs. 4.12-4.13 The predicted curves were repeatedly matched with the measured curves downstream until the optimal value of the dispersion coefficients were found with the nonlinear multiple regression technique to find the longitudinal and transverse dispersion coefficient at the same time. While the measured curves were incorporated into the equation to calculate the predicted curves, the concentration-time-lateral distance curves were transformed into the concentration-time-normalized cumulative discharge curves. The time-concentration curves then were interpolated by using the kriging method. This interpolation was necessary in order to match the predicted curves that were positioned with measured curves because the actual distances between the concentration curves across the normalized cumulative discharge were not uniform in each section.

The results of the longitudinal and transverse dispersion coefficients calculated from 2D-STRP are shown in Figs. 7.7 and 7.8. In this figure the values 'from section' mean that the concentration profiles acquired from the section were used as the input data to route the concentration profile in later sections. Therefore each

sections have several different values of dispersion coefficients starting from different areas. The results showed that the longitudinal dispersion coefficient higher values to the averaged dispersion coefficients derived from velocity profile measurements. This was assumed to be that the peak points of the concentration curve were important in the routing procedures, so even though the 2D-STRP calculated dispersion coefficients were a single value for a section, it was similar to the point value from the velocity driven dispersion coefficients. This was shown in both cases of each sinuosity, as the difference between both methods were not large. The results of the calculations for the REC15 and REC 17 channel showed that the size of the predicted longitudinal dispersion coefficients using velocity data were comparable to observed dispersion coefficients from the routing methods. This shows that the predicted coefficients served as an acceptable tool for calculation without the need for additional tracer tests.

However, the case is somewhat different with the values of the transverse coefficient, as the velocity driven dispersion coefficients are large in the apex of the bend and smaller in the straight part of the meander, but the 2D-STRP driven dispersion coefficients do not show clearly the difference between the apex and straight parts of the meandering channel. This is shown especially in the A317 channel with 1.7 sinuosity. Additional analysis shows that the 1.7 sinuosity had early mixing of the transverse dispersion due to its strong curvature, so the latter sections did not seem to show dispersion as much as the results of the 1.5 sinuosity. Also, the A317 channel had strong curves with multiple meanders, so the direction

of the secondary flow changed going through the apexes and the strength of the secondary flow would decrease as the flow moved to the straight part of the channels. Therefore, this result shows that even with the stream-tube method, the 2D-STRP has some limits in the channels with higher sinuosity since the transverse mixing took place very early, so the routing was not properly executed as well as the routing in less curved channels. These results may require an additional tracer test for routing procedures, and showed that for strong curved meandering channels, the dispersion calculation by velocity could be more appropriate.

Due to the difference between both methods, the velocity driven dispersion coefficients would only represent the dispersion at the velocity measured parts of the channel such as the apex or the straight section, and the 2D-STRP would have the mixing results starting from the apex to the straight section. So the 2D-STRP showed the mixing characteristics of the routing areas, while the velocity driven dispersion showed the mixing characteristics of certain sections only, so the STRP would be better to represent storage zones that could be formed between the measured sections. Thorough measurements of the velocity could be undertaken to all areas of the channel, instead of using interpolation between the sections to get detailed spatial dispersion coefficients of the channels; but the additional effort could be comparable with the effort in additional tracer tests. Also, the storage zones may not be shown with the velocity profiles of the channel, so the appropriate selection of the method to derive dispersion coefficients should be chosen according the characteristics of the channel.

Another point is that most of the values of the longitudinal dispersion coefficient from this study and the previous study were much higher than the theoretical value suggested by Elder (1959), as mentioned earlier. Elder's equation was derived under the assumption of uniform flow with a vertical shear in an infinitely wide, open channel, in which he employed the logarithmic law for the vertical profile of the longitudinal flow, in the derivation of the longitudinal dispersion coefficient. However, unlike the infinitely wide, open channel, the transverse shear also exists in natural rivers, as well as the vertical shear, in terms of velocity variation. Thus, in the tracer tests conducted in natural streams of finite width, the effect of the transverse shear, in addition to the vertical shear, contributes to the longitudinal dispersion. In fact, as Fischer et al. (1979) maintained, the contribution of the transverse variation of the primary velocity is far more significant than that of the vertical variation, because the width is usually much bigger than the depth of the channel.

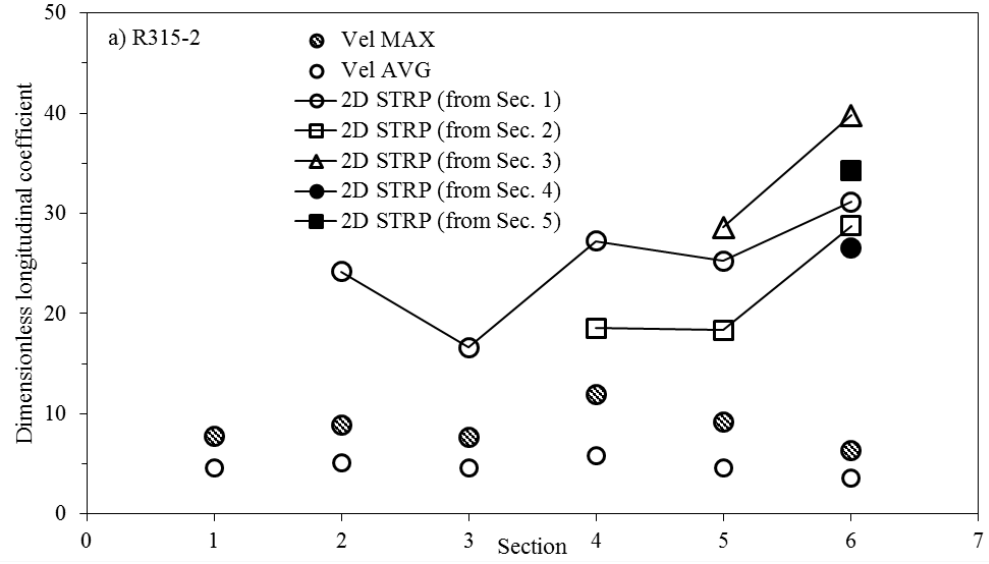

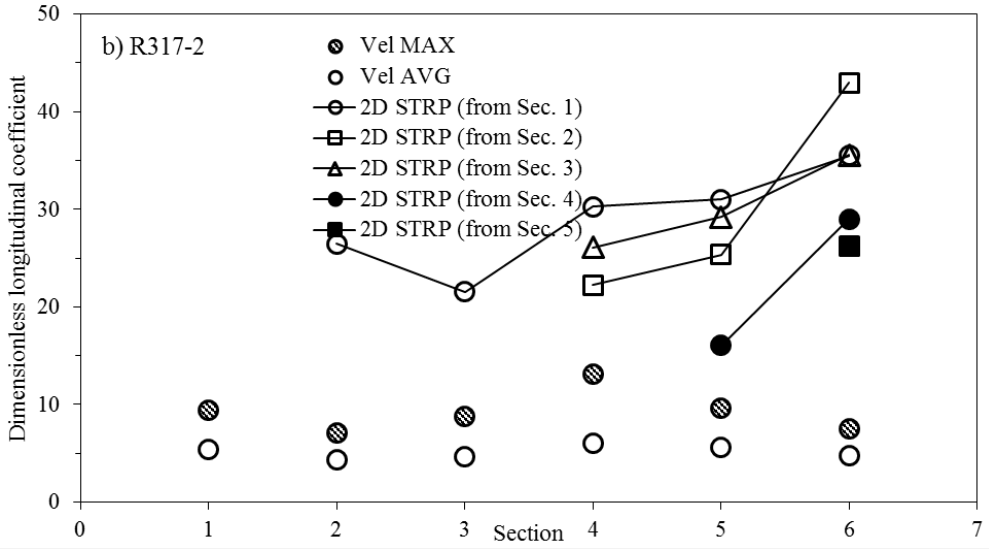

Fig. 7.7 Comparisons of longitudinal dispersion by velocity and routing methods

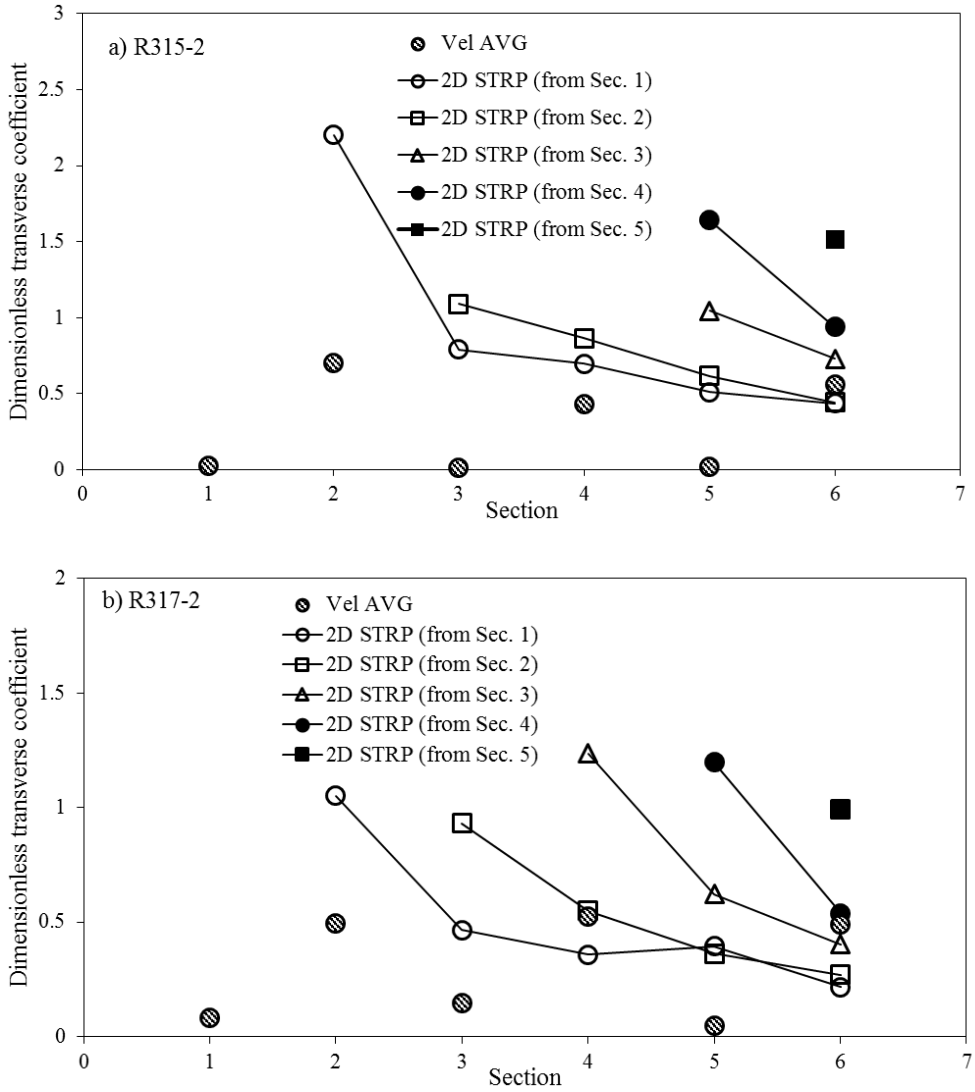

Fig. 7.8 Comparisons of transverse dispersion by velocity and routing methods

7.3 Empirical Equation for Dispersion Coefficients

The non-dimensional term D_L/HU^* is plotted with the dimensionless parameters of the rivers in Fig. 7.9. Data sets from previous field tests (Seo et al, 2006, Seo et al., 2016) are also plotted in this figure for comparison. From Fig. 7.9 (a) and (b), it might be assumed that D_L/HU^* has the relations with W/H and U/U^* in the log-log scale graphs even though test data are somewhat scattered. Another point to note in Fig. 7.9 is that all of the values of the longitudinal dispersion coefficient from this study and the previous study using tracer test concentration data results were much higher than the theoretical value suggested by Elder (1959), which is 5.93. Of course, Elder's equation derivation of the longitudinal dispersion coefficient was under the assumption of uniform flow with a vertical shear in an infinitely wide open channel, in which the derivation utilized the logarithmic law for the vertical profile of the longitudinal flow. However, the infinitely wide open channel is conceptual, and for the real natural rivers the vertical shear terms of velocity variation, and the transverse shear both exist instead of using a logarithmic law. Therefore, the tracer tests conducted in real natural rivers with the effect of the transverse shear and vertical shear also with limited width across the channel has these effects to enlarge the longitudinal dispersion coefficient compared to the theory by Elder. Also, according Fischer et al. (1979) the natural channels have the transverse variation of the primary velocity is far more significant than that of the vertical variation due to width size compared to depth size

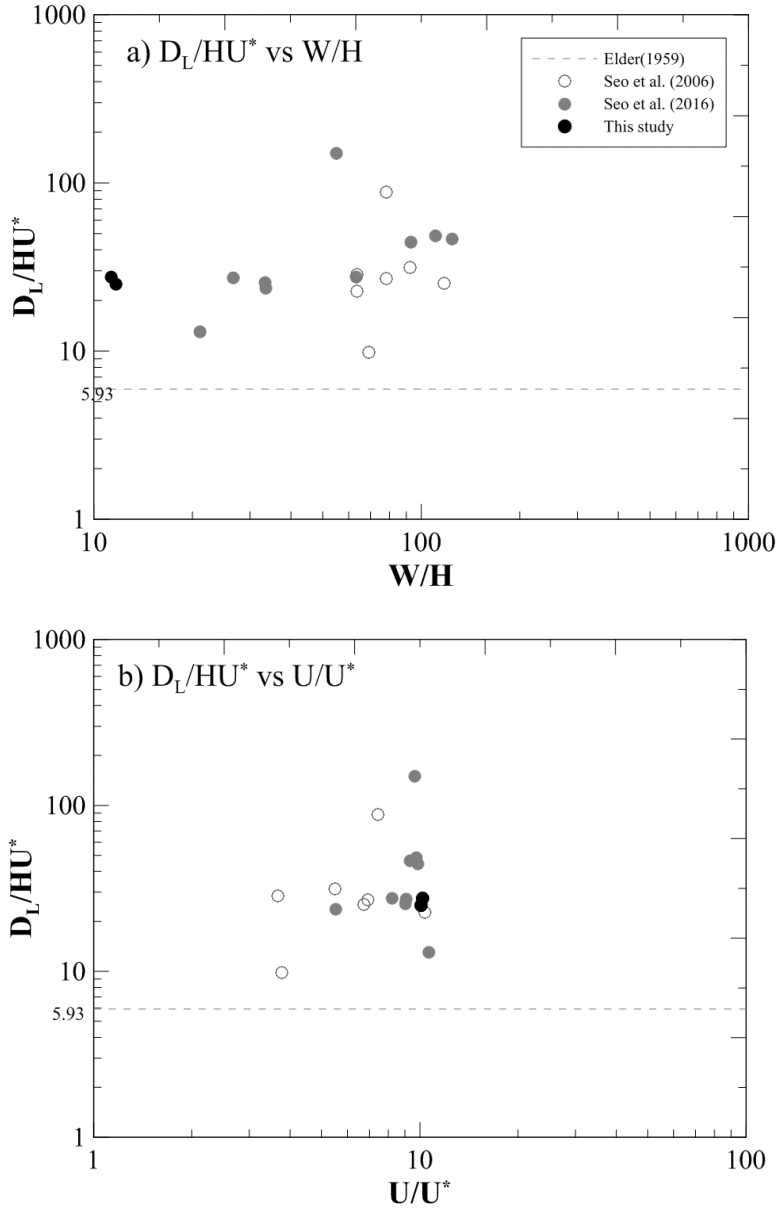

Fig 7.9. Longitudinal dispersion coefficients by hydraulic parameters

The relation between the non-dimensional transverse dispersion coefficient D_T/HU^* and dimensionless values of the hydraulic parameters of the river channel are plotted in a log-log scale in Fig. 7.10. Data sets available from previous field tests using data from the starting from the 70s are also shown in this figure. As seen in Fig. 7.10(a) it is difficult to find a relationship between D_T/HU^* and W/H, but Fig 7.10(b) shows that U/U^* shows some positive relation between the dimensionless transverse mixing coefficient in the log-log scale. The D_T/HU^* increases as the curvature of the stream increases in the form of W/R_c increase in Fig. 7.11 (c). This is because of the strength of the secondary current which was also shown in the experimental data in the research, became stronger to enhance the transverse mixing. To analyze the effects of the channel curvature on the rate of transverse mixing more quantitatively, a relation between $\frac{D_T}{HU^*}$ and $\frac{U}{U^*}\frac{W}{R_c}$ was plotted in a log-log scale in Fig. 7.11(d). In this figure, this relations are the same ones that were introduced before in Yotsukura and Sayre (1976) and Fischer et al. (1979) had shown to be linear, the slope was slope was 2, based on Yotsukura et al. (1970) and Sayre and Yeh (1973). But in this research the slope of the line was shown to be 0.35, which was much smaller than the previous slope due to the additional data acquired after the 80s. Then these parameters were used for the empirical equations using the regression analysis by the relationship between the 2D dispersion coefficients and the hydraulic and geometric parameters to a form of the standard nonlinear multiple models.

$$\frac{D_L}{HU_*}, \frac{D_T}{HU_*} = F\left(\frac{UH\rho}{\mu}, \frac{W}{R_c}, \frac{U}{U_*}, \frac{W}{H}\right) \tag{7.2}$$

where $\frac{UH\rho}{\mu}$ is the Reynolds number. For fully turbulent flow in open channels, the Reynolds number is negligible, and the remaining terms were used for the equation.

$$\frac{D_L}{HU_*} = a_0\left(\frac{U}{U_*}\right)^{a_1}\left(\frac{W}{H}\right)^{a_2} \tag{7.3a}$$

$$\frac{D_T}{HU_*} = a_3\left(\frac{U}{U_*}\times\frac{W}{R_c}\right)^{a_4} \tag{7.3b}$$

The coefficients for the transformed equations using the least-square regression method than becomes the following empirical equations.

$$\frac{D_L}{HU_*} = 1.4573\left(\frac{U}{U_*}\right)^{0.8047}\left(\frac{W}{H}\right)^{0.3583} \tag{7.3a}$$

$$\frac{D_T}{HU_*} = 0.5058\left(\frac{U}{U_*}\times\frac{W}{R_c}\right)^{0.5664} \tag{7.3a}$$

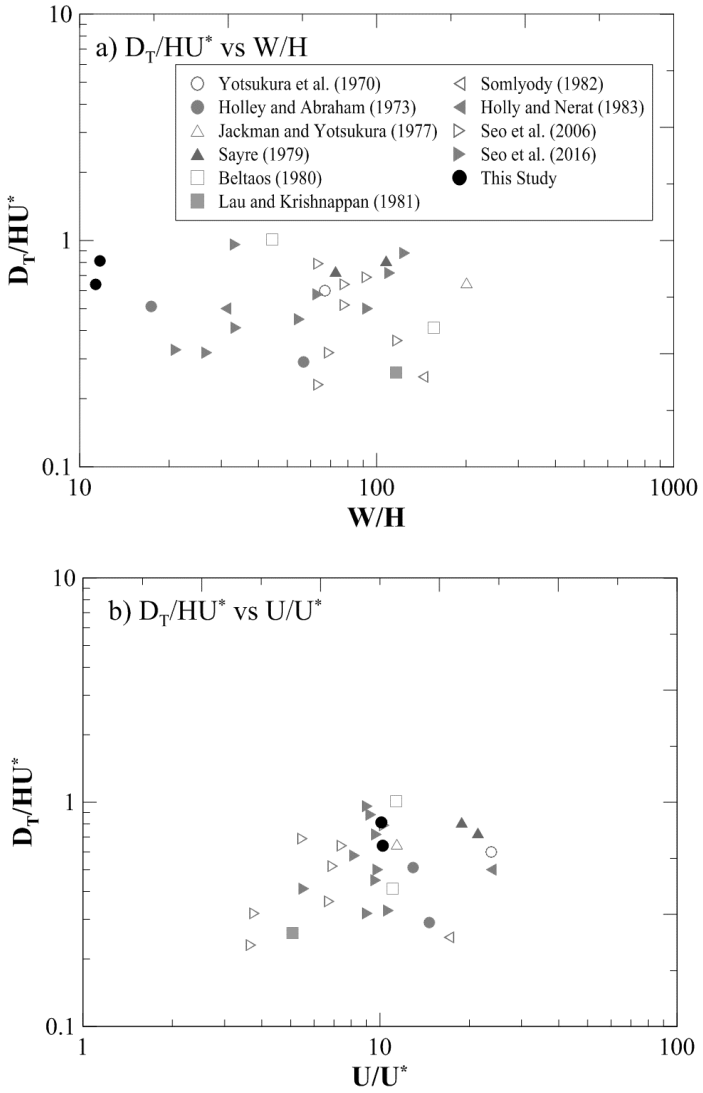

Fig 7.10. Transverse dispersion coefficients by hydraulic parameters

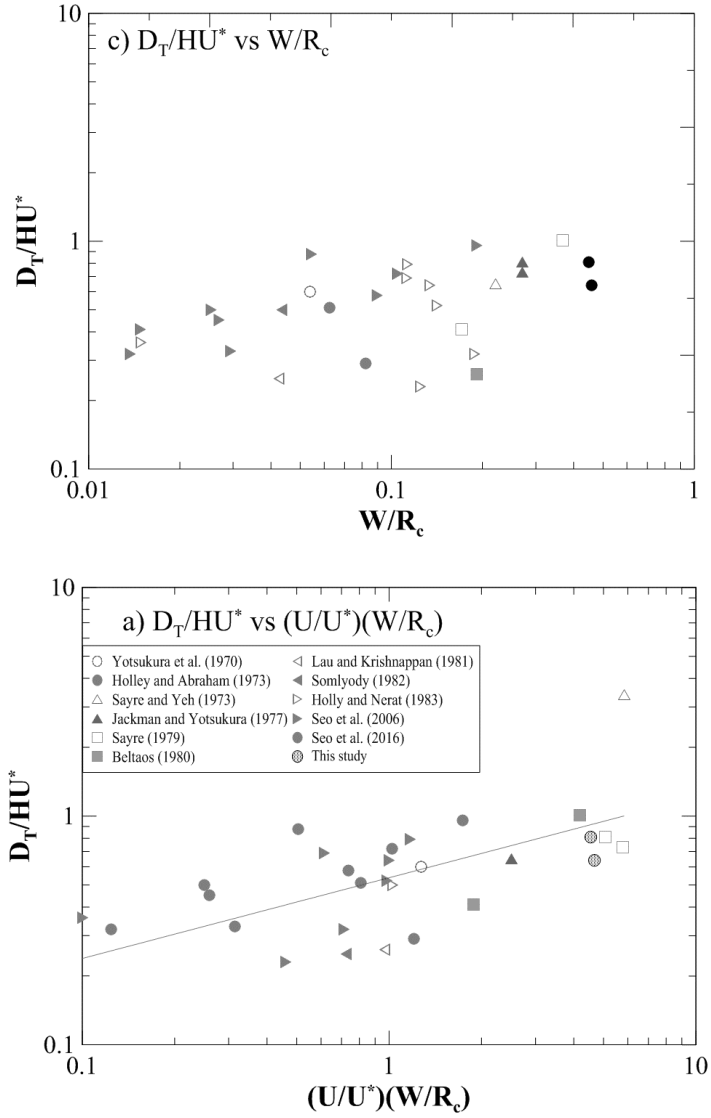

Fig 7.10. Transverse dispersion coefficients by hydraulic parameters (cont)

Chapter 8. Application of 2D Mixing Model

8.1 Calibration of Dispersion Coefficients

To compare the velocity driven 2D dispersion coefficients and the former equation based dispersion coefficients by Elder (1959) and Fischer (1979) for the longitudinal and transverse dispersion coefficients respectively, the advection-dispersion model CTM-2D was used. The velocity driven 2D dispersion coefficients were applied with the calculated coefficients with the Fischer triple integration equation using the measured vertical velocity data. Sectional averaged values were used, and was applied as an interpolated form throughout the channel, since the values were measured at the sectional points only. The former equation based dispersion coefficients used the following.

$$D_L = 5.93hu^* \tag{8.1}$$

$$D_T = 0.6hu^* \tag{8.2}$$

First, the results of the cumulative dosage tracer test results were compared with the equation, STRP, velocity driven results as in Figs 8.1-8.2, and showed that the velocity driven dispersion results had better fit with the tracer test results while the equation based dispersion results overestimated the mixing that occurred in the open channel. Since the velocity driven coefficients were derived using the actual data from the channel it led to better accuracy even in the CTM-2D model application.

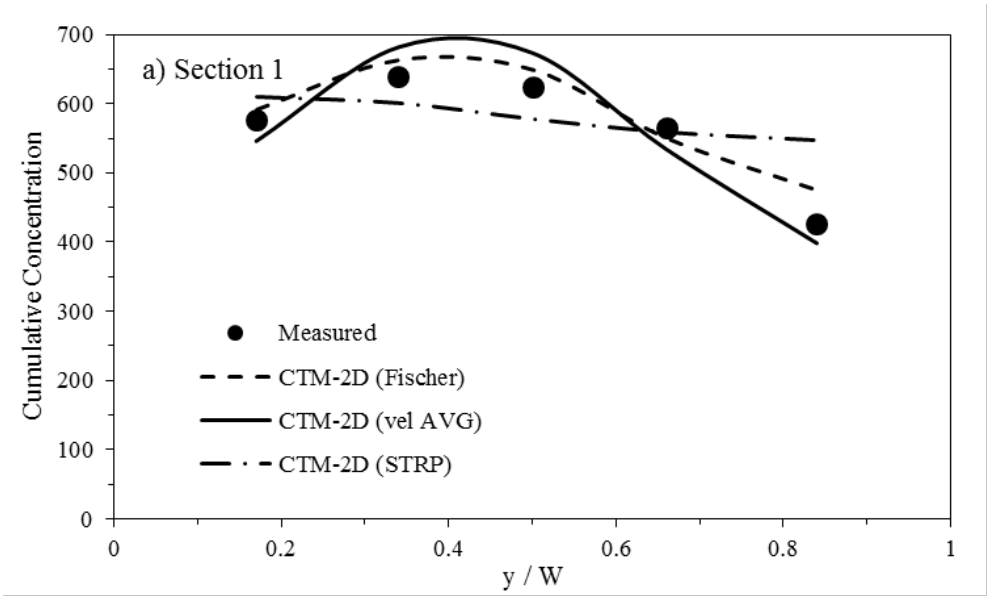

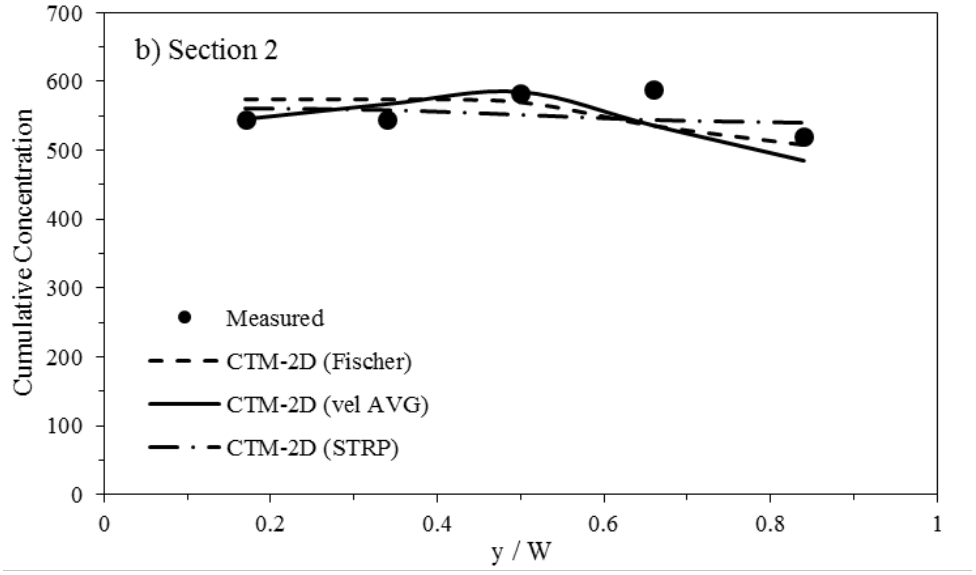

Fig. 8.1 Cumulative concentration by dispersion coefficients in Case R315-2

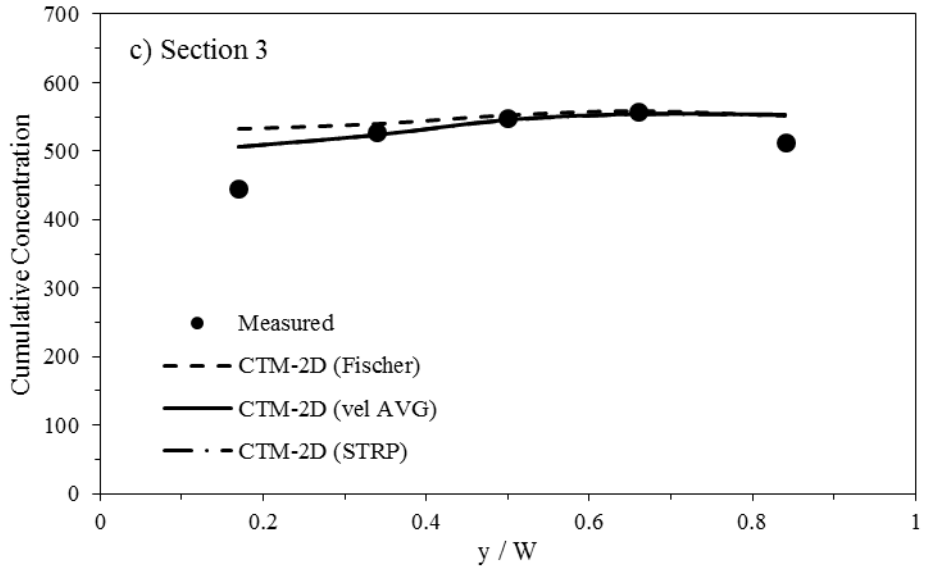

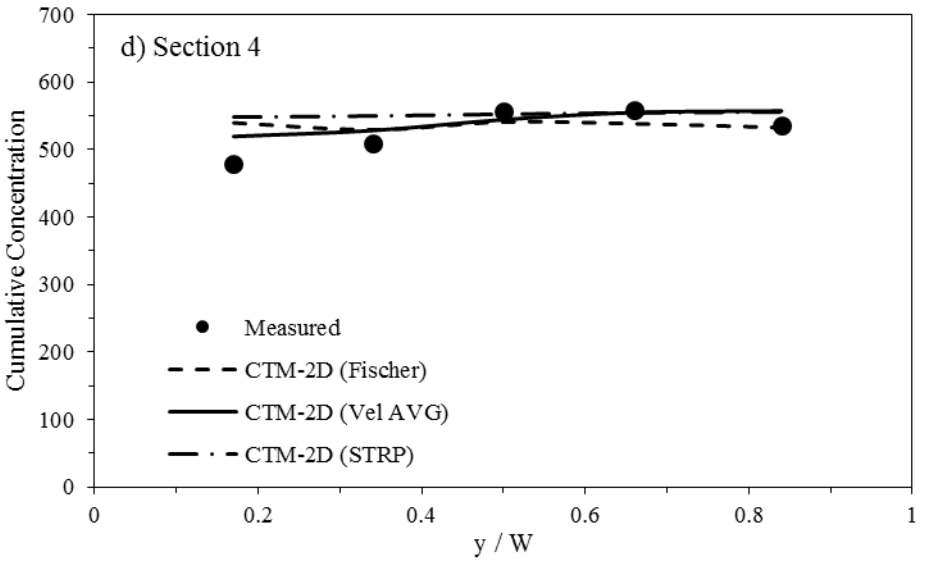

Fig. 8.1 Cumulative concentration by dispersion coefficients in Case R315-2 (cont)

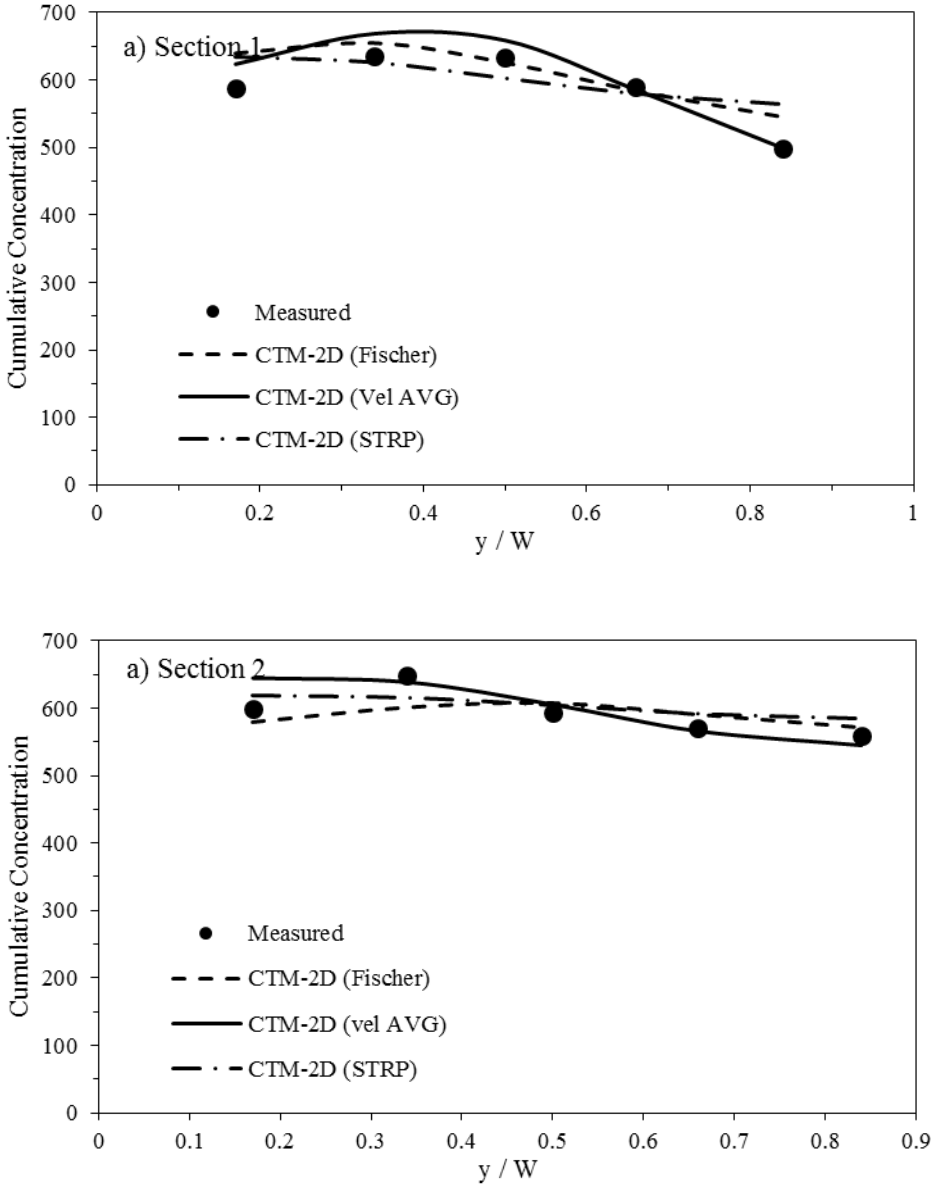

Fig. 8.2 Cumulative concentration by dispersion coefficients in Case R317-2

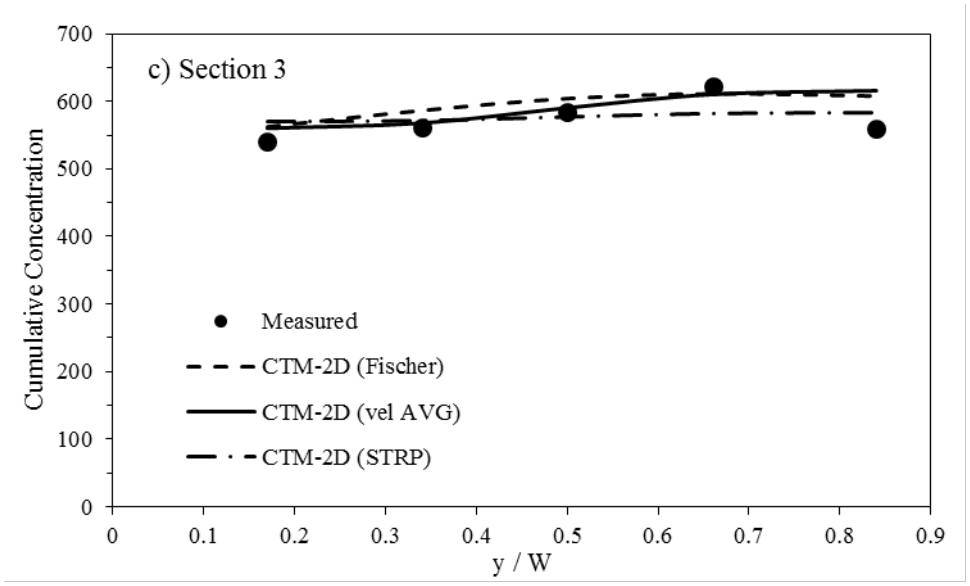

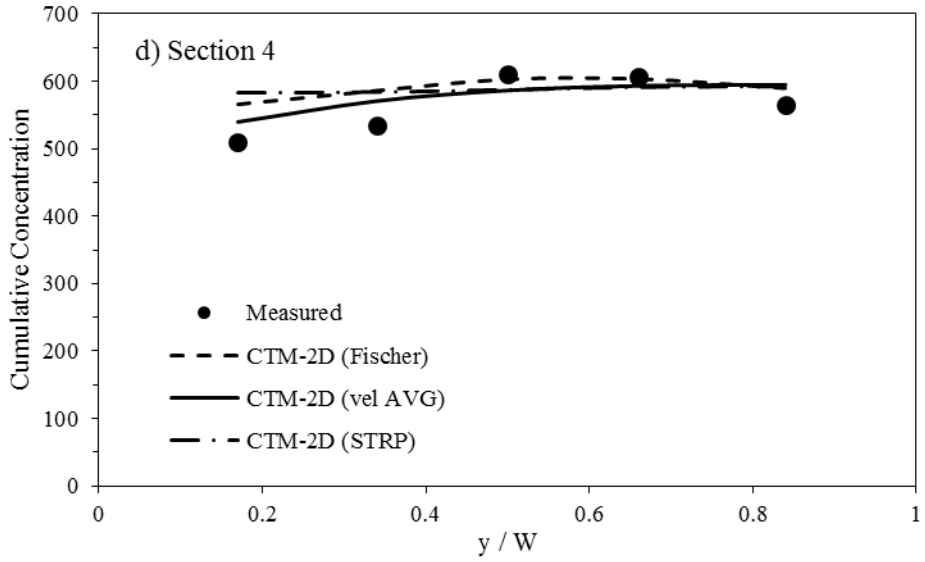

Fig. 8.2 Cumulative concentration by dispersion coefficients in Case R317-2(cont)

A point to note however, is that the Fischer equation value of non-dimensional transverse coefficient 0.6 is the average of the recommended value which was originally 0.3 - 0.9. Since the transverse dispersion coefficient value produced by the ADCP velocity driven method was 0.05-0.4, it was actually within the Fischer recommended values. Of course, the STRP driven results proved to be overestimated when applied to the CTM-2D model. In the case of longitudinal dispersion coefficients, the Elder equation value of non-dimensional longitudinal dispersion coefficient value of 5.93 proved to be too small when applied into the CTM-2D model as shown in Figs 8.3-8.4. This is similar to the average value of the ADCP velocity driven methods which led to coefficients ranging from 4-5. The STRP values still proved to be overestimation when applied to the CTM-2D model, and calibrated results of the longitudinal dispersion coefficients showed to be 10-14, which is about the middle value of the ADCP velocity driven methods and STRP driven methods. Therefore the STRP driven methods contained dispersion other than the ones by shear flow and turbulence driven, such as the equation below.

$$D_L = D_l + \varepsilon_l + \Delta D_L \tag{8.3}$$

where D_l is shear flow dispersion, ε_l is turbulence driven dispersion, ΔD_L is residual dispersion. The dispersion coefficient calculated by shear velocity by the vertical profile velocities only consider the vertical shear that creates the pollutant movement, while the dispersion coefficient by the concentration data are based on

the observed concentration curves and contains the irregularity of the channel, storage zones, and numerical dispersion if considering the turbulence driven dispersion to be relatively small. Therefore, both the ADCP velocity driven method for shear dispersion and STRP method for the total dispersion must be taken into consideration for transport modeling in natural channels. To find the numerical dispersion the simulations were conducted by variation of the mesh size and time steps for change of the Courant number and its effects. Of course, the model was run with the fully implicit schemes which did not require the Courant number to be always lower than 1.

The result of Fig. 8.5(a) show the MAPE at peak concentrations by the difference of Courant numbers by changing times steps for the R317-2 simulation using the calibrated dispersion coefficients. Courant numbers below 2 seem have errors below 5%, but is shows a large increase as the time step is changed. With the log-log scale in the numerical dispersion shows to have a slope of 3, which shows that the plot slope expects a third order scheme so the error is reduced by 3 orders of magnitude when the time spacing is reduced to the first order of magnitude. Fig. 8.5(b) shows the MAPE by multiplied mesh size differences, which shows great difference between the original mesh size and shows the importance of mesh size effecting the simulation. But in the case of tail size differences not specified in this research would be due to the residual dispersion related to storage zones in the channel, but this is not the scope of this research as the pollutant model used is a non-Fickian 2D advection-dispersion model without storage zones.

Through examination of the time-step and mesh-size effects on the accuracy of the simulation showed the differences between the concentration data and calibrated simulation, it was not large enough to show the discrepancy between the calibrated dispersion coefficient and the 2D STRP calculated dispersion coefficient since all the calibrated simulation had courant numbers below 2. Since the 2D-STRP values are based on the concentration data and had to account for the falling tail size due to the residual dispersion of storage zones since the method is based on the theoretical observation curves to predict the actual concentration curves, it overestimated the dispersion coefficients for the model. In some verification cases however, such as the section 2, 6 in R315-1 shown later, the 2D-STRP showed better comparison to the measured data with the tails. Therefore, the main reason for the difference between the calibrated dispersion coefficients and the concentration data driven dispersion coefficients by 2D-STRP method, were caused by the residual dispersion with irregularity of channel and storage zones to take account of the falling tail of the observed concentration.

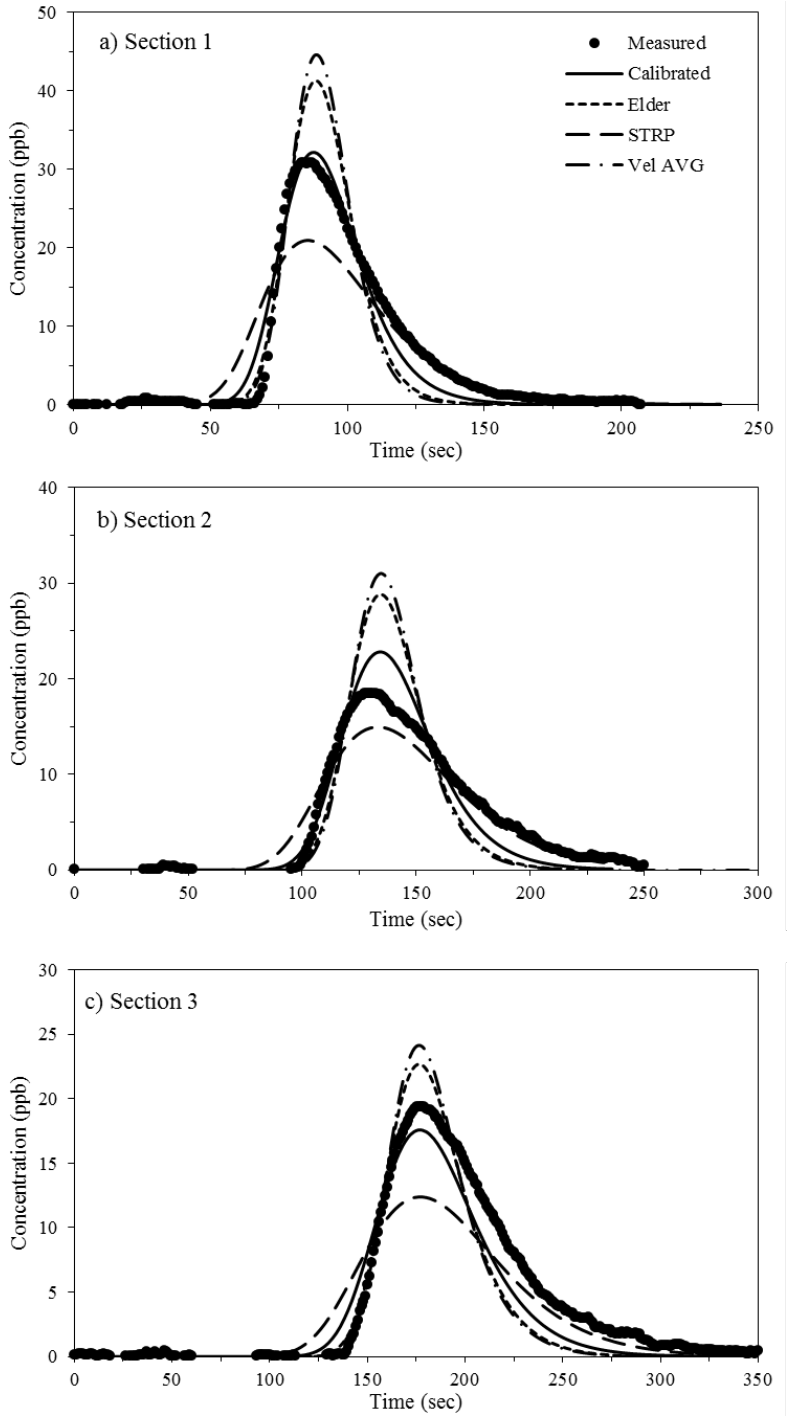

Fig. 8.3 Time-concentration comparisons by dispersion methods in R315-2

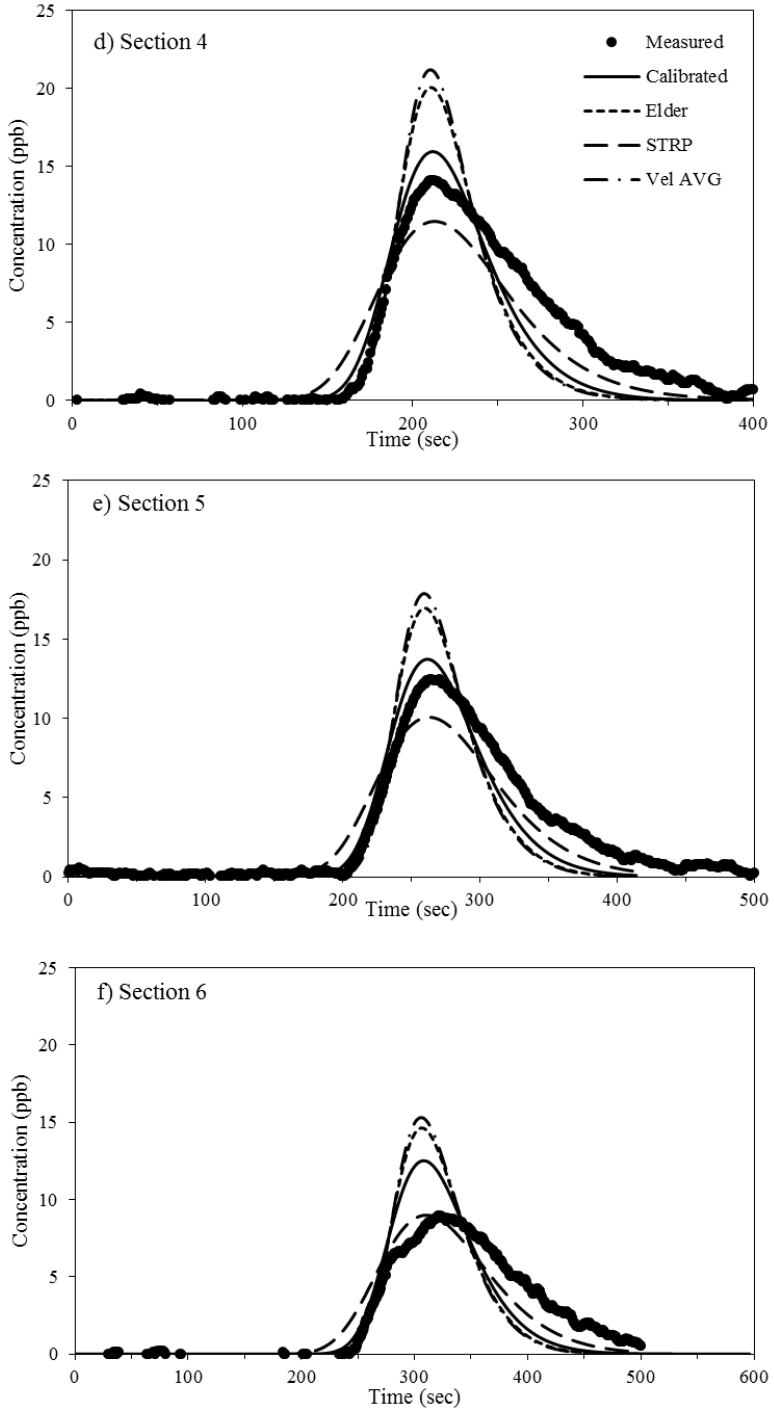

Fig. 8.3 Time-concentration comparisons by dispersion methods in R315-2 (cont)

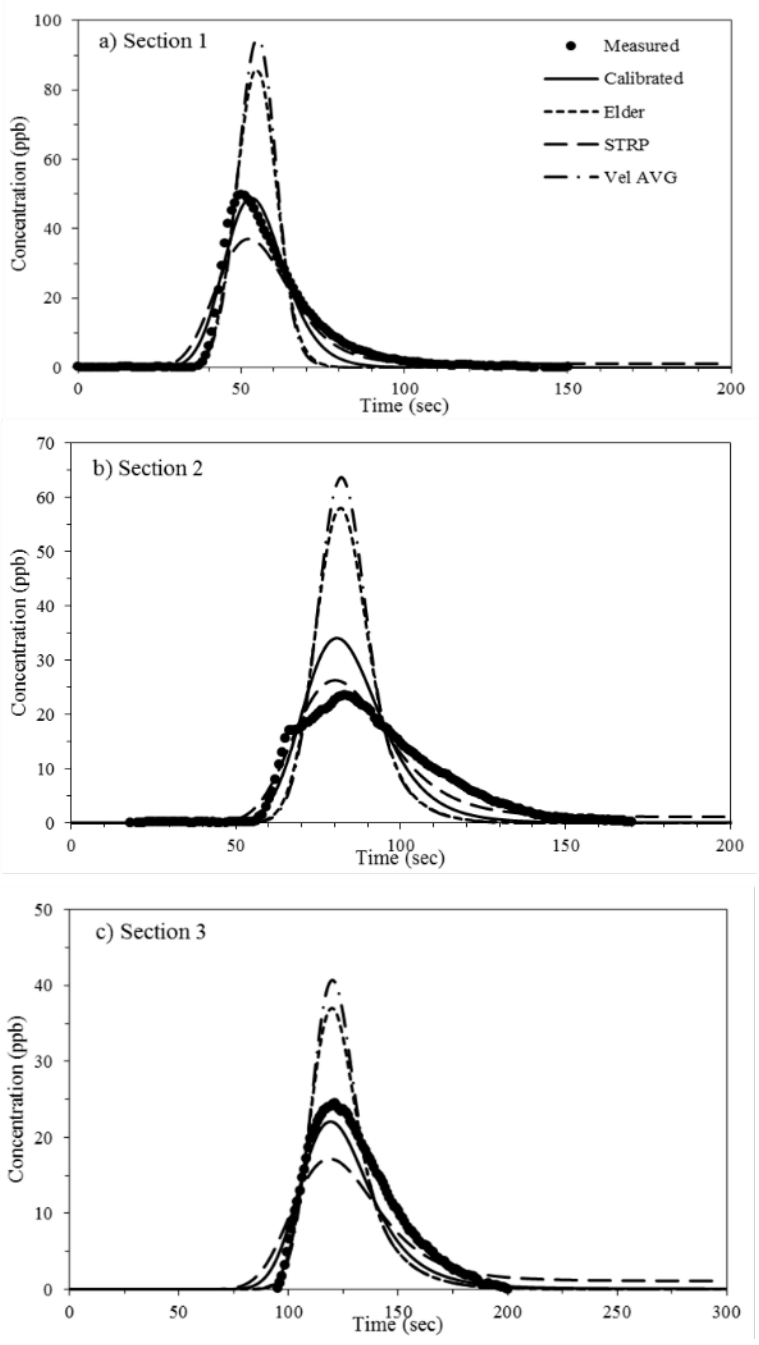

Fig. 8.4 Time-concentration comparisons by dispersion methods in R317-2

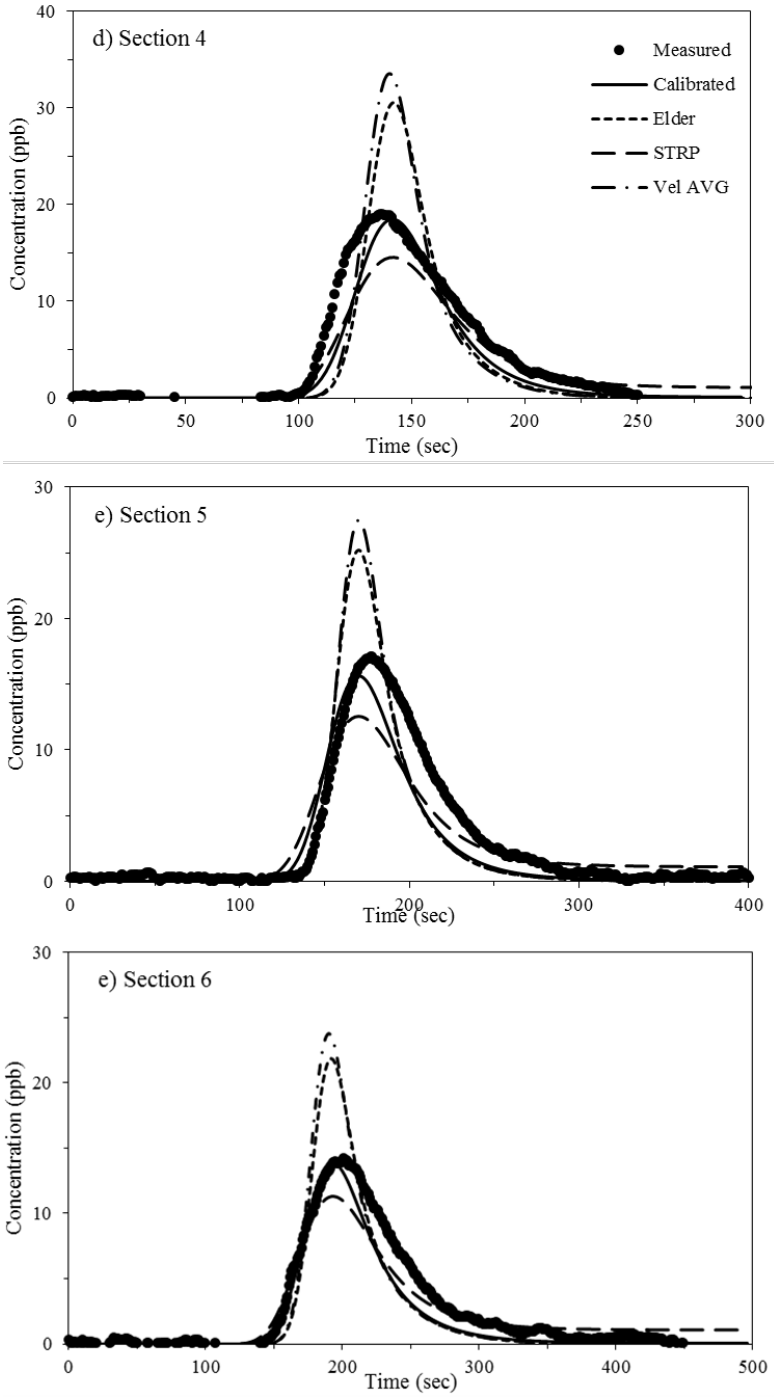

Fig. 8.4 Time-concentration comparisons by dispersion methods in R317-2 (cont)

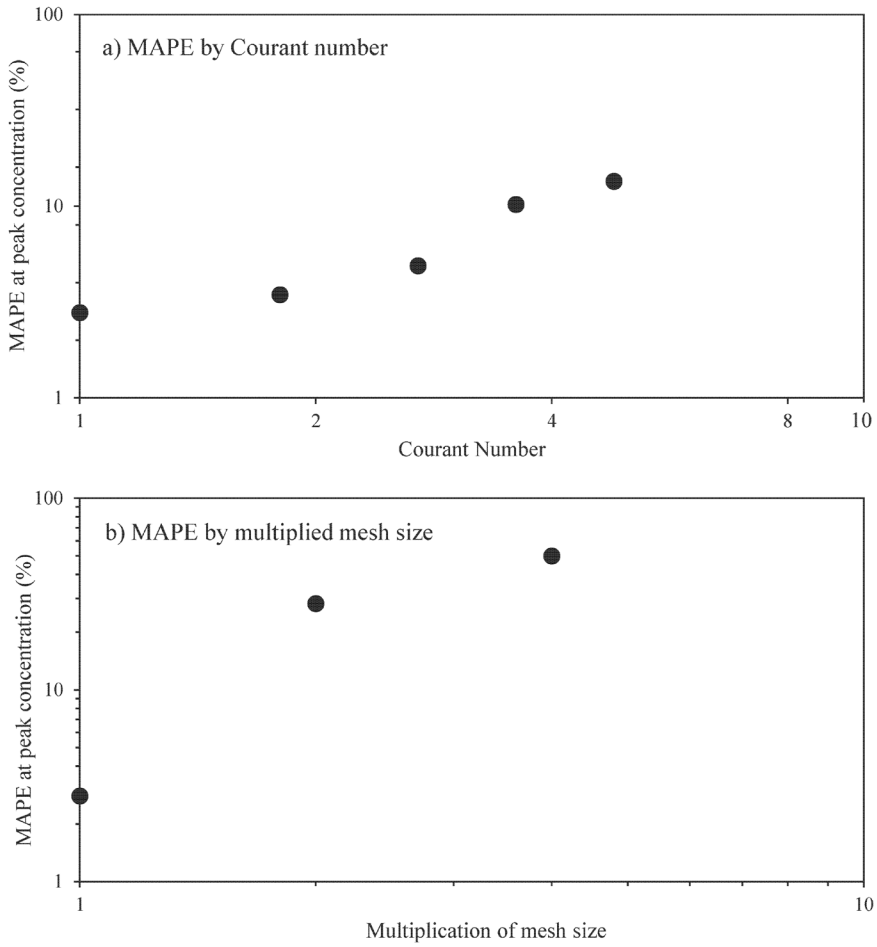

Fig. 8.5 MAPE of peak concentration by Courant number and mesh size

8.2 Concentration Distributions

The calibrated results of the 2D longitudinal and transverse dispersion coefficient results from Figs. 8.3-8.4 were verified for the case R315-1 and case R317-1. Using the HDM-2D results for the two different cases, the CTM-2D was used for comparison between each different coefficient methods. The results of Figs. 8.6-8.7 show that the calibrated coefficients are verified for a close match with the tracer test concentration data with an average MAP error of 8-10% as in Table 8.1 using the dispersion stress method applied flows. For the case of non-dispersion flows, the results showed to be 9-11%, which is not a large difference but the accuracy was improved with the dispersion stress in most of the section comparisons. The CTM-2D model had its limits in reproducing the falling limb tails that were shown in the concentration curve data, but it succeeded in reproducing the rising limbs. The value of about 1/2 of the 2D STRP results, and twice of the velocity-driven results show that although the shear velocity is an important factor in the contaminant transport, the factors such as residual dispersion other than shear dispersion, affect the concentration curves. Of course, the STRP still overestimates the dispersion coefficients since it takes the concentration tails to account, but in certain cases were actually closer to the concentration curves than the calibrated coefficients. The CTM-2D advection-dispersion model, is also dependent on the velocity produced by the flow model. Although the flow model showed to have accuracy of 8-9% from Table 6.3, this is could be the one reason why there is a deficit between the measured concentration curves and the simulated concentration curves.

Table 8.1 Average MAP errors of CTM2D verification simulations using dispersion stress

Section / Case	DS	1	2	3	4	5	6	Average
R315-1	X	7.1%	8.5%	4.7%	10.8%	12.8%	10.2%	9.1%
R317-1	X	13.2%	10.4%	8.5%	6.2%	11.2%	15.7%	10.9%
R315-1	O	4.6 %	9.6 %	3.8 %	11.2 %	11.8 %	7.2%	8.0%
R317-1	O	11.5 %	9.3 %	7.4 %	6.7 %	8.6%	14.4%	9.7%

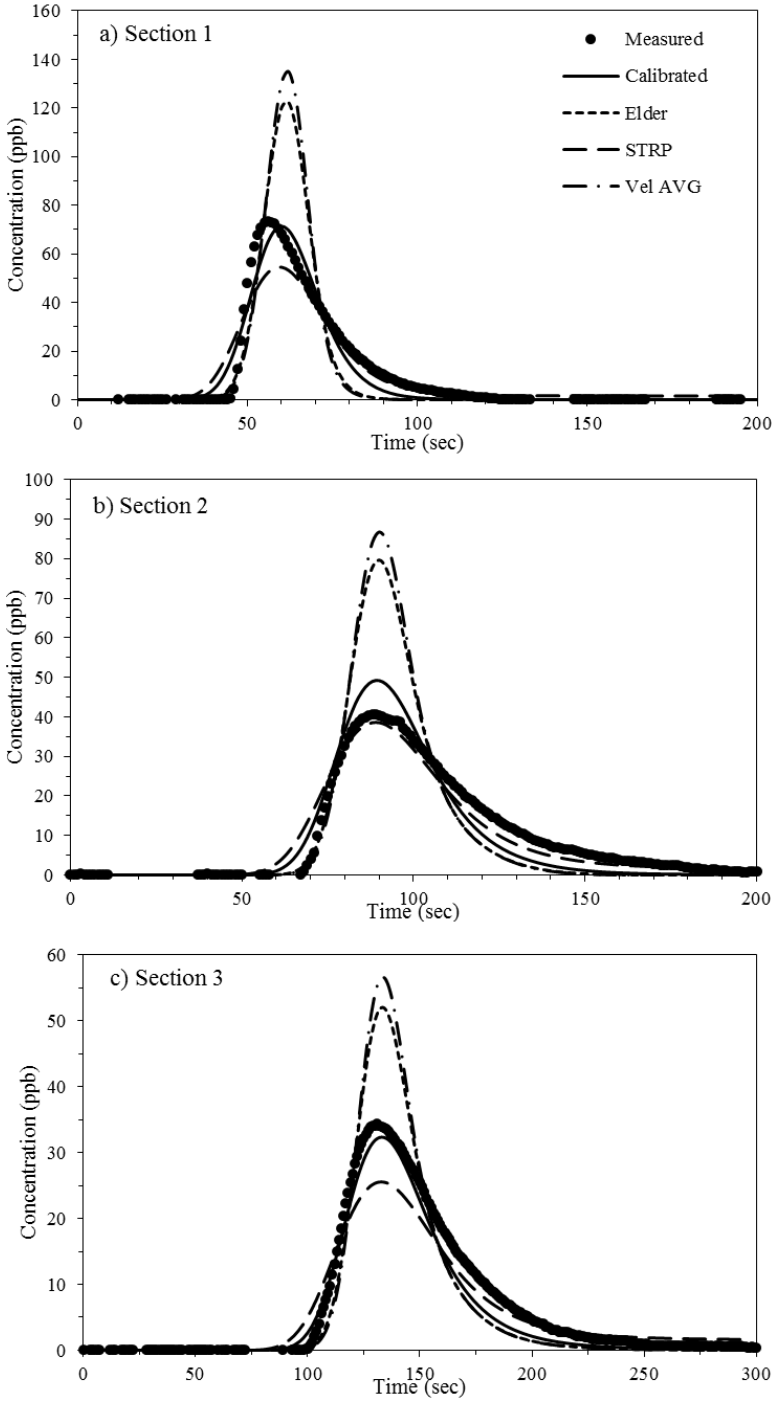

Fig. 8.6 Verification by dispersion methods in R315-1

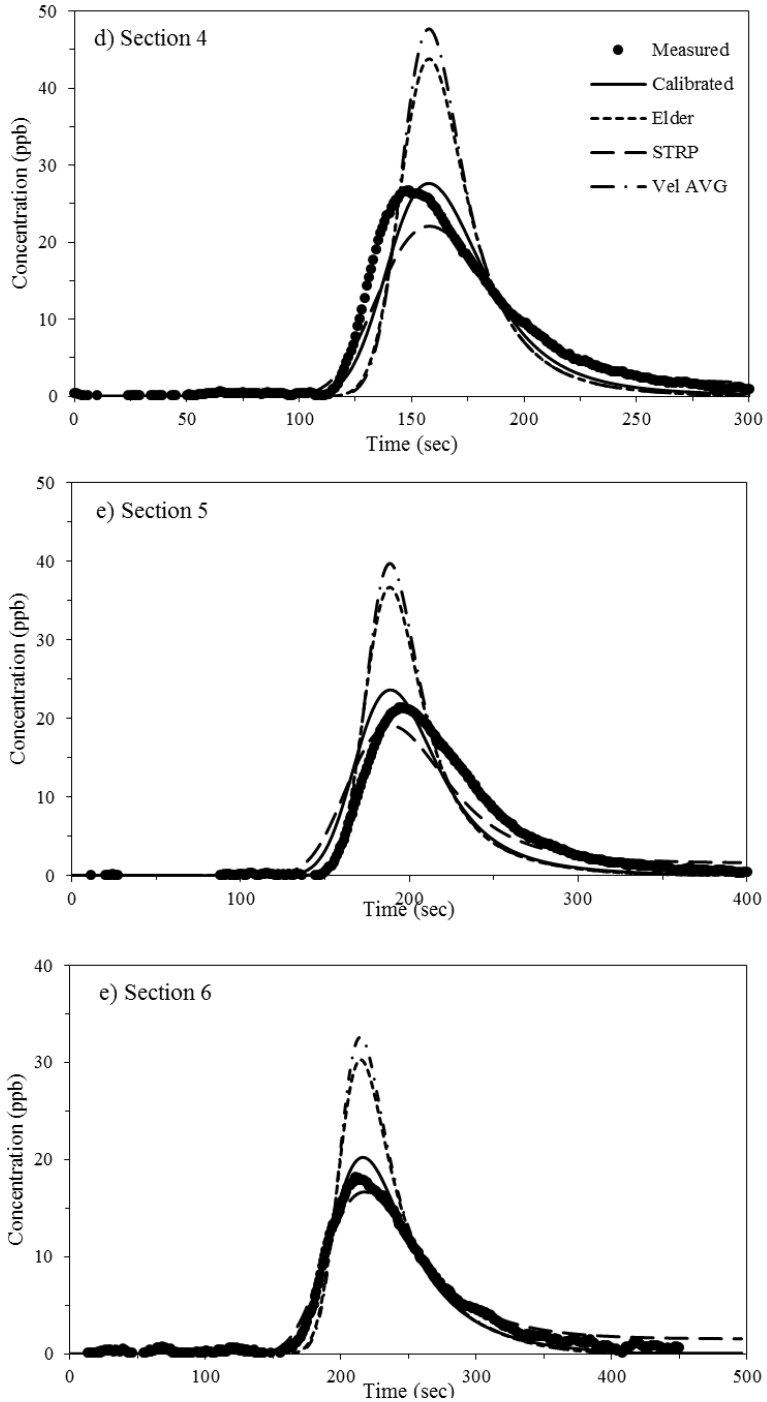

Fig. 8.6 Verification by dispersion methods in R315-1(cont)

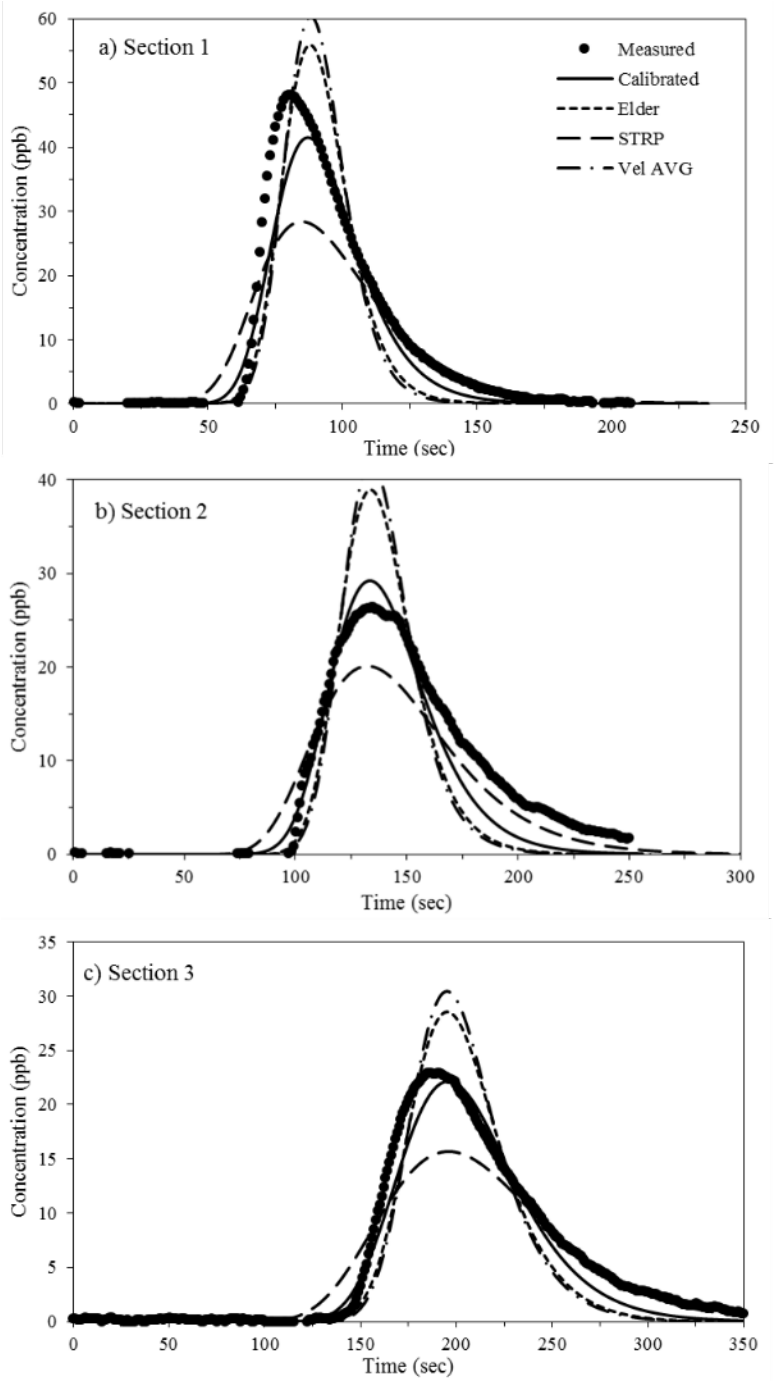

Fig. 8.7 Verification by dispersion methods in R317-1

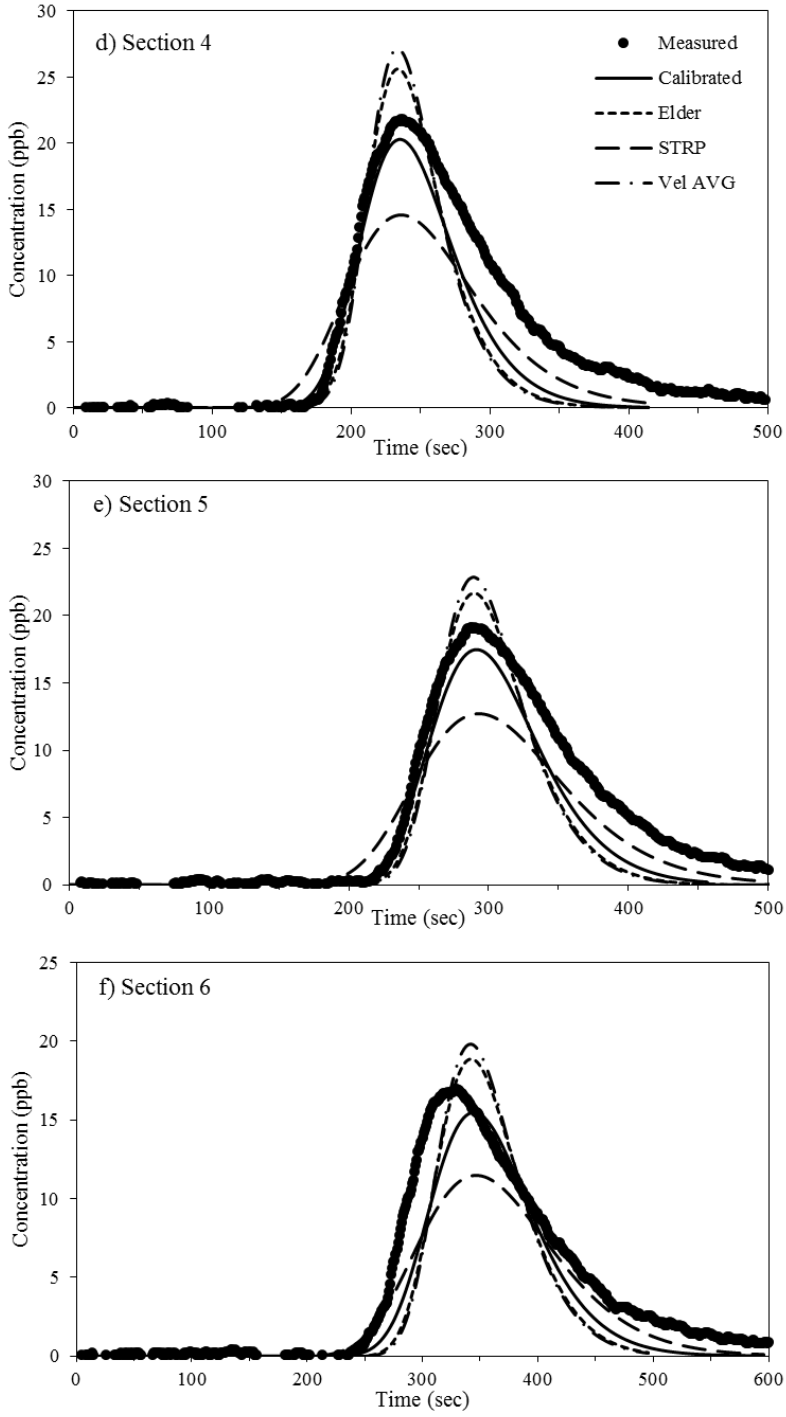

Fig. 8.7 Verification by dispersion methods in R317-1(cont)

Chapter 9. Conclusions and Future Study

In this study, large-scale experiments were conducted in the REC meandering channels, to find the shear effect to the flow and pollutant transport characteristics in meandering channels. First, the effect of the secondary current on the primary flow distribution was analyzed. The experimental results allowed the relations of the secondary flow strength to the depth to radius-of-curvature of the channel and channel roughness to be found. Then, the vertical profile equation for the secondary flow was developed to reflect the nonlinear term effects on the secondary flow. The proposed equation generated a vertical profile that showed a decrease in the maximum secondary flow strength at the top and bottom of the profile, compared to the existing equations, which omitted the nonlinear term.

The proposed velocity profile equation was inserted into the momentum equations with the dispersion stress method, in order to induce the effect of secondary flow, which is normally neglected in the depth averaging process. The simulation results using the proposed equation to the dispersion stress method for the two-dimensional flow solver HDM-2D showed that the simulation of the SNU M2, and Shumate channel fits well with the experimental results. Especially, the Rozovskii channel showed improvement over the dispersion stress model using Kikkawa's velocity equation, which was based on the linear behavior between the secondary flow and primary flow, as well as over the non-dispersion stress results in the distributions of primary flow velocity. The validation results with REC meandering channels revealed that the 2D hydrodynamic model with dispersion

stress term gave a better fit to the experimental data, than the simulation without the dispersion stress term with an MAP error at the peak concentration of 8-10% with about 1% improvement to the simulation results. This effect of the sharp bend was adequately represented by adopting the proposed velocity profile of the secondary flow to the dispersion stress term and secondary flow strength at the bends were further illuminated by comparisons with increasing depth to radius-of-curvature terms. The proposed equation incorporating nonlinearity showed the limitations to the growth of the secondary flow strength, and the HDM-2D with dispersion stress proves useful for assessing the secondary flow effect in meandering channels.

Second, the two dimensional dispersion coefficients were calculated from the vertical profile of the measured sections of the KICT REC channel by ADCP velocity using the triple integration method by Elder (1959) using the equation by Fischer (1954). This approach is useful since it does not require the tracer test experiments that must be conducted in order to calculate dispersion coefficients using conventional methods, such as the 2D stream-tube routing procedure. In order to compare the applicability of the velocity driven dispersion coefficients, experiments were conducted to compare the results with tracer test results using the 2D-STRP. The results showed that non-dimensional longitudinal dispersion coefficient, D_L / hu^*, by velocity profile ranges 4-6 which is close to Elder's result, while non-dimensional transverse dispersion coefficient, D_T / hu^*, ranges 0.05-0.4. However, the dispersion coefficients calculated using the 2D stream-tube routing procedure were quite large: 4-5 times larger than velocity driven values for

longitudinal dispersion coefficients, 1-3 times larger for the transverse dispersion coefficients. These differences could be explained by the fact that the concentration-driven dispersion coefficient included the mixing effects due to the irregularities of the channel, storage zones and numerical dispersion while velocity-driven coefficients only accounted for shear flow effects. In the case of transverse dispersion coefficients, the velocity driven dispersion showed less differences than the routing methods compared to the longitudinal dispersion, but large differences were shown in the apex of the channels. This showed that in strong meandering channels the difference between methods should be considered in their selection.

The dispersion coefficients were then inserted into the advection-dispersion model CTM-2D for the calculation and comparison to tracer test results. The calibrated dispersion coefficients by the CTM-2D model were between the velocity-driven results and concentration driven results by STRP with values of 10-14, due to the numerical dispersion of the model, which showed the importance of using both methods. The STRP values based on the concentration data had to account for the falling tail size, which overestimated the dispersion coefficients for the model. The MAP error of the validation of the dispersion coefficients averaged 8-10%, which was better than the non-dispersion stress model results of 9-11%. Overall, the simulation results proved the applicability of the CTM-2D model in reproducing concentration curves in meandering channels.

The flow model and pollutant transport model in this research are based on the depth-averaged momentum equations, and may have limitations in conditions where

the three dimensional flow characteristics are totally dominant such as near structures, or has very large depth compared to the width of the channel such as open estuaries, and oceans. Also, the pollutant transport model is based on the Fickian dispersion model for simulation of two-dimensional pollutant mixing, in which the model is applicable in the Taylor period. The near-field calculations would require a non-Fickian dispersion model for accurate simulations. Future studies could be focused on other comparison cases of dispersion coefficient calculation by velocity and tracer based tests, to find the discrepancy between the shear-driven dispersion and other types of residual dispersion. For accurate description of the residual dispersion or the representation of concentration curve tails, research concerning storage zones, recirculation zones and its application could be applied to this research. Also the continuous utilization of drone and aerial imagery techniques could be used for not only acquisition of the topographic data, but the concentration curves itself.

References

Alavian, V. (1986). "Dispersion tensor in rotating flows." *Journal of Hydraulic Engineering*, 112(8), 771-777.

Almquist, C. W., & Holley, E. R. (1985). "Transverse mixing in meandering laboratory channels with rectangular and naturally varying cross sections." *Center for Research in Water Resources,* Technical Report-205 September, University of Texas.

Akhtar, M. P., Sharma, N., Ojha, C. S. P. (2015). "2-D depth averaged modelling for curvilinear braided stretch of river Brahmaputra in India." *International Journal of Research in Engineering and Advanced Technology*, 3(1), 217-230.

Baek, K. O., Seo, I. W., Lee, K. W. (2006). "New equation on streamwise variation of secondary flow in meandering channels." *Journal of the Korean Society of Civil Engineers*, 26(4B), 371-378. (in Korean).

Baek, K. O., and Seo, I. W. (2008). "Prediction of transverse dispersion coefficient using vertical profile of secondary flow in meandering channels." *KSCE Journal of Civil Engineering*, 12(6), 417-426.

Baek, K. O., and Seo, I. W. (2011). "Transverse dispersion caused by secondary flow in curved channels." *Journal of Hydraulic Engineering*, 137(10), 1126-1134.

Baek, K. O., and Seo, I. W. (2013). "Empirical equation for transverse dispersion coefficient based on theoretical background in river bends." *Environmental fluid mechanics*, 13(5), 465-477.

Beltaos, S. (1980). “Transverse mixing tests in natural streams.” *J. Hydraul. Div., Am. Soc. Civ. Eng.,* 106(10), 1607–1625.

Bernard, R.S., Schneider. M.L. (1992). “Depth averaged numerical modeling for curved channels” *US Army Corps Engineers*, Technical Report HL 92-9.

Begnudelli, L., Valiani, A., Sanders, B.F. (2010). “A balanced treatment of secondary currents, turbulence and dispersion in a depth-integrated hydrodynamic and bed deformation model for channel bends.” *Adv. Water Resources*, 33(1), 17-33.

Blanckaert, K., and Graf, W. H. (2001). “Mean flow and turbulence in open-channel bend.” *J. Hydr. Engrg*., ASCE, 127(10), 835-847.

Blanckaert, K., and Graf, W. H. (2004). “Momentum transport in sharp open-channel bends.” *Journal of Hydraulic Engineering*, 130(3), 186-198.

Blanckaert, K., and de Vriend H. J. (2003). “Nonlinear modeling of mean flow redistribution in curved open channels.” *Water Resources Research*, 39(12), 1375-1389.

Blanckaert, K., and De Vriend H. J. (2004). “Secondary flow in sharp open-channel bends” *J. Fluid Mech.,* Cambridge, England, 498, 353-380.

Blanckaert, K., and de Vriend H. J. (2010). “Meander dynamics: a nonlinear model without curvature restrictions for flow in open-channel bends.” *Journal of Geophysical Research: Earth Surface.* 115(F4).

Bogle, G. V. (1997). Stream velocity profiles and longitudinal dispersion. *Journal of Hydraulic Engineering*, *123*(9), 816-820.

Boxall, J. B., & Guymer, I. (2003). "Analysis and prediction of transverse mixing coefficients in natural channels." *Journal of Hydraulic Engineering*, 129(2), 129-139.

Carr, M. L., and Rehmann, C. R. (2007). Measuring the dispersion coefficient with acoustic Doppler current profilers. *Journal of Hydraulic Engineering*, *133*(8), 977-982.

Chang, Y.C. (1971). *Lateral mixing in meandering channels*, Ph. D. thesis, University of Iowa, USA.

Chang, H. H. (1988). *Fluvial processes in river engineering*. John Wiley & Sons. Canada.

Chow, V. T. (1973*). Open-channel hydraulics*. International ed. McGraw-Hill.

Demuren, A. O., and Rodi W. (1986). " Calculation of flow and pollutant dispersion in meandering channels" *J. Fluid Mech.,* Cambridge, England, 172, 63-92.

Duan, J. G. (2004). "Simulation of flow and mass dispersion in meandering channels." *Journal of Hydraulic Engineering*, 130(10), 964-976.

Elder, J. W. (1959). "The dispersion of marked fluid in turbulent shear flow." *Journal of Fluid Mechanics*, 5(04), 544-560.

Engelund, F. (1974). "Flow and bed topography in channel bends." *J. Hydr. Div.,* ASCE, 100(11), 1631-1648.

Erwin, S. O., and Jacobson, R. B. (2015). Influence of Channel Morphology and Flow Regime on Larval Drift of Pallid Sturgeon in the Lower Missouri River. *River Research and Applications*, *31*(5), 538-551.

Falcon (1984), Secondary flow in curved open channels. *Annual Rev. Fluid Mech*. 16, 179-93.

Finnie, J., Donnell, B., Letter, J., Bernard, R. S. (1999). "Secondary flow correction for depth-averaged flow calculations." *Journal of Engineering Mechanics*, 125(7), 848-863.

Fischer, H. B. (1969). The effect of bends on dispersion in streams. *Water Resources Research*, 5(2), 496-506.

Fischer, H.B., List, J.E., Koh, R.C.Y., Imberger, J., and Brooks, N.H., (1979). *Mixing in Inland and Coastal Waters*, Academic Press.

Flokstra, C., (1977). "The closure problem for depth averaged two dimensional flow." *International Association for Hydraulic Res.,* Baden-Baden, Aug 15-19.

Gharmry, H. K., and Steffler, P. M. (2002). "Two dimensional vertically averaged and moment equations for rapidly varied flows." *Journal of Hydraulic Research*, 40(5), 579-587.

Henderson (1966), *Open channel flow*. MacMillian Publishing Company, New York.

Holley Jr, F. M., & Nerat, G. (1983). Field calibration of stream-tube dispersion model. *Journal of hydraulic engineering*, *109*(11), 1455-1470.

Hsieh, T.Y., Yang, J.C. (2003). "Investigation on the suitability of two-dimensional depth-averaged models for bend-flow simulation." *Journal of Hydraulic. Eng*., 129(8), 597-612.

Jeon, T. M., Baek, K. O., and Seo, I. W. (2007). "Development of an empirical

equation for the transverse dispersion coefficient in natural streams." *Envir. Fluid Mech.*, Springer, 7, 317-329.

Jia, Y., Wang, S. S. (1999). "Numerical model for channel flow and morphological change studies." *J. Hydr. Engrg*., ASCE, 924-933.

Jing, H. F., Li, C. G., Guo, Y. K., Zhu, L. J., Li, Y.T. (2014). "Numerical modeling of flow in continuous bends from Daliushu to Shapotou in Yellow River." *Water Science and Engineering*, 7(2), 194-207.

Johannesson, H., Parker, G. (1989). "Secondary flow in mildly sinuous channel." *Journal of Hydraulic Engineering*, 115(3), 289-309.

Kikkawa, H., Ikeda, S., Ohkawa, H., Kawamura, Y. (1973). "Secondary flow in a bend of turbulent stream." *Proceedings of the Japan Society of Civil Engineers*, No. 219, 107-114.

Kikkawa, H., Ikeda, S., Kitagawa, A. (1976). ''Flow and bed topography in curved open channels.'' *Journal of the Hydraulics Division*, 102(9), 1327–1342.

Kilpatrick, F. A. (1970). Dosage requirements for slug injections of Rhodamine BA and WT dyes. *Geological Survey research*, 250-253.

Kim, D. (2012). "Assessment of longitudinal dispersion coefficients using Acoustic Doppler Current Profilers in large river.", *Journal of Hydro-environment Research*, Vol. 6, No. 1, pp. 29-39.

Kim, T. W. (2007) *"Evolution of Velocity Distribution Due to Secondary Currents in Sharp Open Channel Bend,*" PhD. thesis, Seoul National University, Korea. (in Korean)

Kimura, I., Onda, S., Hosoda, T., Shimizu, Y. (2010) “Computations of suspended sediment transport in a shallow side-cavity using depth-averaged 2D models with effects of secondary currents.” *Journal of Hydro-environment Research*, 4(2), 153-161.

Knighton, D. (2014). *Fluvial forms and processes: a new perspective*. Routledge.

Lane, S. N., Bradbrook, K. F., Richards, K. S., Biron, P.A., Roy, A.G. (1999). “The application of computational fluid dynamics to natural river channels: three-dimensional versus two-dimensional approaches.” *Geomorphology*, 29(1), 1-20.

Launay, M., Le Coz, J., Camenen, B., Walter, C., Angot, H., Dramais, G., Faure, J.B., and Coquery, M. (2015). Calibrating pollutant dispersion in 1-D hydraulic models of river networks. *Journal of Hydro-environment Research*, 9(1), 120-132.

Lee, K. H. (2006) “*Experimental investigation of flow characteristics in meandering channels*” Master thesis, Seoul National University, Korea.

Lee, M. E., and Seo, I. W., (2013). "Spatially variable dispersion coefficients in meandering channels." *Journal of Hydraulic Engineering*, 139(2), 141-153.

Lien, H. C., Hsieh, T. Y., Yang, J. C., Yeh, K. C. (1999). “Bend flow simulation using 2D depth-averaged model.” *Journal of Hydraulic Engineering*, 125(10), 1097-1108

Molls, T., Chaudhry, M.H., “Depth averaged open channel flow model.” *J. Hydr. Engrg.*, ASCE, 121(6), 453-465.

Mueller, D. S., Wagner, C. R., Rehmel, M. S., Oberg, K. A., and Rainville, F. (2009).

Measuring discharge with Acoustic Doppler Current Profilers from a moving boat US Department of the Interior, US Geological Survey.

Muste, M., Yu, K., & Spasojevic, M. (2004). Practical aspects of ADCP data use for quantification of mean river flow characteristics; Part I: moving-vessel measurements. *Flow measurement and instrumentation*, 15(1), 1-16.

Odgaard, A. J. (1986). "River-meander model. I: Development." *Journal of Hydraulic. Engineering*, 115(11), 1433–1450.

Olsen, N. R. B. (2003). "Three-dimensional CFD modeling of self-forming meandering channel." *J. Hydr. Engrg*., ASCE, 129(5), 366-372.

Ottevanger, W., Blanckaert, K. J., Uijttewaal, W. S., de Vriend, H. J. (2013). "Meander dynamics: a reduced-order nonlinear model without curvature restrictions for flow and bed morphology." *Journal of Geophysical Research: Earth Surface,* 118(2), 1118-1131.

Park, I., and Seo, I. W. (2018). "Modeling non-Fickian pollutant mixing in open channel flows using two-dimensional particle dispersion model." *Advances in Water Resources*, 111, 105-120.

Parsons, D. R., Jackson, P. R., Czuba, J. A., Engel, F. L., et al. (2013). "Velocity Mapping Toolbox (VMT): a processing and visualization suite for moving-vessel ADCP measurements." *Earth Surface Processes and Landforms*, 38(11), 1244-1260.

Patra, K. C., Kar, S. K., and Bhattacharya, A. K. (2004). "Flow and velocity distribution in meandering compound channels." *J. Hydr. Engrg*., ASCE, 130(5), 398-411.

Pilechi, A., Mohammadian, A., Rennie, C. D., and Zhu, D. Z. (2016). Efficient method for coupling field data and numerical modeling for the estimation of transverse mixing coefficients in meandering rivers. *Journal of Hydraulic Engineering*, *142*(6), 04016009.

Prandtl, L. (1952). *Essentials of fluid dynamics*. Blackie, London.

Riley, J. D., and Rhoads, B.L. (2011). "Flow structure and channel morphology at a natural confluent meander bend." *Geomorphology*, 163-164, 84-98.

Rhoads, B. L., and Kenworthy, S. T. (1998). "Time-averaged flow structure in the central region of a stream confluence." *Earth Surface Processes and Landforms*, 23(2), 171-191.

Rowiński, P., & Chrzanowski, M. (2011). Influence of selected fluorescent dyes on small aquatic organisms. *Acta Geophysica*, *59*(1), 91-109.

Rozovskii, I. L. (1957). *Flow of water in bends of open channels*. The Israel Program for Scientific Translations, Jerusalem (First published by Academy Sciences of the Ukrainian SSR, Kiev).

Rutherford, J. C. (1994). *River mixing*, Wiley, Chichester, U.K..

Sayre, W. W. (1979). "Shore-attached thermal plumes in rivers." *In: Shen HW (ed) Modelling in Rivers*., Wiley-Interscience, London, 15.1-15.44

Sayre, W. W., and Chang, F. M. (1968). “A laboratory investigation of open-channel dispersion processes for dissolved, suspended, and floating dispersants.” *Professional paper no. 433-E*, USGS, Reston, Va.

Schwab, L. E., and Rehmann, C. R. (2015). Importance of vertical variations of velocity for shear dispersion in rivers. *Journal of Hydraulic Engineering*, *141*(10), 06015011.

Seo, I. W., and Baek, K. O. (2004). “Estimation of the longitudinal dispersion coefficient using the velocity profile in natural streams.” *Journal of Hydraulic Engineering*, 130(3), 227-236.

Seo, I. W., and Jung, Y. J., (2010) "Velocity Distribution of Secondary Currents in Curved Channels." *Journal of Hydrodynamics, Ser. B.*, 22(5), 617-622.

Seo, I. W., Lee, M. E., & Baek, K. O. (2008). “2D modeling of heterogeneous dispersion in meandering channels.” *Journal of Hydraulic Engineering*, 134(2), 196-204.

Seo, I. W., Shin, J., Kim, T. W. (2012). “The vertical profile of transverse velocity of secondary flow in meandering channels.” *10th International Conference on Hydroscience and Engineering,* Orlando, Florida, November 4-8.

Seo, I. W., Choi, H. J., Kim, Y. D., and Han, E. J. (2016). “Analysis of two-dimensional mixing in natural streams based on transient tracer tests.” *Journal of Hydraulic Engineering*, 142(8), 04016020.

Shen, C., Niu, J., Anderson, E. J., & Phanikumar, M. S. (2010). "Estimating longitudinal dispersion in rivers using Acoustic Doppler Current Profilers." *Advances in Water Resources*, 33(6), 615-623.

Shin, J. (2012). "*Development of Transverse Velocity Profile Equation of Secondary Currents in Curved Channels by Numerical Simulation*, Master Thesis, Seoul National University.

Shiono, K., and Knight, D. W. (1991). "Turbulent open-channel flows with variable depth across the channel." *J. Fluid Mech*., Cambridge, England, 222, 617-646.

Shiono, K., and Muto, D. W. (1998). "Complex flow mechanisms in compound meandering channels with overbank flow." *J. Fluid Mech*., Cambridge, England, 376, 222-261.

Shukry, A. (1950) "Flow around bends in an open flume" *ASCE Trans*, ASCE, 115, 7551-779.

Shumate, E. D. (1998). *Experimental description of flow at an open-channel junction*, Master Thesis, Univ. of Iowa.

Song, C. G., Seo, I. W., Kim, Y. D. (2012). "Analysis of secondary current effect in the modelling of shallow water flow in open channels." *Advances in Water Resources*, 41, 29-48.

Sontek, Y. S. I. (2015). RiverSurveyor S5/M9 System Manual. *San Diego*.

Stoesser, T. (2010). "Calculation of primary and secondary flow and boundary stress in a meandering channel" *Advances in Water Resources,* ASCE , 33*,* 158-170.

Sun, Y., Wells, M., Bailey, S., Anderson, E. J., & Schwab, D. J. (2011). Study on the

physical mixing patterns in the St. Clair River by dye release. In *Proc., 15th Workshop on Physical Processes in Natural Waters*. pp. 180-182.

Sukhodolov, A. N. (2012). "Structure of turbulent flow in a meander bend of a lowland river." *Water Resources Research*, 48(1), 1516-1537.

Taylor, G. (1954). "The dispersion of matter in turbulent flow through a pipe." *In Proceedings of the Royal Society of London A: Mathematical, Physical and Engineering Sciences* (Vol. 223, No. 1155, pp. 446-468). The Royal Society.

Thompson, J. (1876). ''On the origin and winding of rivers in alluvial plains, with remarks on flow around bends in pipes.'' *Proc., Royal Soc*., London, 25, 5.

Tominaga, A., and Nezu, I. (1991). "Turbulent structure in compound open channel flows." *J. Hydr. Engrg*., ASCE, 117, 21-41.

Turnipseed, D. P., & Sauer, V. B. (2010). *Discharge measurements at gaging stations* (No. 3-A8). US Geological Survey.

Uijttewaal, W. S. (2014). "Hydrodynamics of shallow flows: application to rivers." *Journal of Hydraulic Research*, 52(2), 157-172.

Vasquez, J. A., Millar, R. G., Steffler, P. M. (2005). "Vertically-averaged and moment of momentum model for alluvial bend morphology." *Proceedings of the 4th IAHR Symposium on River, Coastal and Esturarine Morphodynamics,* Taylor & Francis, London, 711-718.

de Vriend, H. J. (1977), "A mathematical model of steady flow in curved shallow channels." *Journal of Hydraulic Research*, 15(1), 37-54.

Weber, L. J., Schumate, E. D., and Mawer, N. (2001). “Experiments on flow at a 90 open-channel junction.” *Journal of Hydraulic Engineering*, 127(5), 340-350.

Wei, M., Blanckaert, K., Heyman, J., Li, D., and Schleiss, A. J. (2016), “A parametrical study on secondary flow in sharp open-channel bends: experiments and theoretical modeling.” *Journal of Hydro-environment Research*, 13, 1-13.

Wilson, C.A., Bates, P.D., Hervouet, J.M., (2001), “Comparison of turbulence models for stage-discharge rating curve prediction in reach-scale compound channel flows using two-dimensional finite element methods.” *Journal of Hydrology*, 256.42-58.

Yang, Q. Y., Lu, W. Z., Zhou, S. F., Wang, X. K. (2014), “Impact of dissipation and dispersion terms on simulations of open channel confluence flow using two-dimensional depth averaged model.” *Hydrological Processes*, 28(8), 3230-3240.

Yeh, K. C., Kennedy, J. F. (1993). “Momentum model of nonuniform channel bend flow I: Fixed beds.” *Journal of Hydraulic Engineering*, 119(7), 776-795.

Yotsukura, N., Fischer, H. B., & Sayre, W. W. (1970). *Measurement of mixing characteristics of the Missouri River between Sioux City, Iowa, and Plattsmouth, Nebraska* (No. 1899-G). USGS, Washington, DC.

Yotsukura, N., and Sayre, W. W. (1976). “Transverse mixing in natural channels.” *Water Resour. Res.*, 12(4), 695–704.

Zarrati, A. R., Tamai, N., Jin, Y. C. (2005). “Mathematical modeling of meandering channels with a generalized depth averaged model.” *Journal of Hydraulic Engineering*, 131(6), 467-475.

Zhu, Z., Motta, D., Jackson, P. R., & Garcia, M. H. (2017). Numerical modeling of simultaneous tracer release and piscicide treatment for invasive species control in the Chicago Sanitary and Ship Canal, Chicago, Illinois. *Environmental Fluid Mechanics*, 17(2), 211-229.

Appendix A.1 Velocity distributions for Andong Channel Experiment (AMC15)

y(m) / h(m)	Section 1 Velocity magnitude (m/s)																				
	0.5	0.7	0.9	1.1	1.3	1.5	1.7	1.9	2.1	2.3	2.5	2.7	2.9	3.1	3.3	3.5	3.7	3.9	4.1	4.3	4.5
0.15	0.667	0.911	0.980	0.994	0.993	0.960	0.907	0.873	0.847	0.819	0.822	0.731	0.701	0.705	0.686	0.663	0.639	0.593	0.517	0.455	0.430
0.20	0.632	0.896	0.975	0.994	0.985	0.955	0.916	0.892	0.855	0.823	0.826	0.732	0.693	0.692	0.672	0.646	0.619	0.573	0.495	0.435	0.425
0.25	0.639	0.885	0.972	1.011	0.989	0.959	0.930	0.908	0.863	0.822	0.809	0.718	0.677	0.659	0.635	0.605	0.571	0.525	0.458	0.398	0.417
0.30	0.000	0.899	0.982	1.022	0.977	0.956	0.945	0.915	0.845	0.797	0.769	0.699	0.651	0.614	0.594	0.561	0.528	0.500	0.435	0.367	0.000
0.35	0.000	0.931	0.993	1.023	0.971	0.968	0.944	0.894	0.816	0.773	0.708	0.650	0.632	0.588	0.569	0.535	0.499	0.000	0.000	0.000	0.000
0.40	0.000	0.938	1.012	1.012	0.942	0.964	0.917	0.862	0.824	0.786	0.680	0.000	0.000	0.000	0.000	0.000	0.000	0.000	0.000	0.000	0.000
0.45	0.000	0.936	0.000	0.968	0.896	0.936	0.879	0.828	0.814	0.000	0.000	0.000	0.000	0.000	0.000	0.000	0.000	0.000	0.000	0.000	0.000
0.50	0.000	0.000	0.000	0.951	0.832	0.880	0.831	0.814	0.000	0.000	0.000	0.000	0.000	0.000	0.000	0.000	0.000	0.000	0.000	0.000	0.000
0.55	0.000	0.000	0.000	0.000	0.793	0.854	0.814	0.000	0.000	0.000	0.000	0.000	0.000	0.000	0.000	0.000	0.000	0.000	0.000	0.000	0.000

y(m) / h(m)	Section 2 Velocity magnitude (m/s)																				
	0.5	0.7	0.9	1.1	1.3	1.5	1.7	1.9	2.1	2.3	2.5	2.7	2.9	3.1	3.3	3.5	3.7	3.9	4.1	4.3	4.5
0.15	0.279	0.307	0.371	0.439	0.452	0.523	0.529	0.582	0.644	0.659	0.694	0.782	0.807	0.802	0.764	0.738	0.699	0.686	0.660	0.601	0.503
0.20	0.282	0.303	0.368	0.435	0.449	0.524	0.537	0.594	0.663	0.669	0.695	0.787	0.811	0.793	0.756	0.728	0.697	0.689	0.658	0.592	0.525
0.25	0.278	0.274	0.357	0.421	0.447	0.516	0.542	0.604	0.681	0.680	0.707	0.807	0.823	0.798	0.756	0.724	0.699	0.701	0.660	0.579	0.537
0.30	0.000	0.252	0.348	0.410	0.439	0.513	0.534	0.600	0.680	0.695	0.713	0.796	0.819	0.789	0.740	0.724	0.693	0.699	0.667	0.584	0.000
0.35	0.000	0.000	0.000	0.000	0.436	0.492	0.515	0.581	0.663	0.693	0.730	0.796	0.812	0.790	0.737	0.722	0.681	0.692	0.678	0.000	0.000
0.40	0.000	0.000	0.000	0.000	0.000	0.512	0.495	0.552	0.638	0.669	0.718	0.764	0.764	0.757	0.719	0.693	0.664	0.689	0.687	0.000	0.000
0.45	0.000	0.000	0.000	0.000	0.000	0.511	0.477	0.527	0.622	0.647	0.717	0.767	0.744	0.751	0.718	0.681	0.640	0.672	0.000	0.000	0.000
0.50	0.000	0.000	0.000	0.000	0.000	0.000	0.000	0.510	0.608	0.631	0.690	0.735	0.702	0.730	0.710	0.669	0.634	0.000	0.000	0.000	0.000
0.55	0.000	0.000	0.000	0.000	0.000	0.000	0.000	0.000	0.608	0.630	0.698	0.730	0.688	0.730	0.710	0.665	0.629	0.000	0.000	0.000	0.000
0.60	0.000	0.000	0.000	0.000	0.000	0.000	0.000	0.000	0.000	0.633	0.688	0.711	0.664	0.714	0.698	0.654	0.000	0.000	0.000	0.000	0.000

y(m) / h(m)	Section 3 Velocity magnitude (m/s)																				
	0.5	0.7	0.9	1.1	1.3	1.5	1.7	1.9	2.1	2.3	2.5	2.7	2.9	3.1	3.3	3.5	3.7	3.9	4.1	4.3	4.5
0.15	0.507	0.520	0.560	0.580	0.603	0.643	0.664	0.677	0.674	0.706	0.741	0.763	0.787	0.839	0.860	0.862	0.902	0.928	0.931	0.883	0.881
0.20	0.504	0.524	0.562	0.583	0.608	0.647	0.668	0.679	0.680	0.713	0.746	0.767	0.793	0.837	0.860	0.857	0.893	0.920	0.917	0.881	0.886
0.25	0.494	0.527	0.566	0.588	0.615	0.651	0.672	0.683	0.690	0.723	0.757	0.776	0.808	0.837	0.857	0.846	0.873	0.900	0.902	0.879	0.000
0.30	0.000	0.511	0.547	0.577	0.611	0.647	0.671	0.681	0.693	0.726	0.758	0.774	0.808	0.823	0.826	0.819	0.846	0.864	0.864	0.864	0.000
0.35	0.000	0.501	0.528	0.557	0.595	0.634	0.658	0.668	0.688	0.723	0.752	0.765	0.797	0.803	0.788	0.781	0.813	0.830	0.850	0.000	0.000
0.40	0.000	0.000	0.516	0.541	0.571	0.610	0.633	0.644	0.670	0.704	0.727	0.735	0.765	0.764	0.742	0.742	0.778	0.814	0.000	0.000	0.000
0.45	0.000	0.000	0.000	0.529	0.555	0.580	0.603	0.612	0.630	0.661	0.693	0.709	0.725	0.746	0.728	0.725	0.000	0.000	0.000	0.000	0.000
0.50	0.000	0.000	0.000	0.000	0.546	0.562	0.586	0.595	0.607	0.633	0.672	0.000	0.688	0.000	0.000	0.000	0.000	0.000	0.000	0.000	0.000

y(m) / h(m)	Section 4 Velocity magnitude (m/s)																				
	0.5	0.7	0.9	1.1	1.3	1.5	1.7	1.9	2.1	2.3	2.5	2.7	2.9	3.1	3.3	3.5	3.7	3.9	4.1	4.3	4.5
0.15	0.511	0.578	0.603	0.668	0.738	0.772	0.817	0.847	0.872	0.857	0.808	0.737	0.684	0.628	0.533	0.450	0.421	0.396	0.308	0.188	0.076
0.20	0.560	0.596	0.600	0.677	0.742	0.774	0.829	0.858	0.872	0.865	0.810	0.744	0.691	0.635	0.528	0.454	0.422	0.390	0.307	0.183	0.046
0.25	0.000	0.564	0.592	0.687	0.749	0.772	0.838	0.861	0.861	0.863	0.809	0.755	0.705	0.642	0.534	0.460	0.434	0.399	0.308	0.164	0.013
0.30	0.000	0.556	0.576	0.680	0.741	0.763	0.832	0.856	0.838	0.842	0.803	0.762	0.712	0.651	0.547	0.490	0.449	0.419	0.324	0.166	0.000
0.35	0.000	0.000	0.567	0.663	0.724	0.740	0.804	0.825	0.811	0.806	0.781	0.765	0.724	0.674	0.584	0.522	0.474	0.452	0.335	0.000	0.000
0.40	0.000	0.000	0.000	0.657	0.707	0.730	0.778	0.795	0.780	0.762	0.739	0.756	0.726	0.693	0.618	0.564	0.506	0.458	0.353	0.000	0.000
0.45	0.000	0.000	0.000	0.000	0.688	0.712	0.757	0.765	0.744	0.729	0.696	0.733	0.721	0.702	0.637	0.593	0.539	0.468	0.364	0.000	0.000
0.50	0.000	0.000	0.000	0.000	0.000	0.707	0.710	0.720	0.699	0.668	0.628	0.670	0.649	0.642	0.616	0.603	0.573	0.490	0.000	0.000	0.000
0.55	0.000	0.000	0.000	0.000	0.000	0.654	0.656	0.653	0.655	0.613	0.576	0.619	0.598	0.598	0.587	0.572	0.567	0.000	0.000	0.000	0.000
0.60	0.000	0.000	0.000	0.000	0.000	0.000	0.612	0.604	0.632	0.593	0.533	0.544	0.504	0.517	0.550	0.543	0.000	0.000	0.000	0.000	0.000
0.65	0.000	0.000	0.000	0.000	0.000	0.000	0.000	0.568	0.000	0.594	0.000	0.522	0.494	0.507	0.542	0.000	0.000	0.000	0.000	0.000	0.000

y(m) / h(m)	Section 5 Velocity magnitude (m/s)																					
	0.5	0.7	0.9	1.1	1.3	1.5	1.7	1.9	2.1	2.3	2.5	2.7	2.9	3.1	3.3	3.5	3.7	3.9	4.1	4.3	4.5	4.7
0.15	0.628	0.764	0.914	0.985	0.977	0.936	0.909	0.869	0.837	0.821	0.822	0.769	0.752	0.712	0.673	0.597	0.537	0.488	0.420	0.344	0.318	0.257
0.20	0.661	0.778	0.901	0.983	0.975	0.938	0.906	0.867	0.840	0.821	0.821	0.771	0.750	0.712	0.680	0.599	0.531	0.479	0.403	0.339	0.296	0.226
0.25	0.000	0.786	0.887	0.977	0.972	0.942	0.902	0.860	0.843	0.817	0.813	0.769	0.747	0.713	0.690	0.604	0.525	0.460	0.372	0.324	0.276	0.203
0.30	0.000	0.803	0.866	0.941	0.945	0.929	0.889	0.851	0.836	0.802	0.793	0.752	0.718	0.701	0.686	0.597	0.506	0.434	0.344	0.284	0.249	0.000
0.35	0.000	0.000	0.885	0.919	0.913	0.912	0.871	0.827	0.813	0.780	0.770	0.718	0.688	0.675	0.664	0.580	0.484	0.401	0.326	0.257	0.000	0.000
0.40	0.000	0.000	0.000	0.901	0.881	0.879	0.835	0.792	0.783	0.745	0.731	0.682	0.646	0.619	0.616	0.545	0.465	0.383	0.000	0.000	0.000	0.000
0.45	0.000	0.000	0.000	0.000	0.877	0.873	0.798	0.753	0.740	0.719	0.680	0.614	0.610	0.586	0.587	0.527	0.000	0.000	0.000	0.000	0.000	0.000
0.50	0.000	0.000	0.000	0.000	0.000	0.000	0.770	0.734	0.721	0.702	0.646	0.584	0.000	0.000	0.000	0.000	0.000	0.000	0.000	0.000	0.000	0.000

y(m) / h(m)	Section 6 Velocity magnitude (m/s)																				
	0.5	0.7	0.9	1.1	1.3	1.5	1.7	1.9	2.1	2.3	2.5	2.7	2.9	3.1	3.3	3.5	3.7	3.9	4.1	4.3	4.5
0.15	0.389	0.342	0.388	0.428	0.505	0.568	0.613	0.674	0.707	0.734	0.751	0.797	0.802	0.762	0.756	0.736	0.698	0.683	0.639	0.606	0.536
0.20	0.394	0.374	0.395	0.435	0.514	0.570	0.626	0.687	0.715	0.729	0.747	0.797	0.798	0.749	0.745	0.716	0.702	0.686	0.644	0.607	0.557
0.25	0.384	0.383	0.385	0.441	0.529	0.576	0.642	0.699	0.727	0.729	0.740	0.791	0.775	0.737	0.724	0.687	0.688	0.681	0.650	0.606	0.570
0.30	0.000	0.342	0.389	0.436	0.534	0.579	0.640	0.685	0.723	0.704	0.727	0.787	0.754	0.714	0.704	0.655	0.658	0.671	0.645	0.602	0.000
0.35	0.000	0.271	0.412	0.454	0.540	0.564	0.614	0.654	0.704	0.681	0.711	0.766	0.730	0.705	0.681	0.646	0.645	0.652	0.624	0.592	0.000
0.40	0.000	0.000	0.000	0.484	0.556	0.541	0.595	0.637	0.662	0.619	0.670	0.726	0.701	0.685	0.660	0.635	0.643	0.629	0.604	0.000	0.000
0.45	0.000	0.000	0.000	0.000	0.568	0.533	0.585	0.625	0.630	0.599	0.628	0.673	0.663	0.661	0.636	0.629	0.649	0.617	0.000	0.000	0.000
0.50	0.000	0.000	0.000	0.000	0.000	0.536	0.590	0.626	0.628	0.589	0.588	0.612	0.627	0.664	0.628	0.618	0.639	0.605	0.000	0.000	0.000
0.55	0.000	0.000	0.000	0.000	0.000	0.000	0.000	0.000	0.641	0.611	0.577	0.592	0.613	0.000	0.000	0.000	0.000	0.000	0.000	0.000	0.000

A.2 Velocity distributions for Andong Channel Experiment (AMC17)

y(m) / h(m)	Section 1 Velocity magnitude (m/s)																					
	0.5	0.7	0.9	1.1	1.3	1.5	1.7	1.9	2.1	2.3	2.5	2.7	2.9	3.1	3.3	3.5	3.7	3.9	4.1	4.3	4.5	4.7
0.15	0.616	0.573	0.708	0.722	0.706	0.688	0.659	0.657	0.632	0.585	0.575	0.589	0.588	0.568	0.535	0.513	0.469	0.439	0.377	0.317	0.295	0.267
0.20	0.575	0.564	0.704	0.724	0.712	0.690	0.662	0.660	0.636	0.591	0.579	0.593	0.589	0.569	0.539	0.516	0.473	0.443	0.377	0.315	0.292	0.257
0.25	0.000	0.563	0.703	0.722	0.715	0.693	0.666	0.664	0.643	0.600	0.584	0.600	0.585	0.565	0.542	0.519	0.482	0.450	0.379	0.318	0.287	0.238
0.30	0.000	0.535	0.664	0.707	0.712	0.696	0.661	0.654	0.636	0.598	0.584	0.599	0.586	0.567	0.541	0.513	0.486	0.447	0.383	0.317	0.272	0.216
0.35	0.000	0.000	0.649	0.686	0.705	0.691	0.650	0.638	0.620	0.588	0.573	0.590	0.582	0.561	0.536	0.503	0.481	0.438	0.385	0.329	0.263	0.000
0.40	0.000	0.000	0.611	0.644	0.688	0.680	0.608	0.596	0.588	0.557	0.557	0.567	0.574	0.548	0.520	0.493	0.473	0.427	0.393	0.348	0.000	0.000
0.45	0.000	0.000	0.609	0.625	0.673	0.656	0.560	0.557	0.543	0.510	0.525	0.531	0.546	0.523	0.493	0.466	0.453	0.424	0.402	0.000	0.000	0.000
0.50	0.000	0.000	0.000	0.000	0.659	0.644	0.523	0.526	0.505	0.464	0.485	0.504	0.529	0.507	0.474	0.453	0.445	0.423	0.000	0.000	0.000	0.000
0.55	0.000	0.000	0.000	0.000	0.000	0.000	0.000	0.000	0.000	0.442	0.458	0.000	0.000	0.000	0.000	0.000	0.000	0.000	0.000	0.000	0.000	0.000

y(m) / h(m)	Section 2 Velocity magnitude (m/s)																							
	0.5	0.7	0.9	1.1	1.3	1.5	1.7	1.9	2.1	2.3	2.5	2.7	2.9	3.1	3.3	3.5	3.7	3.9	4.1	4.3	4.5	4.7	4.9	5.1	5.3
0.15	0.220	0.239	0.244	0.300	0.317	0.330	0.343	0.370	0.394	0.433	0.448	0.450	0.484	0.493	0.492	0.501	0.521	0.533	0.539	0.573	0.505	0.448	0.434	0.391	0.335
0.20	0.205	0.253	0.256	0.303	0.325	0.338	0.353	0.373	0.398	0.435	0.457	0.463	0.492	0.498	0.504	0.510	0.524	0.535	0.542	0.567	0.512	0.459	0.437	0.382	0.327
0.25	0.207	0.279	0.276	0.307	0.342	0.356	0.376	0.384	0.403	0.441	0.473	0.486	0.504	0.520	0.534	0.517	0.520	0.543	0.546	0.561	0.517	0.465	0.431	0.400	0.353
0.30	0.000	0.290	0.299	0.314	0.350	0.365	0.389	0.397	0.409	0.444	0.484	0.500	0.524	0.529	0.558	0.540	0.527	0.545	0.546	0.560	0.528	0.481	0.455	0.405	0.000
0.35	0.000	0.000	0.321	0.334	0.361	0.381	0.398	0.413	0.420	0.452	0.496	0.511	0.540	0.542	0.576	0.552	0.534	0.549	0.546	0.566	0.537	0.507	0.479	0.000	0.000
0.40	0.000	0.000	0.329	0.348	0.376	0.385	0.392	0.427	0.430	0.443	0.491	0.498	0.526	0.543	0.579	0.567	0.545	0.554	0.544	0.565	0.554	0.567	0.000	0.000	0.000
0.45	0.000	0.000	0.335	0.361	0.401	0.388	0.383	0.432	0.431	0.436	0.477	0.476	0.498	0.532	0.564	0.570	0.554	0.564	0.541	0.571	0.567	0.601	0.000	0.000	0.000
0.50	0.000	0.000	0.000	0.355	0.413	0.388	0.374	0.438	0.434	0.428	0.445	0.447	0.473	0.509	0.544	0.574	0.562	0.572	0.553	0.570	0.575	0.000	0.000	0.000	0.000
0.55	0.000	0.000	0.000	0.000	0.000	0.390	0.373	0.437	0.436	0.432	0.430	0.441	0.470	0.494	0.519	0.566	0.574	0.589	0.572	0.577	0.000	0.000	0.000	0.000	0.000
0.60	0.000	0.000	0.000	0.000	0.000	0.000	0.000	0.000	0.000	0.000	0.000	0.000	0.000	0.000	0.000	0.563	0.575	0.592	0.587	0.000	0.000	0.000	0.000	0.000	0.000

y(m) / h(m)	Section 3 Velocity magnitude (m/s)																						
	0.5	0.7	0.9	1.1	1.3	1.5	1.7	1.9	2.1	2.3	2.5	2.7	2.9	3.1	3.3	3.5	3.7	3.9	4.1	4.3	4.5	4.7	4.9
0.15	0.165	0.209	0.238	0.278	0.322	0.376	0.414	0.433	0.465	0.469	0.501	0.517	0.529	0.546	0.564	0.578	0.610	0.626	0.661	0.674	0.659	0.687	0.668
0.20	0.166	0.206	0.233	0.276	0.320	0.381	0.421	0.440	0.471	0.479	0.508	0.520	0.531	0.547	0.566	0.584	0.611	0.628	0.659	0.669	0.657	0.671	0.657
0.25	0.000	0.204	0.232	0.276	0.317	0.385	0.432	0.456	0.482	0.499	0.521	0.527	0.537	0.550	0.570	0.593	0.614	0.635	0.655	0.667	0.663	0.640	0.642
0.30	0.000	0.000	0.240	0.263	0.307	0.387	0.445	0.469	0.486	0.506	0.524	0.528	0.541	0.556	0.576	0.598	0.617	0.640	0.652	0.668	0.664	0.614	0.000
0.35	0.000	0.000	0.253	0.241	0.303	0.383	0.447	0.474	0.484	0.505	0.516	0.520	0.543	0.559	0.580	0.602	0.620	0.644	0.648	0.662	0.655	0.594	0.000
0.40	0.000	0.000	0.000	0.222	0.303	0.382	0.439	0.462	0.474	0.505	0.486	0.499	0.534	0.552	0.580	0.598	0.614	0.639	0.640	0.644	0.638	0.000	0.000
0.45	0.000	0.000	0.000	0.000	0.000	0.371	0.422	0.444	0.464	0.493	0.448	0.470	0.511	0.533	0.567	0.579	0.598	0.623	0.625	0.617	0.000	0.000	0.000
0.50	0.000	0.000	0.000	0.000	0.000	0.364	0.382	0.432	0.447	0.479	0.410	0.440	0.481	0.504	0.542	0.549	0.576	0.595	0.610	0.603	0.000	0.000	0.000
0.55	0.000	0.000	0.000	0.000	0.000	0.000	0.359	0.429	0.439	0.463	0.396	0.420	0.460	0.470	0.502	0.509	0.542	0.560	0.000	0.000	0.000	0.000	0.000
0.60	0.000	0.000	0.000	0.000	0.000	0.000	0.000	0.000	0.000	0.000	0.000	0.408	0.000	0.448	0.482	0.492	0.527	0.540	0.000	0.000	0.000	0.000	0.000

y(m) / h(m)	Section 4 Velocity magnitude (m/s)																							
	0.5	0.7	0.9	1.1	1.3	1.5	1.7	1.9	2.1	2.3	2.5	2.7	2.9	3.1	3.3	3.5	3.7	3.9	4.1	4.3	4.5	4.7	4.9	5.1
0.15	0.325	0.298	0.397	0.477	0.534	0.568	0.621	0.641	0.630	0.649	0.639	0.609	0.524	0.492	0.484	0.463	0.439	0.437	0.401	0.351	0.294	0.251	0.195	0.127
0.20	0.345	0.315	0.400	0.480	0.537	0.570	0.630	0.639	0.625	0.646	0.644	0.615	0.538	0.507	0.492	0.470	0.446	0.435	0.406	0.354	0.295	0.251	0.194	0.125
0.25	0.357	0.365	0.406	0.487	0.539	0.570	0.635	0.633	0.620	0.648	0.649	0.623	0.561	0.533	0.508	0.480	0.456	0.436	0.415	0.359	0.298	0.251	0.191	0.130
0.30	0.000	0.401	0.414	0.484	0.541	0.570	0.630	0.621	0.613	0.641	0.647	0.616	0.568	0.548	0.516	0.494	0.469	0.447	0.413	0.356	0.284	0.248	0.206	0.000
0.35	0.000	0.409	0.411	0.473	0.529	0.562	0.617	0.606	0.599	0.628	0.623	0.589	0.561	0.553	0.519	0.499	0.478	0.458	0.415	0.349	0.263	0.242	0.212	0.000
0.40	0.000	0.000	0.412	0.482	0.532	0.550	0.600	0.588	0.575	0.591	0.585	0.545	0.537	0.543	0.511	0.502	0.475	0.463	0.414	0.335	0.248	0.241	0.000	0.000
0.45	0.000	0.000	0.000	0.505	0.544	0.545	0.584	0.572	0.546	0.554	0.539	0.503	0.514	0.530	0.501	0.496	0.463	0.447	0.418	0.328	0.000	0.000	0.000	0.000
0.50	0.000	0.000	0.000	0.000	0.557	0.545	0.543	0.524	0.506	0.514	0.480	0.452	0.462	0.482	0.486	0.483	0.440	0.438	0.415	0.000	0.000	0.000	0.000	0.000
0.55	0.000	0.000	0.000	0.000	0.553	0.537	0.504	0.478	0.470	0.480	0.435	0.417	0.425	0.431	0.468	0.485	0.430	0.422	0.000	0.000	0.000	0.000	0.000	0.000
0.60	0.000	0.000	0.000	0.000	0.000	0.532	0.476	0.434	0.435	0.469	0.397	0.377	0.395	0.385	0.447	0.482	0.000	0.000	0.000	0.000	0.000	0.000	0.000	0.000
0.65	0.000	0.000	0.000	0.000	0.000	0.000	0.000	0.000	0.000	0.464	0.392	0.368	0.397	0.375	0.000	0.000	0.000	0.000	0.000	0.000	0.000	0.000	0.000	0.000

y(m) / h(m)	Section 5 Velocity magnitude (m/s)																							
	0.5	0.7	0.9	1.1	1.3	1.5	1.7	1.9	2.1	2.3	2.5	2.7	2.9	3.1	3.3	3.5	3.7	3.9	4.1	4.3	4.5	4.7	4.9	5.1
0.15	0.294	0.479	0.561	0.636	0.690	0.694	0.679	0.649	0.639	0.617	0.568	0.561	0.541	0.516	0.503	0.462	0.465	0.436	0.403	0.375	0.337	0.280	0.225	0.200
0.20	0.330	0.502	0.565	0.627	0.686	0.691	0.675	0.649	0.636	0.618	0.573	0.564	0.545	0.521	0.505	0.473	0.474	0.438	0.409	0.380	0.337	0.279	0.226	0.193
0.25	0.000	0.540	0.544	0.598	0.673	0.681	0.671	0.646	0.632	0.618	0.583	0.574	0.551	0.529	0.507	0.494	0.489	0.442	0.421	0.387	0.336	0.278	0.207	0.176
0.30	0.000	0.000	0.556	0.592	0.648	0.665	0.658	0.637	0.625	0.613	0.579	0.573	0.551	0.534	0.515	0.502	0.496	0.441	0.424	0.383	0.323	0.272	0.213	0.000
0.35	0.000	0.000	0.000	0.607	0.630	0.645	0.645	0.626	0.616	0.604	0.569	0.568	0.549	0.534	0.516	0.500	0.491	0.431	0.414	0.368	0.324	0.268	0.000	0.000
0.40	0.000	0.000	0.000	0.633	0.619	0.639	0.618	0.587	0.586	0.591	0.542	0.548	0.529	0.519	0.506	0.488	0.471	0.409	0.391	0.343	0.329	0.000	0.000	0.000
0.45	0.000	0.000	0.000	0.000	0.615	0.628	0.587	0.554	0.551	0.574	0.516	0.527	0.504	0.484	0.475	0.462	0.438	0.384	0.374	0.338	0.000	0.000	0.000	0.000
0.50	0.000	0.000	0.000	0.000	0.000	0.631	0.543	0.516	0.515	0.556	0.494	0.506	0.467	0.433	0.435	0.429	0.399	0.364	0.365	0.000	0.000	0.000	0.000	0.000
0.55	0.000	0.000	0.000	0.000	0.000	0.000	0.522	0.515	0.505	0.546	0.488	0.499	0.454	0.401	0.411	0.410	0.378	0.353	0.000	0.000	0.000	0.000	0.000	0.000

y(m) / h(m)	Section 6 Velocity magnitude (m/s)																								
	0.5	0.7	0.9	1.1	1.3	1.5	1.7	1.9	2.1	2.3	2.5	2.7	2.9	3.1	3.3	3.5	3.7	3.9	4.1	4.3	4.5	4.7	4.9	5.1	5.3	5.5
0.15	0.284	0.290	0.317	0.328	0.346	0.349	0.399	0.386	0.403	0.453	0.483	0.493	0.489	0.550	0.541	0.597	0.573	0.561	0.556	0.551	0.512	0.480	0.497	0.474	0.495	0.418
0.20	0.278	0.281	0.320	0.334	0.353	0.357	0.398	0.394	0.415	0.455	0.491	0.496	0.492	0.562	0.540	0.588	0.571	0.559	0.549	0.544	0.509	0.472	0.499	0.480	0.493	0.416
0.25	0.279	0.264	0.325	0.357	0.373	0.373	0.404	0.406	0.437	0.467	0.503	0.503	0.501	0.572	0.540	0.576	0.565	0.551	0.541	0.549	0.508	0.465	0.502	0.486	0.496	0.403
0.30	0.000	0.261	0.323	0.378	0.406	0.395	0.424	0.425	0.453	0.479	0.513	0.519	0.511	0.567	0.526	0.570	0.560	0.545	0.536	0.540	0.503	0.472	0.505	0.480	0.485	0.426
0.35	0.000	0.000	0.333	0.395	0.437	0.414	0.447	0.448	0.468	0.489	0.507	0.521	0.526	0.551	0.510	0.574	0.551	0.531	0.528	0.543	0.504	0.499	0.507	0.473	0.468	0.435
0.40	0.000	0.000	0.339	0.400	0.446	0.418	0.448	0.459	0.470	0.487	0.500	0.508	0.513	0.519	0.485	0.551	0.526	0.517	0.522	0.539	0.503	0.511	0.511	0.470	0.461	0.467
0.45	0.000	0.000	0.000	0.409	0.443	0.414	0.432	0.447	0.469	0.486	0.471	0.478	0.497	0.508	0.476	0.548	0.511	0.500	0.514	0.542	0.491	0.505	0.509	0.467	0.443	0.000
0.50	0.000	0.000	0.000	0.000	0.432	0.410	0.425	0.433	0.458	0.485	0.444	0.446	0.459	0.520	0.478	0.526	0.491	0.501	0.517	0.535	0.476	0.498	0.507	0.461	0.000	0.000
0.55	0.000	0.000	0.000	0.000	0.000	0.407	0.422	0.425	0.455	0.489	0.419	0.429	0.450	0.538	0.489	0.532	0.491	0.503	0.515	0.533	0.464	0.498	0.503	0.000	0.000	0.000

Appendix A.3 Concentration data for Andong Channel Experiment

AMC 15 Section 1

y(m) / t(sec)	Concentration (ppb)				
	0.9	1.8	2.7	3.6	4.5
30.0	0.00	0.00	0.13	0.19	0.00
31.0	0.00	0.00	0.23	0.00	0.00
32.0	0.00	0.00	0.03	0.00	0.00
33.0	0.00	0.00	0.13	0.09	0.00
34.0	0.00	0.00	0.03	0.19	0.00
35.0	0.47	0.00	0.03	0.29	0.08
36.0	2.97	0.00	0.00	0.19	0.18
37.0	6.37	0.00	0.53	0.09	0.08
38.0	12.57	0.22	1.63	0.49	0.00
39.0	18.97	1.12	3.63	0.99	0.00
40.0	26.77	3.02	6.43	1.59	0.00
41.0	35.07	7.32	10.43	3.09	0.00
42.0	42.67	12.12	15.63	5.29	0.00
43.0	47.27	19.22	22.43	8.59	0.00
44.0	49.97	26.72	29.53	13.39	0.18
45.0	50.67	34.72	35.93	17.89	0.88
46.0	49.57	41.42	41.63	22.59	1.48
47.0	48.67	46.82	45.43	27.69	2.18
48.0	47.67	50.62	47.63	31.69	3.58
49.0	46.07	52.32	49.63	35.29	5.18
50.0	44.97	53.12	50.03	37.99	7.38
51.0	43.27	53.22	49.53	40.09	9.98
52.0	41.07	52.52	48.63	41.49	12.58
53.0	38.57	51.92	47.53	42.59	15.18
54.0	36.07	50.22	45.83	43.19	17.28
55.0	33.87	48.02	43.73	43.19	19.18
56.0	31.87	45.42	41.73	42.49	21.28
57.0	29.77	43.02	39.83	41.39	23.18
58.0	27.77	40.92	38.13	39.79	24.78
59.0	25.97	38.82	36.23	38.29	25.68
60.0	24.27	36.72	33.93	36.89	26.38
61.0	22.77	34.62	31.93	34.99	27.08
62.0	21.07	32.32	30.13	33.19	27.68
63.0	19.67	30.22	28.43	31.59	27.88
64.0	18.37	28.32	26.63	29.89	28.28
65.0	16.97	26.42	24.63	28.19	27.88
66.0	15.77	24.52	22.93	26.59	27.88
67.0	14.67	22.72	21.13	24.89	27.38
68.0	13.57	21.22	19.53	23.19	26.58
69.0	12.47	19.72	18.13	21.89	25.48
70.0	11.57	18.42	16.83	20.39	24.68
71.0	10.57	16.72	15.83	19.09	23.58
72.0	9.77	15.62	14.73	17.59	22.48
73.0	8.97	14.42	13.53	16.49	21.48
74.0	8.37	13.42	12.63	15.19	20.28
75.0	7.77	12.42	11.73	14.29	19.28
76.0	7.17	11.52	10.93	13.39	18.18
77.0	6.57	10.62	10.13	12.49	17.08
78.0	6.07	10.02	9.23	11.49	15.98
79.0	5.47	9.22	8.63	10.59	14.98
80.0	5.17	8.52	8.13	9.59	14.28
81.0	4.87	7.92	7.43	8.89	13.28
82.0	4.57	7.22	6.93	8.09	12.38
83.0	4.27	6.62	6.43	7.39	11.58
84.0	3.97	6.22	5.93	6.79	10.88
85.0	3.47	5.62	5.33	6.39	10.08

86.0	3.07	5.22	5.13	5.89	9.58
87.0	3.07	4.62	4.93	5.39	9.18
88.0	2.77	4.32	4.63	4.99	8.48
89.0	2.47	4.02	4.33	4.69	7.88
90.0	2.27	3.62	3.83	4.19	7.38
91.0	1.87	3.22	3.63	4.09	6.78
92.0	1.87	2.92	3.43	3.79	6.28
93.0	1.87	2.62	3.13	3.39	5.88
94.0	1.67	2.42	2.73	3.19	5.38
95.0	1.57	2.22	2.53	2.99	4.98
96.0	1.47	2.12	2.43	2.89	4.78
97.0	1.47	2.02	2.43	2.59	4.78
98.0	1.37	1.92	2.23	2.29	4.28
99.0	1.27	1.82	2.13	2.19	3.88
100.0	1.07	1.62	2.03	2.09	3.88
101.0	0.87	1.52	1.73	1.79	3.58
102.0	0.87	1.32	1.63	1.69	3.28
103.0	0.77	1.02	1.73	1.69	3.08
104.0	0.67	0.92	1.63	1.39	2.78
105.0	0.77	1.02	1.43	1.29	2.68
106.0	0.67	0.92	1.33	1.19	2.38
107.0	0.67	0.92	1.13	1.09	2.38
108.0	0.67	0.72	1.13	0.89	2.18
109.0	0.47	0.72	1.03	0.79	2.18
110.0	0.37	0.72	0.93	0.79	2.08
111.0	0.27	0.62	0.83	0.69	1.98
112.0	0.27	0.42	0.83	0.59	1.98
113.0	0.27	0.32	0.83	0.49	1.68
114.0	0.27	0.22	0.73	0.49	1.68
115.0	0.17	0.02	0.63	0.39	1.48
116.0	0.00	0.00	0.83	0.39	1.58
117.0	0.00	0.00	0.83	0.39	1.38
118.0	0.00	0.00	0.83	0.39	1.18
119.0	0.00	0.00	0.83	0.49	0.98
120.0	0.00	0.00	0.83	0.49	0.88
121.0	0.00	0.00	0.73	0.39	0.68
122.0	0.00	0.00	0.63	0.39	0.48
123.0	0.00	0.00	0.63	0.29	0.48
124.0	0.00	0.00	0.63	0.29	0.38
125.0	0.27	0.00	0.43	0.19	0.48
126.0	0.17	0.00	0.53	0.29	0.38
127.0	0.17	0.00	0.53	0.19	0.28
128.0	0.37	0.00	0.43	0.19	0.28
129.0	0.37	0.02	0.43	0.09	0.28
130.0	0.37	0.00	0.53	0.00	0.28
131.0	0.27	0.02	0.53	0.00	0.00
132.0	0.47	0.00	0.63	0.00	0.08
133.0	0.57	0.02	0.63	0.09	0.18
134.0	0.47	0.12	0.53	0.00	0.00
135.0	0.47	0.02	0.43	0.00	0.00
136.0	0.37	0.00	0.33	0.00	0.00
137.0	0.47	0.00	0.33	0.00	0.00
138.0	0.27	0.00	0.33	0.00	0.00
139.0	0.07	0.00	0.23	0.00	0.00
140.0	0.07	0.12	0.03	0.00	0.00

AMC 15 Section 2

y(m) / 1t(sec)	Concentration (ppb)				
	0.9	1.8	2.7	3.6	4.5
50.0	0.32	0.41	0.30	0.39	0.00
51.0	0.32	0.21	0.30	0.49	0.00
52.0	0.12	0.21	0.30	0.39	0.00
53.0	0.02	0.11	0.30	0.29	0.00
54.0	0.02	0.11	0.20	0.19	0.00
55.0	0.02	0.11	0.30	0.39	0.00
56.0	0.00	0.01	0.50	0.49	0.00
57.0	0.00	0.00	1.20	0.49	0.00
58.0	0.00	0.01	1.50	2.39	0.00
59.0	0.00	0.21	3.10	3.49	0.00
60.0	0.00	0.31	4.50	6.29	0.00
61.0	0.00	0.81	5.90	7.89	0.22
62.0	0.00	1.51	8.10	13.39	0.32
63.0	0.00	2.71	10.80	14.79	0.62
64.0	0.22	4.11	13.00	16.69	3.12
65.0	0.62	5.21	15.60	18.69	5.42
66.0	1.12	6.81	17.10	20.59	6.02
67.0	1.82	8.71	17.20	21.79	7.42
68.0	2.82	10.41	17.10	22.89	9.62
69.0	4.42	13.01	17.40	24.29	12.52
70.0	6.42	15.41	17.80	25.69	15.82
71.0	8.62	17.51	18.60	26.69	18.52
72.0	11.42	18.51	18.70	27.49	20.52
73.0	14.22	19.51	19.10	27.99	21.72
74.0	16.92	20.11	19.70	28.49	22.62
75.0	19.42	20.41	20.20	28.49	23.02
76.0	21.62	20.81	20.80	28.49	23.52
77.0	23.62	21.61	21.10	28.59	24.42
78.0	25.22	21.91	21.40	27.89	25.42
79.0	26.42	22.11	21.90	28.19	26.62
80.0	27.72	22.31	22.70	27.99	27.22
81.0	28.92	22.41	23.30	27.89	27.52
82.0	30.12	22.31	23.40	27.79	27.12
83.0	30.92	22.41	23.70	26.89	26.62
84.0	31.32	22.31	23.50	26.79	25.92
85.0	31.62	22.01	23.30	26.39	25.12
86.0	31.72	22.01	22.90	25.79	24.32
87.0	31.62	21.71	22.40	25.19	23.82
88.0	31.52	21.71	21.80	24.79	23.32
89.0	31.52	21.51	21.50	24.39	22.92
90.0	31.22	21.31	21.20	23.89	22.32
91.0	30.62	20.91	20.60	23.09	21.42
92.0	29.82	20.61	19.30	21.69	20.42
93.0	29.32	20.21	18.50	20.49	19.92
94.0	28.52	20.01	18.00	19.49	19.32
95.0	27.82	19.71	17.60	18.79	18.62
96.0	27.12	19.51	17.30	17.79	18.02
97.0	26.52	19.11	16.60	16.89	17.12
98.0	25.92	18.81	16.00	16.19	16.12
99.0	24.92	18.41	15.50	14.99	15.42
100.0	23.92	18.01	14.70	14.09	15.02
101.0	23.32	17.61	14.20	13.59	14.52
102.0	22.62	17.01	13.60	12.89	13.82
103.0	21.42	16.51	13.30	12.39	13.22
104.0	20.72	16.11	12.90	11.99	12.82

105.0	20.12	15.71	12.40	11.39	12.42
106.0	19.42	15.11	11.80	11.19	11.92
107.0	18.62	14.61	11.40	10.59	11.22
108.0	18.02	14.01	10.90	10.09	10.82
109.0	16.92	13.61	10.50	9.49	10.62
110.0	16.22	12.91	10.00	8.89	10.02
111.0	15.32	12.51	9.70	8.39	9.32
112.0	14.42	12.01	9.40	7.99	8.82
113.0	13.72	11.21	9.10	7.59	8.32
114.0	12.82	10.61	8.90	7.09	8.02
115.0	12.22	10.11	8.50	6.59	7.62
116.0	11.62	9.51	8.00	6.39	7.22
117.0	11.12	8.91	7.60	6.09	6.72
118.0	10.72	8.71	7.30	5.69	6.62
119.0	10.32	8.41	6.90	5.49	6.22
120.0	9.82	8.11	6.60	5.19	5.72
121.0	9.42	7.61	6.10	5.09	5.52
122.0	8.92	7.41	5.80	4.99	5.42
123.0	8.72	7.11	5.60	4.89	5.22
124.0	8.32	7.01	5.20	4.49	4.82
125.0	8.02	6.71	5.00	4.19	4.62
126.0	7.52	6.31	4.70	3.99	4.52
127.0	7.12	6.01	4.40	3.89	4.42
128.0	6.72	5.71	4.00	3.59	4.32
129.0	6.32	5.51	3.90	3.29	4.12
130.0	6.02	5.21	3.60	2.99	3.72
131.0	5.82	5.11	3.60	2.69	3.72
132.0	5.62	4.91	3.40	2.49	3.62
133.0	5.62	4.61	3.20	2.39	3.52
134.0	5.42	4.31	2.80	2.29	3.42
135.0	5.02	4.11	2.70	2.19	3.02
136.0	4.62	3.91	2.60	2.19	2.92
137.0	4.32	3.81	2.40	2.29	2.72
138.0	4.32	3.61	2.20	2.09	2.62
139.0	4.22	3.31	2.10	1.99	2.82
140.0	3.92	3.11	1.70	1.69	2.82
141.0	3.72	2.91	1.50	1.69	2.72
142.0	3.52	2.91	1.50	1.49	2.52
143.0	3.32	2.91	1.30	1.49	2.42
144.0	3.42	2.71	1.20	1.39	2.42
145.0	3.22	2.61	1.20	1.39	2.52
146.0	3.12	2.41	1.10	1.29	2.42
147.0	2.72	2.41	1.20	1.39	2.32
148.0	2.62	2.31	1.10	1.19	2.12
149.0	2.52	2.31	1.10	1.19	2.22
150.0	2.52	2.21	1.00	1.09	2.22
151.0	2.62	2.11	0.90	0.89	2.22
152.0	2.32	1.91	0.80	0.69	1.92
153.0	2.12	1.61	0.70	0.69	1.82
154.0	1.92	1.51	0.90	0.59	1.82
155.0	1.52	1.51	0.80	0.49	1.82
156.0	1.42	1.31	0.70	0.49	1.82
157.0	1.42	1.21	0.80	0.59	1.62
158.0	1.42	1.21	0.90	0.59	1.52
159.0	1.22	1.21	0.70	0.69	1.52
160.0	1.22	1.01	0.60	0.59	1.42
161.0	0.92	1.01	0.60	0.49	1.32
162.0	0.82	0.91	0.50	0.59	1.52
163.0	0.92	0.91	0.60	0.59	1.42
164.0	0.82	0.71	0.50	0.49	1.22
165.0	0.72	0.81	0.50	0.39	1.12
166.0	0.72	0.71	0.50	0.29	1.12

167.0	0.62	0.71	0.40	0.29	1.02
168.0	0.62	0.61	0.30	0.09	1.02
169.0	0.62	0.61	0.30	0.19	0.92
170.0	0.62	0.61	0.30	0.19	0.92
171.0	0.42	0.61	0.30	0.19	0.62
172.0	0.52	0.51	0.10	0.29	0.72
173.0	0.32	0.31	0.10	0.19	0.82
174.0	0.32	0.41	0.10	0.19	0.82
175.0	0.32	0.31	0.00	0.29	0.72
176.0	0.42	0.31	0.00	0.29	0.72
177.0	0.42	0.31	0.00	0.29	0.52
178.0	0.22	0.31	0.00	0.39	0.42
179.0	0.32	0.31	0.00	0.19	0.32
180.0	0.22	0.31	0.00	0.09	0.22
181.0	0.02	0.31	0.00	0.00	0.32
182.0	0.02	0.31	0.00	0.09	0.42
183.0	0.12	0.31	0.00	0.09	0.22
184.0	0.12	0.51	0.00	0.19	0.12
185.0	0.02	0.31	0.00	0.19	0.22
186.0	0.00	0.31	0.00	0.19	0.12
187.0	0.00	0.41	0.00	0.29	0.32
188.0	0.00	0.41	0.00	0.49	0.22
189.0	0.00	0.31	0.00	0.39	0.22
190.0	0.00	0.31	0.00	0.39	0.12
191.0	0.00	0.21	0.00	0.39	0.12
192.0	0.00	0.31	0.00	0.49	0.12
193.0	0.00	0.11	0.00	0.39	0.22
194.0	0.00	0.01	0.00	0.39	0.42
195.0	0.00	0.01	0.00	0.49	0.42
196.0	0.00	0.01	0.00	0.49	0.22
197.0	0.00	0.11	0.00	0.39	0.12
198.0	0.00	0.01	0.00	0.39	0.02
199.0	0.00	0.01	0.00	0.29	0.00
200.0	0.00	0.00	0.00	0.19	0.00
201.0	0.00	0.00	0.00	0.09	0.00
202.0	0.00	0.00	0.00	0.29	0.00
203.0	0.00	0.00	0.00	0.19	0.00
204.0	0.00	0.01	0.00	0.29	0.02
205.0	0.00	0.01	0.00	0.49	0.00
206.0	0.00	0.00	0.00	0.39	0.00
207.0	0.00	0.00	0.00	0.49	0.02
208.0	0.00	0.00	0.00	0.49	0.00
209.0	0.00	0.00	0.00	0.49	0.02
210.0	0.00	0.01	0.00	0.59	0.00
211.0	0.00	0.01	0.00	0.49	0.00
212.0	0.00	0.11	0.00	0.39	0.00
213.0	0.00	0.11	0.00	0.39	0.00
214.0	0.00	0.11	0.00	0.39	0.00
215.0	0.00	0.21	0.00	0.29	0.00
216.0	0.00	0.31	0.00	0.09	0.02
217.0	0.00	0.31	0.10	0.19	0.12
218.0	0.00	0.31	0.00	0.19	0.02
219.0	0.00	0.21	0.10	0.19	0.12
220.0	0.00	0.31	0.00	0.29	0.12

AMC 15 Section 3

y(m) / t(sec)	Concentration (ppb)				
	0.9	1.8	2.7	3.6	4.5
80.0	0.00	0.20	0.00	0.20	0.00
81.0	0.00	0.20	0.00	0.30	0.00
82.0	0.00	0.20	0.00	0.10	0.00
83.0	0.00	0.10	0.00	0.10	0.00
84.0	0.00	0.00	0.00	0.00	0.00
85.0	0.00	0.00	0.00	0.00	0.00
86.0	0.00	0.00	0.00	0.20	0.07
87.0	0.00	0.00	0.00	0.50	0.17
88.0	0.00	0.00	0.00	0.60	0.37
89.0	0.00	0.00	0.00	1.00	1.07
90.0	0.00	0.20	0.00	1.30	2.27
91.0	0.00	0.10	0.00	2.10	3.67
92.0	0.00	0.30	0.00	2.50	4.47
93.0	0.00	0.40	0.00	3.30	5.77
94.0	0.00	0.20	0.00	4.80	7.47
95.0	0.00	0.30	0.22	6.20	9.17
96.0	0.00	0.40	0.92	7.60	10.77
97.0	0.00	0.70	1.82	9.60	12.57
98.0	0.03	0.90	3.22	11.80	13.77
99.0	0.03	1.00	4.92	13.80	15.37
100.0	0.53	1.40	6.72	15.50	16.97
101.0	0.73	1.90	8.02	17.00	18.47
102.0	1.03	2.40	9.22	18.50	19.57
103.0	1.13	3.60	10.42	19.60	20.77
104.0	1.23	4.20	11.52	20.90	21.77
105.0	1.83	5.00	13.02	22.10	22.67
106.0	1.83	5.70	14.72	23.10	23.37
107.0	2.33	6.50	15.82	24.20	24.17
108.0	2.73	7.40	17.32	24.90	24.87
109.0	3.13	8.30	18.72	25.70	24.87
110.0	3.53	9.60	19.92	26.30	25.17
111.0	4.83	10.80	20.72	26.20	25.07
112.0	5.63	12.00	21.32	26.30	24.77
113.0	6.23	13.00	22.12	26.60	24.37
114.0	6.73	14.10	22.72	26.90	24.07
115.0	7.23	15.60	23.12	26.60	23.77
116.0	7.73	16.70	23.62	26.60	23.27
117.0	8.03	17.40	23.82	26.50	23.07
118.0	8.63	17.80	24.02	26.10	22.97
119.0	9.13	18.50	24.12	25.80	22.77
120.0	10.23	18.90	24.42	25.50	22.27
121.0	10.83	19.20	24.52	25.00	21.57
122.0	11.33	19.90	24.12	24.50	21.27
123.0	11.93	20.60	23.72	24.20	20.77
124.0	12.33	20.80	23.52	23.50	20.07
125.0	12.43	21.00	23.72	23.20	19.37
126.0	12.43	21.20	23.32	22.90	18.97
127.0	12.73	21.60	22.92	22.20	18.37
128.0	13.33	21.80	22.22	21.60	17.57
129.0	13.83	22.00	21.72	20.90	17.07
130.0	14.33	21.70	21.42	20.50	16.57
131.0	14.83	21.60	20.72	19.60	15.97
132.0	15.13	21.50	20.12	18.60	15.47
133.0	15.53	21.20	19.22	18.30	14.97
134.0	15.53	20.70	18.72	17.70	14.57
135.0	15.73	20.20	18.32	17.10	14.27
136.0	16.13	19.90	17.72	16.50	13.77

137.0	16.33	19.80	17.22	15.80	13.37
138.0	16.43	19.20	16.72	15.00	12.77
139.0	16.73	19.20	16.02	14.20	12.07
140.0	16.53	18.70	15.32	13.70	11.67
141.0	16.23	18.30	15.02	13.00	11.27
142.0	16.33	17.80	14.62	12.40	10.87
143.0	16.33	17.60	14.12	11.80	10.37
144.0	16.13	17.10	13.42	11.30	10.17
145.0	15.93	16.40	12.82	10.80	9.77
146.0	15.53	16.20	12.12	10.40	9.37
147.0	15.23	16.00	11.42	9.90	9.07
148.0	15.03	15.20	10.92	9.40	8.57
149.0	14.73	14.90	10.72	9.00	8.37
150.0	14.33	14.50	10.32	8.70	8.17
151.0	14.03	13.80	9.72	8.30	7.57
152.0	13.73	13.20	9.42	7.80	7.27
153.0	13.33	12.70	8.92	7.40	6.87
154.0	12.83	12.50	8.32	6.90	6.37
155.0	12.33	12.30	7.72	6.60	5.77
156.0	11.83	11.70	7.72	6.30	5.57
157.0	11.53	11.10	7.32	5.90	5.07
158.0	11.23	10.20	7.02	5.50	4.77
159.0	11.03	9.70	6.52	5.20	4.77
160.0	10.63	9.40	6.32	4.80	4.37
161.0	10.33	8.80	5.92	4.60	4.17
162.0	10.13	8.70	5.82	4.60	3.87
163.0	9.93	8.30	5.72	4.30	3.57
164.0	9.73	7.90	5.42	4.10	3.47
165.0	9.63	7.70	5.12	3.90	3.47
166.0	9.33	7.20	4.92	3.60	2.97
167.0	9.23	6.80	4.42	3.50	2.57
168.0	9.03	6.40	4.22	3.20	2.57
169.0	8.53	6.20	3.92	2.80	2.47
170.0	8.33	6.00	3.82	2.70	2.37
171.0	8.33	6.00	3.72	2.50	2.17
172.0	8.53	5.50	3.42	2.60	2.07
173.0	8.43	5.40	3.12	2.40	1.97
174.0	8.33	5.30	2.92	2.40	1.87
175.0	8.03	4.90	2.62	2.30	1.87
176.0	7.83	4.80	2.72	2.10	1.57
177.0	7.63	4.40	2.52	2.10	1.67
178.0	7.43	4.20	2.32	2.20	1.47
179.0	6.93	4.00	2.12	2.00	1.37
180.0	6.63	3.80	2.02	1.80	1.27
181.0	6.43	3.60	1.92	1.70	1.17
182.0	6.13	3.60	1.92	1.70	1.27
183.0	6.03	3.30	1.72	1.60	1.47
184.0	6.03	3.20	1.72	1.50	1.57
185.0	5.73	3.20	1.52	1.30	1.37
186.0	5.13	2.90	1.32	1.20	1.57
187.0	5.03	2.80	1.02	1.00	1.37
188.0	4.53	2.90	0.72	0.90	1.37
189.0	4.63	2.70	0.62	0.80	1.27
190.0	4.63	2.60	0.72	1.00	1.27
191.0	4.53	2.50	0.82	0.90	1.17
192.0	4.43	2.30	0.62	1.00	0.97
193.0	4.33	2.30	0.62	1.10	0.97
194.0	3.93	2.20	0.62	1.00	0.67
195.0	3.63	2.00	0.62	1.00	0.57
196.0	3.43	1.90	0.42	0.90	0.57
197.0	3.33	1.80	0.32	0.80	0.67
198.0	3.13	1.70	0.32	0.70	0.87

199.0	2.93	1.50	0.22	0.80	0.77
200.0	2.63	1.60	0.12	0.80	0.67
201.0	2.63	1.20	0.00	0.80	0.67
202.0	2.43	1.50	0.00	0.50	0.67
203.0	2.33	1.40	0.00	0.60	0.47
204.0	2.33	1.40	0.00	0.40	0.67
205.0	2.13	1.40	0.12	0.30	0.67
206.0	1.93	1.30	0.02	0.30	0.57
207.0	1.93	1.40	0.02	0.40	0.57
208.0	1.83	1.10	0.02	0.40	0.37
209.0	1.83	1.30	0.02	0.30	0.37
210.0	1.63	1.40	0.12	0.40	0.57
211.0	1.83	1.10	0.12	0.60	0.47
212.0	1.73	1.10	0.02	0.50	0.17
213.0	1.53	1.00	0.00	0.50	0.07
214.0	1.53	1.10	0.00	0.50	0.27
215.0	1.33	1.10	0.00	0.50	0.27
216.0	1.13	1.00	0.00	0.50	0.37
217.0	1.03	0.80	0.00	0.60	0.27
218.0	0.93	0.70	0.00	0.40	0.27
219.0	1.23	0.80	0.00	0.50	0.00
220.0	1.13	0.70	0.00	0.60	0.00
221.0	0.93	1.00	0.00	0.60	0.00
222.0	1.03	0.80	0.00	0.50	0.00
223.0	0.93	0.80	0.00	0.40	0.00
224.0	1.03	0.40	0.00	0.40	0.00
225.0	1.13	0.60	0.00	0.20	0.00
226.0	0.93	0.50	0.00	0.00	0.00
227.0	0.93	0.40	0.00	0.20	0.00
228.0	0.93	0.50	0.00	0.10	0.00
229.0	0.73	0.60	0.00	0.30	0.07
230.0	0.63	0.50	0.00	0.40	0.07
231.0	0.83	0.50	0.00	0.40	0.00
232.0	0.83	0.50	0.00	0.30	0.00
233.0	0.73	0.10	0.00	0.20	0.00
234.0	0.63	0.10	0.00	0.00	0.07
235.0	0.53	0.10	0.00	0.00	0.00
236.0	0.33	0.20	0.00	0.00	0.00
237.0	0.13	0.20	0.00	0.00	0.00
238.0	0.23	0.10	0.00	0.00	0.00
239.0	0.33	0.30	0.00	0.00	0.00
240.0	0.43	0.20	0.00	0.00	0.07
241.0	0.53	0.30	0.00	0.00	0.00
242.0	0.73	0.30	0.00	0.00	0.17
243.0	0.83	0.40	0.00	0.00	0.27
244.0	0.93	0.00	0.00	0.00	0.17
245.0	0.93	0.00	0.00	0.00	0.00
246.0	1.03	0.00	0.00	0.00	0.07
247.0	1.23	0.00	0.00	0.00	0.07
248.0	0.93	0.00	0.00	0.00	0.07
249.0	0.73	0.00	0.00	0.10	0.00
250.0	0.53	0.10	0.00	0.20	0.00

AMC 15 Section 4

y(m) / t(sec)	Concentration (ppb)				
	1.0	2.0	3.0	4.0	5.0
90.0	0.00	0.16	0.17	0.29	0.00
91.0	0.00	0.06	0.27	0.29	0.00
92.0	0.00	0.00	0.27	0.39	0.00
93.0	0.00	0.06	0.17	0.39	0.00
94.0	0.00	0.16	0.07	0.39	0.00
95.0	0.00	0.26	0.00	0.29	0.00
96.0	0.00	0.06	0.07	0.59	0.00
97.0	0.00	0.00	0.17	0.49	0.00
98.0	0.00	0.06	0.37	0.49	0.00
99.0	0.00	0.00	0.47	0.59	0.05
100.0	0.00	0.06	0.57	0.79	0.00
101.0	0.00	0.00	0.57	0.79	0.25
102.0	0.00	0.06	0.77	0.79	0.05
103.0	0.00	0.06	0.97	1.09	0.15
104.0	0.00	0.00	1.37	1.19	0.25
105.0	0.00	0.00	1.77	1.79	0.25
106.0	0.00	0.00	2.27	2.29	0.05
107.0	0.00	0.00	3.27	2.79	0.15
108.0	0.00	0.56	4.17	3.59	0.25
109.0	0.00	1.06	4.57	4.49	0.35
110.0	0.00	1.36	5.37	5.59	0.45
111.0	0.00	1.86	6.47	6.19	0.55
112.0	0.00	2.96	7.27	7.49	0.85
113.0	0.00	3.66	7.67	8.59	1.15
114.0	0.00	3.86	8.37	9.09	1.45
115.0	0.00	4.46	9.37	9.89	1.65
116.0	0.08	5.36	10.77	10.99	1.85
117.0	0.58	6.66	11.97	11.99	2.45
118.0	0.78	7.46	12.67	12.69	3.15
119.0	1.78	7.76	12.87	13.49	4.05
120.0	3.08	7.96	13.97	13.89	4.55
121.0	4.18	8.56	14.87	14.69	5.15
122.0	4.78	9.36	15.37	15.49	6.05
123.0	5.38	10.06	15.67	16.19	6.65
124.0	6.48	11.06	15.97	16.19	7.75
125.0	7.28	12.16	16.17	16.49	8.45
126.0	8.38	13.26	16.67	16.89	9.25
127.0	9.18	13.96	17.07	17.69	10.15
128.0	10.28	14.66	17.47	18.29	10.85
129.0	11.08	15.06	17.87	18.79	11.55
130.0	11.68	15.26	18.17	19.09	12.25
131.0	12.48	15.56	18.47	19.49	12.95
132.0	13.18	15.86	18.47	19.79	13.45
133.0	14.08	16.26	18.57	20.09	14.05
134.0	14.48	16.56	18.67	20.09	14.55
135.0	14.78	16.96	18.87	20.29	14.85
136.0	15.28	17.16	18.97	20.39	15.35
137.0	15.18	17.36	18.97	20.59	15.85
138.0	15.68	17.66	18.87	20.39	15.95
139.0	16.28	17.76	18.87	20.39	16.25
140.0	16.88	18.16	18.87	20.49	16.45
141.0	17.38	18.36	18.67	20.39	16.75
142.0	17.78	18.46	18.07	20.19	16.95
143.0	18.18	18.36	17.77	19.89	16.95
144.0	18.38	18.36	17.47	19.59	17.05

145.0	18.38	18.56	17.57	19.29	17.35
146.0	18.48	18.66	17.17	18.89	17.25
147.0	18.48	18.66	16.97	18.59	17.35
148.0	18.58	18.26	16.27	18.19	17.55
149.0	18.48	18.26	16.17	17.99	17.55
150.0	18.28	18.06	15.67	17.59	17.45
151.0	18.18	17.76	15.47	17.29	17.55
152.0	17.88	17.36	15.17	16.69	17.45
153.0	17.78	17.16	14.87	16.29	17.35
154.0	17.48	16.86	14.67	15.79	17.35
155.0	17.08	16.76	14.37	15.39	17.15
156.0	16.78	16.36	14.07	15.19	17.05
157.0	16.48	15.66	13.47	14.89	17.05
158.0	16.38	15.36	13.47	14.39	16.65
159.0	15.88	14.96	12.97	14.09	16.35
160.0	15.78	14.66	12.67	13.79	16.15
161.0	15.58	14.36	12.47	13.49	15.85
162.0	15.18	13.86	12.17	12.99	15.65
163.0	14.88	13.46	12.07	12.49	15.35
164.0	14.98	13.26	11.47	12.19	15.05
165.0	14.68	12.96	11.17	11.79	14.75
166.0	14.58	12.56	10.87	11.39	14.35
167.0	14.08	12.26	10.67	11.19	13.95
168.0	13.88	12.06	10.37	10.89	13.65
169.0	13.58	11.76	10.07	10.69	13.35
170.0	13.08	11.36	9.67	10.49	13.05
171.0	12.68	10.86	9.27	9.99	12.75
172.0	12.28	10.46	9.07	9.59	12.35
173.0	11.98	10.16	8.67	9.19	12.05
174.0	11.78	9.76	8.37	8.89	11.85
175.0	11.58	9.46	8.27	8.49	11.45
176.0	11.18	9.16	7.97	8.19	11.25
177.0	11.18	8.86	7.77	7.99	10.85
178.0	10.78	8.46	7.67	7.79	10.55
179.0	10.58	8.16	7.47	7.39	10.25
180.0	10.18	7.96	6.97	7.19	10.25
181.0	9.88	7.86	6.47	6.99	10.05
182.0	9.28	7.36	6.07	6.69	9.65
183.0	9.28	7.06	5.77	6.49	9.55
184.0	8.98	6.96	5.57	6.29	9.15
185.0	8.68	6.86	5.37	5.99	8.45
186.0	8.58	6.46	5.17	5.79	8.15
187.0	8.38	6.16	5.07	5.49	7.95
188.0	8.08	6.06	5.07	5.19	7.65
189.0	7.88	6.06	4.87	5.09	7.35
190.0	7.68	6.06	4.87	5.09	7.05
191.0	7.48	5.96	4.77	4.99	6.85
192.0	7.18	5.76	4.47	4.79	6.65
193.0	7.08	5.46	4.47	4.69	6.45
194.0	6.98	5.16	4.17	4.59	6.25
195.0	6.98	4.86	4.07	4.39	6.05
196.0	6.68	4.56	3.77	4.29	5.85
197.0	6.48	4.36	3.47	4.09	5.75
198.0	6.38	4.06	3.17	4.09	5.65
199.0	5.98	3.86	2.97	3.99	5.55
200.0	5.98	3.86	2.87	3.89	5.35
201.0	5.68	3.66	2.77	3.69	4.95
202.0	5.68	3.56	2.67	3.59	4.85
203.0	5.48	3.56	2.47	3.39	4.85
204.0	5.18	3.46	2.67	3.19	4.65
205.0	4.98	3.46	2.57	2.99	4.35
206.0	4.98	3.36	2.67	2.79	4.25

207.0	4.58	3.16	2.57	2.49	4.05
208.0	4.58	3.06	2.47	2.39	3.85
209.0	4.58	3.06	2.37	2.39	3.65
210.0	4.58	2.86	2.27	2.39	3.45
211.0	4.38	2.66	2.17	2.09	3.35
212.0	4.28	2.66	2.17	2.09	3.15
213.0	4.38	2.56	2.07	1.99	3.05
214.0	4.18	2.26	2.07	1.89	3.05
215.0	3.88	2.16	1.97	1.89	2.85
216.0	3.68	2.16	1.87	1.69	2.85
217.0	3.38	2.16	1.97	1.39	2.75
218.0	3.18	2.16	1.87	1.29	2.75
219.0	3.08	2.06	1.77	1.39	2.65
220.0	3.18	1.96	1.77	1.29	2.55
221.0	2.98	2.06	1.57	1.29	2.55
222.0	2.78	1.96	1.57	1.09	2.45
223.0	2.68	2.06	1.67	1.19	2.25
224.0	2.48	2.16	1.47	1.09	2.15
225.0	2.38	2.06	1.57	0.89	2.15
226.0	2.38	1.96	1.37	0.79	1.95
227.0	2.18	1.86	1.27	0.79	1.95
228.0	2.18	1.46	1.27	0.99	1.85
229.0	2.18	1.36	1.27	0.79	1.85
230.0	1.98	1.16	1.27	0.79	1.75
231.0	2.08	1.16	1.17	0.69	1.65
232.0	1.98	1.06	1.07	0.59	1.55
233.0	1.98	1.06	1.07	0.59	1.45
234.0	2.08	0.96	1.17	0.69	1.35
235.0	1.88	1.06	1.17	0.59	1.25
236.0	1.78	1.16	0.97	0.49	1.35
237.0	1.68	1.06	1.07	0.69	1.45
238.0	1.68	0.96	0.87	0.59	1.25
239.0	1.88	0.86	0.87	0.69	1.35
240.0	1.78	0.86	0.97	0.69	1.25
241.0	1.68	0.86	0.87	0.69	1.25
242.0	1.68	0.86	0.67	0.69	1.25
243.0	1.58	0.96	0.67	0.59	1.35
244.0	1.48	0.96	0.67	0.59	1.35
245.0	1.38	0.96	0.57	0.59	1.45
246.0	1.28	1.06	0.57	0.69	1.45
247.0	1.38	0.96	0.47	0.59	1.55
248.0	1.18	0.86	0.27	0.69	1.45
249.0	1.38	0.76	0.37	0.49	1.35
250.0	1.38	0.66	0.37	0.49	1.35
251.0	1.28	0.66	0.37	0.39	1.25
252.0	1.18	0.56	0.47	0.49	1.15
253.0	1.38	0.66	0.57	0.29	1.15
254.0	1.28	0.76	0.57	0.29	1.05
255.0	1.08	0.66	0.47	0.39	0.95
256.0	0.88	0.86	0.47	0.39	1.05
257.0	0.88	0.86	0.27	0.39	0.85
258.0	0.68	0.66	0.47	0.39	0.75
259.0	0.58	0.86	0.47	0.49	0.85
260.0	0.58	0.86	0.27	0.29	0.65
261.0	0.58	0.96	0.17	0.39	0.65
262.0	0.48	0.96	0.27	0.29	0.65
263.0	0.38	0.86	0.27	0.49	0.75
264.0	0.18	0.66	0.17	0.59	0.65
265.0	0.48	0.66	0.27	0.59	0.65
266.0	0.58	0.56	0.17	0.49	0.85
267.0	0.58	0.66	0.27	0.39	0.85
268.0	0.48	0.66	0.27	0.29	0.75

269.0	0.58	0.56	0.27	0.39	0.65
270.0	0.58	0.66	0.27	0.49	0.65
271.0	0.68	0.56	0.17	0.49	0.55
272.0	0.58	0.56	0.27	0.49	0.65
273.0	0.48	0.56	0.07	0.59	0.65
274.0	0.58	0.46	0.00	0.69	0.65
275.0	0.58	0.56	0.00	0.79	0.65
276.0	0.38	0.56	0.00	0.79	0.55
277.0	0.28	0.46	0.00	0.69	0.55
278.0	0.18	0.46	0.00	0.69	0.45
279.0	0.18	0.36	0.07	0.79	0.45
280.0	0.00	0.36	0.00	0.89	0.45
281.0	0.00	0.26	0.00	0.79	0.65
282.0	0.00	0.36	0.00	0.49	0.65
283.0	0.00	0.26	0.17	0.49	0.55
284.0	0.00	0.46	0.07	0.59	0.45
285.0	0.00	0.16	0.00	0.69	0.55
286.0	0.00	0.16	0.00	0.59	0.65
287.0	0.00	0.16	0.00	0.79	0.75
288.0	0.08	0.06	0.00	0.89	0.75
289.0	0.08	0.16	0.00	0.69	0.55
290.0	0.08	0.16	0.00	0.59	0.55
291.0	0.00	0.26	0.00	0.49	0.45
292.0	0.00	0.16	0.00	0.29	0.35
293.0	0.00	0.06	0.00	0.29	0.35
294.0	0.00	0.26	0.00	0.39	0.25
295.0	0.00	0.26	0.00	0.39	0.35
296.0	0.00	0.16	0.00	0.09	0.25
297.0	0.00	0.16	0.17	0.19	0.25
298.0	0.00	0.26	0.07	0.29	0.25
299.0	0.00	0.16	0.07	0.29	0.25
300.0	0.00	0.26	0.27	0.39	0.15

AMC 15 Section 5

y(m) / t(sec)	Concentration (ppb)				
	0.9	1.8	2.7	3.6	4.5
120.0	0.07	0.18	0.28	0.17	0.08
121.0	0.17	0.28	0.38	0.07	0.08
122.0	0.17	0.18	0.28	0.17	0.08
123.0	0.27	0.28	0.28	0.17	0.08
124.0	0.17	0.28	0.28	0.17	0.00
125.0	0.17	0.28	0.28	0.27	0.00
126.0	0.27	0.18	0.38	0.37	0.00
127.0	0.17	0.28	0.38	0.27	0.00
128.0	0.17	0.28	0.38	0.27	0.00
129.0	0.37	0.38	0.38	0.17	0.00
130.0	0.37	0.38	0.48	0.17	0.00
131.0	0.47	0.58	0.38	0.17	0.00
132.0	0.67	0.68	0.28	0.27	0.00
133.0	0.97	0.98	0.28	0.17	0.00
134.0	1.27	1.38	0.48	0.17	0.00
135.0	1.67	2.18	0.38	0.17	0.00
136.0	2.17	2.58	0.58	0.17	0.00
137.0	2.57	3.08	0.78	0.27	0.00
138.0	2.97	3.58	0.78	0.37	0.00
139.0	3.37	4.18	0.88	0.57	0.00
140.0	4.07	4.68	1.18	0.67	0.00
141.0	4.57	5.08	1.58	0.77	0.00
142.0	5.17	5.58	1.98	1.07	0.00
143.0	5.77	6.38	2.28	1.17	0.00
144.0	6.57	6.78	2.78	1.37	0.00
145.0	7.47	7.48	3.48	1.57	0.00
146.0	8.17	8.28	4.08	1.67	0.00
147.0	8.87	8.98	4.28	2.07	0.00
148.0	9.77	9.58	4.88	2.57	0.00
149.0	10.57	10.28	5.28	3.07	0.00
150.0	11.27	10.98	6.18	3.37	0.00
151.0	11.57	11.78	6.68	3.87	0.00
152.0	12.27	12.38	7.18	4.37	0.00
153.0	12.87	12.98	7.88	4.87	0.00
154.0	13.47	13.48	8.48	5.27	0.00
155.0	13.97	13.98	9.18	5.67	0.00
156.0	14.37	14.48	9.78	6.17	0.00
157.0	14.87	14.88	10.38	6.57	0.00
158.0	15.17	15.38	10.98	7.27	0.00
159.0	15.57	15.88	11.48	7.87	0.00
160.0	15.87	16.18	12.08	8.47	0.18
161.0	16.17	16.58	12.58	9.17	0.38
162.0	16.37	16.88	13.08	9.87	0.48
163.0	16.67	17.18	13.68	10.57	0.68
164.0	16.87	17.48	14.08	11.27	0.68
165.0	16.97	17.68	14.58	11.87	0.88
166.0	17.07	17.78	14.88	12.47	1.08
167.0	17.17	18.18	15.28	13.07	1.28
168.0	17.17	18.18	15.68	13.67	1.28
169.0	17.17	18.28	15.98	13.97	1.28
170.0	17.07	18.48	16.28	14.47	1.48
171.0	17.07	18.38	16.38	14.77	1.38
172.0	16.97	18.28	16.58	15.17	1.68
173.0	16.87	18.28	16.68	15.57	1.98
174.0	16.67	18.18	16.88	15.97	2.48
175.0	16.37	17.98	16.98	16.27	2.78
176.0	16.17	17.88	16.98	16.37	3.08

177.0	16.07	17.88	17.08	16.67	3.38
178.0	15.77	17.48	17.08	16.87	3.88
179.0	15.67	17.18	16.88	17.07	4.28
180.0	15.37	16.88	16.78	17.17	4.88
181.0	15.07	16.68	16.78	17.47	5.18
182.0	14.77	16.28	16.58	17.57	5.48
183.0	14.67	15.98	16.48	17.67	5.68
184.0	14.47	15.78	16.28	17.67	5.98
185.0	14.17	15.48	16.18	17.77	6.28
186.0	13.97	15.18	15.98	17.67	6.38
187.0	13.67	14.88	15.68	17.67	6.68
188.0	13.37	14.78	15.48	17.57	6.98
189.0	13.17	14.48	15.28	17.47	7.38
190.0	12.87	14.08	15.18	17.37	7.88
191.0	12.57	13.78	14.88	17.27	8.18
192.0	12.27	13.28	14.68	17.07	8.58
193.0	11.97	12.98	14.28	16.97	8.78
194.0	11.67	12.68	14.08	16.67	9.08
195.0	11.37	12.28	13.78	16.37	9.38
196.0	11.17	11.98	13.58	16.27	9.58
197.0	10.87	11.78	13.38	16.07	9.78
198.0	10.47	11.48	13.08	15.87	9.98
199.0	10.17	11.08	12.78	15.57	10.28
200.0	9.87	10.88	12.38	15.17	10.48
201.0	9.47	10.68	12.08	14.87	10.58
202.0	9.27	10.28	11.78	14.67	10.68
203.0	9.07	9.98	11.48	14.47	10.88
204.0	8.77	9.68	11.18	14.07	10.78
205.0	8.47	9.38	10.88	13.67	10.78
206.0	8.17	9.08	10.58	13.37	10.78
207.0	7.97	8.78	10.38	13.07	10.98
208.0	7.77	8.38	9.98	12.77	10.88
209.0	7.47	7.98	9.68	12.47	10.98
210.0	7.27	7.78	9.28	12.27	11.18
211.0	6.97	7.48	8.98	11.97	11.08
212.0	6.87	7.28	8.68	11.67	11.08
213.0	6.87	7.08	8.58	11.37	11.18
214.0	6.77	6.98	8.18	10.97	11.18
215.0	6.57	6.98	7.88	10.67	11.38
216.0	6.37	6.78	7.68	10.47	11.48
217.0	6.07	6.68	7.58	10.07	11.48
218.0	5.87	6.48	7.38	9.87	11.38
219.0	5.67	6.38	7.18	9.57	11.28
220.0	5.47	6.08	6.98	9.37	11.08
221.0	5.37	5.78	6.68	9.17	10.98
222.0	5.17	5.58	6.48	8.87	10.78
223.0	4.97	5.28	6.28	8.57	10.68
224.0	4.87	5.18	6.08	8.17	10.58
225.0	4.77	5.08	5.88	7.87	10.48
226.0	4.47	4.88	5.68	7.67	10.38
227.0	4.57	4.78	5.58	7.47	10.18
228.0	4.37	4.58	5.38	7.07	10.28
229.0	4.27	4.48	5.28	6.87	10.18
230.0	4.07	4.38	5.08	6.67	10.18
231.0	3.97	4.18	4.88	6.37	9.98
232.0	3.87	4.08	4.68	6.07	9.98
233.0	3.77	3.78	4.48	5.97	9.88
234.0	3.67	3.78	4.38	5.87	9.78
235.0	3.47	3.78	4.28	5.87	9.78
236.0	3.37	3.48	4.08	5.67	9.58
237.0	3.37	3.38	3.88	5.57	9.48
238.0	3.27	3.18	3.78	5.37	9.18

239.0	3.27	3.18	3.68	5.27	9.08
240.0	3.17	3.18	3.48	5.17	8.98
241.0	3.07	3.08	3.28	5.07	8.78
242.0	3.07	2.88	3.18	4.97	8.48
243.0	3.07	2.98	3.08	4.77	8.48
244.0	2.87	3.08	2.98	4.57	8.18
245.0	2.67	3.18	2.88	4.37	7.98
246.0	2.67	3.18	2.78	4.17	7.98
247.0	2.57	2.98	2.68	3.97	7.88
248.0	2.57	2.98	2.58	3.87	7.68
249.0	2.47	2.68	2.48	3.77	7.78
250.0	2.37	2.88	2.38	3.67	7.58
251.0	2.27	2.78	2.38	3.57	7.48
252.0	2.27	2.58	2.58	3.47	7.48
253.0	2.17	2.58	2.48	3.37	7.28
254.0	1.97	2.58	2.28	3.27	6.98
255.0	1.77	2.38	2.28	3.37	6.78
256.0	1.77	2.18	2.08	3.27	6.58
257.0	1.67	2.18	1.98	3.07	6.38
258.0	1.67	2.08	1.98	3.07	6.18
259.0	1.57	2.08	1.88	3.07	6.08
260.0	1.47	1.98	2.08	2.87	5.78
261.0	1.57	1.98	1.98	2.67	5.78
262.0	1.57	1.98	2.08	2.77	5.58
263.0	1.67	1.78	2.08	2.67	5.48
264.0	1.77	1.88	1.88	2.47	5.28
265.0	1.67	1.68	1.78	2.27	5.18
266.0	1.57	1.48	1.88	2.27	4.98
267.0	1.47	1.48	1.78	2.17	4.98
268.0	1.37	1.58	1.88	2.17	4.88
269.0	1.37	1.58	1.88	2.07	4.98
270.0	1.47	1.48	1.78	2.07	5.08
271.0	1.47	1.58	1.68	2.07	5.08
272.0	1.47	1.48	1.58	2.07	4.88
273.0	1.37	1.38	1.68	1.97	4.68
274.0	1.47	1.38	1.58	1.87	4.58
275.0	1.47	1.38	1.48	1.87	4.38
276.0	1.37	1.38	1.38	1.67	4.28
277.0	1.27	1.08	1.48	1.47	4.28
278.0	1.27	1.18	1.48	1.47	4.18
279.0	1.27	1.28	1.38	1.47	3.98
280.0	1.37	1.28	1.28	1.27	4.08
281.0	1.27	1.28	1.08	1.27	3.88
282.0	1.17	1.28	1.08	1.37	3.78
283.0	0.97	1.18	0.98	1.37	3.58
284.0	0.97	1.08	1.08	1.27	3.48
285.0	0.87	0.98	1.08	1.27	3.48
286.0	0.87	0.98	1.08	1.17	3.38
287.0	0.87	0.98	0.88	1.17	3.28
288.0	0.87	0.98	0.88	1.17	3.28
289.0	0.77	0.88	0.68	1.17	3.18
290.0	0.87	0.88	0.68	1.17	3.18
291.0	0.77	0.78	0.68	1.17	3.08
292.0	0.87	0.88	0.68	1.07	2.88
293.0	0.87	0.78	0.58	0.97	2.88
294.0	0.87	0.88	0.48	0.97	2.88
295.0	0.67	0.88	0.58	0.97	2.88
296.0	0.57	0.78	0.58	1.07	2.78
297.0	0.47	0.78	0.58	0.97	2.78
298.0	0.37	0.78	0.68	1.07	2.78
299.0	0.27	0.68	0.78	1.07	2.58
300.0	0.37	0.68	0.78	0.97	2.48

301.0	0.47	0.78	0.68	0.87	2.38
302.0	0.37	0.98	0.68	0.87	2.38
303.0	0.37	0.78	0.68	0.87	2.38
304.0	0.37	0.88	0.68	0.97	2.28
305.0	0.27	0.78	0.68	0.77	2.18
306.0	0.37	0.78	0.78	0.67	1.98
307.0	0.47	0.78	0.88	0.67	1.98
308.0	0.57	0.88	0.78	0.57	1.98
309.0	0.47	0.98	0.78	0.47	1.98
310.0	0.47	0.98	0.58	0.47	1.98
311.0	0.57	0.88	0.58	0.37	1.98
312.0	0.57	0.98	0.58	0.47	1.98
313.0	0.57	1.08	0.58	0.57	1.88
314.0	0.57	0.98	0.58	0.67	1.88
315.0	0.57	0.98	0.58	0.67	1.78
316.0	0.57	0.98	0.58	0.67	1.68
317.0	0.47	0.98	0.68	0.67	1.68
318.0	0.47	0.78	0.58	0.77	1.68
319.0	0.37	0.78	0.48	0.77	1.78
320.0	0.37	0.78	0.38	0.77	1.78
321.0	0.37	0.78	0.48	0.67	1.78
322.0	0.37	0.98	0.48	0.57	1.78
323.0	0.47	0.88	0.28	0.57	1.88
324.0	0.37	0.88	0.18	0.47	1.78
325.0	0.37	0.88	0.18	0.47	1.48
326.0	0.37	0.78	0.18	0.57	1.48
327.0	0.37	0.88	0.28	0.57	1.38
328.0	0.17	0.78	0.08	0.67	1.38
329.0	0.27	0.88	0.08	0.77	1.28
330.0	0.17	0.98	0.08	0.87	1.28
331.0	0.27	0.98	0.18	0.87	1.38
332.0	0.37	1.08	0.18	0.67	1.38
333.0	0.37	0.98	0.18	0.77	1.48
334.0	0.37	0.88	0.18	0.77	1.48
335.0	0.27	0.78	0.28	0.77	1.48
336.0	0.27	0.68	0.28	0.67	1.48
337.0	0.27	0.68	0.28	0.57	1.38
338.0	0.37	0.78	0.28	0.57	1.28
339.0	0.27	0.68	0.38	0.57	1.08
340.0	0.27	0.68	0.28	0.47	1.08
341.0	0.27	0.58	0.38	0.47	1.18
342.0	0.17	0.68	0.28	0.47	1.08
343.0	0.07	0.78	0.18	0.67	1.08
344.0	0.17	0.68	0.18	0.67	1.18
345.0	0.17	0.38	0.28	0.67	1.18
346.0	0.17	0.48	0.28	0.57	1.18
347.0	0.17	0.38	0.38	0.67	1.18
348.0	0.07	0.38	0.58	0.57	1.18
349.0	0.17	0.28	0.48	0.47	1.28
350.0	0.17	0.38	0.48	0.47	1.28
351.0	0.27	0.28	0.48	0.37	1.18
352.0	0.17	0.28	0.48	0.47	1.08
353.0	0.27	0.28	0.38	0.27	1.08
354.0	0.17	0.18	0.38	0.27	1.18
355.0	0.07	0.18	0.28	0.17	1.28
356.0	0.17	0.18	0.28	0.17	1.18
357.0	0.17	0.18	0.28	0.27	1.18
358.0	0.27	0.08	0.38	0.17	1.18
359.0	0.07	0.18	0.38	0.07	1.08
360.0	0.07	0.28	0.48	0.17	1.08
361.0	0.07	0.28	0.38	0.17	0.98
362.0	0.07	0.28	0.48	0.17	0.98

363.0	0.07	0.28	0.38	0.27	0.78
364.0	0.07	0.38	0.48	0.27	0.68
365.0	0.07	0.38	0.68	0.27	0.68
366.0	0.17	0.28	0.68	0.37	0.68
367.0	0.17	0.18	0.38	0.37	0.58
368.0	0.17	0.28	0.58	0.37	0.48
369.0	0.17	0.38	0.58	0.37	0.38
370.0	0.07	0.28	0.48	0.37	0.28
371.0	0.07	0.38	0.48	0.37	0.28
372.0	0.17	0.48	0.48	0.27	0.18
373.0	0.17	0.28	0.48	0.37	0.28
374.0	0.17	0.38	0.38	0.47	0.38
375.0	0.17	0.28	0.48	0.47	0.28
376.0	0.07	0.38	0.38	0.47	0.28
377.0	0.17	0.48	0.28	0.47	0.18
378.0	0.17	0.48	0.28	0.47	0.18
379.0	0.17	0.48	0.18	0.47	0.18
380.0	0.17	0.48	0.38	0.47	0.18
381.0	0.17	0.58	0.28	0.37	0.18
382.0	0.17	0.38	0.28	0.37	0.18
383.0	0.07	0.28	0.28	0.47	0.28
384.0	0.07	0.28	0.38	0.37	0.28
385.0	0.00	0.38	0.28	0.27	0.28
386.0	0.07	0.38	0.28	0.47	0.28
387.0	0.17	0.38	0.28	0.37	0.38
388.0	0.17	0.38	0.28	0.27	0.28
389.0	0.17	0.48	0.28	0.37	0.28
390.0	0.07	0.38	0.48	0.27	0.38
391.0	0.17	0.38	0.48	0.17	0.48
392.0	0.27	0.48	0.48	0.17	0.48
393.0	0.27	0.38	0.48	0.17	0.58
394.0	0.27	0.38	0.48	0.27	0.38
395.0	0.27	0.38	0.58	0.27	0.48
396.0	0.27	0.28	0.68	0.17	0.68
397.0	0.17	0.38	0.68	0.27	0.68
398.0	0.17	0.38	0.48	0.17	0.58
399.0	0.07	0.48	0.48	0.17	0.68
400.0	0.17	0.48	0.28	0.17	0.58

AMC 15 Section 6

y(m) / t(sec)	Concentration (ppb)				
	0.9	1.8	2.7	3.6	4.5
140.0	0.13	0.00	0.09	0.03	0.29
141.0	0.13	0.09	0.00	0.00	0.29
142.0	0.03	0.00	0.09	0.03	0.39
143.0	0.03	0.00	0.09	0.03	0.29
144.0	0.00	0.19	0.29	0.13	0.39
145.0	0.03	0.19	0.39	0.13	0.39
146.0	0.00	0.39	0.39	0.13	0.29
147.0	0.00	0.39	0.49	0.13	0.39
148.0	0.00	0.49	0.59	0.23	0.59
149.0	0.00	0.59	0.69	0.13	0.39
150.0	0.00	0.79	0.79	0.13	0.19
151.0	0.03	1.09	0.99	0.13	0.19
152.0	0.03	1.29	1.39	0.13	0.29
153.0	0.23	1.59	1.49	0.33	0.19
154.0	0.23	1.89	1.69	0.53	0.19
155.0	0.33	2.19	1.79	0.63	0.29
156.0	0.63	2.39	1.99	0.53	0.29
157.0	0.73	2.79	2.59	0.53	0.29
158.0	1.03	2.99	2.79	0.73	0.29
159.0	1.23	3.49	3.29	0.93	0.49
160.0	1.43	3.79	3.59	1.23	0.49
161.0	1.73	4.19	4.49	1.33	0.59
162.0	1.83	4.39	5.09	1.43	0.79
163.0	2.03	4.89	5.59	1.63	0.99
164.0	2.23	5.29	5.89	1.73	0.99
165.0	2.33	5.59	5.99	2.13	0.99
166.0	2.73	5.99	6.09	2.53	1.29
167.0	3.13	6.49	6.59	3.13	1.59
168.0	3.63	6.79	6.69	3.63	1.99
169.0	4.13	7.19	6.89	4.03	2.29
170.0	4.53	7.49	7.39	4.63	2.39
171.0	5.03	7.89	7.99	5.03	2.49
172.0	5.33	8.39	8.29	5.13	2.89
173.0	5.73	8.79	8.89	5.43	3.39
174.0	6.13	9.29	9.29	5.83	3.89
175.0	6.43	9.89	9.49	6.43	4.19
176.0	6.93	10.39	9.79	7.03	4.39
177.0	7.33	10.79	9.99	7.53	4.39
178.0	7.73	11.09	10.19	8.03	4.49
179.0	8.03	11.39	10.09	8.63	4.49
180.0	8.53	11.99	10.59	9.33	4.59
181.0	8.93	12.59	10.99	9.73	4.89
182.0	9.23	13.09	11.39	10.13	5.39
183.0	9.53	13.59	11.89	10.63	6.09
184.0	9.93	13.69	12.09	11.13	6.49
185.0	10.13	13.99	12.39	11.43	7.19
186.0	10.43	14.19	12.69	11.63	7.49
187.0	10.83	14.49	12.79	11.83	8.29
188.0	11.33	14.49	12.99	12.03	8.49
189.0	11.63	14.59	13.09	12.43	8.79
190.0	11.93	14.59	13.29	12.73	8.99
191.0	12.13	14.69	13.39	13.03	9.29
192.0	12.43	14.69	13.69	13.43	9.39
193.0	12.53	14.69	13.89	13.63	9.59
194.0	12.73	14.79	13.89	13.93	9.99

195.0	12.83	14.79	13.99	14.23	10.29
196.0	13.13	14.79	13.79	14.33	10.69
197.0	13.23	14.79	13.89	14.33	10.69
198.0	13.33	14.79	13.89	14.73	11.09
199.0	13.33	14.69	13.89	14.93	11.39
200.0	13.43	14.59	14.09	14.93	11.39
201.0	13.43	14.49	14.19	15.13	11.79
202.0	13.53	14.29	14.09	15.03	12.09
203.0	13.53	14.29	14.09	15.03	12.29
204.0	13.63	13.99	13.89	15.03	12.49
205.0	13.73	13.69	13.69	14.93	12.69
206.0	13.73	13.59	13.69	15.03	12.79
207.0	13.73	13.49	13.59	15.03	12.79
208.0	13.73	13.29	13.59	15.13	12.79
209.0	13.53	13.19	13.39	15.03	12.89
210.0	13.43	13.19	13.39	14.83	12.99
211.0	13.33	13.09	13.29	14.93	13.09
212.0	13.33	12.89	12.99	14.93	13.19
213.0	13.33	12.69	12.79	14.83	13.19
214.0	13.33	12.39	12.49	14.63	13.19
215.0	13.23	12.09	12.09	14.63	13.09
216.0	13.13	11.89	11.79	14.43	12.99
217.0	13.03	11.79	11.79	14.33	12.89
218.0	12.93	11.69	11.69	14.23	12.89
219.0	12.73	11.59	11.49	13.93	12.79
220.0	12.53	11.19	11.19	13.63	12.69
221.0	12.33	10.79	10.89	13.43	12.59
222.0	12.03	10.59	10.69	13.23	12.69
223.0	11.93	10.29	10.39	13.13	12.49
224.0	11.63	10.09	10.39	12.83	12.39
225.0	11.33	9.79	10.29	12.53	12.29
226.0	11.23	9.59	10.19	12.33	12.09
227.0	11.03	9.49	9.89	11.93	11.99
228.0	10.93	9.29	9.69	11.73	12.09
229.0	10.73	9.09	9.59	11.23	11.99
230.0	10.53	8.89	9.29	10.93	11.79
231.0	10.33	8.79	9.09	10.53	11.59
232.0	10.03	8.49	8.89	10.33	11.59
233.0	9.83	8.39	8.59	10.03	11.49
234.0	9.73	8.19	8.39	9.93	11.39
235.0	9.63	8.19	8.39	9.73	11.19
236.0	9.43	7.89	8.09	9.63	11.09
237.0	9.33	7.89	7.89	9.53	10.89
238.0	9.03	7.69	7.69	9.23	10.79
239.0	8.93	7.49	7.59	9.13	10.49
240.0	8.83	7.39	7.19	9.03	10.19
241.0	8.63	7.29	7.09	8.83	9.99
242.0	8.43	6.99	6.89	8.53	9.89
243.0	8.23	6.69	6.89	8.43	9.69
244.0	8.03	6.59	6.79	8.23	9.59
245.0	7.93	6.49	6.69	8.13	9.39
246.0	7.83	6.39	6.59	7.93	9.19
247.0	7.73	6.19	6.39	7.53	8.89
248.0	7.53	5.99	6.29	7.33	8.69
249.0	7.23	5.89	6.19	7.23	8.49
250.0	7.13	5.79	5.99	7.03	8.39
251.0	6.93	5.59	5.79	6.83	8.19
252.0	6.73	5.39	5.49	6.63	7.89
253.0	6.43	5.29	5.39	6.43	7.79
254.0	6.33	4.99	5.29	6.23	7.69
255.0	6.23	4.69	5.09	6.03	7.59
256.0	6.13	4.59	4.89	5.93	7.19

257.0	6.03	4.49	4.79	5.83	6.89
258.0	5.83	4.39	4.59	5.63	6.69
259.0	5.63	4.29	4.49	5.53	6.59
260.0	5.43	4.19	4.29	5.43	6.49
261.0	5.33	4.29	4.19	5.43	6.29
262.0	5.13	4.19	4.29	5.33	5.99
263.0	4.93	3.99	4.19	5.13	5.69
264.0	4.93	3.89	4.09	5.03	5.59
265.0	4.63	3.89	3.89	4.93	5.69
266.0	4.53	3.99	3.69	4.73	5.49
267.0	4.33	3.89	3.49	4.63	5.29
268.0	4.33	3.89	3.39	4.43	4.89
269.0	4.23	3.79	3.49	4.43	4.79
270.0	4.03	3.79	3.29	4.33	4.69
271.0	3.83	3.59	3.19	4.23	4.49
272.0	3.73	3.29	2.99	4.03	4.49
273.0	3.63	3.19	2.89	4.03	4.49
274.0	3.53	2.99	2.79	3.83	4.39
275.0	3.43	2.89	2.79	3.73	4.29
276.0	3.43	2.69	2.69	3.63	4.39
277.0	3.33	2.59	2.79	3.63	4.39
278.0	3.23	2.59	2.59	3.63	4.29
279.0	3.13	2.59	2.69	3.53	4.19
280.0	3.03	2.39	2.59	3.33	4.19
281.0	3.03	2.39	2.29	3.33	4.19
282.0	3.13	2.29	2.29	3.03	3.99
283.0	3.03	2.19	2.19	2.83	3.79
284.0	2.83	1.99	2.09	2.63	3.99
285.0	2.83	1.99	2.19	2.53	3.89
286.0	2.73	1.99	2.09	2.43	3.69
287.0	2.63	1.99	2.09	2.33	3.69
288.0	2.63	2.09	2.09	2.23	3.69
289.0	2.53	1.99	2.09	2.23	3.49
290.0	2.43	1.99	2.19	2.23	3.59
291.0	2.33	1.79	2.09	2.33	3.69
292.0	2.43	1.79	2.19	2.13	3.49
293.0	2.33	1.69	2.09	2.13	3.49
294.0	2.23	1.59	2.09	2.03	3.29
295.0	2.13	1.49	1.89	2.03	3.19
296.0	2.13	1.49	1.89	1.93	3.09
297.0	2.03	1.49	1.79	1.93	3.09
298.0	1.83	1.39	1.79	1.83	2.89
299.0	1.83	1.39	1.89	1.83	2.89
300.0	1.83	1.29	1.79	1.93	2.69
301.0	1.73	1.19	1.59	1.93	2.69
302.0	1.73	1.19	1.59	1.93	2.59
303.0	1.63	1.09	1.49	1.83	2.59
304.0	1.63	1.09	1.49	1.83	2.39
305.0	1.53	1.19	1.49	1.73	2.19
306.0	1.53	0.99	1.59	1.73	2.19
307.0	1.63	1.09	1.59	1.63	2.19
308.0	1.63	1.19	1.49	1.53	2.19
309.0	1.63	0.99	1.49	1.53	2.19
310.0	1.53	0.99	1.59	1.53	2.19
311.0	1.33	1.09	1.59	1.63	2.09
312.0	1.33	1.09	1.69	1.53	1.99
313.0	1.13	0.89	1.59	1.53	1.89
314.0	1.13	0.89	1.49	1.53	1.79
315.0	1.13	0.89	1.39	1.53	1.49
316.0	1.13	0.79	1.39	1.43	1.59
317.0	1.13	0.99	1.29	1.33	1.49
318.0	1.03	0.89	1.29	1.33	1.39

319.0	0.93	1.09	1.29	1.33	1.49
320.0	0.83	0.99	1.19	1.33	1.39
321.0	0.73	0.89	1.09	1.33	1.39
322.0	0.73	0.79	1.09	1.13	1.39
323.0	0.83	0.69	1.09	1.13	1.49
324.0	0.93	0.59	0.99	1.23	1.49
325.0	0.83	0.69	0.99	1.13	1.49
326.0	0.83	0.79	0.89	1.13	1.49
327.0	0.83	0.79	0.89	1.03	1.39
328.0	0.73	0.79	0.79	0.93	1.29
329.0	0.63	0.79	0.79	0.93	1.29
330.0	0.63	0.69	0.79	0.83	1.39
331.0	0.63	0.49	0.89	0.73	1.49
332.0	0.73	0.39	0.69	0.73	1.39
333.0	0.73	0.39	0.89	0.83	1.39
334.0	0.63	0.39	0.99	0.83	1.39
335.0	0.73	0.49	0.89	0.93	1.29
336.0	0.73	0.49	0.99	0.93	1.29
337.0	0.63	0.49	0.99	1.03	1.29
338.0	0.63	0.39	0.99	1.03	1.39
339.0	0.63	0.39	0.99	1.03	1.39
340.0	0.73	0.39	0.99	1.03	1.39
341.0	0.63	0.29	1.09	1.03	1.29
342.0	0.63	0.29	1.09	1.03	1.39
343.0	0.63	0.29	1.19	0.83	1.29
344.0	0.73	0.19	1.19	0.83	1.39
345.0	0.53	0.29	1.19	0.73	1.19
346.0	0.63	0.19	1.19	0.73	1.19
347.0	0.63	0.29	1.09	0.73	1.09
348.0	0.63	0.19	1.09	0.63	0.99
349.0	0.53	0.09	1.09	0.73	0.89
350.0	0.63	0.19	1.09	0.73	0.89
351.0	0.63	0.19	0.99	0.73	0.89
352.0	0.63	0.09	0.89	0.63	0.89
353.0	0.73	0.00	0.79	0.63	0.99
354.0	0.73	0.00	0.79	0.63	0.89
355.0	0.63	0.09	0.79	0.53	0.89
356.0	0.73	0.19	0.79	0.63	0.69
357.0	0.63	0.19	0.59	0.73	0.69
358.0	0.63	0.29	0.69	0.73	0.69
359.0	0.53	0.39	0.59	0.83	0.69
360.0	0.63	0.49	0.59	0.73	0.69
361.0	0.63	0.39	0.59	0.73	0.69
362.0	0.53	0.29	0.49	0.63	0.69
363.0	0.53	0.29	0.39	0.63	0.59
364.0	0.43	0.29	0.39	0.43	0.49
365.0	0.53	0.39	0.39	0.43	0.59
366.0	0.53	0.39	0.39	0.53	0.69
367.0	0.43	0.39	0.39	0.43	0.69
368.0	0.53	0.39	0.29	0.43	0.79
369.0	0.43	0.49	0.29	0.53	0.79
370.0	0.53	0.29	0.49	0.53	0.59
371.0	0.43	0.29	0.49	0.53	0.69
372.0	0.43	0.29	0.49	0.63	0.69
373.0	0.43	0.29	0.59	0.73	0.69
374.0	0.33	0.29	0.49	0.63	0.59
375.0	0.43	0.29	0.49	0.63	0.69
376.0	0.43	0.19	0.49	0.63	0.59
377.0	0.43	0.00	0.39	0.63	0.49
378.0	0.33	0.09	0.39	0.73	0.59
379.0	0.43	0.19	0.39	0.63	0.59
380.0	0.43	0.19	0.39	0.53	0.49

381.0	0.43	0.39	0.29	0.53	0.39
382.0	0.53	0.29	0.29	0.43	0.49
383.0	0.53	0.39	0.29	0.43	0.49
384.0	0.43	0.29	0.39	0.43	0.49
385.0	0.53	0.39	0.39	0.33	0.49
386.0	0.33	0.39	0.39	0.13	0.39
387.0	0.33	0.39	0.49	0.03	0.39
388.0	0.33	0.39	0.49	0.13	0.39
389.0	0.43	0.29	0.49	0.03	0.49
390.0	0.43	0.39	0.39	0.00	0.49
391.0	0.43	0.39	0.39	0.00	0.49
392.0	0.33	0.39	0.39	0.03	0.39
393.0	0.33	0.39	0.49	0.03	0.49
394.0	0.33	0.49	0.39	0.00	0.39
395.0	0.23	0.59	0.49	0.00	0.39
396.0	0.33	0.59	0.49	0.03	0.39
397.0	0.33	0.69	0.49	0.03	0.49
398.0	0.23	0.69	0.49	0.13	0.49
399.0	0.23	0.79	0.59	0.13	0.49
400.0	0.23	0.69	0.59	0.13	0.59
401.0	0.13	0.69	0.49	0.13	0.69
402.0	0.13	0.59	0.59	0.23	0.69
403.0	0.13	0.49	0.69	0.23	0.69
404.0	0.13	0.49	0.69	0.23	0.69
405.0	0.23	0.49	0.59	0.23	0.69
406.0	0.13	0.39	0.59	0.33	0.69
407.0	0.03	0.39	0.69	0.23	0.69
408.0	0.00	0.29	0.69	0.23	0.79
409.0	0.03	0.39	0.59	0.03	0.59
410.0	0.00	0.49	0.59	0.13	0.59
411.0	0.03	0.39	0.69	0.23	0.69
412.0	0.00	0.49	0.59	0.23	0.49
413.0	0.00	0.39	0.69	0.23	0.49
414.0	0.00	0.39	0.69	0.23	0.29
415.0	0.00	0.29	0.49	0.23	0.39
416.0	0.00	0.29	0.49	0.13	0.39
417.0	0.03	0.19	0.59	0.13	0.39
418.0	0.03	0.29	0.59	0.03	0.39
419.0	0.00	0.39	0.49	0.00	0.29
420.0	0.00	0.09	0.49	0.03	0.29

A.4 Concentration data for Andong Channel Experiment

AMC 17 Section 1

y(m) / t(sec)	Concentration (ppb)				
	0.9	1.8	2.7	3.6	4.5
50.0	0.00	0.00	0.00	0.00	0.23
51.0	0.00	0.00	0.12	0.00	0.33
52.0	0.00	0.00	0.12	0.00	0.33
53.0	0.00	0.00	0.12	0.00	0.43
54.0	0.00	0.00	0.12	0.00	0.33
55.0	0.00	0.00	0.12	0.00	0.33
56.0	0.00	0.00	0.12	0.00	0.43
57.0	0.00	0.00	0.12	0.00	0.53
58.0	0.00	0.00	0.22	0.00	0.43
59.0	0.00	0.00	0.22	0.00	0.43
60.0	0.00	0.00	0.22	0.00	0.33
61.0	0.00	0.00	0.22	0.00	0.33
62.0	0.00	0.00	0.12	0.00	0.43
63.0	0.00	0.00	0.12	0.00	0.43
64.0	0.20	0.00	0.12	0.00	0.43
65.0	0.90	0.00	0.22	0.00	0.43
66.0	2.40	0.00	0.22	0.00	0.63
67.0	4.00	0.00	0.72	0.00	0.53
68.0	6.90	0.00	1.22	0.00	0.53
69.0	11.00	0.25	2.22	0.29	0.53
70.0	15.80	1.15	3.52	1.09	0.43
71.0	20.20	2.85	6.22	2.29	0.43
72.0	23.30	5.05	10.62	4.29	0.53
73.0	25.80	8.45	14.22	6.59	0.43
74.0	27.50	13.95	17.42	9.29	0.63
75.0	28.70	18.45	20.02	11.99	0.63
76.0	29.60	21.55	22.52	14.59	0.83
77.0	30.30	24.35	24.82	17.09	1.13
78.0	30.70	26.45	26.82	19.59	2.23
79.0	30.70	28.05	28.22	21.79	3.23
80.0	30.80	29.35	29.12	23.69	4.33
81.0	31.20	30.45	29.82	25.19	5.73
82.0	31.40	31.25	30.42	26.69	7.43
83.0	31.00	31.65	30.92	27.89	8.83
84.0	30.60	31.95	30.82	28.89	9.93
85.0	30.40	31.95	30.72	29.49	10.93
86.0	29.90	31.75	30.82	29.89	11.83
87.0	29.30	31.35	30.82	30.49	12.53
88.0	28.40	30.85	30.62	30.69	13.63
89.0	27.50	30.35	30.02	30.89	14.73
90.0	26.30	29.65	29.62	30.99	15.83
91.0	25.50	29.15	29.12	30.99	17.13
92.0	24.80	28.35	28.72	30.69	18.53
93.0	24.10	27.95	28.12	30.39	19.63
94.0	23.20	27.45	27.42	29.99	20.63
95.0	22.50	26.65	26.82	29.39	21.53
96.0	21.80	25.95	26.22	28.69	22.23
97.0	21.30	25.05	25.52	27.89	22.83
98.0	20.50	24.05	24.52	27.29	23.43
99.0	19.50	23.25	23.62	26.89	23.83
100.0	18.80	22.45	22.52	26.19	24.13
101.0	18.20	21.45	21.62	25.59	24.53
102.0	17.60	20.85	20.92	24.99	24.53
103.0	17.00	20.45	20.12	24.29	24.43
104.0	16.20	19.75	19.32	23.59	24.53

105.0	15.10	18.85	18.52	22.79	24.53
106.0	14.20	17.95	17.82	21.89	24.43
107.0	13.40	17.25	17.32	20.99	24.43
108.0	12.90	16.45	16.62	20.19	24.23
109.0	12.10	15.85	15.82	19.29	24.03
110.0	11.60	14.95	15.22	18.49	23.83
111.0	11.10	14.25	14.42	17.89	23.53
112.0	10.60	13.55	13.72	17.29	23.13
113.0	9.90	12.95	13.22	16.39	22.73
114.0	9.30	12.25	12.62	15.79	22.23
115.0	8.80	11.75	12.12	15.19	21.63
116.0	8.40	11.15	11.52	14.59	21.03
117.0	8.00	10.75	10.92	13.79	20.63
118.0	7.60	10.15	10.42	13.29	20.13
119.0	7.10	9.75	9.92	12.69	19.63
120.0	6.80	9.45	9.52	11.99	19.03
121.0	6.40	9.05	8.92	11.39	18.53
122.0	6.20	8.55	8.72	10.99	18.03
123.0	5.80	8.05	8.32	10.39	17.53
124.0	5.50	7.45	7.82	9.89	17.13
125.0	5.20	7.05	7.42	9.29	16.73
126.0	4.90	6.75	7.02	8.79	16.33
127.0	4.50	6.55	6.72	8.29	15.73
128.0	4.10	6.35	6.32	7.89	15.33
129.0	3.90	5.85	6.22	7.39	14.83
130.0	3.80	5.55	5.92	6.89	14.33
131.0	3.70	5.25	5.52	6.49	14.13
132.0	3.50	4.95	5.22	6.19	13.63
133.0	3.50	4.65	4.82	5.89	13.23
134.0	3.20	4.45	4.62	5.69	12.73
135.0	3.20	4.35	4.52	5.29	12.33
136.0	3.10	3.95	4.22	4.99	11.73
137.0	3.00	3.65	4.12	4.69	11.23
138.0	2.90	3.45	3.82	4.39	10.63
139.0	2.60	3.15	3.62	4.09	10.13
140.0	2.50	3.05	3.32	3.89	9.83
141.0	2.20	2.85	3.12	3.79	9.63
142.0	2.00	2.85	3.02	3.79	9.23
143.0	1.70	2.65	2.82	3.69	8.83
144.0	1.60	2.45	2.72	3.59	8.33
145.0	1.50	2.35	2.52	3.39	8.13
146.0	1.50	2.15	2.32	3.09	7.73
147.0	1.30	1.95	2.32	2.89	7.63
148.0	1.20	1.85	2.12	2.69	7.23
149.0	1.00	1.75	2.12	2.49	7.03
150.0	0.90	1.75	1.92	2.49	6.83
151.0	0.90	1.75	1.72	2.39	6.53
152.0	0.80	1.55	1.72	2.19	6.53
153.0	0.80	1.45	1.52	2.09	6.33
154.0	0.70	1.45	1.42	1.89	6.03
155.0	0.70	1.45	1.32	1.79	5.73
156.0	0.50	1.25	1.22	1.69	5.63
157.0	0.40	1.15	1.22	1.59	5.33
158.0	0.20	1.25	1.22	1.49	5.13
159.0	0.20	1.25	1.22	1.49	4.83
160.0	0.20	1.15	1.32	1.39	4.63
161.0	0.20	1.25	1.12	1.39	4.43
162.0	0.10	1.05	1.12	1.29	4.13
163.0	0.00	1.05	1.12	1.09	3.93
164.0	0.00	0.95	1.02	0.99	3.73
165.0	0.00	0.95	1.02	0.89	3.53
166.0	0.00	0.95	0.92	0.79	3.43

167.0	0.00	0.85	0.92	0.69	3.23
168.0	0.00	0.85	1.02	0.69	3.03
169.0	0.00	0.75	0.92	0.69	2.93
170.0	0.00	0.65	0.82	0.69	2.83
171.0	0.00	0.55	0.72	0.59	2.63
172.0	0.00	0.35	0.72	0.59	2.63
173.0	0.00	0.35	0.72	0.49	2.63
174.0	0.00	0.35	0.62	0.49	2.53
175.0	0.00	0.35	0.62	0.29	2.43
176.0	0.00	0.45	0.62	0.19	2.13
177.0	0.00	0.25	0.72	0.19	2.03
178.0	0.00	0.15	0.72	0.19	1.93
179.0	0.10	0.25	0.72	0.19	1.83
180.0	0.10	0.15	0.62	0.09	1.73
181.0	0.10	0.25	0.52	0.09	1.53
182.0	0.20	0.15	0.42	0.00	1.53
183.0	0.20	0.15	0.52	0.00	1.53
184.0	0.30	0.15	0.62	0.00	1.53
185.0	0.50	0.05	0.62	0.00	1.53
186.0	0.40	0.25	0.62	0.00	1.63
187.0	0.40	0.35	0.42	0.00	1.63
188.0	0.50	0.25	0.52	0.00	1.53
189.0	0.50	0.25	0.52	0.00	1.53
190.0	0.50	0.25	0.42	0.00	1.33
191.0	0.60	0.15	0.32	0.19	1.43
192.0	0.70	0.35	0.52	0.00	1.43
193.0	0.60	0.35	0.52	0.00	1.43
194.0	0.40	0.35	0.42	0.00	1.43
195.0	0.50	0.25	0.42	0.00	1.13
196.0	0.50	0.15	0.42	0.00	1.03
197.0	0.40	0.15	0.52	0.00	1.23
198.0	0.40	0.05	0.62	0.00	0.83
199.0	0.30	0.05	0.52	0.00	1.13
200.0	0.20	0.05	0.52	0.00	1.03
201.0	0.10	0.00	0.62	0.00	0.93
202.0	0.00	0.00	0.52	0.00	0.93
203.0	0.00	0.00	0.52	0.00	0.93
204.0	0.00	0.00	0.42	0.00	1.03
205.0	0.00	0.00	0.32	0.00	0.63
206.0	0.00	0.00	0.12	0.00	0.73
207.0	0.00	0.00	0.12	0.00	0.83
208.0	0.00	0.00	0.12	0.00	0.63
209.0	0.00	0.00	0.22	0.00	0.73
210.0	0.00	0.05	0.22	0.00	0.53
211.0	0.00	0.05	0.32	0.00	0.73
212.0	0.00	0.00	0.32	0.00	0.63
213.0	0.00	0.00	0.22	0.00	0.73
214.0	0.00	0.00	0.32	0.00	0.63
215.0	0.00	0.00	0.22	0.00	0.33
216.0	0.00	0.00	0.32	0.00	0.23
217.0	0.00	0.00	0.22	0.00	0.13
218.0	0.00	0.05	0.22	0.00	0.33
219.0	0.00	0.15	0.42	0.00	0.23
220.0	0.00	0.35	0.42	0.00	0.13
221.0	0.00	0.25	0.52	0.00	0.23
222.0	0.00	0.25	0.52	0.00	0.23
223.0	0.10	0.25	0.62	0.00	0.33
224.0	0.00	0.15	0.52	0.00	0.23
225.0	0.00	0.15	0.42	0.00	0.13
226.0	0.00	0.25	0.42	0.00	0.03
227.0	0.00	0.35	0.42	0.00	0.00
228.0	0.00	0.25	0.42	0.00	0.00

229.0	0.00	0.25	0.42	0.00	0.13
230.0	0.00	0.35	0.52	0.00	0.13
231.0	0.00	0.25	0.32	0.00	0.13
232.0	0.10	0.35	0.52	0.00	0.03
233.0	0.10	0.25	0.52	0.00	0.00
234.0	0.20	0.15	0.52	0.00	0.03
235.0	0.10	0.15	0.42	0.00	0.13
236.0	0.00	0.15	0.22	0.00	0.13
237.0	0.00	0.05	0.12	0.00	0.13
238.0	0.00	0.05	0.12	0.00	0.13
239.0	0.00	0.15	0.22	0.00	0.00
240.0	0.00	0.15	0.12	0.00	0.03
241.0	0.10	0.25	0.22	0.00	0.00
242.0	0.00	0.35	0.12	0.00	0.00
243.0	0.00	0.25	0.22	0.00	0.00
244.0	0.10	0.25	0.12	0.00	0.03
245.0	0.10	0.15	0.12	0.00	0.13
246.0	0.00	0.35	0.12	0.00	0.03
247.0	0.00	0.35	0.22	0.00	0.23
248.0	0.00	0.35	0.22	0.00	0.03
249.0	0.10	0.25	0.12	0.00	0.00
250.0	0.00	0.25	0.22	0.00	0.03
251.0	0.00	0.35	0.32	0.00	0.03
252.0	0.00	0.45	0.32	0.00	0.00
253.0	0.00	0.45	0.32	0.00	0.00
254.0	0.00	0.45	0.32	0.00	0.00
255.0	0.00	0.65	0.32	0.00	0.00
256.0	0.00	0.65	0.22	0.00	0.00
257.0	0.00	0.75	0.22	0.00	0.00
258.0	0.00	0.65	0.02	0.00	0.00
259.0	0.00	0.75	0.00	0.00	0.00
260.0	0.00	0.85	0.02	0.00	0.00
261.0	0.00	0.85	0.12	0.00	0.00
262.0	0.00	0.75	0.12	0.00	0.00
263.0	0.00	0.65	0.22	0.00	0.00
264.0	0.00	0.75	0.22	0.00	0.00
265.0	0.00	0.65	0.12	0.00	0.00
266.0	0.00	0.55	0.02	0.00	0.00
267.0	0.00	0.45	0.00	0.00	0.00
268.0	0.00	0.45	0.00	0.00	0.00
269.0	0.00	0.35	0.00	0.00	0.03
270.0	0.00	0.35	0.00	0.00	0.13
271.0	0.00	0.35	0.00	0.00	0.03
272.0	0.00	0.35	0.02	0.00	0.03
273.0	0.00	0.45	0.12	0.00	0.03
274.0	0.00	0.35	0.02	0.00	0.03
275.0	0.00	0.25	0.02	0.00	0.23
276.0	0.00	0.15	0.02	0.00	0.33
277.0	0.00	0.05	0.12	0.00	0.33
278.0	0.00	0.00	0.12	0.00	0.23
279.0	0.00	0.00	0.02	0.00	0.03
280.0	0.00	0.00	0.00	0.00	0.03
281.0	0.00	0.00	0.00	0.00	0.03
282.0	0.00	0.00	0.00	0.00	0.13
283.0	0.00	0.00	0.12	0.00	0.33
284.0	0.00	0.00	0.12	0.00	0.43
285.0	0.00	0.00	0.00	0.00	0.33
286.0	0.00	0.00	0.00	0.00	0.33
287.0	0.00	0.00	0.00	0.00	0.23
288.0	0.00	0.00	0.00	0.00	0.33
289.0	0.00	0.00	0.00	0.00	0.23
290.0	0.00	0.00	0.00	0.00	0.33

291.0	0.00	0.00	0.00	0.00	0.33
292.0	0.00	0.00	0.00	0.00	0.33
293.0	0.00	0.00	0.00	0.00	0.23
294.0	0.00	0.00	0.00	0.09	0.33
295.0	0.00	0.00	0.00	0.09	0.33
296.0	0.00	0.00	0.00	0.00	0.33
297.0	0.00	0.00	0.00	0.00	0.23
298.0	0.00	0.00	0.00	0.00	0.23
299.0	0.00	0.00	0.00	0.00	0.23
300.0	0.00	0.00	0.02	0.00	0.23

AMC 17 Section 2

y(m) / t(sec)	Concentration (ppb)				
	1.0	2.0	3.0	4.0	5.0
80.0	0.00	0.00	0.00	0.21	0.00
81.0	0.06	0.00	0.00	0.41	0.00
82.0	0.06	0.00	0.00	0.51	0.00
83.0	0.00	0.00	0.00	0.51	0.00
84.0	0.00	0.00	0.00	0.41	0.00
85.0	0.06	0.00	0.00	0.31	0.00
86.0	0.16	0.00	0.00	0.51	0.00
87.0	0.26	0.00	0.00	0.51	0.00
88.0	0.26	0.00	0.00	0.51	0.00
89.0	0.16	0.00	0.00	0.31	0.00
90.0	0.16	0.00	0.00	0.21	0.00
91.0	0.06	0.00	0.00	0.21	0.00
92.0	0.06	0.00	0.00	0.41	0.00
93.0	0.00	0.00	0.00	0.61	0.00
94.0	0.06	0.00	0.00	0.81	0.00
95.0	0.00	0.00	0.07	1.01	0.00
96.0	0.00	0.00	0.27	1.11	0.07
97.0	0.00	0.00	0.27	1.31	0.07
98.0	0.00	0.00	0.37	1.81	0.27
99.0	0.00	0.00	0.57	2.21	0.27
100.0	0.00	0.00	0.97	2.81	0.77
101.0	0.00	0.00	1.47	3.61	1.07
102.0	0.00	0.00	2.17	4.31	1.17
103.0	0.00	0.00	2.87	5.11	1.37
104.0	0.00	0.02	3.47	5.41	1.47
105.0	0.06	0.22	4.47	5.91	1.67
106.0	0.00	0.52	5.77	6.81	1.47
107.0	0.06	1.02	6.87	8.21	1.47
108.0	0.06	1.62	7.77	9.71	1.57
109.0	0.26	2.22	8.57	11.51	2.07
110.0	0.36	2.82	9.47	13.11	2.37
111.0	0.96	3.32	10.17	14.71	2.47
112.0	1.46	3.72	10.97	15.91	2.67
113.0	2.16	4.32	11.67	17.31	2.97
114.0	2.66	4.72	12.07	18.41	3.37
115.0	3.36	5.32	12.87	19.11	3.87
116.0	3.86	5.72	13.87	19.91	4.27
117.0	4.46	6.32	14.67	20.51	5.17
118.0	4.96	7.12	15.27	21.01	6.07
119.0	5.56	7.92	15.77	21.51	6.87
120.0	6.26	8.82	16.37	21.91	8.07
121.0	7.06	9.72	16.87	21.91	8.87
122.0	7.86	10.52	17.17	21.81	9.57
123.0	8.76	11.22	17.57	21.81	9.97
124.0	9.56	12.12	17.87	22.01	10.77
125.0	10.46	12.82	18.17	22.31	11.47
126.0	11.26	13.52	18.27	22.71	12.27
127.0	11.76	14.12	18.47	22.91	13.07
128.0	12.16	14.62	18.47	22.91	13.87
129.0	12.66	15.02	18.57	23.11	14.27
130.0	12.96	15.42	18.57	23.01	14.67
131.0	13.26	15.52	18.57	22.41	14.97
132.0	13.36	15.82	18.47	22.11	15.07
133.0	13.96	16.22	18.37	21.61	15.27
134.0	14.36	16.32	18.37	21.41	15.37
135.0	14.76	16.62	18.17	20.71	15.67
136.0	15.16	16.72	17.97	20.31	16.07

137.0	15.36	17.02	17.67	19.51	16.27
138.0	15.56	17.12	17.27	19.21	16.67
139.0	15.76	17.12	16.87	18.91	16.67
140.0	15.96	17.12	16.57	18.81	16.57
141.0	16.06	17.02	16.57	18.51	16.27
142.0	16.26	16.92	16.57	18.11	16.17
143.0	16.36	16.92	16.37	17.61	16.07
144.0	16.66	16.82	16.07	17.01	15.97
145.0	16.66	16.62	15.87	16.61	15.87
146.0	16.86	16.62	15.57	16.21	16.17
147.0	17.06	16.52	15.37	16.01	16.27
148.0	17.16	16.52	15.37	15.71	16.37
149.0	17.16	16.42	15.07	15.21	16.17
150.0	17.16	16.22	14.77	14.71	16.17
151.0	16.86	16.12	14.57	14.41	15.77
152.0	16.76	16.02	14.27	14.01	15.57
153.0	16.46	15.92	14.07	13.91	15.17
154.0	16.36	15.62	13.87	13.41	15.27
155.0	16.16	15.42	13.67	13.11	15.27
156.0	15.86	15.12	13.27	12.71	15.07
157.0	15.66	14.82	13.07	12.41	14.87
158.0	15.46	14.42	12.47	12.01	14.47
159.0	15.06	14.12	12.17	11.41	13.87
160.0	14.96	13.92	11.67	11.01	13.87
161.0	14.56	13.62	11.47	10.81	13.67
162.0	14.06	13.42	11.07	10.51	13.67
163.0	13.86	13.32	10.67	10.31	13.47
164.0	13.66	13.12	10.17	9.91	13.27
165.0	13.36	12.82	9.97	9.61	13.07
166.0	13.26	12.62	9.67	9.21	12.47
167.0	13.16	12.42	9.47	9.11	11.97
168.0	12.96	12.12	9.07	8.71	11.67
169.0	12.66	11.82	8.97	8.41	11.57
170.0	12.56	11.52	8.77	8.01	11.17
171.0	12.36	11.32	8.27	7.71	10.77
172.0	12.16	11.02	8.17	7.31	10.57
173.0	11.86	10.62	7.87	7.11	10.27
174.0	11.76	10.42	7.77	6.61	10.07
175.0	11.46	10.22	7.57	6.21	9.97
176.0	11.36	9.82	7.37	6.01	10.07
177.0	11.16	9.52	7.27	5.81	10.07
178.0	11.06	9.22	7.07	5.71	9.97
179.0	10.76	8.82	6.97	5.31	9.47
180.0	10.46	8.72	6.67	5.21	9.27
181.0	10.06	8.32	6.27	5.01	9.07
182.0	9.76	8.12	6.07	4.71	8.87
183.0	9.56	7.82	5.77	4.61	8.77
184.0	9.26	7.62	5.57	4.41	8.67
185.0	9.16	7.52	5.27	4.01	8.37
186.0	9.06	7.22	5.07	3.91	7.97
187.0	8.86	7.12	5.07	3.81	7.87
188.0	8.56	6.92	4.87	3.81	7.77
189.0	8.36	6.52	4.87	3.71	7.87
190.0	8.26	6.32	4.97	3.71	7.87
191.0	8.16	6.12	4.87	3.41	7.67
192.0	8.06	5.92	4.57	3.21	7.37
193.0	7.76	5.82	4.47	2.91	7.47
194.0	7.46	5.62	4.57	2.91	7.37
195.0	7.16	5.62	4.27	2.91	7.27
196.0	6.76	5.42	4.07	2.81	6.97
197.0	6.56	5.32	3.77	2.71	6.57
198.0	6.26	5.32	3.57	2.61	6.47

199.0	5.96	5.02	3.57	2.61	6.27
200.0	5.86	4.82	3.57	2.51	5.97
201.0	5.56	4.52	3.57	2.31	5.87
202.0	5.56	4.32	3.37	2.21	5.87
203.0	5.36	4.22	3.17	2.31	5.67
204.0	5.06	3.92	2.87	2.31	5.57
205.0	4.96	3.82	2.77	2.31	5.37
206.0	4.96	3.72	2.57	2.11	5.37
207.0	4.66	3.52	2.37	2.11	5.27
208.0	4.56	3.42	2.37	2.01	4.97
209.0	4.46	3.22	2.27	2.01	4.87
210.0	4.46	3.02	2.17	2.01	4.87
211.0	4.16	3.02	2.17	1.71	4.57
212.0	4.16	2.72	2.17	1.81	4.37
213.0	3.96	2.72	1.97	1.71	4.17
214.0	3.96	2.92	1.87	1.61	4.07
215.0	3.86	3.02	1.87	1.61	4.07
216.0	3.76	3.02	1.77	1.71	3.77
217.0	3.56	2.82	1.77	1.61	3.47
218.0	3.36	2.82	1.67	1.81	3.37
219.0	3.36	2.72	1.47	1.91	3.17
220.0	3.36	2.52	1.47	2.01	3.37
221.0	3.26	2.42	1.27	1.91	3.67
222.0	3.16	2.32	1.37	1.91	3.47
223.0	2.96	2.22	1.27	1.81	3.47
224.0	2.96	2.02	1.27	1.81	3.47
225.0	2.96	1.92	1.37	1.71	3.27
226.0	2.76	2.12	1.37	1.71	3.07
227.0	2.56	1.92	1.67	1.81	2.77
228.0	2.46	1.92	1.57	1.71	2.87
229.0	2.36	1.82	1.47	1.51	2.67
230.0	2.26	1.72	1.27	1.51	2.47
231.0	2.26	1.72	1.27	1.41	2.67
232.0	2.26	1.72	1.27	1.21	2.57
233.0	2.26	1.72	1.17	1.01	2.57
234.0	2.06	1.62	1.27	0.91	2.57
235.0	1.96	1.42	1.27	0.91	2.47
236.0	2.06	1.42	1.37	0.81	2.47
237.0	2.16	1.42	1.37	0.81	2.47
238.0	2.06	1.42	1.17	0.81	2.37
239.0	2.06	1.32	0.97	0.91	2.47
240.0	1.96	1.22	1.07	0.81	2.67
241.0	1.96	1.22	1.07	0.71	2.77
242.0	1.66	1.22	0.87	0.71	2.67
243.0	1.66	1.12	0.87	0.61	2.57
244.0	1.46	0.92	0.87	0.61	2.27
245.0	1.36	0.92	0.77	0.61	1.97
246.0	1.36	0.72	0.47	0.61	1.87
247.0	1.26	0.62	0.37	0.71	1.77
248.0	1.06	0.82	0.47	0.61	1.77
249.0	0.96	0.82	0.37	0.51	1.77
250.0	0.76	0.72	0.57	0.51	1.67
251.0	0.86	0.82	0.67	0.41	1.67
252.0	0.76	0.72	0.67	0.51	1.67
253.0	0.76	0.82	0.57	0.51	1.67
254.0	0.66	0.82	0.47	0.61	1.87
255.0	0.46	0.92	0.37	0.61	1.87
256.0	0.46	0.82	0.37	0.61	1.87
257.0	0.46	0.82	0.37	0.61	2.07
258.0	0.66	0.72	0.37	0.61	2.07
259.0	0.66	0.62	0.37	0.71	1.97
260.0	0.66	0.52	0.27	0.81	1.77

261.0	0.66	0.42	0.17	0.81	1.67
262.0	0.56	0.42	0.27	0.71	1.67
263.0	0.56	0.52	0.17	0.81	1.47
264.0	0.36	0.52	0.17	0.81	1.37
265.0	0.36	0.62	0.27	0.71	1.47
266.0	0.36	0.82	0.07	0.91	1.47
267.0	0.56	0.72	0.07	0.71	1.17
268.0	0.56	0.82	0.17	0.81	1.17
269.0	0.46	0.72	0.07	0.91	1.17
270.0	0.36	0.62	0.17	0.91	1.17
271.0	0.46	0.52	0.00	0.71	0.97
272.0	0.46	0.52	0.00	0.61	0.67
273.0	0.56	0.52	0.00	0.81	0.77
274.0	0.36	0.52	0.00	0.71	0.77
275.0	0.36	0.52	0.00	0.71	0.67
276.0	0.16	0.32	0.00	0.81	0.57
277.0	0.26	0.32	0.07	0.81	0.57
278.0	0.26	0.22	0.27	0.71	0.67
279.0	0.26	0.22	0.07	0.71	0.47
280.0	0.26	0.22	0.00	0.61	0.47
281.0	0.16	0.22	0.00	0.61	0.57
282.0	0.16	0.12	0.00	0.51	0.57
283.0	0.16	0.12	0.00	0.41	0.67
284.0	0.26	0.12	0.00	0.41	0.67
285.0	0.26	0.02	0.00	0.51	0.67
286.0	0.26	0.12	0.00	0.61	0.57
287.0	0.36	0.00	0.00	0.61	0.57
288.0	0.16	0.02	0.00	0.61	0.57
289.0	0.26	0.02	0.00	0.71	0.47
290.0	0.36	0.22	0.00	0.61	0.47
291.0	0.36	0.32	0.00	0.51	0.47
292.0	0.46	0.32	0.00	0.51	0.57
293.0	0.56	0.12	0.00	0.51	0.67
294.0	0.56	0.22	0.00	0.71	0.47
295.0	0.66	0.12	0.00	0.71	0.57
296.0	0.56	0.22	0.00	0.71	0.37
297.0	0.76	0.22	0.00	0.61	0.37
298.0	0.76	0.02	0.00	0.71	0.67
299.0	0.66	0.22	0.00	0.61	0.57
300.0	0.56	0.22	0.00	0.71	0.47
301.0	0.56	0.12	0.00	0.71	0.47
302.0	0.46	0.12	0.17	0.61	0.47
303.0	0.46	0.12	0.17	0.71	0.47
304.0	0.36	0.02	0.00	0.51	0.47
305.0	0.26	0.00	0.07	0.41	0.37
306.0	0.26	0.02	0.17	0.41	0.37
307.0	0.16	0.00	0.37	0.31	0.37
308.0	0.06	0.02	0.27	0.41	0.47
309.0	0.00	0.00	0.27	0.51	0.47
310.0	0.00	0.00	0.37	0.41	0.47
311.0	0.00	0.00	0.07	0.31	0.47
312.0	0.00	0.00	0.07	0.21	0.37
313.0	0.00	0.00	0.00	0.21	0.27
314.0	0.00	0.00	0.00	0.41	0.37
315.0	0.00	0.00	0.00	0.51	0.37
316.0	0.00	0.00	0.07	0.51	0.37
317.0	0.00	0.00	0.00	0.51	0.47
318.0	0.00	0.00	0.00	0.41	0.37
319.0	0.00	0.00	0.07	0.41	0.37
320.0	0.00	0.00	0.07	0.41	0.37
321.0	0.00	0.00	0.07	0.41	0.27
322.0	0.16	0.00	0.00	0.21	0.47

323.0	0.06	0.00	0.07	0.31	0.47
324.0	0.00	0.00	0.00	0.31	0.47
325.0	0.16	0.00	0.00	0.41	0.57
326.0	0.26	0.00	0.00	0.41	0.57
327.0	0.16	0.00	0.07	0.41	0.57
328.0	0.16	0.00	0.07	0.51	0.57
329.0	0.26	0.00	0.00	0.41	0.67
330.0	0.26	0.00	0.00	0.41	0.57
331.0	0.16	0.00	0.00	0.61	0.47
332.0	0.16	0.00	0.00	0.51	0.47
333.0	0.16	0.00	0.00	0.51	0.67
334.0	0.26	0.00	0.00	0.41	0.57
335.0	0.06	0.00	0.00	0.31	0.57
336.0	0.00	0.00	0.00	0.41	0.47
337.0	0.00	0.00	0.00	0.51	0.37
338.0	0.00	0.00	0.00	0.51	0.27
339.0	0.00	0.00	0.00	0.51	0.27
340.0	0.00	0.00	0.00	0.51	0.07
341.0	0.00	0.02	0.00	0.51	0.27
342.0	0.00	0.00	0.00	0.51	0.37
343.0	0.00	0.00	0.00	0.61	0.37
344.0	0.00	0.00	0.00	0.61	0.37
345.0	0.00	0.00	0.00	0.41	0.37
346.0	0.00	0.00	0.00	0.41	0.47
347.0	0.00	0.00	0.00	0.61	0.47
348.0	0.00	0.00	0.00	0.61	0.37
349.0	0.06	0.00	0.00	0.71	0.17
350.0	0.00	0.00	0.00	0.81	0.27

AMC 17 Section 3

y(m) / t(sec)	Concentration (ppb)				
	0.9	1.8	2.7	3.6	4.5
130.0	0.77	0.01	0.09	0.10	0.11
131.0	0.67	0.11	0.09	0.10	0.21
132.0	0.47	0.01	0.00	0.10	0.31
133.0	0.57	0.11	0.00	0.30	0.21
134.0	0.57	0.21	0.00	0.40	0.11
135.0	0.57	0.21	0.09	0.70	0.31
136.0	0.47	0.21	0.09	0.80	0.51
137.0	0.57	0.31	0.00	1.30	0.91
138.0	0.37	0.21	0.00	1.60	1.21
139.0	0.37	0.41	0.19	2.20	1.41
140.0	0.27	0.41	0.59	2.70	1.71
141.0	0.17	0.51	0.99	3.30	2.01
142.0	0.17	0.41	1.29	4.20	2.31
143.0	0.17	0.41	1.59	5.10	2.71
144.0	0.27	0.41	2.19	5.80	3.41
145.0	0.17	0.51	2.69	6.50	3.81
146.0	0.17	0.71	3.39	7.00	4.21
147.0	0.27	0.81	3.79	8.20	4.51
148.0	0.27	0.91	4.09	9.20	4.71
149.0	0.27	1.11	4.49	10.10	5.01
150.0	0.27	1.31	5.39	10.90	5.61
151.0	0.17	1.51	6.09	11.80	6.21
152.0	0.07	1.81	7.09	12.40	6.71
153.0	0.17	2.21	7.99	13.00	7.31
154.0	0.27	2.51	8.69	13.70	7.81
155.0	0.37	2.81	9.49	14.60	8.31
156.0	0.37	3.41	10.29	15.10	8.91
157.0	0.37	3.81	10.99	15.80	9.61
158.0	0.57	4.31	11.59	16.50	10.21
159.0	0.67	4.91	12.29	17.10	10.91
160.0	0.87	5.41	12.99	17.70	11.41
161.0	0.87	5.81	13.79	18.10	11.91
162.0	1.07	6.41	14.49	18.50	12.31
163.0	1.17	7.11	15.09	19.00	12.71
164.0	1.47	7.81	15.59	19.40	12.91
165.0	1.87	8.31	16.19	19.60	13.41
166.0	2.07	8.91	16.59	19.70	13.91
167.0	2.27	9.61	16.89	19.90	14.21
168.0	2.67	10.11	17.29	20.20	14.41
169.0	2.87	10.51	17.69	20.20	14.51
170.0	3.37	11.11	17.89	20.50	14.61
171.0	3.77	11.61	18.19	20.70	14.81
172.0	4.17	12.21	18.59	20.50	14.91
173.0	4.57	12.91	18.79	20.30	15.01
174.0	5.07	13.41	19.09	20.40	15.11
175.0	5.67	14.01	19.19	20.40	15.31
176.0	6.17	14.51	19.19	20.20	15.51
177.0	6.47	14.71	19.19	20.00	15.61
178.0	6.67	15.01	19.19	19.80	15.81
179.0	6.97	15.31	19.19	19.50	15.81
180.0	6.97	15.61	19.09	19.10	15.71
181.0	7.37	16.11	18.99	18.90	15.71
182.0	7.77	16.31	18.99	18.60	15.61
183.0	7.87	16.31	18.79	18.30	15.61
184.0	8.37	16.61	18.69	18.00	15.51
185.0	8.67	16.71	18.39	17.70	15.51
186.0	9.17	17.01	18.29	17.40	15.51

187.0	9.57	16.91	17.99	17.00	15.41
188.0	9.87	17.01	17.69	16.60	15.31
189.0	10.27	17.11	17.39	16.40	15.21
190.0	10.37	16.91	17.19	16.30	15.01
191.0	10.57	17.01	16.89	15.80	14.81
192.0	10.87	17.01	16.79	15.60	14.71
193.0	11.07	17.01	16.59	15.40	14.61
194.0	11.37	17.01	16.49	15.10	14.41
195.0	11.67	16.91	16.29	14.70	14.21
196.0	11.87	16.91	16.19	14.50	14.11
197.0	11.87	16.71	15.89	14.20	14.01
198.0	11.97	16.51	15.59	13.60	13.81
199.0	12.27	16.51	15.19	13.10	13.51
200.0	12.47	16.21	14.89	12.90	13.21
201.0	12.57	16.11	14.59	12.70	12.71
202.0	12.77	15.91	14.19	12.50	12.51
203.0	12.77	15.61	13.89	12.40	12.21
204.0	12.97	15.31	13.69	12.20	12.11
205.0	12.87	15.11	13.29	11.90	11.81
206.0	12.87	14.91	13.09	11.80	11.51
207.0	12.97	14.61	12.59	11.60	11.21
208.0	12.97	14.61	12.39	11.20	10.91
209.0	13.17	14.31	12.19	10.90	10.61
210.0	13.37	14.01	11.89	10.60	10.31
211.0	13.57	14.01	11.49	10.30	10.01
212.0	13.57	13.81	11.29	10.10	9.81
213.0	13.67	13.51	10.99	9.80	9.51
214.0	13.67	13.41	10.89	9.50	9.41
215.0	13.57	13.11	10.49	9.30	9.31
216.0	13.47	12.71	10.29	9.00	9.31
217.0	13.17	12.51	10.09	8.60	9.21
218.0	13.07	12.11	9.79	8.30	9.01
219.0	12.87	11.81	9.39	8.30	8.91
220.0	12.67	11.61	8.99	8.30	8.91
221.0	12.67	11.41	8.69	8.10	8.71
222.0	12.37	11.11	8.29	7.80	8.41
223.0	12.47	10.71	8.19	7.70	8.31
224.0	12.27	10.41	7.99	7.50	8.21
225.0	12.27	10.21	7.89	7.30	7.91
226.0	12.27	10.01	7.59	7.20	7.81
227.0	11.97	10.01	7.49	6.90	7.51
228.0	11.97	9.71	7.39	6.60	7.31
229.0	11.67	9.41	6.99	6.60	7.11
230.0	11.57	9.11	6.79	6.30	6.91
231.0	11.47	9.01	6.49	6.20	6.61
232.0	11.27	8.71	6.29	6.20	6.41
233.0	11.27	8.51	6.09	5.80	6.31
234.0	10.97	8.31	5.89	5.50	6.11
235.0	10.87	8.11	5.49	5.40	6.11
236.0	10.87	7.91	5.39	5.20	5.81
237.0	10.67	7.61	5.19	5.00	5.61
238.0	10.57	7.51	4.89	4.70	5.61
239.0	10.17	7.21	4.79	4.50	5.51
240.0	10.07	7.01	4.69	4.30	5.21
241.0	9.97	6.81	4.59	4.10	5.01
242.0	9.67	6.71	4.49	4.00	4.91
243.0	9.57	6.31	4.39	4.00	4.91
244.0	9.37	6.21	4.09	3.90	4.91
245.0	9.37	6.11	4.09	3.80	4.71
246.0	9.27	5.81	3.99	3.70	4.71
247.0	9.17	5.71	3.79	3.70	4.61
248.0	9.07	5.51	3.69	3.70	4.51

249.0	8.87	5.31	3.79	3.60	4.41
250.0	8.87	5.31	3.59	3.50	4.21
251.0	8.67	5.41	3.39	3.40	4.11
252.0	8.47	5.31	3.49	3.10	4.01
253.0	8.37	5.21	3.29	3.10	3.81
254.0	8.17	5.01	3.19	3.00	3.61
255.0	7.97	4.91	3.19	2.90	3.51
256.0	7.87	4.71	2.89	2.70	3.31
257.0	7.77	4.61	2.89	2.70	3.31
258.0	7.67	4.21	2.89	2.60	3.21
259.0	7.67	4.11	2.79	2.40	3.11
260.0	7.47	3.91	2.79	2.40	3.31
261.0	7.37	3.71	2.79	2.40	3.21
262.0	7.27	3.71	2.79	2.40	3.41
263.0	7.37	3.61	2.89	2.10	3.31
264.0	7.27	3.31	2.69	1.90	3.21
265.0	7.07	3.21	2.49	1.80	3.01
266.0	7.07	3.21	2.19	1.90	2.81
267.0	6.87	3.11	2.09	1.90	2.81
268.0	6.77	3.01	2.09	1.80	2.71
269.0	6.57	2.91	2.19	1.80	2.61
270.0	6.27	2.91	1.99	1.80	2.71
271.0	5.97	2.81	1.89	1.80	2.61
272.0	5.67	2.61	1.89	1.80	2.51
273.0	5.57	2.51	1.89	1.60	2.71
274.0	5.57	2.51	1.89	1.50	2.61
275.0	5.57	2.41	1.69	1.20	2.51
276.0	5.37	2.31	1.69	1.30	2.41
277.0	5.37	2.21	1.59	1.40	2.31
278.0	5.17	2.11	1.69	1.30	2.21
279.0	5.07	2.21	1.59	1.50	2.21
280.0	5.07	2.11	1.79	1.40	2.21
281.0	4.97	1.91	1.69	1.50	2.31
282.0	4.67	1.91	1.59	1.60	2.51
283.0	4.67	2.01	1.79	1.50	2.71
284.0	4.77	1.81	1.69	1.50	2.61
285.0	4.67	1.71	1.59	1.70	2.51
286.0	4.57	1.61	1.59	1.80	2.61
287.0	4.57	1.71	1.69	1.60	2.61
288.0	4.47	1.71	1.59	1.50	2.51
289.0	4.47	1.71	1.59	1.50	2.51
290.0	4.27	1.61	1.29	1.30	2.41
291.0	4.17	1.61	1.19	1.10	2.41
292.0	3.97	1.51	1.09	1.30	2.21
293.0	3.87	1.51	1.09	1.30	2.11
294.0	3.97	1.61	0.99	1.20	2.11
295.0	3.77	1.61	0.89	1.20	2.01
296.0	3.77	1.71	0.79	1.10	2.01
297.0	3.77	1.61	0.69	1.20	1.91
298.0	3.67	1.61	0.59	1.20	1.91
299.0	3.57	1.71	0.59	1.30	1.91
300.0	3.57	1.71	0.69	1.40	1.91
301.0	3.57	1.51	0.69	1.30	1.91
302.0	3.47	1.51	0.69	1.10	1.71
303.0	3.47	1.41	0.69	1.20	1.61
304.0	3.37	1.41	0.69	1.20	1.71
305.0	3.37	1.31	0.59	1.30	1.61
306.0	3.37	1.21	0.69	1.20	1.71
307.0	3.27	1.21	0.79	1.00	1.71
308.0	3.17	1.21	0.79	1.00	1.61
309.0	2.97	1.21	0.79	1.00	1.41
310.0	2.97	1.21	0.79	1.00	1.31

311.0	2.87	1.21	0.69	1.10	1.21
312.0	2.77	1.11	0.59	1.00	1.21
313.0	2.67	1.01	0.59	1.00	1.21
314.0	2.57	0.91	0.49	1.10	1.21
315.0	2.47	0.91	0.49	1.10	1.41
316.0	2.57	0.81	0.49	1.00	1.31
317.0	2.47	0.81	0.49	1.00	1.41
318.0	2.57	0.71	0.49	0.90	1.31
319.0	2.27	0.81	0.39	0.90	1.21
320.0	2.17	0.71	0.29	0.70	1.11
321.0	1.97	0.71	0.39	0.60	1.11
322.0	2.07	0.81	0.29	0.50	1.01
323.0	1.97	0.71	0.39	0.40	0.91
324.0	1.87	0.71	0.39	0.30	1.01
325.0	1.77	0.81	0.39	0.30	1.11
326.0	1.87	0.61	0.39	0.20	1.11
327.0	1.77	0.61	0.29	0.20	1.21
328.0	1.67	0.61	0.29	0.20	1.21
329.0	1.47	0.61	0.29	0.20	1.01
330.0	1.37	0.61	0.29	0.20	1.01
331.0	1.37	0.61	0.29	0.20	0.81
332.0	1.47	0.71	0.29	0.20	0.71
333.0	1.47	0.61	0.19	0.10	0.71
334.0	1.37	0.61	0.19	0.00	0.61
335.0	1.37	0.51	0.29	0.00	0.71
336.0	1.37	0.51	0.29	0.00	0.71
337.0	1.47	0.61	0.19	0.00	0.71
338.0	1.67	0.71	0.29	0.00	0.71
339.0	1.47	0.71	0.29	0.00	0.51
340.0	1.37	0.51	0.19	0.00	0.51
341.0	1.37	0.51	0.19	0.00	0.61
342.0	1.37	0.51	0.19	0.00	0.51
343.0	1.47	0.51	0.19	0.00	0.61
344.0	1.27	0.51	0.09	0.00	0.61
345.0	1.27	0.51	0.09	0.00	0.71
346.0	1.37	0.61	0.29	0.00	0.71
347.0	1.57	0.51	0.19	0.00	0.71
348.0	1.67	0.61	0.09	0.00	0.71
349.0	1.57	0.51	0.19	0.00	0.61
350.0	1.47	0.61	0.29	0.00	0.71
351.0	1.37	0.71	0.29	0.00	0.61
352.0	1.37	0.61	0.19	0.00	0.61
353.0	1.47	0.61	0.19	0.00	0.51
354.0	1.47	0.61	0.19	0.10	0.51
355.0	1.37	0.61	0.09	0.30	0.51
356.0	1.47	0.51	0.19	0.40	0.51
357.0	1.27	0.51	0.09	0.30	0.51
358.0	1.37	0.21	0.09	0.30	0.51
359.0	1.27	0.41	0.09	0.10	0.31
360.0	1.27	0.21	0.09	0.00	0.31
361.0	1.07	0.31	0.00	0.00	0.41
362.0	0.97	0.31	0.09	0.10	0.41
363.0	0.97	0.41	0.19	0.00	0.41
364.0	0.97	0.31	0.09	0.00	0.51
365.0	1.27	0.21	0.00	0.00	0.51
366.0	1.37	0.31	0.00	0.10	0.41
367.0	1.27	0.31	0.00	0.00	0.31
368.0	1.27	0.31	0.00	0.00	0.11
369.0	1.27	0.31	0.00	0.00	0.01
370.0	1.17	0.41	0.00	0.00	0.01
371.0	1.07	0.41	0.00	0.00	0.11
372.0	1.07	0.31	0.00	0.10	0.11

373.0	0.97	0.31	0.00	0.20	0.11
374.0	1.07	0.31	0.00	0.10	0.21
375.0	0.87	0.31	0.09	0.00	0.21
376.0	1.17	0.41	0.09	0.10	0.21
377.0	0.97	0.41	0.00	0.10	0.21
378.0	0.87	0.51	0.09	0.20	0.21
379.0	0.77	0.51	0.09	0.10	0.01
380.0	0.87	0.41	0.00	0.20	0.01
381.0	0.77	0.21	0.00	0.10	0.01
382.0	0.97	0.31	0.00	0.00	0.01
383.0	0.97	0.31	0.00	0.00	0.11
384.0	0.87	0.21	0.00	0.10	0.01
385.0	1.07	0.21	0.00	0.10	0.21
386.0	1.07	0.31	0.00	0.00	0.21
387.0	1.17	0.00	0.00	0.10	0.11
388.0	1.07	0.01	0.00	0.10	0.11
389.0	1.07	0.01	0.00	0.20	0.11
390.0	0.87	0.11	0.00	0.30	0.00
391.0	0.87	0.11	0.00	0.40	0.00
392.0	0.97	0.01	0.09	0.50	0.00
393.0	0.97	0.11	0.09	0.50	0.00
394.0	0.87	0.01	0.09	0.50	0.01
395.0	0.57	0.01	0.19	0.30	0.01
396.0	0.57	0.00	0.19	0.20	0.11
397.0	0.57	0.00	0.09	0.20	0.01
398.0	0.77	0.00	0.00	0.10	0.11
399.0	0.67	0.01	0.00	0.30	0.01
400.0	0.57	0.11	0.00	0.10	0.01

AMC 17 Section 4

y(m) / t(sec)	Concentration (ppb)				
	1.0	2.0	3.0	4.0	5.0
150.0	0.00	0.00	0.04	0.18	0.17
151.0	0.00	0.00	0.00	0.18	0.00
152.0	0.00	0.00	0.00	0.08	0.17
153.0	0.06	0.00	0.00	0.08	0.27
154.0	0.16	0.00	0.00	0.18	0.47
155.0	0.00	0.00	0.04	0.00	0.57
156.0	0.06	0.00	0.00	0.08	0.57
157.0	0.16	0.00	0.04	0.18	0.77
158.0	0.06	0.00	0.14	0.08	0.67
159.0	0.00	0.00	0.14	0.18	0.67
160.0	0.00	0.00	0.24	0.28	0.67
161.0	0.00	0.00	0.34	0.38	0.77
162.0	0.00	0.00	0.54	0.48	0.47
163.0	0.00	0.00	0.64	0.38	0.67
164.0	0.00	0.00	0.84	0.38	0.47
165.0	0.06	0.00	0.74	0.58	0.47
166.0	0.06	0.00	0.84	0.88	0.37
167.0	0.26	0.00	0.94	0.98	0.37
168.0	0.16	0.00	0.94	0.98	0.27
169.0	0.26	0.00	1.14	1.28	0.37
170.0	0.16	0.01	1.54	1.58	0.47
171.0	0.36	0.11	1.84	1.68	0.37
172.0	0.36	0.41	2.04	1.88	0.47
173.0	0.46	1.01	2.04	2.28	0.27
174.0	0.36	1.41	2.44	2.58	0.37
175.0	0.56	1.71	3.04	3.18	0.47
176.0	0.56	1.71	3.74	3.48	0.47
177.0	0.56	1.81	3.94	3.78	0.47
178.0	0.66	2.01	4.14	4.28	0.47
179.0	0.56	2.01	4.64	4.58	0.67
180.0	0.76	2.01	5.14	4.88	0.77
181.0	0.86	1.91	5.54	5.88	0.97
182.0	0.96	2.21	5.94	6.18	1.07
183.0	0.96	2.71	6.34	6.68	1.27
184.0	0.96	3.11	7.14	7.18	1.37
185.0	1.06	3.31	7.94	7.48	1.37
186.0	0.96	3.21	8.34	7.68	1.57
187.0	1.06	3.31	8.54	8.08	1.67
188.0	1.16	3.51	8.64	8.58	1.97
189.0	1.26	3.81	9.14	9.18	2.27
190.0	1.36	4.21	9.54	9.48	2.57
191.0	1.36	4.81	9.74	9.78	3.07
192.0	1.66	5.11	10.34	10.18	3.17
193.0	1.86	5.31	10.64	10.68	3.37
194.0	2.16	5.41	10.84	11.08	3.67
195.0	2.46	6.21	11.14	11.38	4.17
196.0	2.56	6.81	11.54	11.68	4.47
197.0	2.66	7.31	11.74	12.08	4.67
198.0	2.56	7.71	12.14	12.28	4.87
199.0	2.36	8.11	12.34	12.38	5.07
200.0	2.36	8.61	12.64	12.58	5.37
201.0	2.66	9.11	12.94	12.58	5.57
202.0	2.96	9.61	13.04	12.78	5.87
203.0	3.26	10.11	13.24	13.08	6.37
204.0	3.66	10.61	13.34	13.38	6.87

205.0	4.06	11.21	13.44	13.38	7.27
206.0	4.16	11.71	13.64	13.48	7.67
207.0	4.36	11.81	13.74	13.68	8.07
208.0	4.36	12.01	13.84	13.98	8.47
209.0	4.66	12.11	14.04	13.98	8.87
210.0	4.76	12.11	14.14	14.08	9.07
211.0	4.86	12.41	14.14	14.08	9.37
212.0	5.16	12.51	14.14	14.18	9.67
213.0	5.86	12.51	14.14	14.28	9.77
214.0	6.26	12.61	14.04	14.18	9.77
215.0	6.36	12.71	14.04	14.28	10.07
216.0	6.56	12.91	13.94	14.08	10.27
217.0	6.86	13.11	13.84	14.28	10.67
218.0	7.46	13.01	13.84	14.18	10.87
219.0	7.86	12.91	13.64	14.08	11.27
220.0	8.26	12.91	13.44	14.08	11.57
221.0	8.76	13.01	13.34	13.78	11.77
222.0	9.36	12.71	13.24	13.78	11.97
223.0	9.66	12.71	13.14	13.68	12.17
224.0	10.06	12.51	13.24	13.58	12.37
225.0	10.56	12.51	13.24	13.58	12.57
226.0	10.76	12.41	13.04	13.58	12.57
227.0	10.86	12.41	13.04	13.38	12.87
228.0	11.16	12.31	12.94	13.48	12.87
229.0	11.36	12.41	12.74	13.38	12.97
230.0	11.66	12.41	12.64	13.08	13.07
231.0	11.86	12.51	12.54	12.88	13.17
232.0	11.86	12.41	12.34	12.78	13.27
233.0	12.16	12.41	12.14	12.88	13.27
234.0	12.16	12.41	12.14	12.58	13.47
235.0	12.16	12.31	11.94	12.58	13.47
236.0	12.26	12.21	11.74	12.58	13.57
237.0	12.26	12.11	11.64	12.38	13.57
238.0	12.26	11.91	11.54	12.18	13.47
239.0	12.16	11.61	11.54	11.98	13.37
240.0	12.36	11.21	11.34	11.78	13.37
241.0	12.26	10.91	11.24	11.58	13.27
242.0	12.06	10.71	11.14	11.68	13.07
243.0	12.16	10.61	11.04	11.58	13.07
244.0	11.96	10.51	10.84	11.28	12.87
245.0	11.76	10.51	10.64	10.98	12.77
246.0	11.76	10.41	10.44	10.78	12.67
247.0	11.66	10.51	10.14	10.68	12.47
248.0	11.56	10.61	10.04	10.58	12.27
249.0	11.56	10.41	9.84	10.38	12.27
250.0	11.36	10.11	9.64	10.08	12.27
251.0	11.36	10.01	9.54	9.98	11.97
252.0	11.16	10.01	9.44	9.68	11.77
253.0	10.96	9.91	9.54	9.18	11.57
254.0	10.66	9.71	9.54	8.98	11.37
255.0	10.46	9.61	9.34	8.98	11.27
256.0	10.26	9.61	9.24	8.68	11.07
257.0	10.26	9.41	9.14	8.58	10.77
258.0	10.26	9.51	8.94	8.28	10.67
259.0	9.96	9.31	8.74	8.28	10.57
260.0	9.86	9.11	8.84	8.18	10.47
261.0	9.46	8.91	8.74	8.08	10.37
262.0	9.36	8.81	8.54	8.08	10.27
263.0	9.06	8.91	8.44	8.28	10.17
264.0	9.16	8.71	8.54	8.18	9.97
265.0	9.16	8.51	8.24	7.98	9.77
266.0	9.16	8.31	8.04	7.88	9.77

267.0	9.16	8.11	7.74	7.68	9.57
268.0	9.16	7.91	7.64	7.68	9.57
269.0	8.96	7.71	7.44	7.58	9.57
270.0	8.56	7.61	7.34	7.48	9.47
271.0	8.16	7.41	7.34	7.28	9.37
272.0	8.06	7.21	7.14	7.18	9.17
273.0	7.86	6.91	6.94	6.98	8.97
274.0	7.86	6.81	6.84	6.88	9.07
275.0	7.56	6.71	6.74	6.58	8.97
276.0	7.36	6.51	6.64	6.58	8.87
277.0	7.36	6.51	6.44	6.68	8.67
278.0	7.36	6.51	6.34	6.68	8.27
279.0	7.06	6.21	6.34	6.38	8.07
280.0	6.96	6.21	6.24	6.48	7.87
281.0	6.66	6.11	6.04	6.18	7.87
282.0	6.76	6.11	5.94	6.08	7.77
283.0	6.46	5.81	5.84	5.98	7.57
284.0	6.56	5.61	5.64	5.98	7.47
285.0	6.66	5.41	5.54	5.78	7.17
286.0	6.66	5.11	5.64	5.58	6.77
287.0	6.56	5.11	5.54	5.38	6.57
288.0	6.46	4.91	5.44	5.18	6.57
289.0	6.36	4.61	5.14	5.08	6.57
290.0	6.16	4.51	5.14	5.08	6.37
291.0	5.96	4.61	4.94	4.88	6.17
292.0	5.76	4.61	4.94	4.68	5.97
293.0	5.96	4.51	4.84	4.48	5.77
294.0	6.06	4.41	4.94	4.28	5.67
295.0	5.76	4.31	4.84	4.08	5.77
296.0	5.76	4.21	4.84	4.18	5.57
297.0	5.76	4.31	4.74	4.08	5.57
298.0	5.76	4.41	4.34	3.98	5.47
299.0	5.76	4.41	4.24	3.88	5.27
300.0	5.66	4.41	4.24	3.78	5.07
301.0	5.66	4.21	4.14	3.68	5.07
302.0	5.56	4.01	3.94	3.68	4.97
303.0	5.56	3.81	3.84	3.58	5.07
304.0	5.46	3.81	3.74	3.48	4.87
305.0	5.46	3.81	3.54	3.38	4.77
306.0	5.36	3.61	3.24	3.28	4.57
307.0	5.26	3.51	3.04	3.18	4.47
308.0	5.06	3.31	3.14	2.98	4.47
309.0	4.96	3.21	3.14	2.88	4.27
310.0	4.86	3.01	3.04	2.68	4.07
311.0	4.66	2.91	2.84	2.58	3.77
312.0	4.86	2.71	2.84	2.48	3.67
313.0	4.86	2.71	2.74	2.38	3.67
314.0	4.76	2.71	2.54	2.28	3.57
315.0	4.76	2.71	2.54	2.28	3.47
316.0	4.76	2.61	2.54	2.18	3.47
317.0	4.76	2.51	2.44	2.18	3.27
318.0	4.76	2.41	2.24	2.18	3.27
319.0	4.66	2.31	2.34	2.08	3.17
320.0	4.56	2.31	2.34	2.08	3.27
321.0	4.46	2.21	2.34	2.08	3.17
322.0	4.46	2.01	2.24	2.08	3.37
323.0	4.46	2.01	2.24	2.18	3.37
324.0	4.36	2.01	2.14	2.28	3.37
325.0	3.96	2.01	2.24	2.38	3.27
326.0	3.96	1.91	2.14	2.28	3.27
327.0	3.86	1.91	2.14	2.28	3.27
328.0	3.76	1.81	2.14	2.08	3.27

329.0	3.76	1.71	2.24	1.98	2.97
330.0	3.66	1.71	2.24	2.08	2.87
331.0	3.86	1.81	2.04	1.98	2.57
332.0	3.66	1.91	1.94	1.88	2.47
333.0	3.76	1.91	1.94	1.78	2.67
334.0	3.66	1.91	1.84	1.68	2.67
335.0	3.36	1.91	1.84	1.78	2.67
336.0	3.16	1.71	1.84	1.88	2.47
337.0	3.16	1.71	1.94	1.68	2.67
338.0	2.96	1.61	1.94	1.48	2.67
339.0	2.76	1.61	1.84	1.48	2.67
340.0	2.86	1.51	1.84	1.48	2.47
341.0	2.66	1.41	1.74	1.48	2.37
342.0	2.46	1.51	1.64	1.48	2.27
343.0	2.46	1.51	1.64	1.38	2.07
344.0	2.46	1.61	1.64	1.28	2.17
345.0	2.16	1.41	1.74	1.48	2.07
346.0	2.06	1.31	1.74	1.48	2.07
347.0	1.96	1.41	1.54	1.38	1.97
348.0	2.16	1.41	1.54	1.58	2.17
349.0	2.16	1.31	1.34	1.58	1.97
350.0	2.36	1.41	1.34	1.38	1.87
351.0	2.46	1.41	1.34	1.28	1.87
352.0	2.36	1.31	1.44	1.38	1.77
353.0	2.36	1.11	1.64	1.28	1.87
354.0	2.26	1.11	1.54	1.18	1.87
355.0	2.06	1.11	1.44	1.08	1.97
356.0	1.96	1.21	1.34	1.08	1.97
357.0	2.06	1.01	1.34	1.08	1.77
358.0	2.06	1.01	1.14	1.08	1.77
359.0	2.16	0.91	1.14	1.08	1.67
360.0	2.06	0.71	1.14	1.08	1.57
361.0	2.16	0.61	1.14	1.08	1.47
362.0	2.06	0.61	1.24	1.08	1.27
363.0	2.06	0.71	1.34	0.88	1.17
364.0	2.06	0.61	1.34	0.78	1.17
365.0	2.06	0.81	1.34	0.78	1.07
366.0	2.26	0.81	1.34	0.78	0.97
367.0	2.16	0.91	1.24	0.58	0.97
368.0	2.06	1.01	1.14	0.38	1.07
369.0	2.16	1.01	1.04	0.38	1.07
370.0	1.96	1.11	1.04	0.28	1.07
371.0	1.96	1.01	0.94	0.48	1.07
372.0	1.76	0.81	0.74	0.58	0.97
373.0	1.86	0.81	0.74	0.48	0.97
374.0	1.86	0.71	0.84	0.48	1.07
375.0	1.66	0.61	0.64	0.48	1.17
376.0	1.76	0.51	0.64	0.48	1.27
377.0	1.96	0.61	0.54	0.48	1.37
378.0	1.76	0.71	0.44	0.48	1.17
379.0	1.66	0.71	0.54	0.58	1.27
380.0	1.66	0.71	0.44	0.68	1.27
381.0	1.76	0.81	0.34	0.58	1.17
382.0	1.76	0.81	0.24	0.48	1.17
383.0	1.76	0.81	0.34	0.48	0.87
384.0	1.76	0.81	0.14	0.58	0.87
385.0	1.76	0.71	0.14	0.48	0.97
386.0	1.86	0.71	0.24	0.58	1.07
387.0	1.86	0.71	0.34	0.68	1.17
388.0	1.76	0.71	0.34	0.58	1.07
389.0	1.76	0.91	0.34	0.58	1.17
390.0	1.66	0.81	0.24	0.48	1.07

391.0	1.56	0.41	0.34	0.48	1.07
392.0	1.46	0.41	0.34	0.58	0.97
393.0	1.66	0.51	0.54	0.48	0.87
394.0	1.56	0.41	0.54	0.48	0.87
395.0	1.46	0.41	0.64	0.58	0.97
396.0	1.36	0.41	0.74	0.58	0.87
397.0	1.26	0.41	0.64	0.48	0.77
398.0	1.36	0.51	0.74	0.58	0.67
399.0	1.26	0.41	0.74	0.58	0.67
400.0	1.06	0.41	0.74	0.48	0.67
401.0	1.06	0.41	0.74	0.48	0.77
402.0	1.16	0.41	0.64	0.28	0.77
403.0	1.06	0.41	0.64	0.28	0.77
404.0	1.06	0.31	0.64	0.38	0.67
405.0	0.96	0.21	0.64	0.38	0.67
406.0	0.86	0.21	0.64	0.38	0.57
407.0	0.96	0.11	0.54	0.48	0.57
408.0	0.96	0.21	0.64	0.38	0.47
409.0	0.96	0.11	0.64	0.58	0.47
410.0	0.96	0.01	0.54	0.38	0.57
411.0	1.06	0.01	0.54	0.48	0.47
412.0	1.16	0.11	0.74	0.38	0.57
413.0	1.16	0.11	0.74	0.38	0.57
414.0	1.16	0.11	0.74	0.48	0.57
415.0	1.16	0.21	0.64	0.38	0.47
416.0	1.06	0.01	0.64	0.38	0.57
417.0	1.16	0.01	0.74	0.48	0.47
418.0	1.16	0.00	0.64	0.48	0.57
419.0	1.06	0.01	0.74	0.48	0.57
420.0	1.06	0.00	0.84	0.48	0.57
421.0	0.96	0.00	0.74	0.48	0.47
422.0	1.16	0.00	0.74	0.38	0.37
423.0	1.16	0.00	0.64	0.48	0.37
424.0	1.06	0.00	0.64	0.28	0.37
425.0	0.96	0.00	0.64	0.18	0.37
426.0	0.96	0.00	0.54	0.08	0.17
427.0	0.96	0.00	0.44	0.08	0.17
428.0	0.96	0.00	0.24	0.18	0.27
429.0	1.06	0.00	0.34	0.08	0.37
430.0	0.96	0.00	0.44	0.00	0.47
431.0	0.96	0.11	0.64	0.08	0.47
432.0	0.86	0.11	0.74	0.08	0.47
433.0	0.66	0.21	0.64	0.00	0.47
434.0	0.66	0.21	0.74	0.08	0.47
435.0	0.86	0.21	0.64	0.00	0.57
436.0	0.76	0.41	0.64	0.00	0.37
437.0	0.76	0.51	0.74	0.08	0.37
438.0	0.76	0.41	0.74	0.08	0.37
439.0	0.66	0.21	0.74	0.00	0.47
440.0	0.76	0.31	0.74	0.00	0.37
441.0	0.56	0.31	0.74	0.00	0.57
442.0	0.76	0.31	0.64	0.00	0.57
443.0	0.56	0.31	0.64	0.08	0.47
444.0	0.66	0.31	0.54	0.28	0.47
445.0	0.76	0.21	0.74	0.28	0.47
446.0	0.76	0.01	0.74	0.08	0.57
447.0	0.66	0.01	0.64	0.00	0.57
448.0	0.56	0.01	0.74	0.00	0.47
449.0	0.56	0.00	0.54	0.00	0.47
450.0	0.56	0.00	0.54	0.00	0.57

AMC 17 Section 5

y(m) / t(sec)	Concentration (ppb)				
	0.9	1.8	2.7	3.6	4.5
190.0	0.00	0.09	0.28	0.00	0.18
191.0	0.00	0.09	0.28	0.08	0.08
192.0	0.00	0.09	0.28	0.00	0.00
193.0	0.00	0.09	0.28	0.18	0.00
194.0	0.09	0.19	0.28	0.18	0.00
195.0	0.09	0.19	0.18	0.08	0.08
196.0	0.19	0.29	0.28	0.08	0.08
197.0	0.29	0.29	0.18	0.00	0.00
198.0	0.39	0.29	0.28	0.08	0.00
199.0	0.29	0.39	0.08	0.08	0.00
200.0	0.39	0.39	0.08	0.18	0.00
201.0	0.49	0.49	0.08	0.08	0.00
202.0	0.59	0.69	0.18	0.18	0.18
203.0	0.59	0.69	0.18	0.28	0.18
204.0	0.49	0.59	0.38	0.38	0.08
205.0	0.49	0.79	0.58	0.38	0.00
206.0	0.59	0.89	0.58	0.48	0.08
207.0	0.69	1.09	0.68	0.58	0.08
208.0	0.89	1.29	0.88	0.68	0.08
209.0	0.99	1.39	1.18	0.58	0.00
210.0	1.09	1.49	1.38	0.68	0.00
211.0	1.09	1.69	1.48	0.88	0.00
212.0	1.29	1.99	1.48	0.78	0.00
213.0	1.29	2.19	1.68	0.78	0.08
214.0	1.39	2.59	1.88	0.88	0.08
215.0	1.49	2.99	2.18	0.88	0.18
216.0	1.69	3.29	2.38	0.98	0.28
217.0	1.89	3.59	2.68	1.08	0.08
218.0	2.09	3.79	2.88	1.18	0.18
219.0	2.19	4.19	3.08	1.38	0.18
220.0	2.29	4.49	3.28	1.48	0.18
221.0	2.69	4.79	3.48	1.48	0.18
222.0	2.99	4.99	3.58	1.68	0.08
223.0	3.19	5.19	3.78	1.78	0.18
224.0	3.49	5.69	4.08	2.08	0.28
225.0	3.89	5.99	4.28	2.38	0.48
226.0	4.19	6.29	4.68	2.38	0.58
227.0	4.59	6.59	4.88	2.58	0.68
228.0	4.89	6.79	5.18	2.78	0.78
229.0	5.09	7.09	5.38	3.08	1.08
230.0	5.39	7.59	5.68	3.28	1.08
231.0	5.69	7.99	6.08	3.58	1.28
232.0	6.09	8.19	6.38	3.88	1.28
233.0	6.29	8.49	6.68	4.08	1.38
234.0	6.49	8.69	6.88	4.38	1.58
235.0	6.89	8.99	7.08	4.68	1.78
236.0	7.09	9.19	7.38	4.98	1.98
237.0	7.49	9.49	7.68	5.28	1.98
238.0	7.69	9.69	7.98	5.68	2.18
239.0	7.89	9.79	8.28	5.98	2.38
240.0	8.09	9.89	8.38	6.38	2.58
241.0	8.49	10.09	8.68	6.58	2.98
242.0	8.69	10.49	8.98	6.98	3.18
243.0	8.79	10.69	9.28	7.38	3.38
244.0	8.99	10.89	9.58	7.78	3.68

245.0	9.19	11.09	9.88	8.08	3.78
246.0	9.29	11.29	9.98	8.38	3.98
247.0	9.49	11.49	10.28	8.68	4.38
248.0	9.59	11.49	10.48	8.78	4.78
249.0	9.89	11.69	10.78	8.98	4.78
250.0	9.99	11.89	10.88	9.28	5.08
251.0	10.09	11.99	11.08	9.48	5.28
252.0	10.29	12.19	11.28	9.78	5.38
253.0	10.39	12.19	11.48	9.98	5.38
254.0	10.59	12.39	11.68	10.28	5.58
255.0	10.69	12.39	11.78	10.48	5.78
256.0	10.79	12.49	11.88	10.68	6.08
257.0	10.89	12.59	11.98	10.98	6.28
258.0	10.79	12.59	12.08	11.08	6.38
259.0	10.79	12.59	12.18	11.08	6.58
260.0	10.79	12.69	12.18	11.38	6.78
261.0	10.79	12.69	12.38	11.68	6.78
262.0	10.79	12.69	12.38	11.68	7.08
263.0	10.79	12.69	12.48	11.88	7.28
264.0	10.79	12.69	12.48	11.98	7.68
265.0	10.79	12.59	12.48	12.08	7.88
266.0	10.89	12.49	12.38	12.08	8.08
267.0	10.79	12.49	12.38	12.28	8.28
268.0	10.89	12.49	12.38	12.38	8.38
269.0	10.89	12.39	12.38	12.38	8.48
270.0	10.79	12.39	12.48	12.48	8.58
271.0	10.79	12.19	12.48	12.58	8.78
272.0	10.79	12.09	12.18	12.58	8.98
273.0	10.79	12.09	12.18	12.58	9.28
274.0	10.79	11.99	12.18	12.68	9.38
275.0	10.69	11.99	12.08	12.68	9.68
276.0	10.59	11.89	12.08	12.78	9.68
277.0	10.49	11.69	11.88	12.78	9.98
278.0	10.39	11.59	11.78	12.78	10.28
279.0	10.39	11.39	11.68	12.68	10.38
280.0	10.29	11.19	11.58	12.68	10.48
281.0	10.09	11.09	11.58	12.58	10.38
282.0	10.09	10.99	11.58	12.68	10.48
283.0	9.99	10.89	11.38	12.68	10.48
284.0	9.99	10.89	11.38	12.68	10.68
285.0	9.89	10.79	11.18	12.58	10.78
286.0	9.69	10.69	11.08	12.48	10.78
287.0	9.69	10.49	11.08	12.28	10.98
288.0	9.59	10.29	10.98	12.28	11.08
289.0	9.49	9.99	10.88	12.18	11.08
290.0	9.39	9.99	10.68	12.08	10.98
291.0	9.39	9.99	10.58	11.88	10.88
292.0	9.19	9.99	10.48	11.68	10.88
293.0	9.19	9.89	10.38	11.78	10.98
294.0	9.19	9.69	10.08	11.68	10.88
295.0	9.09	9.59	9.88	11.58	10.78
296.0	8.99	9.49	9.78	11.48	10.68
297.0	8.89	9.29	9.58	11.38	10.58
298.0	8.79	9.29	9.38	11.18	10.58
299.0	8.69	9.19	9.48	10.98	10.38
300.0	8.59	9.09	9.38	10.88	10.48
301.0	8.39	8.99	9.38	10.58	10.38
302.0	8.29	8.89	9.28	10.48	10.38
303.0	8.19	8.79	9.08	10.38	10.28
304.0	8.09	8.69	8.88	10.18	10.28
305.0	7.99	8.59	8.78	10.08	10.28
306.0	7.69	8.39	8.78	9.98	10.18

307.0	7.59	8.29	8.58	9.88	10.18
308.0	7.39	8.09	8.48	9.68	10.08
309.0	7.29	8.09	8.38	9.48	10.08
310.0	7.29	7.99	8.28	9.48	9.98
311.0	7.09	7.89	7.98	9.38	9.98
312.0	6.99	7.89	7.88	9.28	9.98
313.0	6.89	7.69	7.68	9.08	9.98
314.0	6.79	7.59	7.58	9.08	9.88
315.0	6.69	7.29	7.48	8.98	9.78
316.0	6.69	7.19	7.48	8.88	9.68
317.0	6.49	6.99	7.28	8.68	9.58
318.0	6.39	6.99	7.38	8.68	9.48
319.0	6.29	6.89	7.18	8.38	9.48
320.0	6.29	6.99	6.98	8.28	9.38
321.0	6.29	6.99	6.88	8.18	9.28
322.0	6.19	6.89	6.78	7.88	9.18
323.0	6.09	6.59	6.48	7.68	9.18
324.0	6.09	6.59	6.38	7.48	8.98
325.0	5.99	6.49	6.28	7.28	8.88
326.0	5.99	6.19	6.08	7.18	8.68
327.0	5.89	6.09	6.18	7.08	8.58
328.0	5.79	5.89	5.98	6.98	8.48
329.0	5.69	5.89	5.88	6.78	8.28
330.0	5.49	5.89	5.78	6.68	8.18
331.0	5.39	5.79	5.68	6.58	8.08
332.0	5.29	5.79	5.48	6.58	7.78
333.0	5.09	5.59	5.38	6.28	7.68
334.0	4.89	5.49	5.18	6.08	7.48
335.0	4.89	5.39	4.98	5.98	7.48
336.0	4.79	5.39	4.78	5.98	7.48
337.0	4.69	5.29	4.58	5.88	7.48
338.0	4.59	5.19	4.58	5.68	7.38
339.0	4.59	5.09	4.58	5.58	7.28
340.0	4.49	4.79	4.48	5.48	7.08
341.0	4.39	4.69	4.38	5.58	6.98
342.0	4.39	4.49	4.38	5.48	6.78
343.0	4.29	4.49	4.18	5.38	6.78
344.0	4.19	4.49	4.18	5.28	6.68
345.0	3.99	4.29	3.98	5.28	6.68
346.0	3.99	4.19	3.88	5.28	6.58
347.0	3.89	4.09	3.98	5.18	6.48
348.0	3.79	4.09	3.88	5.18	6.38
349.0	3.69	3.99	3.88	5.08	6.38
350.0	3.59	4.09	3.68	4.88	6.28
351.0	3.59	3.79	3.58	4.58	6.18
352.0	3.69	3.69	3.48	4.58	6.08
353.0	3.59	3.69	3.48	4.48	5.98
354.0	3.59	3.59	3.58	4.48	5.88
355.0	3.49	3.49	3.68	4.38	5.78
356.0	3.49	3.39	3.68	4.08	5.58
357.0	3.39	3.39	3.58	4.08	5.58
358.0	3.29	3.39	3.58	3.98	5.48
359.0	3.19	3.39	3.48	3.88	5.48
360.0	3.09	3.29	3.48	3.88	5.28
361.0	3.09	3.09	3.28	3.88	5.28
362.0	2.99	3.19	3.28	3.68	5.18
363.0	2.99	3.09	3.18	3.78	5.08
364.0	2.99	3.09	3.08	3.68	4.98
365.0	2.89	3.09	3.08	3.58	4.88
366.0	2.79	2.99	3.08	3.38	4.88
367.0	2.69	3.09	2.98	3.28	4.78
368.0	2.49	2.99	2.98	3.18	4.68

369.0	2.39	2.99	3.08	3.18	4.78
370.0	2.39	2.79	2.88	2.98	4.78
371.0	2.49	2.69	2.98	2.98	4.68
372.0	2.49	2.69	2.88	2.98	4.58
373.0	2.39	2.69	2.78	2.78	4.48
374.0	2.29	2.69	2.78	2.78	4.38
375.0	2.19	2.69	2.68	2.68	4.38
376.0	2.29	2.69	2.68	2.78	4.18
377.0	2.29	2.69	2.68	2.68	4.28
378.0	2.29	2.69	2.48	2.48	3.98
379.0	2.29	2.39	2.38	2.48	3.78
380.0	2.09	2.39	2.38	2.48	3.78
381.0	2.19	2.29	2.28	2.38	3.78
382.0	2.09	2.19	2.18	2.38	3.58
383.0	1.99	2.19	2.08	2.38	3.48
384.0	1.89	2.09	2.18	2.38	3.48
385.0	1.79	1.99	2.18	2.38	3.48
386.0	1.69	1.89	1.98	2.28	3.38
387.0	1.69	1.79	1.88	2.28	3.28
388.0	1.59	1.79	1.88	2.18	3.28
389.0	1.49	1.69	1.78	2.18	3.08
390.0	1.39	1.69	1.68	2.08	3.18
391.0	1.49	1.69	1.78	2.08	2.98
392.0	1.39	1.79	1.78	1.98	2.98
393.0	1.39	1.79	1.78	1.88	2.98
394.0	1.29	1.79	1.58	1.98	2.98
395.0	1.19	1.79	1.58	1.88	2.88
396.0	1.29	1.69	1.68	1.78	2.88
397.0	1.39	1.49	1.68	1.78	2.88
398.0	1.39	1.49	1.58	1.78	2.88
399.0	1.39	1.49	1.48	1.78	2.78
400.0	1.39	1.49	1.58	1.78	2.88
401.0	1.39	1.49	1.38	1.78	2.78
402.0	1.39	1.49	1.38	1.88	2.68
403.0	1.39	1.39	1.28	1.88	2.58
404.0	1.39	1.39	1.08	1.98	2.58
405.0	1.39	1.39	1.18	1.98	2.48
406.0	1.39	1.39	1.08	1.88	2.48
407.0	1.29	1.49	1.18	1.88	2.58
408.0	1.39	1.49	1.28	1.78	2.48
409.0	1.29	1.39	1.28	1.68	2.58
410.0	1.29	1.59	1.08	1.58	2.58
411.0	1.29	1.59	1.28	1.48	2.58
412.0	1.29	1.39	1.28	1.48	2.58
413.0	1.39	1.29	1.38	1.38	2.48
414.0	1.39	1.29	1.38	1.38	2.48
415.0	1.29	1.29	1.28	1.28	2.48
416.0	1.29	1.39	1.18	1.38	2.28
417.0	1.19	1.39	1.18	1.38	2.28
418.0	1.19	1.39	1.18	1.38	2.18
419.0	1.19	1.29	1.18	1.28	2.18
420.0	1.19	1.49	1.08	1.18	2.18
421.0	1.19	1.39	1.08	1.38	2.08
422.0	1.09	1.29	0.98	1.38	2.08
423.0	1.09	1.29	1.08	1.38	2.08
424.0	0.99	1.19	0.98	1.28	2.08
425.0	1.09	1.09	0.88	1.28	1.98
426.0	0.89	0.99	0.88	1.28	1.88
427.0	0.89	1.09	0.88	1.38	1.88
428.0	0.89	0.99	0.88	1.38	1.98
429.0	0.99	0.99	0.88	1.38	1.88
430.0	0.89	0.89	0.88	1.48	1.68

431.0	0.89	0.99	0.78	1.38	1.48
432.0	0.99	0.99	0.78	1.28	1.48
433.0	0.79	1.09	0.78	1.08	1.28
434.0	0.79	1.09	0.78	1.08	1.28
435.0	0.69	0.99	0.78	0.98	1.28
436.0	0.69	1.09	0.68	0.98	1.18
437.0	0.69	0.99	0.68	0.98	1.28
438.0	0.59	0.89	0.68	0.98	1.38
439.0	0.69	0.89	0.58	1.08	1.38
440.0	0.69	0.99	0.58	0.98	1.28
441.0	0.69	0.89	0.48	1.08	1.38
442.0	0.79	0.69	0.38	0.98	1.38
443.0	0.89	0.79	0.38	0.88	1.18
444.0	0.89	0.79	0.48	0.88	1.18
445.0	0.89	0.79	0.48	0.78	0.98
446.0	0.79	0.89	0.48	0.78	0.98
447.0	0.89	0.89	0.38	0.68	0.98
448.0	0.89	0.99	0.48	0.78	0.98
449.0	0.89	0.89	0.68	0.58	0.88
450.0	0.89	0.89	0.78	0.58	0.88
451.0	0.79	0.79	0.78	0.58	0.88
452.0	0.79	0.79	0.78	0.58	0.88
453.0	0.79	0.69	0.68	0.58	0.98
454.0	0.79	0.69	0.68	0.58	0.88
455.0	0.79	0.79	0.68	0.68	0.98
456.0	0.79	0.79	0.68	0.68	0.98
457.0	0.69	0.79	0.78	0.78	0.98
458.0	0.79	0.89	0.78	0.68	0.98
459.0	0.79	0.89	0.78	0.68	0.78
460.0	0.79	0.79	0.78	0.58	0.78
461.0	0.79	0.69	0.78	0.68	0.88
462.0	0.89	0.69	0.78	0.78	0.88
463.0	0.79	0.59	0.78	0.68	0.78
464.0	0.79	0.59	0.78	0.58	0.68
465.0	0.59	0.69	0.78	0.68	0.78
466.0	0.69	0.79	0.88	0.68	0.78
467.0	0.59	0.59	0.78	0.88	0.78
468.0	0.59	0.59	0.68	0.88	0.88
469.0	0.49	0.49	0.68	0.88	0.78
470.0	0.49	0.59	0.68	0.88	0.78
471.0	0.49	0.69	0.68	0.88	0.78
472.0	0.29	0.79	0.68	0.88	0.88
473.0	0.29	0.89	0.58	0.78	0.98
474.0	0.29	0.89	0.58	0.78	0.98
475.0	0.29	0.89	0.68	0.88	0.98
476.0	0.29	0.79	0.68	0.78	0.98
477.0	0.29	0.69	0.78	0.68	1.08
478.0	0.19	0.49	0.68	0.78	1.08
479.0	0.19	0.49	0.78	0.78	1.08
480.0	0.19	0.49	0.78	0.68	0.98
481.0	0.19	0.59	0.68	0.68	0.88
482.0	0.19	0.59	0.68	0.58	0.88
483.0	0.29	0.49	0.78	0.58	0.88
484.0	0.29	0.59	0.58	0.48	0.78
485.0	0.19	0.59	0.58	0.48	0.78
486.0	0.09	0.39	0.48	0.38	0.78
487.0	0.09	0.39	0.48	0.48	0.68
488.0	0.19	0.49	0.38	0.38	0.68
489.0	0.19	0.49	0.38	0.38	0.58
490.0	0.29	0.49	0.28	0.48	0.68
491.0	0.19	0.49	0.28	0.28	0.68
492.0	0.19	0.49	0.28	0.28	0.58

493.0	0.39	0.39	0.28	0.38	0.38
494.0	0.29	0.39	0.28	0.48	0.48
495.0	0.29	0.39	0.18	0.58	0.48
496.0	0.19	0.29	0.18	0.58	0.48
497.0	0.29	0.09	0.08	0.48	0.28
498.0	0.19	0.09	0.18	0.48	0.28
499.0	0.29	0.19	0.18	0.48	0.28
500.0	0.19	0.00	0.28	0.58	0.38
501.0	0.19	0.09	0.28	0.38	0.28
502.0	0.19	0.09	0.28	0.38	0.28
503.0	0.19	0.19	0.38	0.38	0.38
504.0	0.19	0.29	0.58	0.48	0.48
505.0	0.29	0.29	0.48	0.58	0.38
506.0	0.29	0.29	0.58	0.58	0.38
507.0	0.29	0.19	0.68	0.48	0.38
508.0	0.19	0.29	0.68	0.38	0.38
509.0	0.19	0.29	0.68	0.48	0.38
510.0	0.19	0.29	0.68	0.38	0.48
511.0	0.19	0.19	0.78	0.38	0.48
512.0	0.19	0.19	0.68	0.28	0.58
513.0	0.29	0.09	0.78	0.28	0.58
514.0	0.19	0.19	0.78	0.18	0.58
515.0	0.19	0.29	0.78	0.08	0.48
516.0	0.19	0.29	0.68	0.08	0.48
517.0	0.19	0.39	0.68	0.08	0.48
518.0	0.29	0.29	0.78	0.18	0.58
519.0	0.29	0.29	0.68	0.18	0.68
520.0	0.19	0.39	0.68	0.18	0.58
521.0	0.29	0.39	0.58	0.18	0.48
522.0	0.29	0.49	0.48	0.18	0.58
523.0	0.39	0.39	0.38	0.18	0.58
524.0	0.49	0.39	0.28	0.18	0.58
525.0	0.49	0.39	0.08	0.38	0.58
526.0	0.49	0.49	0.08	0.18	0.58
527.0	0.49	0.49	0.18	0.18	0.48
528.0	0.49	0.59	0.18	0.18	0.48
529.0	0.49	0.59	0.08	0.18	0.48
530.0	0.39	0.59	0.08	0.08	0.48
531.0	0.39	0.59	0.00	0.18	0.48
532.0	0.49	0.59	0.18	0.08	0.38
533.0	0.49	0.69	0.18	0.18	0.48
534.0	0.49	0.49	0.08	0.28	0.38
535.0	0.49	0.59	0.18	0.18	0.38
536.0	0.39	0.49	0.18	0.28	0.38
537.0	0.39	0.59	0.38	0.28	0.38
538.0	0.39	0.59	0.38	0.18	0.38
539.0	0.49	0.59	0.38	0.28	0.38
540.0	0.49	0.69	0.38	0.18	0.28
541.0	0.49	0.59	0.58	0.28	0.38
542.0	0.39	0.59	0.68	0.38	0.38
543.0	0.29	0.49	0.68	0.28	0.28
544.0	0.29	0.69	0.78	0.38	0.28
545.0	0.29	0.59	0.68	0.38	0.38
546.0	0.29	0.79	0.48	0.28	0.38
547.0	0.39	0.79	0.48	0.38	0.28
548.0	0.29	0.89	0.48	0.28	0.38
549.0	0.29	0.69	0.38	0.18	0.48
550.0	0.39	0.79	0.28	0.08	0.38

AMC 17 Section 6

y(m) / t(sec)	Concentration (ppb)				
	1.0	2.0	3.0	4.0	5.0
220.0	0.09	0.06	0.00	0.02	0.21
221.0	0.09	0.06	0.00	0.00	0.21
222.0	0.09	0.06	0.00	0.00	0.21
223.0	0.00	0.06	0.00	0.00	0.31
224.0	0.00	0.06	0.00	0.00	0.31
225.0	0.09	0.00	0.00	0.00	0.31
226.0	0.09	0.00	0.00	0.00	0.31
227.0	0.09	0.00	0.00	0.00	0.31
228.0	0.09	0.00	0.00	0.00	0.41
229.0	0.09	0.00	0.00	0.02	0.51
230.0	0.00	0.00	0.00	0.02	0.51
231.0	0.00	0.00	0.00	0.12	0.51
232.0	0.00	0.00	0.00	0.12	0.41
233.0	0.00	0.00	0.04	0.02	0.31
234.0	0.00	0.00	0.04	0.12	0.41
235.0	0.00	0.00	0.04	0.12	0.41
236.0	0.00	0.06	0.04	0.02	0.31
237.0	0.00	0.06	0.04	0.02	0.31
238.0	0.00	0.06	0.04	0.00	0.21
239.0	0.00	0.00	0.14	0.00	0.31
240.0	0.00	0.00	0.14	0.00	0.41
241.0	0.00	0.16	0.14	0.02	0.51
242.0	0.09	0.46	0.14	0.00	0.51
243.0	0.00	0.46	0.04	0.02	0.51
244.0	0.00	0.56	0.24	0.12	0.51
245.0	0.00	0.76	0.24	0.12	0.51
246.0	0.09	0.76	0.34	0.22	0.51
247.0	0.19	0.76	0.34	0.32	0.51
248.0	0.19	0.96	0.34	0.42	0.61
249.0	0.19	1.16	0.54	0.52	0.71
250.0	0.19	1.26	0.84	0.62	0.71
251.0	0.19	1.46	0.94	0.72	0.71
252.0	0.29	1.36	1.14	0.92	0.81
253.0	0.29	1.56	1.14	1.12	0.61
254.0	0.39	1.66	1.54	1.22	0.61
255.0	0.39	1.86	1.74	1.32	0.71
256.0	0.49	2.06	2.04	1.52	0.71
257.0	0.59	2.36	2.24	1.52	0.61
258.0	0.59	2.36	2.24	1.62	0.71
259.0	0.79	2.26	2.34	1.62	0.71
260.0	0.79	2.36	2.64	1.62	0.61
261.0	0.89	2.56	2.84	1.82	0.51
262.0	0.99	2.76	2.94	1.92	0.61
263.0	1.09	2.96	3.14	2.02	0.71
264.0	1.19	3.26	3.24	2.12	0.71
265.0	1.29	3.56	3.34	2.22	0.91
266.0	1.39	3.66	3.64	2.62	0.91
267.0	1.59	4.06	3.84	2.92	1.01
268.0	1.59	4.26	3.94	3.22	1.21
269.0	1.79	4.56	4.04	3.22	1.41
270.0	1.99	4.86	4.24	3.42	1.51
271.0	2.09	5.16	4.64	3.72	1.61
272.0	2.19	5.46	4.84	4.12	1.71
273.0	2.39	5.56	5.04	4.42	1.91
274.0	2.59	5.86	5.14	4.52	2.01

275.0	2.69	5.96	5.14	4.52	2.11
276.0	2.89	6.26	5.64	4.62	2.11
277.0	2.99	6.46	5.94	4.62	2.21
278.0	2.99	6.56	6.14	4.72	2.21
279.0	3.19	6.66	6.14	4.92	2.21
280.0	3.39	6.66	6.24	5.12	2.31
281.0	3.69	6.86	6.34	5.22	2.41
282.0	3.89	6.96	6.54	5.42	2.51
283.0	4.09	7.06	6.54	5.82	2.71
284.0	4.29	7.26	6.54	6.22	2.91
285.0	4.39	7.36	6.54	6.42	3.21
286.0	4.59	7.46	6.64	6.72	3.41
287.0	4.89	7.66	6.64	6.92	3.61
288.0	5.09	7.76	6.64	7.32	3.71
289.0	5.39	7.86	6.54	7.42	3.91
290.0	5.59	7.96	6.64	7.62	4.11
291.0	5.89	7.96	6.74	7.72	4.31
292.0	5.99	8.16	6.84	7.82	4.51
293.0	6.29	8.26	6.94	7.82	4.61
294.0	6.39	8.36	7.04	7.82	4.81
295.0	6.49	8.36	7.14	8.02	5.11
296.0	6.79	8.46	7.24	8.22	5.41
297.0	6.99	8.56	7.14	8.12	5.81
298.0	7.09	8.56	7.24	8.22	6.01
299.0	7.19	8.76	7.24	8.42	6.21
300.0	7.39	8.86	7.34	8.72	6.41
301.0	7.59	8.86	7.44	8.82	6.61
302.0	7.69	8.86	7.44	8.82	6.71
303.0	7.69	8.96	7.64	8.92	6.91
304.0	7.89	8.96	7.74	9.22	7.21
305.0	8.09	9.06	7.74	9.32	7.21
306.0	8.19	9.16	7.94	9.32	7.41
307.0	8.29	9.16	8.04	9.22	7.61
308.0	8.39	9.26	8.04	9.22	7.61
309.0	8.49	9.36	8.24	9.32	7.61
310.0	8.69	9.36	8.34	9.22	7.71
311.0	8.69	9.36	8.34	9.42	7.91
312.0	8.69	9.36	8.54	9.42	8.01
313.0	8.79	9.26	8.44	9.52	8.21
314.0	8.89	9.36	8.44	9.62	8.31
315.0	9.09	9.36	8.54	9.62	8.51
316.0	9.09	9.46	8.64	9.72	8.61
317.0	9.29	9.36	8.74	9.72	8.81
318.0	9.29	9.46	8.74	9.62	8.81
319.0	9.39	9.56	8.74	9.62	8.71
320.0	9.39	9.46	8.84	9.62	8.81
321.0	9.49	9.36	8.94	9.52	8.91
322.0	9.59	9.36	8.94	9.52	9.01
323.0	9.59	9.26	8.94	9.62	9.01
324.0	9.59	9.36	8.84	9.72	9.01
325.0	9.59	9.26	8.84	9.62	9.01
326.0	9.49	9.36	8.84	9.52	8.91
327.0	9.49	9.26	8.74	9.62	8.91
328.0	9.49	9.36	8.64	9.72	8.91
329.0	9.39	9.26	8.84	9.62	8.91
330.0	9.49	9.26	8.74	9.52	9.01
331.0	9.39	9.26	8.74	9.42	9.01
332.0	9.49	9.26	8.74	9.42	9.11
333.0	9.39	9.16	8.74	9.42	9.11
334.0	9.29	9.16	8.74	9.42	9.21
335.0	9.29	9.16	8.64	9.42	9.11
336.0	9.29	9.16	8.54	9.42	9.21

337.0	9.29	9.16	8.54	9.42	9.01
338.0	9.39	9.16	8.54	9.42	9.11
339.0	9.39	9.06	8.54	9.32	9.01
340.0	9.39	8.86	8.54	9.22	9.21
341.0	9.49	9.06	8.54	9.22	9.11
342.0	9.39	8.96	8.54	9.12	9.11
343.0	9.49	8.76	8.44	9.12	9.01
344.0	9.39	8.66	8.24	9.02	9.01
345.0	9.29	8.56	8.24	8.82	9.01
346.0	9.29	8.56	8.14	8.82	9.11
347.0	9.19	8.46	8.24	8.72	9.01
348.0	8.99	8.36	8.14	8.52	8.91
349.0	8.89	8.26	8.04	8.52	8.91
350.0	8.79	8.26	8.04	8.42	8.91
351.0	8.69	7.96	7.84	8.42	8.81
352.0	8.69	7.86	7.74	8.32	8.71
353.0	8.69	7.66	7.74	8.12	8.61
354.0	8.59	7.56	7.64	8.12	8.51
355.0	8.59	7.36	7.64	8.12	8.51
356.0	8.59	7.46	7.54	8.02	8.41
357.0	8.49	7.46	7.44	8.02	8.41
358.0	8.49	7.46	7.64	7.92	8.41
359.0	8.49	7.36	7.54	7.72	8.31
360.0	8.29	7.46	7.54	7.72	8.21
361.0	8.29	7.26	7.44	7.62	8.11
362.0	8.19	7.26	7.24	7.42	8.11
363.0	8.09	7.16	7.14	7.52	8.01
364.0	8.09	6.96	7.04	7.42	8.01
365.0	7.89	6.86	6.94	7.42	7.91
366.0	7.79	6.56	6.94	7.22	7.91
367.0	7.59	6.46	6.84	7.02	7.91
368.0	7.59	6.26	6.74	6.92	7.81
369.0	7.49	6.16	6.74	6.92	7.91
370.0	7.49	6.16	6.54	7.02	7.81
371.0	7.29	6.06	6.34	6.92	7.81
372.0	7.19	5.86	6.34	6.92	7.71
373.0	7.09	5.76	6.44	6.82	7.71
374.0	6.99	5.76	6.24	6.72	7.61
375.0	6.89	5.56	6.04	6.52	7.41
376.0	6.79	5.46	6.04	6.42	7.41
377.0	6.79	5.56	6.04	6.22	7.41
378.0	6.69	5.36	5.94	6.02	7.41
379.0	6.69	5.36	5.74	6.02	7.31
380.0	6.69	5.16	5.54	5.92	7.21
381.0	6.49	5.06	5.54	5.82	7.11
382.0	6.49	4.86	5.44	5.72	7.01
383.0	6.39	4.86	5.34	5.62	6.81
384.0	6.39	4.76	5.14	5.42	6.71
385.0	6.29	4.66	5.04	5.32	6.71
386.0	6.19	4.56	5.04	5.32	6.51
387.0	6.09	4.56	5.04	5.42	6.41
388.0	5.99	4.46	5.04	5.22	6.31
389.0	5.99	4.46	5.04	5.22	6.21
390.0	5.89	4.46	5.04	5.22	6.21
391.0	5.69	4.46	4.94	5.22	6.01
392.0	5.69	4.46	5.04	5.22	5.91
393.0	5.49	4.56	4.94	5.12	5.81
394.0	5.49	4.56	4.84	5.02	5.81
395.0	5.39	4.46	4.74	4.92	5.81
396.0	5.29	4.26	4.74	4.82	5.81
397.0	5.19	4.26	4.74	4.92	5.71
398.0	4.99	4.26	4.84	4.92	5.71

399.0	4.89	4.16	4.74	4.72	5.81
400.0	4.89	4.16	4.44	4.62	5.71
401.0	4.89	4.26	4.34	4.52	5.51
402.0	4.89	4.06	4.24	4.52	5.41
403.0	4.89	4.06	4.14	4.52	5.31
404.0	4.79	3.96	3.94	4.32	5.21
405.0	4.69	3.96	3.94	4.22	5.11
406.0	4.69	3.76	4.04	4.12	5.01
407.0	4.59	3.86	4.14	4.22	5.11
408.0	4.59	3.76	4.24	4.12	5.11
409.0	4.59	3.76	4.24	4.02	5.11
410.0	4.49	3.76	4.14	3.92	5.01
411.0	4.29	3.66	4.14	3.82	4.81
412.0	4.19	3.66	3.84	3.82	4.71
413.0	4.09	3.56	3.74	3.72	4.61
414.0	4.09	3.56	3.44	3.72	4.71
415.0	3.99	3.46	3.34	3.62	4.71
416.0	3.89	3.36	3.14	3.62	4.71
417.0	3.99	3.26	3.14	3.62	4.61
418.0	3.99	3.26	3.04	3.62	4.61
419.0	3.89	3.06	3.04	3.62	4.51
420.0	3.79	2.96	2.94	3.62	4.31
421.0	3.69	2.96	3.04	3.72	4.31
422.0	3.59	2.96	3.14	3.52	4.11
423.0	3.59	2.76	3.04	3.42	4.11
424.0	3.69	2.66	2.94	3.42	4.21
425.0	3.49	2.66	2.84	3.32	4.11
426.0	3.39	2.56	2.84	3.22	4.01
427.0	3.39	2.56	2.74	3.12	3.81
428.0	3.29	2.66	2.74	3.22	3.91
429.0	3.19	2.46	2.74	3.22	3.81
430.0	2.99	2.36	2.74	3.12	3.81
431.0	2.99	2.36	2.74	3.22	3.71
432.0	2.89	2.36	2.64	3.12	3.61
433.0	2.89	2.26	2.64	3.22	3.61
434.0	2.89	2.26	2.64	3.12	3.41
435.0	2.89	2.26	2.74	3.22	3.31
436.0	2.79	2.36	2.54	3.22	3.21
437.0	2.79	2.36	2.54	3.12	3.21
438.0	2.69	2.26	2.54	3.12	3.21
439.0	2.69	2.36	2.34	3.02	3.01
440.0	2.69	2.26	2.14	2.92	2.91
441.0	2.69	2.16	2.04	2.92	3.01
442.0	2.49	1.96	1.94	2.92	2.91
443.0	2.49	2.06	1.84	2.72	2.81
444.0	2.49	1.96	1.84	2.82	2.91
445.0	2.39	1.96	1.74	2.82	2.91
446.0	2.39	1.96	1.74	2.62	3.01
447.0	2.39	1.86	1.74	2.52	3.01
448.0	2.49	1.86	1.84	2.32	3.11
449.0	2.29	1.66	1.94	2.42	3.01
450.0	2.29	1.66	1.94	2.32	3.01
451.0	2.29	1.66	2.04	2.22	3.01
452.0	2.29	1.76	1.94	2.22	3.01
453.0	2.29	1.56	2.04	2.32	2.91
454.0	2.19	1.46	2.04	2.32	2.71
455.0	2.09	1.36	2.04	2.12	2.81
456.0	2.09	1.26	1.84	2.02	2.81
457.0	1.99	1.36	1.84	1.92	2.61
458.0	1.99	1.36	1.84	1.92	2.51
459.0	1.99	1.26	1.74	1.82	2.61
460.0	1.89	1.16	1.74	1.82	2.61

461.0	1.89	1.26	1.64	1.82	2.71
462.0	1.89	1.26	1.64	1.82	2.71
463.0	1.79	1.16	1.54	1.92	2.71
464.0	1.69	1.16	1.44	1.82	2.51
465.0	1.79	1.16	1.44	1.82	2.51
466.0	1.79	1.16	1.54	1.82	2.41
467.0	1.79	1.16	1.54	1.82	2.41
468.0	1.79	1.06	1.44	1.92	2.41
469.0	1.79	1.16	1.34	1.82	2.51
470.0	1.69	1.16	1.24	1.62	2.51
471.0	1.59	0.96	1.24	1.72	2.31
472.0	1.49	0.96	1.24	1.72	2.21
473.0	1.69	1.06	1.24	1.72	2.01
474.0	1.69	1.16	1.24	1.72	2.01
475.0	1.69	0.96	1.24	1.62	1.71
476.0	1.69	0.96	1.24	1.62	1.81
477.0	1.59	1.16	1.14	1.42	1.81
478.0	1.59	1.06	1.14	1.32	1.81
479.0	1.59	1.16	0.94	1.22	1.81
480.0	1.59	1.06	0.94	1.22	1.71
481.0	1.59	1.06	0.84	1.12	1.81
482.0	1.59	1.06	0.84	1.22	1.71
483.0	1.59	0.96	0.84	1.32	1.81
484.0	1.49	0.86	0.84	1.22	1.71
485.0	1.49	0.76	0.94	1.22	1.81
486.0	1.49	0.76	0.94	1.12	1.81
487.0	1.29	0.86	1.04	1.12	1.61
488.0	1.19	0.76	0.94	1.02	1.51
489.0	1.19	0.76	0.94	0.92	1.61
490.0	1.29	0.76	0.94	0.92	1.71
491.0	1.29	0.76	0.84	0.92	1.61
492.0	1.19	0.76	0.84	0.92	1.71
493.0	1.19	0.86	0.74	0.92	1.61
494.0	1.09	0.66	0.84	0.72	1.61
495.0	0.99	0.56	0.74	0.72	1.61
496.0	0.99	0.66	0.74	0.62	1.51
497.0	0.99	0.56	0.74	0.72	1.51
498.0	0.99	0.66	0.64	0.82	1.41
499.0	1.09	0.66	0.64	0.72	1.41
500.0	1.09	0.66	0.54	0.72	1.31
501.0	1.09	0.66	0.54	0.62	1.21
502.0	0.99	0.76	0.54	0.72	1.21
503.0	1.09	0.76	0.44	0.62	1.31
504.0	1.09	0.56	0.34	0.82	1.31
505.0	1.09	0.66	0.44	0.82	1.41
506.0	1.09	0.56	0.34	0.82	1.31
507.0	1.09	0.56	0.44	0.72	1.31
508.0	1.09	0.56	0.34	0.82	1.21
509.0	1.09	0.66	0.34	0.92	1.21
510.0	1.19	0.76	0.24	1.02	1.11
511.0	1.09	0.76	0.24	0.92	1.11
512.0	1.09	0.86	0.34	1.02	1.11
513.0	1.09	0.66	0.34	1.02	1.21
514.0	1.09	0.76	0.34	0.92	1.21
515.0	0.99	0.76	0.44	0.92	1.11
516.0	0.89	0.66	0.54	0.92	1.01
517.0	0.89	0.66	0.54	0.82	1.01
518.0	0.79	0.46	0.64	0.72	1.01
519.0	0.79	0.46	0.64	0.72	1.01
520.0	0.79	0.36	0.74	0.82	1.11
521.0	0.79	0.46	0.54	0.72	1.11
522.0	0.79	0.66	0.64	0.72	1.11

523.0	0.69	0.66	0.84	0.62	1.11
524.0	0.79	0.66	0.84	0.72	1.21
525.0	0.79	0.66	0.74	0.82	1.11
526.0	0.69	0.66	0.84	0.72	1.11
527.0	0.79	0.56	0.74	0.62	1.11
528.0	0.79	0.46	0.74	0.62	1.11
529.0	0.89	0.46	0.64	0.62	1.11
530.0	0.89	0.56	0.74	0.52	1.01
531.0	0.89	0.46	0.74	0.82	1.01
532.0	0.89	0.46	0.74	0.82	1.21
533.0	0.89	0.46	0.84	0.72	1.31
534.0	0.89	0.46	0.64	0.62	1.21
535.0	0.89	0.46	0.64	0.62	1.11
536.0	0.89	0.36	0.54	0.52	1.11
537.0	0.79	0.36	0.54	0.32	1.11
538.0	0.69	0.26	0.64	0.42	1.11
539.0	0.69	0.26	0.54	0.32	1.11
540.0	0.69	0.26	0.54	0.32	1.11
541.0	0.59	0.26	0.54	0.32	1.01
542.0	0.69	0.26	0.64	0.32	0.81
543.0	0.59	0.26	0.74	0.32	1.01
544.0	0.49	0.36	0.74	0.42	1.01
545.0	0.49	0.26	0.84	0.42	1.01
546.0	0.49	0.36	0.84	0.42	0.91
547.0	0.39	0.26	0.74	0.32	0.91
548.0	0.39	0.26	0.54	0.42	0.91
549.0	0.49	0.26	0.54	0.32	0.91
550.0	0.59	0.16	0.54	0.32	0.91
551.0	0.49	0.06	0.64	0.32	0.91
552.0	0.49	0.06	0.64	0.32	0.81
553.0	0.49	0.00	0.74	0.32	0.81
554.0	0.49	0.06	0.64	0.32	0.81
555.0	0.49	0.16	0.74	0.32	0.81
556.0	0.49	0.06	0.54	0.32	0.81
557.0	0.39	0.06	0.54	0.32	0.91
558.0	0.59	0.06	0.54	0.32	0.81
559.0	0.59	0.00	0.54	0.22	0.71
560.0	0.49	0.06	0.44	0.12	0.81
561.0	0.49	0.16	0.34	0.02	0.81
562.0	0.59	0.36	0.44	0.12	0.71
563.0	0.49	0.26	0.44	0.02	0.81
564.0	0.49	0.36	0.34	0.12	0.81
565.0	0.49	0.26	0.44	0.22	0.91
566.0	0.49	0.36	0.44	0.32	0.81
567.0	0.49	0.26	0.44	0.32	0.81
568.0	0.49	0.16	0.54	0.32	0.91
569.0	0.59	0.36	0.44	0.32	0.91
570.0	0.49	0.26	0.44	0.22	0.91
571.0	0.49	0.26	0.34	0.22	0.81
572.0	0.29	0.26	0.34	0.22	0.61
573.0	0.39	0.36	0.34	0.32	0.51
574.0	0.39	0.16	0.14	0.32	0.61
575.0	0.39	0.06	0.04	0.22	0.61
576.0	0.49	0.26	0.00	0.22	0.71
577.0	0.39	0.16	0.14	0.22	0.71
578.0	0.49	0.06	0.04	0.22	0.81
579.0	0.49	0.06	0.04	0.32	0.81
580.0	0.49	0.16	0.14	0.32	0.71
581.0	0.49	0.16	0.14	0.42	0.71
582.0	0.49	0.26	0.04	0.32	0.81
583.0	0.49	0.26	0.14	0.32	0.81
584.0	0.39	0.16	0.14	0.32	0.81

585.0	0.39	0.26	0.14	0.32	0.71
586.0	0.39	0.16	0.14	0.42	0.61
587.0	0.39	0.26	0.24	0.52	0.71
588.0	0.29	0.16	0.14	0.52	0.81
589.0	0.49	0.16	0.24	0.42	0.91
590.0	0.39	0.16	0.14	0.42	0.91
591.0	0.39	0.06	0.24	0.52	0.91
592.0	0.59	0.06	0.34	0.42	0.91
593.0	0.59	0.06	0.44	0.52	0.91
594.0	0.59	0.00	0.54	0.42	1.01
595.0	0.59	0.00	0.74	0.52	1.01
596.0	0.59	0.00	0.74	0.32	1.01
597.0	0.59	0.06	0.74	0.42	1.01
598.0	0.49	0.00	0.74	0.32	0.81
599.0	0.49	0.00	0.54	0.32	0.91
600.0	0.39	0.00	0.54	0.32	0.91
601.0	0.39	0.00	0.54	0.42	0.91
602.0	0.29	0.00	0.44	0.52	0.81
603.0	0.29	0.00	0.34	0.52	0.81
604.0	0.19	0.00	0.44	0.42	0.71
605.0	0.29	0.00	0.44	0.42	0.61
606.0	0.19	0.06	0.44	0.32	0.71
607.0	0.19	0.06	0.44	0.32	0.81
608.0	0.19	0.06	0.54	0.22	0.71
609.0	0.19	0.16	0.54	0.22	0.61
610.0	0.29	0.06	0.54	0.22	0.61
611.0	0.29	0.16	0.54	0.12	0.71
612.0	0.39	0.06	0.54	0.22	0.81
613.0	0.29	0.06	0.44	0.32	0.81
614.0	0.19	0.16	0.44	0.22	0.71
615.0	0.09	0.06	0.54	0.22	0.71
616.0	0.09	0.06	0.44	0.32	0.61
617.0	0.09	0.16	0.64	0.42	0.61
618.0	0.09	0.26	0.64	0.32	0.51
619.0	0.00	0.06	0.54	0.32	0.61
620.0	0.00	0.16	0.54	0.32	0.51
621.0	0.00	0.00	0.44	0.32	0.51
622.0	0.00	0.06	0.34	0.22	0.61
623.0	0.00	0.00	0.44	0.22	0.61
624.0	0.00	0.06	0.44	0.12	0.51
625.0	0.00	0.00	0.44	0.22	0.51
626.0	0.00	0.00	0.34	0.22	0.41
627.0	0.00	0.00	0.34	0.32	0.41
628.0	0.09	0.00	0.44	0.42	0.51
629.0	0.19	0.00	0.54	0.32	0.51
630.0	0.19	0.00	0.54	0.42	0.31
631.0	0.09	0.00	0.44	0.32	0.31
632.0	0.19	0.16	0.54	0.42	0.41
633.0	0.19	0.00	0.54	0.42	0.41
634.0	0.29	0.00	0.54	0.42	0.41
635.0	0.29	0.00	0.54	0.52	0.51
636.0	0.39	0.00	0.44	0.42	0.41
637.0	0.39	0.00	0.54	0.32	0.41
638.0	0.39	0.00	0.64	0.22	0.41
639.0	0.39	0.00	0.54	0.32	0.61
640.0	0.39	0.00	0.54	0.32	0.71
641.0	0.29	0.00	0.44	0.32	0.61
642.0	0.29	0.00	0.44	0.32	0.61
643.0	0.39	0.00	0.34	0.42	0.61
644.0	0.39	0.00	0.34	0.42	0.71
645.0	0.29	0.00	0.34	0.32	0.61
646.0	0.29	0.00	0.24	0.32	0.61

647.0	0.19	0.00	0.24	0.32	0.61
648.0	0.19	0.00	0.24	0.22	0.61
649.0	0.19	0.00	0.24	0.22	0.61
650.0	0.19	0.00	0.24	0.22	0.71
651.0	0.19	0.00	0.24	0.22	0.71
652.0	0.19	0.00	0.24	0.22	0.81
653.0	0.29	0.00	0.34	0.22	0.71
654.0	0.29	0.00	0.24	0.22	0.71
655.0	0.29	0.00	0.14	0.12	0.61
656.0	0.29	0.00	0.04	0.22	0.51
657.0	0.19	0.00	0.14	0.32	0.51
658.0	0.19	0.00	0.14	0.32	0.51
659.0	0.00	0.00	0.14	0.32	0.41
660.0	0.00	0.00	0.14	0.42	0.41
661.0	0.00	0.00	0.14	0.32	0.51
662.0	0.00	0.00	0.14	0.32	0.41
663.0	0.00	0.00	0.24	0.32	0.51
664.0	0.00	0.00	0.34	0.42	0.41
665.0	0.00	0.00	0.34	0.42	0.41
666.0	0.00	0.00	0.34	0.32	0.41
667.0	0.00	0.00	0.34	0.42	0.41
668.0	0.00	0.00	0.34	0.42	0.21
669.0	0.00	0.00	0.34	0.32	0.31
670.0	0.00	0.00	0.34	0.32	0.41
671.0	0.00	0.06	0.34	0.32	0.21
672.0	0.00	0.16	0.34	0.32	0.21
673.0	0.00	0.16	0.34	0.32	0.31
674.0	0.09	0.06	0.24	0.22	0.31
675.0	0.19	0.06	0.14	0.32	0.41

국문 초록

사행수로에서 흐름 및 오염물질 혼합에 미치는 2차원 전단효과에 대한 연구

서울대학교 대학원
건설환경공학부
신 재 현

본 연구에서는 전단 효과가 사행수로에서 흐름 및 오염물질 혼합에 미치는 영향을 수심 적분 수치 모형을 사용하여 정확하고 효율적으로 모의를 구현하였다. 수치 모형의 검증을 위해서 대규모 실험을 하천실험센터에서 수행하여 acoustic Doppler current profiler (ADCP)를 통하여 유속자료를, 추적자 실험을 통하여 농도곡선 자료를 취득하였다. 유속자료를 사용하여 이차류가 주 흐름 분포에 미치는 영향을 먼저 분석하였다. 이차류 강도와 사행수로의 수심 대비 곡률반경과의 관계를 발견하였고, 기존의 연구에서 제외된 비선형항을 고려한 이차류 연직분포 공식을 개발하였다. 제시된 연직분포 공식은 기존의 공식과는 다르게 상단부와 하단부에 상대적으로 감소되는 이차류 크기를 나타내었다.

개발된 연직분포 공식을 분산응력항 형태로 운동량 방정식에 도입하여 2차원 흐름 모형 HDM-2D에 적용하였고, 이를 통해 수심적분 과정에서 제외되는 이차류에 의해 발생하는 전단효과를 추가하였다. 분산응력항을 사용한 모형의 모의 결과는 Rozovskii 실험에 적용되어 기존에 사용되었던 주 흐름과 이차류 흐름간의 선형 관계로 이루어진 deVriend 및 Kikkawa 공식을 이용한 모형과, 분산응력항을 사용하지 않은 모형보다 정확한 결과를 보여주었다. 또한 하천실험센터의 사행수로에 적용된 분산응력항이 적용된 모의 결과 역시 주 흐름 분포를 정확하게 재현하였다.

사행수로에서 오염물질 혼합 특성을 발견하기 위해서 ADCP를 통해 취득한 유속의 연직 분포를 이용하여 전단류 분산에 의한 2차원 분산 계수를 구하였고, 이를 추적자 실험에서 취득한 농도곡선을 이용하여 2차원 유관추적법을 수행하여 서로 비교하였다. 유속 분포를 이용한 2차원 분산 계수는 Fischer 등 (1979)의 공식을 이용하여 전단류 분산을 계산할 수 있어 추적자 실험 없이 상대적으로 간편하게 분산계수를 구할 수 있는 장점이 있다. 유속을 이용한 분산계수 계산 결과, 무차원 종분산 계수 D_L / hu^* 는 범위가 4-6으로 Elder (1959)의 결과와 비슷하였으며, 무차원 횡분산 계수 D_T / hu^* 의 경우 0.05-0.4의 범위를 나타내었다. 2차원 유관 추적법을 사용한 결과, 종분산 계수는 유속을 이용하여 계산한 결과의 4-5배, 횡분산 계수는 1-3배의 결과가

나타났다. 이러한 차이는 농도장 기반으로 유관추적법으로 구한 분산계수의 경우 하천의 불균질성, 저장대 효과를 가지고 있어 전단류 분산 효과만 반영되는 유속 연직 분포 기반 분산 계수보다 크게 계산된 것이다. 이후 2차원 이송-분산 모형인 CTM-2D를 이용하여 계산한 결과, 분산응력항의 도입으로 계산 정확도가 1% 증가하였으며, 모형 결과에 보정된 분산계수는 유속 기반 분산계수 결과와 농도장 기반 분산계수 결과의 중간 값으로 판단되었다. 모의 결과 CTM-2D 모형이 사행수로에서 추적자 실험을 통해 구한 농도장을 재현할 수 있는 적용성이 높다는 것이 확인되었으며, HDM-2D 와 더불어 흐름 및 오염물질 혼합 검토에 유용한 모형으로 사용될 것으로 기대된다.

주요어: 2차원 천수흐름 모형, 2차원 이송분산 모형, 사행수로, 분산응력항, 분산 계수, 주 흐름 분포, 이차류, 유속 연직분포, 비선형 효과

학번: 2012-30246